Structural Fire Design Considerations for High Strength Steel

Dorothy Abigail Adjoa Anoa Winful

A thesis submitted to Brunel University, London for the degree of Doctor of Philosophy in College of Engineering, Design and Physical Sciences

December 2018

"And people should eat and drink and enjoy the fruits of their labour, for these are gifts from God".

Ecclesiastes 3:13

(New Living Translation)

Preface

The research described herein was conducted by the author under the supervision of Dr Katherine A. Cashell, Dr Sheida Afshan at Brunel University, London and Adrienne M. Barnes and Richard J. Pargeter at TWI Ltd, Great Abington, Cambridge, between October 2014 and April 2018. Material from published or unpublished work is referenced, when used.

Copyright declaration

The copyright of this thesis rests with the author, Dorothy Winful and is made available under a Creative Commons Attribution Non-Commercial No Derivatives licence. Researchers are free to copy, distribute or transmit the thesis on the condition that they attribute it, that they do not use it for commercial purposes and that they do not alter, transform or build upon it. For any reuse or redistribution, researchers must make clear to others the licence terms of this work.

Abstract

High strength steels (HSS) defined herein as material with a yield strength between 460 and 700 N/mm^2 are increasingly being employed in structures as an alternative to conventional steel grades (i.e. steel grades with yield strengths below 460 N/mm^2) due to economic and environmental benefits related to reductions in section thickness and hence reduced weight (and overall material usage) as well as potentially lower transport and fabrication costs. The European structural design guidelines (Eurocodes) are based on previous work on conventional steel grades, which currently limit the use of HSS. Hence there has been a surge in research activity with the aim to enhancing the current understanding relating to the behaviour of HSS structural members under various loading conditions and including their performance in fire scenarios.

This thesis examines the behaviour of various HSS grades at elevated temperature for structural fire design purposes. Fundamental to the understanding and safe design of structures under fire conditions is a detailed understanding of material properties at elevated temperatures. To this end, the material response of various commercial HSS grades, including quenched and tempered (QT) and thermomechanically control processed (TMCP) steels, were determined from elevated temperature tensile tests under two conditions: isothermal (steady-state) and anisothermal (transient-state), at temperatures up to 800°C. The strength and stiffness were obtained and converted into reduction factors, defined as the elevated temperature property normalised by the property at room temperature in line with the current Eurocode approach. The results demonstrate the variability in strength retention at elevated temperatures; this is attributed to the material history particularly the alloying elements and highlight the danger in generalising the material properties of different types of HSS for structural fire design purposes.

Heat treatments and microstructural studies were conducted on the two HSS grades which demonstrated the best strength retention properties at elevated temperatures to deduce possible metallurgical effects, which could account for the better strength retention. The study highlighted that a sufficient amount of elements including molybdenum and chromium, as well as microalloying elements, niobium, vanadium and titanium can cause strength enhancement between 500 and 700°C through secondary hardening.

Additionally, with the scarcity of performance data on HSS columns at elevated temperature, a numerical model, which considered geometric imperfections and material nonlinearity, was developed in ABAQUS and validated using experimental data on HSS at room temperature and mild steel grades at elevated temperature. After the model was validated, parametric studies were conducted, incorporating material properties of QT and TMCP steels, in order to determine the influence of the material history on the buckling behaviour and assess the suitability of the buckling curves provided in Eurocode 3 Part 1-2 (2005). The results showed that the Eurocode generally provides conservative (i.e. safe) results for TMCP steel columns with respect to the buckling coefficients and safely predicts the buckling resistance, but a lower buckling curve may be needed for QT columns. In addition, because of the various alloying and production routes employed to produce HSS, variations in the stress-strain response was also observed, in turn, this influenced the buckling response and highlighted possible unconservativisms (i.e. unsafe) in the Eurocode design approach as a result of generalising the material response.

Acknowledgements

To God be the glory! There are countless individuals to thank for their support, wisdom and love throughout this endeavour; I will not attempt to list everyone before this turns into an essay but there are the few individuals I will single out.

Firstly, special thanks to my academic supervisors, Dr Katherine Cashell and Dr Sheida Afshan and my industrial supervisors Adrienne Barnes and Richard Pargeter. Thank you for your guidance, encouragement, patience, invaluable knowledge and ensuring I stay on track to finish this work.

Many thanks to Imperial College, London and the organisations for providing the high strength steels used in this study. This research was funded by the UK Engineering and Physical Sciences Research Council (EPSRC) and TWI Ltd and is greatly acknowledged. In addition, this research was undertaken at TWI Ltd, Great Abington, Cambridge and I must extend my gratitude to the technicians, particularly Jerry Godden, Mark Tinkler, Phillip Cossey, Jack Bradford, Ashley Spencer and Tom Adams. Thank you for your knowledge, banter and the positive attitude which was much needed during the numerous “failures”.

Many thanks to my fellow researchers including Lisa Blanchard, Michael Walker and Rosa Griñon Echaniz as well as my colleagues Michael Dodge, David Griffths, Imran Bhaji and Philip McNutt for the countless joyful moments, support and delicious ‘feasts’.

I would like to express my deep gratitude to those who have not only made my time in Cambridge wonderful but challenged and nurtured my faith through some tough personal circumstances. These include the Grahams, Cherish Nicholson, Esther Sharman, Lydia Lowe, Joanna Lunt and Catherine Hildersly.

To the few friends who have known me long before this venture began, thank you for your constant stream of love and belief that I will leave a positive dent in this world, I will always be working towards this.

Finally, I would like to express sincere gratitude to my biological and spiritual family including those in the Motherland. Your emotional and spiritual support has been invaluable. In particular,

special thanks to my mother Amanda - you have been a physical rock for Ekow, Emma and me. Thank you from the bottom of my heart.

List of publications

Journals

- Winful, D.A., Cashell, K.A., Afshan, S., Barnes, A.M., Pargeter, R.J. (2018) "Behaviour of high strength steel columns under fire conditions", Journal of constructional research
- Winful, D.A., Cashell, K.A., Afshan, S., Barnes, A.M., Pargeter, R.J. (2017) "Elevated temperature material properties of high strength steel", ICE Building and structures

Conferences

- Winful, D.A., Afshan, S., Cashell, K.A., Barnes, A.M., Pargeter, R.J. (2017) "Flexural buckling behaviour of high strength steel columns under fire conditions", in Eurosteel 2017, Copenhagen, Denmark
- Winful, D.A., Cashell, K.A., Afshan, S., Barnes, A.M., Pargeter, R.J. (2017) "Material properties of high strength steel under fire conditions", in Eurosteel 2017, Copenhagen, Denmark
- Winful, D.A., Cashell, K.A., Barnes, A.M., Pargeter, R.J. (2015) "Influence of metallurigcal properties on the mechanical behaviour of high stength steels". In proceedings of the first international conference on structural safety under fire and blast CONFAB 2017. Brunel University, London, UK
- Winful, D.A., Cashell, K.A., Barnes, A.M., Pargeter, R.J. (2016) "Behaviour of high strength steel under fire conditions", In Proceedings of 9th International Conference on Structures in Fire (SiF), Princeton University, USA
- Winful, D.A., Cashell, K.A., Barnes, A.M., Pargeter, R.J. (2015) "High strength steel in fire". In proceedings of the first international conference on structural safety under fire and blast CONFAB 2015. Glasgow, UK

Awards and grants

First place oral presentation (2018)

Awarded by the Institution of Structural Engineers at the 20th Young Researchers' Conference in London in April 2018

Best final year PhD student (2017)

Awarded by The Armourers & Brasiers Gauntlet Trust and presented at The Welding Institute's Annual Awards and Dinner in June 2017

First place poster prize (2017)

Awarded at Brunel University, London Research Student Poster Conference in July 2017

Brunel University Vice Chancellor travel prize (2016)

Awarded by the Brunel Graduate School, this award was used to attend and present at the 9th International Conference on Structures in Fire at Princeton, USA in June 2016

Armourers and Brasiers travel award (2016)

Awarded by The Armourers & Brasiers Gauntlet Trust, this award was used to attend and present at the 9th International Conference on Structures in Fire at Princeton, USA in June 2016

Runner-up poster prize (2015)

National structural integrity research (NSIRC) Conference in June 2015

List of contents

List of tables

List of figures

List of notations

A	cross-section area of the structural member
A_{eff}	effective cross-sectional area
A_o	cross-sectional area of tensile specimen
b	width of the cross-section
C	suitable for cold-forming/cold-formed
COV	Coefficient of variation
E_a	elastic modulus
$E_{a,\theta}$	elastic modulus at temperature θ
$E_{0.2}$	tangent modulus at 0.2% proof strength
f_{cr}	elastic critical buckling stress of the most slender constitute plate element in the section
$f_{0.2p}$	0.2% proof strength
$f_{0.2p,\theta}$	0.2% proof strength at temperature θ
$f_{1.0p}$	1.0% proof strength
f_p	proportional limit
$f_{p,\theta}$	proportional limit at temperature θ
$f_{1.0p}$	1.0% proof strength
f_y	nominal or design yield strength
$f_{y,20}$	effective yield strength based on 2% total strain at room temperature θ (20°C)
$f_{y,\theta}$	effective yield strength based on 2% total strain at temperature θ
f_u	ultimate strength
H	hollow section
h	depth of the cross-section
H-J	Hollomon Jaffe
HSS	High strength steels
$k_{p,\theta}$	reduction factor for the proportional limit at steel temperature θ

$k_{0.2p,\theta}$	reduction factor for the 0.2% proof strength at steel temperature θ
$k_{y,\theta}$	reduction factor for the effective yield strength at steel temperature θ
$k_{Ea,\theta}$	reduction factor for elastic modulus at steel temperature θ
L	column length
L_c	parallel length
L_o	gauge length
L_t	total length of tensile specimen
L_u	final gauge length after fracture
m	strain hardening parameter determined from the points ($f_{0.2p}$, $\varepsilon_{0.2p}$) and ($f_{1.0p}$, $\varepsilon_{1.0p}$).
N	normalized
n	strain hardening parameter
$N_{b,fi,tRd}$	design buckling resistance at time t of a compression member
Q	quenched and tempered
RHS	Rectangular hollow section
r_i	internal radius of curvature
S	structural steel
SHS	Square hollow section
T/TMCP	Thermomechanically controlled processed steel
t	thickness of cross-section
t_o	thickness of tensile specimen
α	imperfection factor
$\gamma_{M,fi}$	the partial safety factor, for fire situation the recommended value is 1.0
ε	parameter used to determine cross section classification or strain
$\varepsilon_{0.2p}$	total strain at 0.2% proof strength $f_{0.2p}$
$\varepsilon_{1.0p}$	total strain at 1.0% proof strength $f_{1.0p}$
ε_f	elongation at fracture
ε_{nom}	engineering strain
ε_{pl}^{ln}	logarithmic plastic strain
$\varepsilon_{p,\theta}$	strain at the proportional limit
$\varepsilon_{t,\theta}$	limiting strain for yield strength
$\varepsilon_{y,\theta}$	yield strain
$\varepsilon_{u,\theta}$	strain at ultimate tensile strength
θ	temperature
σ	stress

σ_{nom}	engineering stress
σ_{true}	true stress
$\bar{\lambda}$	non-dimensional slenderness at room temperature
$\bar{\lambda}_{\theta}$	non-dimensional slenderness at temperature θ
φ_{θ}	parameter used to calculate χ_{fi}
χ_{fi}	reduction factor for the flexural buckling in the fire
ω_0	local imperfection amplitude

Chapter

1

Introduction

1.1 General

This research is concerned with the behaviour of various HSS grades (defined here as materials with yield strength between 460 and 700 N/mm^2 in accordance with Eurocode 3 part 1-12 (2007) at elevated temperature for structural fire design purposes. Fundamental to the understanding and safe design of structures under fire conditions is a detailed understanding of material properties at elevated temperatures. The material properties are dependent on the metallurgical properties which stem from material history, particularly the chemical composition and production route. Often, the metallurgical influences are overlooked because there are so many variables to take into account, which only adds another layer of complexity to the design process. However, neglecting these influences may compromise the safety of the design. Before discussing the previous work on the material properties of HSS at elevated temperature, it is worth considering the industrial need for HSS in structural applications.

1.2 The industrial need for HSS in structural applications

Steel is a versatile and popular material in the construction industry because of its excellent strength to weight ratio compared to other common building materials such a concrete, brick and wood. According to the World Steel Association (World Steel Association, 2017a), 1.5 billion tons of steel was consumed worldwide in 2014 – more than 50% of this was utilised in buildings and

infrastructure. The use of steel in construction will continue to grow as the population in urban areas rises. By 2050, the UN has projected the population in urban areas to grow by 2.5 to 3 billion people (Rhodan, 2013). In turn, there will be a great demand in infrastructure including buildings for people to live, work, socialise and study in. At the same time, there is a great concern over the decline of natural resources, rising carbon emissions and the effect on climate change as well as the environment. Thus infrastructure must be designed to strike a balance between social, economic and environmental needs. The choice of material is important in the design process and this is where HSS is potentially advantageous over conventional steel grades with lower yield strengths (e.g. S235, S355) as their use can result in reduced weight and cost of structures when employed in appropriate applications. The use of HSS can reduce the overall material usage of steel in structures by 25-50% (Hechler, 2015; World Steel Association, 2017b). However, there are still a number of challenges including increased likelihood of stability issues relating to the reduction in section thickness, and lack of performance data and design guidelines under fire conditions. The aforementioned challenges and knowledge gaps are being addressed to help provide reliable and economical design guidance for HSS in structural application.

1.3 Previous research on the material properties of HSS at elevated temperatures

As mentioned in Section 1.1, the material properties form the basis of understanding the structural performance at elevated temperatures. The material properties of steels at elevated temperature presented in the European structural fire design guidelines (EN 1993-1-2, 2005) are derived from conventional steel grades and assumed to be applicable to HSS grades. There is conflicting information about whether the Eurocodes (EN 1993-1-2, 2005) are conservative (i.e. safe) or unconservative (unsafe) for the design of HSS in case of fire. For example, studies by Chen and Young (2006) and the Rules on High Strength Steel (RUOSTE) report commissioned by the EU Research Fund for Coal and Steel (European Commission, 2016) concluded that the Eurocode approach is conservative and adequate for predicting strength degradation of HSS at elevated temperature. However, studies by Chen et al., (2006), Schneider and Lange (2009), Qiang (2013), Choi et al. (2014), Chiew et al. (2014), Xiong and Liew (2016) and Neuenschwander et al. (2017) have shown that the strength degradation presented in Eurocode is unconservative (i.e. unsafe), thus incorporating the Eurocode approach could compromise the overall performance of HSS components under fire conditions. Whether the Eurocode is conservative or unconservative with respect to elevated temperature performance of HSS is dependent on at least two things which are often not considered:

1. Experimental parameters used to obtain the data
2. The material history, in particular the chemical composition and/or production route

A variety of production routes and chemical compositions are used to produce HSS complaint with the standards at ambient temperature, however, this in turn could lead to a wide variation in material responses in fire. Further clarity is needed to differentiate which HSS grades are safely predicted by the Eurocode (EN 1993-1-2, 2005) and why? This thesis will examine the material and metallurgical properties of different types of HSS at elevated temperatures in order to explore and understand which HSS grades have better strength retention properties than others. The HSS grades to be examined here differ from HSS grades tested previously in the literature because of the differences in chemical composition and/or heat treatment.

1.4 Research objectives

The aim of this research is to explore how the material history including chemical composition and production route of various HSS will influence the material properties (i.e. strength and stiffness) and hence structural response in a fire scenario. The findings from this study will be compared with design guidelines provided in the Eurocodes and support the growing research on the material properties of HSS at elevated temperature. A further aim is to explore whether any benefits can be derived (when compared to lower strength alternatives) from metallurgical effects including secondary hardening gained from the microalloying additions, such to improve the strength retardation at elevated temperatures. The work which comprises in-depth experimental and numerical studies is intended to provide engineers and designers with essential and reliable information to support the safe design of structures made from HSS. In addition, this work should offer wider potential application of current HSS grades for structural applications as well as providing the necessary input for improved material design.

1.5 Thesis outline

This thesis is divided into seven further chapters which are summarised hereafter:

Chapter 2 presents an overview of published research into the behaviour and design of high strength steel, considering the metallurgical and structural aspects including the prescriptive and performance based design processes, with emphasis given to the fire response.

Chapter 3 introduces the procured HSS grades used in this research and presents an experimental study on the material properties of different types of HSS grades at room temperature. These material properties are used as a baseline in chapter 4, to characterise how the material properties of different types of HSS change at elevated temperature.

Chapter 4 presents a detailed experimental study on the material properties of different HSS grades at elevated temperatures. Isothermal (steady-state) and anisothermal (transient-state) test methods are conducted to obtain information on how the strength and stiffness change at temperatures up to 800°C and the results are compared with the literature and the recommendations given in Eurocode 3 Part 1-12 (2007).

Chapter 5 presents a metallurgical study, characterising the microstructure of the HSS in the as-received condition as well as capturing the microstructural changes, including grain size, of the HSS grades with the best strength retention properties at elevated temperature. To achieve the latter, selected steel grades are heat-treated to simulate the heat treatments in the tensile tests and examined using optical microscopy and scanning electron microscopy.

The application of the material properties of HSS obtained in Chapters 3 and 4 are presented in Chapter 6, with the aim to demonstrate how the material history influences the buckling behaviour of HSS columns in fire scenarios. Firstly, the stress-strain responses obtained in Chapters 4 and 5 are mathematically represented using the modified Ramberg-Osgood model proposed by Gardner and Nethercot (2004). Following on, a numerical model is created in the finite element package ABAQUS which is validated using experimental data on high strength steel and mild strength steel at room and elevated temperature, respectively. Parametric studies are then performed utilising the material properties in Chapters 3 and 4 to investigate the influence of material history on the buckling behaviour at elevated temperatures. The results are assessed using the current Eurocode approach and suggestions are made for future design consideration.

Chapter 7 collates the key points from Chapters 3 to 6 to discuss the links between the material history, including chemical composition, production and fabrication route of different HSS grades tested with the changes in the microstructure at elevated temperature and relates this to material and buckling performance at elevated temperature.

Finally, Chapter 8 summarises the important findings from this research and identifies possible areas for future research.

Chapter

2

Literature review

2.1 Introduction

The most commonly used steel grade in construction, S355 was considered a high strength steel 20 years ago. Nowadays, higher strength steel grades with nominal yield strengths greater than 460 N/mm^2 are being used in structures because of associated economic, environmental and social benefits compared to conventional steel grades. This suggests that high strength steel grades may become the norm in the future (Baddoo and Brown, 2015). A summary of the various steel types utilised in construction are presented in Table 2-1.

Table 2-1 Examples of steel types used in construction

Type	Yield strength (N/mm^2)	Nominal elastic modulus (GPa)	Typical steel grades
Mild strength steel/conventional steel	<460	210	S235, S275 S355
High strength steel	460-700	210	S460, S500, S690
Very high strength steel	>700	210	S890, S960, S1100

This chapter presents an overview of previous research into the behaviour and design of high strength steel, including the metallurgical and structural aspects, with emphasis given to the fire response. The chapter is generally divided into three sections. Firstly, the benefits and challenges of utilising high strength steel (HSS) in structural applications are presented. Secondly, the role of metallurgy, particularly the allotropy of iron, the iron-carbon phase diagram, strengthening mechanisms and production routes for HSS are described, giving consideration to how this relates

to the material properties and their performance in a fire scenario. “Heat-resistant” steels are also briefly discussed from the viewpoint of the role of alloying elements and its implications on the strength at elevated temperatures. The final section presents a critical review of other relevant research into the structural fire performance and design of high strength steel structures, which includes the material properties of HSS at elevated temperature.

2.2 HSS in structures: the benefits and the challenges

2.2.1 The benefits of using HSS in structural applications

As mentioned in Chapter 1, HSS offer economic, environmental and social benefits when compared to the more conventional steel grades (e.g. S235, S275 and S355) through a reduction in material usage, weight and section size as well as an increase in the load-carrying capacity of structures. The benefits of HSS have been well documented by many (Gresnigt and Steenhuis, 1997; Laogan and Elnashai, 1999; Sedlacek and Müller, 2001; Schröter, 2006; Qiang, 2013). In summary of these studies, economic savings are gained through the potential reduction in the construction time, as lighter structures can be quicker to erect and easier to transport, and the reduced section sizes result in smaller cross sections to weld and inspect. Additional savings can be made because a smaller foundation may be required due to the reduced weight and there are also associated environmental benefits owing to less disruption to the ground. Further environmental benefits include reduced fabrication costs and raw material consumption as well as reduced carbon dioxide emissions due to the transportation of lighter structural components and the production of less material. There is also less material to maintain and dispose of during and after the structure’s life.

HSS has the potential to create more architecturally pleasing solutions, particularly in high rise buildings, as slender sections lead to more open space (i.e. increase in the net to gross area ratio for each floor) and are less of a visual intrusion. Long span beams also allow for great interior flexibility, where spaces are adaptable to meet future needs without the economic burden of demolishing and rebuilding walls. Then there are the social aspects that at times can be difficult to quantify. This could be an indirect benefit as a result of architectural triumphs that improve lifestyle (i.e. housing, workplace, utilities, and transport infrastructure) (Burgan and Sansom, 2006).

The full potential of HSS can be exploited when the design of structural components is governed by strength rather than stiffness (i.e. buckling and deflection) and where there are advantages of

reducing the weight to decrease operating expenses. For such reasons, HSS have been used in other industries for many years, including: automotive, oil and gas, shipbuilding, and heavy industrial plants (Billingham et al., 2003).

In structures, there are several documented instances where HSS have been successfully used. For example, the use of HSS (a hybrid of S460, S690 and S900) in the roof structure of the Friends Arena Stadium in Sweden resulted in a structure 15% lighter when compared with using S355, saving €2.2 million in costs and producing 17% less greenhouse gas emissions (Ruukki, 2013). In addition, the use of HSS in the long span Oresund Bridge between Sweden and Denmark (Figure 2-1) resulted in cost savings of more than €22 million (Rakshe and Patel, 2010). HSS has also been successful used in buildings (e.g. City of Dreams Hotel Tower, Macau), and metro stations (e.g. Olaya Metro Station, Saudi Arabia).

Figure 2-1 The Oresund Bridge at Malmö, Sweden

2.2.2 The challenges of using HSS in structural applications

One of the challenges hindering the exploitation of HSS in structural design is a misconception regarding the price/tonne. HSS sections tend to command a higher price/tonne than conventional

steel grades, with the price of steel being determined by factors such as supply and demand, energy and transportation costs, and the price fluctuation in raw material. Currently the cost of S460 compared to S355 can be between 10-15% higher, whilst the cost of S690 compared to S355 is 40-70% more (Baddoo, 2015). However, the use of HSS can result in a reduction in the required tonnage which could counteract the higher price per tonne. Indeed, HSS, when used appropriately, will have a positive impact considering the holistic costs associated with structures such as raw-material, fabrication and erection costs.

The higher alloying content and hardenability of HSS can pose additional welding challenges compared with lower strength counterparts. For example, careful control of preheating and interpass temperatures is required, as well as thorough postweld non-destructive examination. Several researchers have reported on factors that influence the weldability of HSS, which include weld geometry, consumable selection, preheat and interpass temperature (e.g. Collin and Johansson, 2005; Gladman, 1999; Gyasi and Kah, 2016; Meester, 1997). The challenges are transferring up-to-date knowledge to relevant design guidelines without excessive conservatism, and the lack of qualified welders (Johansson and Collin, 2005; Porter, 2015; Baddoo, 2015).

The use of HSS is further hindered by the increased likelihood of stability and serviceability (i.e. deflection and vibration) issues since HSS sections tend to be smaller or thinner than conventional steel grade equivalents for the same load bearing capacity. The stability and serviceability of structures are governed by the elastic modulus, which, irrespective of the strength of the steel, is bounded between 190-230 GPa (Mahendran, 1996). Thus, HSS have a higher yield to stiffness ratio and a more limited deformation capacity (or larger deflections) than conventional steels. This becomes of paramount importance when loading conditions cause inelastic deformations such as can arise during fire and earthquakes (Varol and Cashell, 2017). In addition, it may not be economical or aesthetically pleasing to introduce additional stiffeners such as braces to justify using HSS. Despite these challenges, it is worth noting that Eurocode 3 Part 1-1 (2005) prescribe a slightly better buckling curve for HSS hot-rolled or formed structural hollow sections compared to conventional steel grade equivalents because the influence of geometric imperfections and residual stresses is less pronounced.

To date, the lack of reliable design guidelines for HSS does not allow the benefits of HSS over mild strength steel to be fully exploited. For example, due to the reduced ductility and to some extent the reduced ratio between the ultimate tensile and yield strength (f_u/f_y) of many HSS, the Eurocode recommends that the guidelines for plastic analysis and semi-rigid joints are not

applicable to HSS members. However, no alternative guidelines are given, even though there are several studies (e.g. (Johansson and Collin, 2005; Sedlacek and Müller, 2001))which imply that plastic hinge analysis is possible. Wang (2016) investigated the ductility requirements of various HSS comparing work from an experimental study with extensive literature surveys and concluded that HSS can satisfy the stricter ductility limits in Eurocode 3 Part 1-1 (2005). Since the current Eurocodes were derived from extensive studies on conventional steel grades, more clarity is needed to assess the uncertainties and knowledge gaps concerning the use of HSS members, such as to further develop appropriate design guidelines for HSS.

New structural solutions may need to be developed to ensure HSS structural members meet deflection and fatigue requirements in order to widen the application of HSS in structural applications (Johansson and Collin, 2005). There has been a considerable amount of work done in Europe (e.g. HILONG and ROUSTE projects both funded by the Research Fund for Coal and Steel (European Commission, 2016, 2017) which has focused on room temperature design and these are likely to expand the scope of Eurocode 3 Part 1-1 (2005) to cover steel grades up to S700, with even higher strengths up to S960 covered in Eurocode 3- Part 1-12 (Baddoo and Brown, 2015). Under fire conditions, it is expected that, like conventional steel grades, the strength of the material decreases as the temperature increases until eventually it can no longer support the load it was designed to carry. Although Eurocode 3 Part 1-2 (2005) is derived from extensive tests on steels with yield strengths below 460 N/mm^2, Eurocode 3 Part 1-12 (2007) states the following for structural fire design guidelines:

> "The standard (EN 1993-1-2, 2005) is applicable to steels with grades greater than S460 and up to S700 without further additional rules"

The above statement was made based on limited information at that time, and since then there has been further research which suggests that alternative/additional rules may be needed to ensure the safe design of HSS structures under fire conditions. For instance, Qiang (2013) concluded that the strength degradation of HSS at elevated temperatures is higher than conventional steel grades, and this may compromise the overall performance under fire conditions. Further research is needed to assess the applicability of Eurocode 3 Part 1-2 (2005) to HSS; to date studies have been limited mainly because of the significant expense associated with high temperature structural testing, as well as a lack of reliable data on the material properties which are needed to develop computational design models. This is one of the key focuses of this research and is discussed further in Chapters 4 and 7.

2.3 The diversity of structural steel

2.3.1 Fundamental steel metallurgy

Steel is an alloy containing iron and up to 2% (by weight) of carbon along with other alloying elements such as manganese, nickel, silicon, chromium, molybdenum, niobium and vanadium. The heat treatments and mechanical working, together with the alloying elements, combine to give steel a wide variety of useful properties for design, including adequate strength, ductility, fracture toughness and creep resistance. The wide range of properties is also related to the allotropic nature of iron, meaning that the crystal structure or phase changes are dependent on temperature (Chadwick, 1972). In pure iron, the phase transformation considered the most important occurs at 910°C, where below this temperature, iron is a body centred cubic (bcc) structure known as ferrite (α), and above this a face centred cubic (fcc), known as austenite (γ). At temperatures above 1390°C, iron reverts back to a bcc structure referred to as delta (δ)-ferrite, which is stable until melting occurs at 1536°C (Bhadeshia and Honeycombe, 2006). A summary of the allotropic forms of iron at atmospheric pressure is presented in Table 2-2.

Table 2-2 The allotropic forms of pure iron at atmospheric pressure (Chadwick, 1972)

Temperature θ (°C)	Phase	Crystal structure
1536 < θ < 1390	delta-ferrite (δ-Fe)	body centred cube
1390 < θ < 910	austenite (γ-Fe)	face centred cube
θ < 910	ferrite (α-Fe)	body centred cube

When steels undergo a phase transformation, the (predominantly iron) atoms rearrange, and new grains nucleate and grow on existing grain boundaries as well as within the grains on sites including slip bands. In addition, elements such as carbon will diffuse and either form precipitates or sit interstitially in the matrix, depending on the solubility of iron (i.e. carbon is more soluble in austenite than ferrite). It should be noted that this process is not instantaneous; time will greatly influence the size and shape of the grains as well as the ability for alloying elements to diffuse to form precipitates. There is a growing body of knowledge on the influence of chemical composition, time and temperature on the microstructure and hence material properties of steel at room and elevated temperatures. Steelmakers use such information to manipulate the microstructure of steel during the manufacturing process to ensure it meets the desired properties for a given application.

The addition of alloying elements to iron influences the temperature at which there is a phase transformation from austenite to ferrite. The best way to demonstrate this is to look at the iron-carbon (Fe-C) phase diagram shown in Figure 2-2. With reference to Figure 2-2, if there is 0.25

weight % of C in Fe, starting at 900°C (marked as 'x', where the steel is 100% austenitic), upon cooling ferrite will begin to form at approximately 830°C onwards. This transformation temperature is often referred to as A_3. As the carbon content in steel increases from 0 to 0.8 weight %, the transformation temperature A_3 decreases from 910 to the eutectoid temperature 723°C. At 723°C, when the carbon content is greater than 0.02%, all the austenite and (soluble) carbon will transform into ferrite and cementite (Fe_3C); this transformation temperature is often defined as A_1. It should be noted that the Fe-C phase diagram shows the phases that would exist under equilibrium conditions, which are representative of very slow cooling times. Under non-equilibrium conditions which are more usually encountered and associated with rapid cooling times, other microstructural constituents, such as bainite and martensite can develop. Martensite is discussed further in Section 2.3.4.3.

In addition to having great significance for the microstructural development of steel, it is worth considering how important allotropic transformation may be for structural fire design purposes. The phase transition from ferrite to austenite which can occur at about 723°C, does influence the material properties (e.g. thermal expansion, specific heat and elastic modulus) of steel. From a prescriptive approach to structural fire design, the limiting temperature of steel where failure is imminent (e.g. 550°C) is lower than the ferrite to austenite (α/γ) transformation temperature. The transition temperature (A_1) may only be critical if the limiting temperature for structural elements coincides in this region.

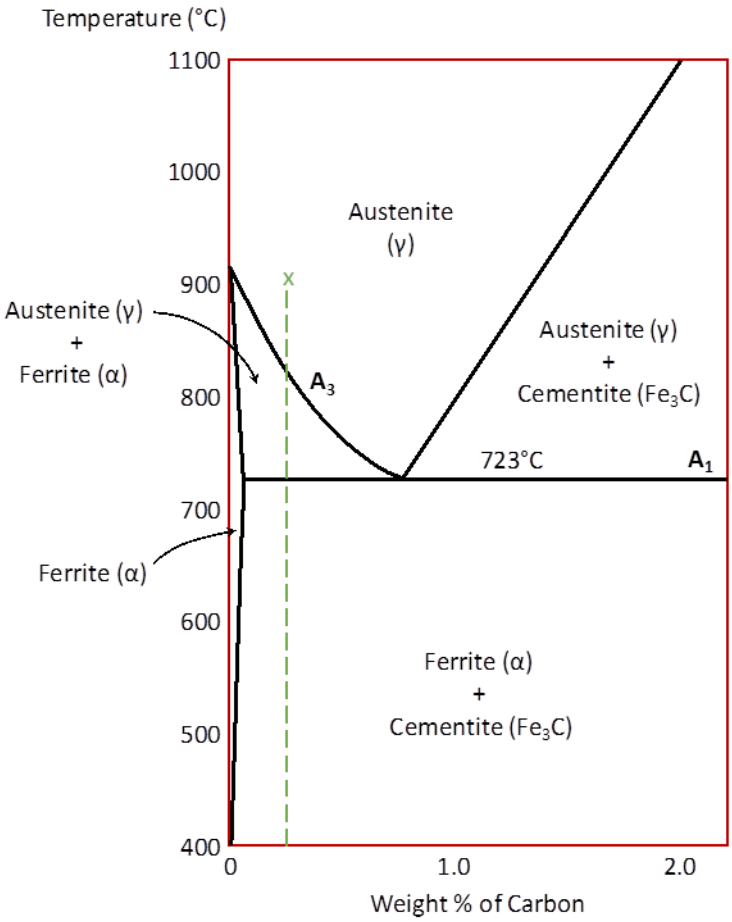

Figure 2-2 The Fe-C phase diagram adopted from Bhadeshia and Honeycombe (1995)

2.3.2 Strengthening mechanisms

2.3.2.1 General

To understand the concept of yield strength, it is important to consider the crystal lattice structure of steel, where the atoms are packed closely together in a regular repeating pattern. The crystal lattice is not perfect; it contains defects known as dislocations which, with the application of an external stress, move through the lattice structure. The cumulative movement of dislocations through the crystal lattice results in plastic deformation where the material yields (Ashby and Jones, 2005). To increase the yield strength, the mobility of dislocations must be restricted such that the dislocations require more stress to move through the crystal lattice. Dislocation movement can be slowed down by the presence of alloying elements in the form of solute atoms (e.g. niobium), or precipitates (e.g. niobium carbides), grain boundaries or other dislocations. Commercial HSS typically achieve this strengthening through a combination of strengthening mechanisms. However, it should be recognised that strength is usually achieved at the expense of ductility. With increasing temperature, dislocations gain thermal energy and can

move around more easily, resulting in a decrease in strength and increase in ductility. The most commonly employed strengthening mechanisms are briefly discussed in the following subsections with discussion on how they are affected by temperature.

2.3.2.2 Grain refinement

Grain refinement is the process of producing a microstructure with fine grains which, in turn, results in greater grain boundary area. Fine grains result in an increase in yield strength because there are more grain boundaries present to slow down the movement of dislocations, making it difficult for a dislocation to move across the boundary into the adjacent grain. The yield strength (f_y) is inversely proportional to the square root of the average grain size (d) as demonstrated in the Hall-Petch relationship in Equation (2.1) (Bhadeshia and Honeycombe, 2006).

$$f_y = f_0 + \frac{k_y}{\sqrt{d}} \tag{2.1}$$

where f_0 and k_y are constants. Grain refinement is considered the most unique strengthening mechanism because it is the only strengthening mechanism that also increases toughness. Available literature regarding the influence of grain size on the strength of steels at elevated temperature is predominately related to long term creep deformation, where a fine grain size will accelerate creep (Sha et al., 2001).

Morozov et al. (2007), reported that the contribution of grain refinement as an effective strengthening mechanism diminishes from 600 ± 50°C. This coincides with the equicohesive temperature where grain boundary sliding becomes significant, as discussed by Sha et al. (2001). To supress grain boundary sliding and hence improve the strength at temperatures above 600°C, coarser grains are preferred (Chijiwa et al., 1993). However, grain boundary sliding is normally associated with long term creep deformation and so it can be considered irrelevant in scenarios where the fire duration is short. Additionally, from temperatures greater than half the absolute melting temperature (i.e. $T > 0.5\ T_m$), the likelihood of grain coarsening increases, in order to minimise the grain boundary energy (Chadwick, 1972). Subsequently, this will limit the effectiveness of grain refinement at elevated temperatures.

2.3.2.3 Solid solution strengthening

By distorting the iron crystal lattice, the movement of dislocations is slowed down, resulting in an increase in yield strength. The atoms of the alloying elements either sit interstitially between the

iron atoms (i.e. as an interstitial solid solution) or replace them by substitution (substitutional solid solution) (Bhadeshia and Honeycombe, 2006) as shown in Figure 2-3.

Information regarding the influence of solid solution strengthening at elevated temperature is limited. It is noted that solid solution strengthening does not adversely affect the ductility and has been describes as a useful strengthening mechanism in "heat-resistant" steels at 550°C (Davis, 1997; Sha et al., 1999). In ferritic steels, a particular combination of interstitial and substitutional alloying elements including manganese-nitrogen and molybdenum-carbon has a better effect on enhancing the resistance to deformation at elevated temperature than the addition of just interstitial or substitutional solutes (Davis, 1997). Solid solution strengthening may become unstable at very high temperature (i.e. >1000°C) as the diffusion rate of solute atoms in the dislocation atmosphere is high and the atoms are dispersed in the atmosphere such that solute atoms are no longer clustered together. Both effects make it easier for dislocation mobility (Davis, 1997).

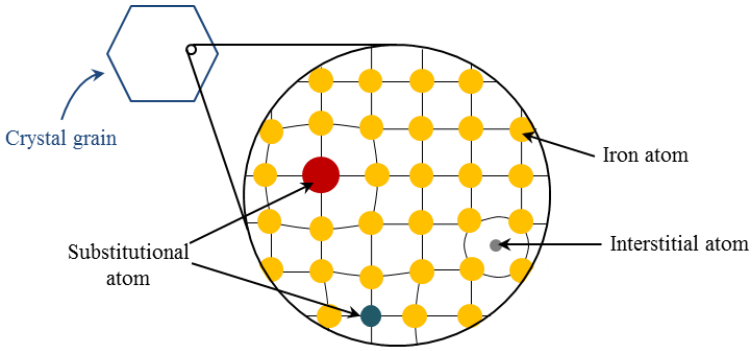

Figure 2-3 Crystal lattice distortion caused by the presence of solute atoms

2.3.2.4 Precipitation hardening

Precipitation hardening differs from solid solution strengthening in that the increase in yield strength is due to the precipitates directly obstructing the motion of dislocations as opposed to indirectly through distorting the iron crystal lattice. Generally, dislocations cut through smaller precipitates and move around larger precipitates; the latter is known as Orowan Bowing. The extent to which precipitates contribute to the strength of steel is dependent on the composition (as this relates to the thermal stability), size, and the space between them (Bhadeshia and Honeycombe, 2006). In steels, the following carbides/nitrides, listed in order of increasing thermal stability, are: chromium, molybdenum, vanadium, niobium, and titanium. These carbides/nitrides form from 500-650°C (Bhadeshia and Honeycombe, 2006). Moreover, there are instances where the precipitation effect can be delayed until the steel is reheated (such as in

a fire scenario) and this is known as secondary hardening. A fine distribution of carbonitride-promoting elements, such as vanadium and niobium, can be thermally stable at temperatures above 600°C, making the precipitation hardening by these strengthening compounds particularly useful at elevated temperatures (Sha et al., 1999). If the precipitates are not thermally stable, they will coarsen and become less effective at impeding dislocation motion.

2.3.2.5 Strain hardening

Strain hardening is when differently oriented dislocations are introduced into the crystal lattice through plastic deformation or cold-working. Since dislocations are themselves obstacles to the movement of other dislocations, increasing the dislocation density leads to an increase in strength (Bolton and Higgins, 2014). This strengthening mechanism is commonly used to obtain adequate strength in wires and rods, but at the expense of ductility.

At elevated temperatures, recovery and then recrystallisation occurs. During recovery, the amount of dislocations introduced through plastic strain is reduced, whilst during recrystallisation, new equiaxed strain free grains are formed. Both recovery and recrystallisation, result in a reduction in strength and increase in ductility (Bolton and Higgins, 2014). From temperatures greater than 700°C, recovery and recrystallisation have been attributed as one of the limiting factors of strength retention of steels at higher temperatures (Assefpour-Dezfuly et al. 1990).

2.3.3 Elastic modulus

The elastic modulus is closely related to the interatomic forces which hold atoms together. Generally, the atomic arrangement of steels consists of predominately iron atoms, thus the elastic moduli of steels are similar to that of pure iron at room temperature (Cleaves and Hiegal, 1942; Meyers and Chawla, 2009).

High alloying amounts of chromium, manganese, nickel and molybdenum can influence the elastic modulus of steel as demonstrated by Date and Andrews (1969). Noticeable deviations in the elastic modulus of ferritic steels were seen when at least 12% chromium, 4% manganese, nickel and molybdenum was added as shown in Figure 2-4. As most HSS considered for structural applications are alloyed with much less alloying amounts, it can be concluded that the elastic moduli of structural steels are unaffected by changes in the chemical composition. The elastic modulus is also considered independent of heat treatment (Bolton, 2013).

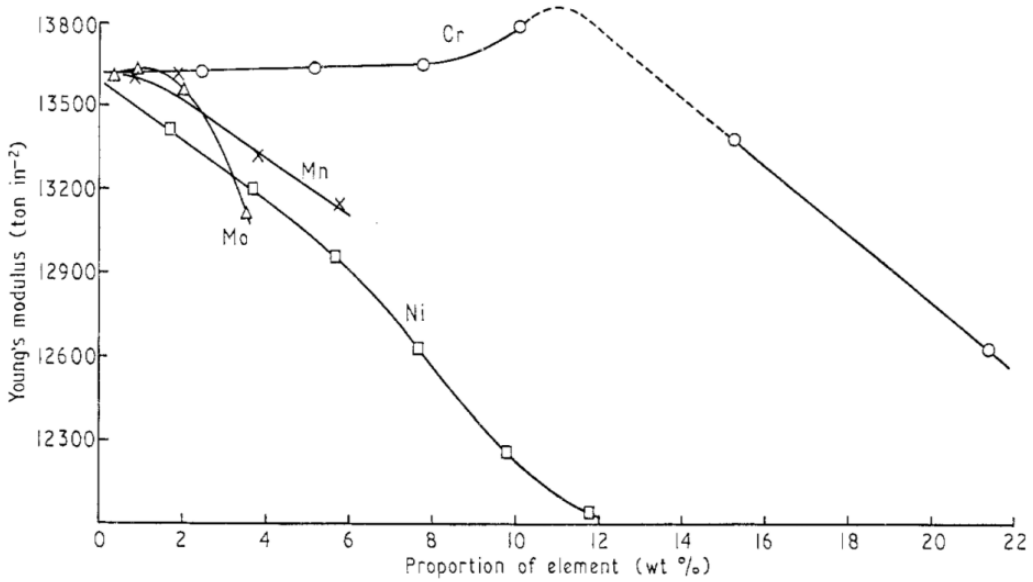

Figure 2-4 Variation of the elastic modulus with composition for ferritic steels (Date and Andrews, 1969)

On a microscopic scale the elastic modulus is highly anisotropic where the individual iron crystal (or grain) is stronger in one compared to another. Reported theoretical values of elastic modulus of iron (ferrite) orientated in (111), (110) and (100) planes are 273, 210 and 125 GPa, respectively (Davis et al., 2008). However, in many engineering applications it is acceptable to assume that the material is homogenous at a macroscopic scale, since the orientation of the iron crystals is random. In such cases the bulk elastic modulus is 210 GPa, which is also the adopted value for structural steels as specified in Eurocode 3 Part 1-1 (2005). Reported values of the elastic modulus for steels can vary between 190 and 230 GPa (Mahendran, 1996). The variation is most certainly related to the testing conditions and to some extent the texture (i.e. the preferred orientation of the grains). There are reports by Lord and Morrell (2010, 2014) which discuss the challenges of obtaining an accurate elastic modulus in greater detail.

Since the elastic modulus is dependent on the orientation of the crystal grains, variations in the elastic modulus can occur as a result of texture introduced through processes such as rolling and extruding where the grains are orientated in a preferred direction (Meyers and Chawla, 2009; Lord and Morrell, 2014; Kizu et al., 2015). Slight variations in the elastic modulus have been observed in as-rolled steel, where the elastic modulus was 207 GPa in the rolling direction and 225 GPa perpendicular to the rolling direction (Boehler, 1987). For commercial steels, the maximum value for the elastic modulus never exceeds 225 GPa (Münstermann et al., 2014). With increasing temperature, the atoms in the crystal structure gain kinetic energy and move further

apart. As the atomic distance increases the interatomic force which holds atoms together decreases and this leads to a reduction in the elastic modulus.

2.3.4 Production routes for HSS

2.3.4.1 Summary of production routes and designation

In addition to the different strengthening methods, high strength steels are produced using various heat treatments and rolling regimes to manipulate the microstructure to obtain optimum properties for a given application. HSS are traditionally hot rolled in the austenitic region which is typically above 900°C, depending on the chemical composition. Prior to rolling, a soaking stage may be implemented to ensure a homogenous temperature distribution and dissolve any coarse precipitates. Following hot-rolling, the steel is then cooled at different rates to get the desired mechanical properties.

In Europe (EN 10027-1, 2005) the steel grades for structural applications are denoted by a prefix 'S' followed by the minimum yield strength in N/mm^2 and then the production route/delivery condition, where N, Q, M and C are used for materials that are; normalised (N), quench and tempered (Q), thermo-mechanically rolled or thermo-mechanically control processed (M) and cold-formed (C), respectively. The most common processing routes used to produce high strength steel at room temperature and the elevated temperature effects of the steel are summarised hereafter.

2.3.4.2 Normalised (N) steel

Normalising steel involves reheating it to a fully austenitic state where the temperature is typically about 100°C above the upper transformation temperature (A_3), to limit grain growth. After a specified time (dependent on thickness), the steel is then air-cooled and the result is a homogenous microstructure of fine grain size with good ductility and toughness properties. This heat treatment is often used after hot rolling, where the high finishing temperature (≥ 900°C) can lead to a coarse microstructure (Bhadeshia and Honeycombe, 2006). Normalised steels are covered in EN 10025-3 (2004) for strength levels up to 460 N/mm^2, as shown in Table 2-3. Higher strengths can be achieved by increasing the alloying content of elements including carbon; however, this is at the expense of toughness and weldability. Hence, for higher strength grades, alternative heat treatments and production routes are used. It should be noted that "L" in the steel grade designation S460NL in Table 2-3, indicates that the material meets the minimum Charpy impact energy of 30J at -40°C. In Eurocode 3 Part 1-1 (2005), normalised steels are

specified up to 80 mm thickness, whilst in EN 10025-3 (2004), S460N steel grades are specified to thicknesses up to and including 200 mm.

Table 2-3 Nominal values of yield strength f_y and ultimate tensile strength f_u in N/mm² for N steel as presented in accordance with EN 10025-3 (2004)

Steel grade and qualities	Nominal thickness of the element t (mm)							
	t≤16 mm		16 mm<t≤40 mm		40 mm<t≤63 mm		63mm<t≤80 mm	
	f_y (N/mm²)	f_u (N/mm²)	f_y (N/mm²)	f_u (N/mm²)	f_y (N/mm²)	f_u (N/mm²)	f_y (N/mm²)	f_u (N/mm²)
S 460 N/NL	460	540	440	540	430	540	410	540

As normalised steels are cooled naturally in air from the austenitic region, the anticipated microstructure is ferrite and pearlite. At elevated temperatures, the cementite in pearlite may spheroidise or "ball up" which generally results in reduction in strength and increased ductility (Samuels, 1999). The rate of spheroidising is dependent on the initial microstructure, with fine pearlite spheroidising more readily compared to coarse pearlite (Samuels, 1999; Bhadeshia, 2010). In normalised steels, significant spheroidising of pearlite is anticipated to occur at temperatures exceeding 600°C following very long exposure times (in the order of thousands of hours). At 700°C, the time is reduced to the order of hundreds of hours (Samuels, 1999). Hence, the rate of spheroidising increases with increasing temperature.

2.3.4.3 Quench and tempered (Q or QT) steel

After hot rolling in the austenitic region (≥ 900°C) the steel is quenched or rapidly cooled, in water or oil to room temperature. Typically, oil is used to quench steels with carbon content of 0.25 to 0.70%, while water quenching is used for lower carbon content steel and thicker plates, which can result in greater uniformity of microstructure and hardness (Du et al., 2017). The result is usually the formation of martensite, a very strong and brittle structure where the carbon has no time to diffuse and the microstructure becomes supersaturated with carbon. Quenching is usually followed by tempering, at temperatures typically between 550-700°C. During tempering, the supersaturated carbon form fine carbide precipitates within the grains and on the grain boundaries, resulting in some restoration in ductility and toughness with a moderate sacrifice in strength (Bhadeshia and Honeycombe, 2006). QT is used to produce steels with yield strengths as high as 1100 N/mm² (Schröter, 2006). Table 2-4 presents, the nominal yield (f_y) and ultimate tensile strength (f_u) for various QT grades suitable for structural applications. (Note that in Table 2-4, the steel grade designation (e.g. S690QL1), L1 indicate that the material meets the minimum impact energy of 30J at -60°C). QT steels such as S690Q are available in thicknesses up to 150 mm making them favourable for situations where payload (weight saving) is significant (note that the

design yield strength also decreases with thickness by up to 10%). However, thicker plates require a higher carbon content to ensure that there is sufficient hardening in the core. This in turn reduces the weldability of the steel, meaning that thicker platers can be more difficult and expensive to weld (Billingham et al., 2003).

Table 2-4 Nominal values of yield strength f_y and ultimate tensile strength f_u in N/mm² for QT steel as presented in EN10025-6 (2004)

Steel grade and qualities	Nominal thickness of the element t (mm)					
	3 mm≤ t≤50 mm		50 mm<t≤100 mm		100 mm<t≤150 mm	
	f_y (N/mm²)	f_u (N/mm²)	f_y (N/mm²)	f_u (N/mm²)	f_y (N/mm²)	f_u (N/mm²)
S 460Q/QL/QL1	460	550	440	550	400	500
S 500Q/QL/QL1	500	590	480	590	440	540
S 550Q/QL/QL1	550	640	530	640	490	590
S 620Q/QL/QL1	620	700	580	700	560	650
S 690Q/QL/QL1	690	770	650	760	630	710

As discussed by Burgan (2001), there are greater uncertainties related to the behaviour of QT steels at elevated temperatures compared to N or M steels. These uncertainties stem from the material history, where there can be significant discrepancies in the chemical composition and the QT process itself. EN 10025-6 (2004) gives a maximum allowance for alloying elements, hence there are various combinations of alloying elements that manufactures can use, and whilst this may result in properties compliant with the standards at room temperature, at elevated temperature the material properties may vastly differ. In addition, QT steels can be produced off-line or on-line, where off-line processed material is sometimes referred to as reheated QT steel. In such cases, mild strength steel grades undergo a QT process to enhance strength; however, there is no change in the chemical composition, and strength is only achieved through heat treatment. It is noted that heating QT steels above their tempering temperatures may result in changes in microstructure and rapid strength degradation compared to mild strength steel. This is particularly so for reheated QT steels because at such temperatures, the strength enhancement due to heat treatment is lost and the steel properties are similar to those of mild strength steel above the tempering temperature (Chijiwa et al., 1993; Wang et al., 2012). QT steels can have better strength degradation properties at elevated temperature, provided that sufficient amounts of alloying elements including molybdenum and niobium are in the steel to retard dislocation motion via solid solution strengthening and precipitation hardening, as demonstrated by Mizutani et al., (2004). Due to the numerous combinations of chemical composition and QT processes manufacturers use, Burgan (2001) concluded that there should be no attempt to generalise the behaviour of QT steels at elevated temperatures as this can lead to misleading results.

2.3.4.4 Thermomechanical control processed (M) steel

Thermomechanical control processing (TMCP) is a production process whereby the steel is rolled in a carefully controlled manner down to relatively lower temperatures than in quench and tempered and normalised processes (i.e. ≥700°C vs. ≥900°C). The process is followed by cooling naturally in air or accelerated cooling, resulting in a fine-grained microstructure with good toughness properties "that cannot be achieved or repeated by heat treatment alone" (EN 10025-4, 2004).

Typically, during hot-rolling processes, the increase in the dislocation density is counteracted by recovery and recrystallisation (Total Materia, 2009). However, in the TMCP process, hot rolling is continued to temperatures below the recrystallisation temperature (≤900°C). As a result, the rate of recrystallisation is slow and the austenite grains remain deformed or "pancaked" shape in (Jacques and Boris, 2004; Nishioka and Ichikawa, 2012). Ferrite will also form on the triple junctions of existing austenite grains if the rolling temperature is below A_3. Upon cooling, the deformed austenite and ferrite grains become potential nucleation sites for new fine grains, as shown in Figure 2-5. The final size of the ferritic grains is heavily influenced by the size of the austenite grains prior to cooling, and the benefit of rolling at lower temperatures is to introduce more nucleation sites (which includes deformation bands within the grains) for new grains leading to grain refinement. Recrystallisation and grain growth are further suppressed using accelerated cooling and/or microalloying amounts of niobium, titanium and vanadium which remain in solid solution or form precipitates. Such precipitates pin to the grain boundaries to restrict the opportunity for grain growth and further strengthen the material through precipitation hardening. As a result, reduced levels of alloying elements such as carbon are needed to contribute to the strength, resulting in improved weldability compared to normalised and QT steel (Meester, 1997; Nishioka and Ichikawa, 2012).

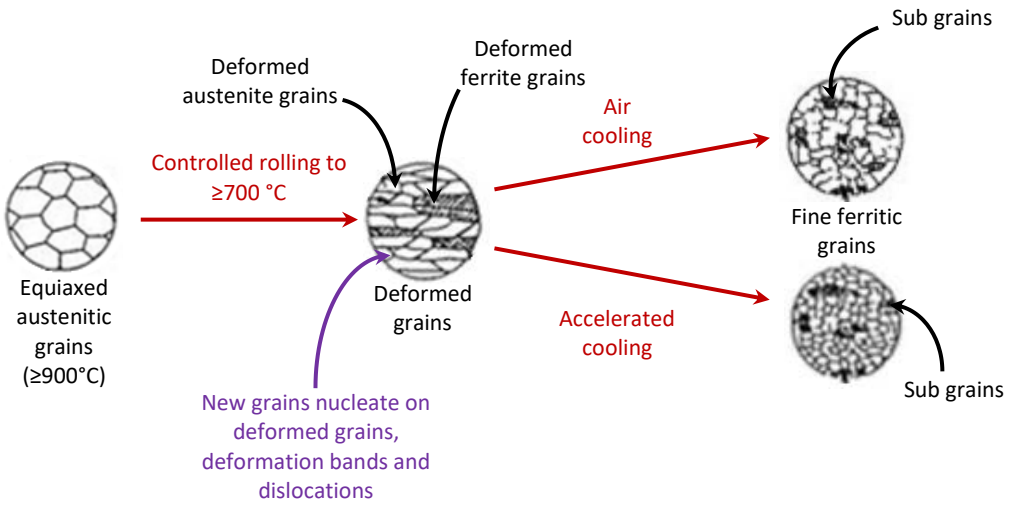

Figure 2-5 Microstructural evolution of TMCP adopted from Total Materia (2009)

TMCP steels are covered in EN 10025-4 (2004) for S460 with thicknesses up to 120 mm and EN 10149-2 (2013) with cold-forming for S500 – S700MC at much smaller thicknesses (1.5 – 16 mm). A summary of the thickness ranges and nominal yield strengths for TMCP steels is presented in Table 2-5. At higher strengths, the thickness range is limited due to the large forces required to roll the steel at relatively low temperatures.

EN 10025-4 (2004) recommends not to heat TMCP steels above 580°C to minimise any adverse effects on the mechanical properties. Elsewhere, it has also been reported that the properties of TMCP steels are retained unless heated above 650°C (SteelConstruction.info, 2017a).

Table 2-5 Nominal values of yield strength f_y and ultimate tensile strength f_u in N/mm² for M steel as presented in EN10025-4 (2004) and EN 10149-2 (2013)

Steel grade and qualities	Nominal thickness of the element t (mm)					
	1.5 mm≤ t≤8 mm		8 mm<t≤16 mm		16mm<t≤40 mm	
	f_y (N/mm²)	f_u (N/mm²)	f_y (N/mm²)	f_u (N/mm²)	f_y (N/mm²)	f_u (N/mm²)
S 460M/ML	460	540	460	540	460	540
S 460MC	460	520	460	520	-	-
S 500MC	500	550	500	550	-	-
S 550MC	550	600	550	600	-	-
S 600MC	600	650	600	650	-	-
S 650MC	650	700	630	700	-	-
S 700MC	700	750	680	750	-	-

2.3.4.5 Cold–formed (C) steel

Cold-formed or cold-worked steels are rolled or formed below their recrystallisation temperature, typically at room temperature. During cold-forming, steel undergoes plastic deformation which results in strength enhancement through strain hardening, leading to

increased strength at the expense of ductility as discussed in Section 2.3.2.5. Thus, it is expected that the strength of cold-formed steels will degrade with increasing temperature as recovery and recrystallisation takes place. The temperature required to bring about full recrystallisation for a given time (typically 1 hour), is dependent on the degree of cold work. As the amount of cold work increases, the recrystallisation temperature approaches a limiting temperature, as shown in Figure 2-6. For 0.2% carbon steels, the limiting temperature for recrystallisation, following a 1 hour soaking time is 460°C (Wyatt and Dew-Hughes, 1974).

Strength degradation properties of cold-formed structural sections are presented in Annex E of Eurocode 3 Part 1-2 (2005), and show that the strength retention of cold-formed sections is higher than class 1-3 hot rolled sections from temperatures above 200°C. In addition, studies by British Steel have shown that the strength degradation of galvanised cold formed steel in accordance with EN 10147 (1992), in the temperature range of 400 to 600°C, is higher than hot-rolled steels; the data to support this is based on a 95% confidence limit (Lawson and Newman, 1996).

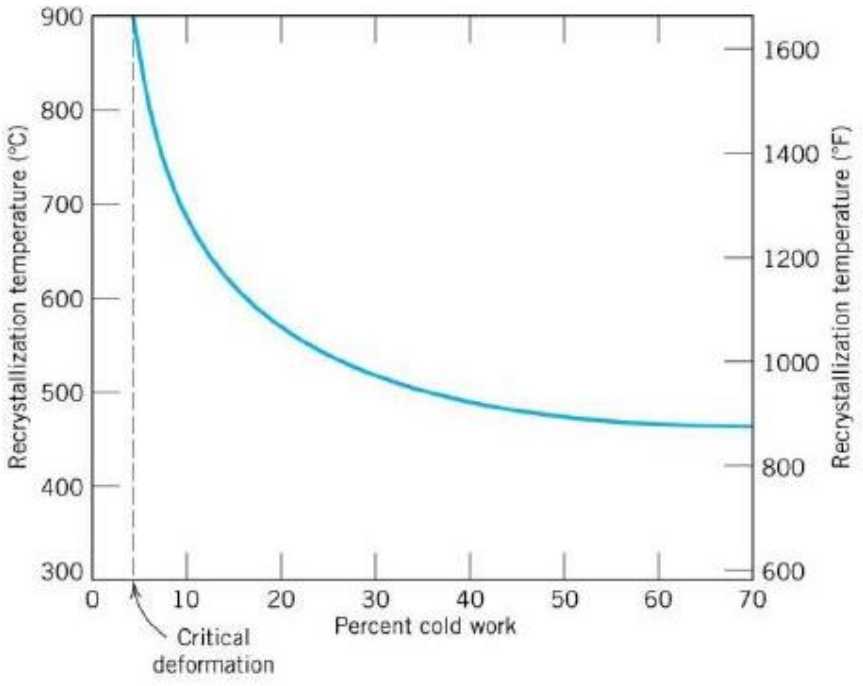

Figure 2-6 The effect of cold working on the recrystallisation temperature (Türköz, 2016)

2.3.4.6 A comparison of different steel grades

The choice of steel is dependent on factors including the application, cost and lead times. M steels have a leaner chemical composition compared to N and Q steels, which could be advantageous because of reduced raw material costs and good weldability. In particular, preheating

temperatures can be reduced or it can be omitted prior to welding for M steels, which allows for significant savings in fabrication time and cost (Schröter, 2006; Nishioka and Ichikawa, 2012).

Although M steels may require more energy to deform the steels at relatively lower temperatures compared to Q steels, no further heat treatment (i.e. tempering) steps are required. However, many mills are not designed to resist additional stresses at the relatively lower rolling temperatures used in TMCP process. The lower rolling temperatures may result in an increased rolling time and subsequent reduction in productivity, because a waiting time is usually incorporated in the rolling schedule to allow for the temperature adjustment (Jacques and Boris, 2004). This suggests that N steels have the lowest associated processing costs because there are no additional deformation or heat treatment steps required after hot-rolling in the austenitic region.

N steels are only available up to 460 N/mm^2, whilst strengths as high as 700 N/mm^2 are available in Q and M steels. The price of S700M can be up to 10% less than S690QL, which may be attributed to the reduced alloying content (Stroetmann, 2011). However, Q steels are available in much larger thicknesses compared with M steels, which make them more suitable for use in large heavily loaded structures and are beneficial in applications where impact toughness is important. The highest impact energy standardised for Q steels is 30J at -60°C (EN 10025-6, 2004), whilst for M steels it is 27J at -50°C (EN 10149-2, 2013).

In terms of the behaviour of these steels in fire, there may be some HSS grades with better strength retention properties at elevated temperatures than others, which could be beneficial for ensuring structures containing HSS members are designed to maintain their structural integrity for an anticipated fire duration. The elevated temperature performance of different types of HSS grades are discussed later in Sections 2.4.2 to 2.4.4

2.3.5 "Heat-resistant" steel

Whilst this research is concerned with the behaviour of high strength steel at elevated temperatures for structural fire design purposes, it is worth mentioning research into so-called heat-resistant steels, which are steels that have been specifically designed for elevated temperature applications. For instance, steel components can be subjected to relatively high temperatures (e.g. 550°C) in turbines used in the power industry (e.g. high pressure – low pressure rotors/disks in steam turbines), pressure vessels, condensers, heat exchangers, and boilers, for much longer periods than anticipated fire durations. In these steels, elements such as chromium, molybdenum, niobium and vanadium are added to enhance the strength and improve

creep performance at elevated temperatures (Davis, 1997). An example, highlighting the influence of molybdenum on the short term tensile strength of 0.15% carbon steel is presented in Figure 2-7, where "short term" is assumed to indicate that the influence of deformation due to creep is minimal. As shown in Figure 2-7, increasing molybdenum addition resulted in minor changes to the tensile strength at room temperature. Whilst at elevated temperatures, the short time tensile strength increased with increasing molybdenum content. For instance, at 600°C, the addition of 1% molybdenum to 0.15% carbon steel, the short term tensile strength increased by 94%, from 18 kg/mm^2 (177 N/mm^2) to 35 kg/mm^2 (343 N/mm^2).

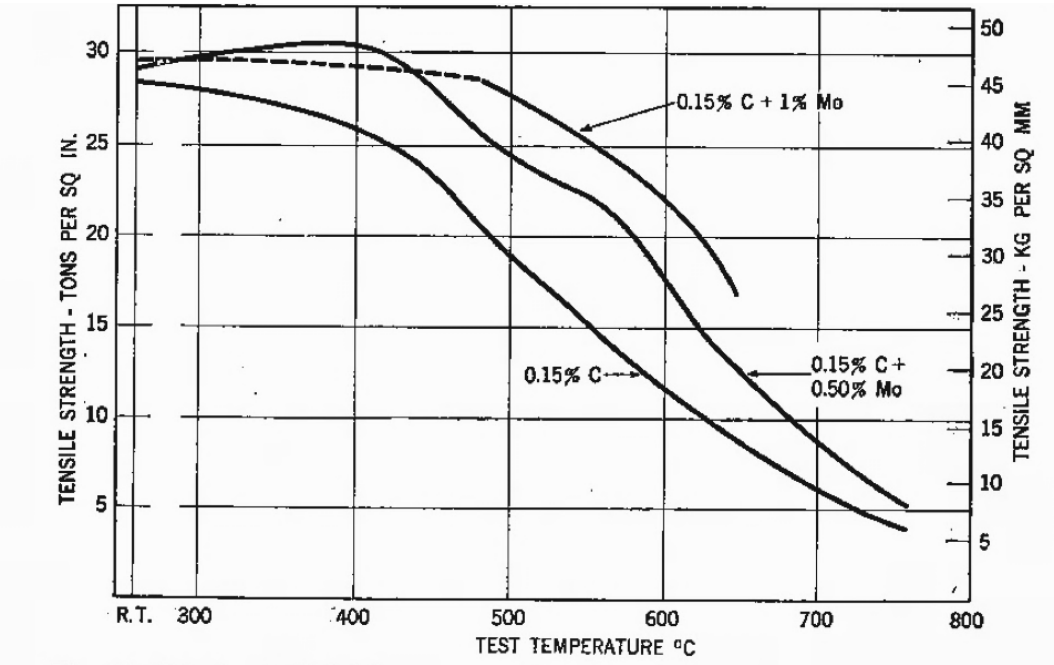

Figure 2-7 The effect of molybdenum on the short time elevated temperature tensile strength of 0.15% C steel (Archer et al., 1948)

Identical alloying elements are also used to retard the strength loss of so-called "fire resistant" (FR) steels; a concept introduced and developed in Japan, following a requirement in 1969 by the Japanese Ministry of Construction (now Ministry of Land, Infrastructure, Transport and Tourism), which dictated that the temperature of steel frames should not exceed 350°C on average, or 450°C at maximum in the event of a fire (Sakumoto, n.d.). This requirement would generally lead to considerable amounts of fire protection which can increase construction costs and impair the competiveness of steel-frame buildings in terms of increased constructions time and reduced effective use of interior space. This restriction was nullified, following a comprehensive project titled "Development of Comprehensive Fire-Resistant Design Systems for Building Fire Safety",

completed in March 1987. The updated design guidance allowed for "the maximum permissible steel temperature to be set in terms of the performance of steel at elevated temperature" (i.e. to consider the changes in strength and stiffness of steels at elevated temperature) (Chijiwa et al., 1993). This became advantageous to FR steel in Japan, which had better strength properties at elevated temperatures than conventional structural steel grades.

FR steels can be regarded as structural steels with enhanced strength performance at elevated temperatures (Sha et al., 2002). It is worth mentioning that FR steels have been developed by Nippon Steel Corporation (now, Nippon Steel and Sumitomo Metal Corporation) and utilised in multi-story carparks and buildings such as the Tobihata building in Japan (Chijiwa et al., 1993). These steels are not currently available on the general construction market and are not economically competitive with steels in Europe and the rest of the world, particularly as the current European design codes are more relaxed than the Japanese construction standards (i.e. the European standards allow for the steel to reach temperatures greater than 350°C, except in the case of class 4 sections) (Sha et al., 2002; Sha et al., 2001).

The historical developments of FR steels, including chemical composition and production routes, have been summarised by Sha et al. (2001), Garcia et al. (2013) and Maślak and Skiba (2015). Key findings suggest that FR steels should include chromium, molybdenum, vanadium and niobium. In addition, a very small addition of boron (e.g. 0.0025 mass %) with reduced carbon content is recommended to achieve good strength retention properties (i.e. retain 60% of room temperature strength) at temperatures in excess of 700°C, however, little is known about other important properties at room temperature, including ductility and fracture toughness. The role of alloying elements in steel is explained further in the next section (2.3.6).

Early research into FR steel, focused on enhancing the elevated temperature strength of the most common structural steels used at that time, namely S275 and S355. What is most intriguing about the design of FR steel is that many of the strengthening mechanisms utilised to retard the strength loss at temperatures greater than 700°C, have resulted in steels with yield strengths in excess of 460 N/mm^2 at room temperature as demonstrated by Kelly (1998) and Morozov et al., (2007). The use of HSS in structural applications may require further fire protection if sections are slender, due to higher associated section factors, which is a measure of the ratio of the heated perimeter to the area or mass to the cross-section (Buchanan and Abu, 2017). If HSS were to have better strength retention properties at elevated temperatures, then there is the potential to reduce the amount of fire protection used, which could help minimise costs.

2.3.6 Alloying elements

2.3.6.1 General

Alloying elements are used in conjunction with heat treatments and mechanical working, to alter the physical properties of steel to achieve desired properties including strength, ductility, fracture toughness, hardenability and creep resistance. The following section, presents the common chemical elements present in steels.

2.3.6.2 Carbon (C)

Carbon is one of the key alloying elements added to steel to increase the hardenability and strength of steel, but typically at the expense of other properties including ductility and weldability. For structural steels, carbon content below 0.2% is preferred to achieve a balance between strength, ductility, toughness and weldability (ArcelorMittal USA, 2015). Thicker steel sections require higher quantities of carbon to ensure that there is sufficient hardening in the core such that the microstructure and hence properties are consistent through the thickness. Carbon increases the short-time tensile, where "short time" is assumed to indicate that the influence of creep deformation is minimal. However, after prolong heating times above 540°C, any carbides present will eventually spherodise, resulting in a reduction in strength (Davis, 1997).

2.3.6.3 Manganese (Mn)

Manganese is present in all commercial steels, and is particularly beneficial in decreasing the critical cooling rate during hardening, which makes steel more stable when quenching (ArcelorMittal USA, 2015). The main role of manganese is as an active deoxidizer which helps prevent the formation of iron sulphide and inclusions that could lead to hot-shortness, or increase the susceptibility to cracking and tearing at rolling temperatures (e.g. ≥900°C) (Prabhudev, 1988). Manganese also appears to enhance the effectiveness of nitrogen in increasing the strength of plain carbon steels at elevated temperature (Davis, 1997). Moderate strengthening effects have been observed due to strain hardening interactions between manganese, nitrogen and carbon in the temperature range 250-550°C (Sha et al., 2001).

2.3.6.4 Chromium (Cr)

Chromium is present in most structural steels and is also added to increase the hardenability; its effectiveness is surpassed only by manganese, molybdenum and boron. The addition of chromium to steels markedly improves the corrosion resistance and increases strength at elevated temperature. However, as reported by Sha et al. (2001), chromium on its own does not contribute to the strength of low carbon steel grades at elevated temperatures and so it is

typically added in combination with molybdenum and vanadium, forming a family of heat-resistant chromium-molybdenum or chromium-molybdenum-vanadium steels. Chromium may form the carbide Cr_7C_3 when at least 1% is added with a carbon content of about 0.2% and the complex carbide $Cr_{23}C_6$ when other metals including molybdenum are present (Bhadeshia and Honeycombe, 2006). Such complex carbides are relatively stable at elevated temperatures provided elements such as molybdenum and vanadium are also present to slow down the rate of coarsening (ArcelorMittal USA, 2015; Bhadeshia and Honeycombe, 2006).

2.3.6.5 Silicon (Si)

Silicon is one of the principal deoxidisers used in the manufacturing of steel and is typically alloyed with manganese. Most structural steels may contain up to 0.35% silicon (Prabhudev, 1988). The addition of silicon can enhance the elevated temperature strength of steel, particularly as it may retard the coarsening of cementite (Sha et al., 2001).

2.3.6.6 Nickel (Ni)

Nickel is added to improve the hardenability and toughness of steels, the latter achieved by limiting the grain growth during heat treatment (Bolton and Higgins, 2014). Nickel does not form any carbide in ferrite and so contributes to strengthening of the ferrite phase thorough grain size control and solid solution strengthening (Steiner, 1990). Nickel can also help reduce distortion and cracking during the quenching stage of heat treatment (Global Metals, 2017).

2.3.6.7 Copper (Cu)

Copper is added to steels in amounts of 0.2 to 0.5% to primarily improve the steels resistance to atmospheric corrosion. Copper is typically added in combination with nickel to prevent copper segregating to the grain boundaries as this can have adverse effects on the surface quality and the hot-working behaviour (ArcelorMittal USA, 2015; Global Metals, 2017).

2.3.6.8 Molybdenum (Mo)

Molybdenum also has a strong effect on the hardenability of steels, though to a lesser extent than those of carbon, boron and manganese. In creep and fire resistant steels, molybdenum is considered “the most effective element in contributing high temperature strength to ferrous alloys” (Archer et al., 1948), with noticeable effects observed even when small amounts (0.1 to 0.5%) are present as depicted in Figure 2-7 (Davis, 1997). Molybdenum typically, first contributes to strength by complex solid solution strengthening (i.e. a mixture of interstitial and substitutional elements). Then, as time progresses, the precipitation of molybdenum carbides, including $M_{23}C_6$ and M_2C, which removes molybdenum from solid solution, further contributes to strength by

precipitation hardening (Bhadeshia and Honeycombe, 2006; Davis, 1997). Several studies on "fire-resistant' structural steels (Uemori et al., 1996; Wan et al., 2012a, 2012b) reveal that most of the molybdenum remains in solid solution and form clusters around niobium carbides. Thus, molybdenum has been linked to reducing the coarsening rate of niobium carbides. Anticipated fire durations may not give sufficient time for molybdenum carbides to form in fire resistant steels and so molybdenum contributes to retaining the strength at elevated temperatures by solid-solution strengthening.

2.3.6.9 Aluminium (Al)

Aluminium is primarily added to control grain size and achieve deoxidation. Aluminium is particularly effective at controlling the grain growth of austenite in reheated steels prior to quenching (Steiner, 1990).

2.3.6.10 Microalloying elements: niobium (Nb), titanium (Ti) and vanadium (V)

Microalloying elements such as niobium, titanium and vanadium are typically added in small amounts totalling up to 0.22%. These elements typically combine with carbon and nitrogen to form a fine dispersion of carbides and nitrides in the steel matrix, which contribute to strength and toughness by grain refinement and precipitation hardening. The resulting carbides formed from microalloying elements are more thermally stable than chromium and molybdenum carbides and play a key role in achieving strength and toughness in TMCP process as well as contributing to strength in QT steels following tempering. Typically, during the tempering of steels, carbides do not form until 500-600°C, because below these temperatures the alloying elements cannot sufficiently diffuse rapidly to allow carbide to nucleate and grow. Their carbides can remain very fine even after prolonged tempering, resulting in increased strength, at room and elevated temperatures (Bhadeshia and Honeycombe, 2006). This phenomenon is known as secondary hardening, and is noted to be a key contributor to ensure superior strength retention properties at temperatures up to 700°C (Assefpour-Dezful et al., 1990). In studies on "fire-resistant" steel manufactured by the Nippon Steel Corporation, a strong secondary wave of precipitates was observed at approximately 650°C (Sha et al., 1999). Small additions of vanadium can also increase the hardenability of steel (as demonstrated in the carbon equivalent calculations presented later in Section 3.4). The chemical composition of many microalloyed steels including TMCP steels are controlled to meet required material properties rather than a specific alloying amount. Thus, microalloyed steels can be less susceptible to price volatility of alloying elements. In addition, the use of microalloying elements is considered a cost-effective

method of achieving a balanced combination of required properties including strength, weldability and toughness (Baddoo, 2015).

2.3.6.11 Boron (B)

Boron significantly increases the hardenability of steel. Its effectiveness is most noticeable at lower carbon levels, diminishing with increasing carbon content. Small additions of boron, typically ranging from 0.0005 to 0.003% can help reduce the amount of other expensive elements such as nickel, chromium and molybdenum, without compromising the hardenability (Dunne, 2016). Although boron is a strong nitride former, alloyed in very small amounts, it is not classified with the microalloying elements mentioned in the previous section. A possible reason for this is that boron can only achieve its hardenability capability as solid solution. Thus, to avoid the formation boron nitrides, sufficient amounts of titanium is added to first combine with the nitrogen in the steel (Kutz, 2002). Diligence is required during subsequent welding processes as the addition of boron is likely to increase the potential for weldment cracking by promoting the formation of martensite in the heat affected zone (HAZ). Although counteractive welding process can be employed, this is likely to result in additional manufacturing costs (Dunne, 2016). The use of boron has also be seen to have a positive influence on the strength of steels at temperatures in excess of 700°C in very low (0.025-0.045%) carbon steel (Morozov et al., 2007).

2.3.6.12 Phosphorus (P) and sulphur (S)

Phosphorus and sulphur are generally considered undesirable impurities in steel. Phosphorus can decrease the ductility, toughness and impact strength, which is more evident in quench and tempered steels, whilst sulphur can have adverse effects on the ductility, weldability and surface quality (Steiner, 1990; ArcelorMittal USA, 2015). The amounts of these elements are typically limited to up to 0.04 and 0.02% for phosphorus and sulphur, respectively, in international standards.

2.3.6.13 Other considerations

Thus far, the influences of individual elements have been discussed with limited attention to how elements interact with each other, which is very complex. It must be emphasised that the effect of an alloying element is strongly dependent upon the interaction with other elements; changing the quantity of one element requires careful consideration of the level of other elements to ensure the right balance between the chemical composition and desired properties. In addition, alloying elements generally fall into two categories: (1) γ-stabilisers, which encourage the formation of austenite over a wider temperatures by expanding the austenite (γ) field and (2) α-

stabilisers, which encourage the formation of ferrite over temperature range by contracting the austenite (γ) field in the iron-carbon diagram (Bhadeshia and Honeycombe, 2006). Elements such as copper, nickel and manganese are classified as γ-stabilisers whilst, chromium, molybdenum and niobium are classified as α–stabilisers. The latter (α–stabilisers), help raise the α–γ transformation temperature, which is the temperature at which ferritic steel loses a large proportion of its strength (Muratov et al., 2007; Sha et al., 2001). This transformation temperature can be considered an upper limit on the strength of steel at elevated temperatures (Sha et al., 2001).

2.4 Structural fire design of steel

2.4.1 An overview of structural fire design

Structural fire design is one of the most fundamental requirements in the design and maintenance of infrastructure, such as buildings and tunnels. Eurocode 3 Part 1-12 (2007) assumes the current structural fire design guidelines (EN 1993-1-2, 2005), which were developed on mild steel are also applicable to HSS. This section summarises the current approach to structural fire design in relation to the prescriptive and performance based approaches presented in the Eurocodes.

As summarised by Wang et al. (2012):

> "The principal aim of fire safety precautions is to minimise the loss of life, but in many cases, fire safety provision will also have to take into account other considerations, such as minimising financial loss incurred as a result of damage, property and contents, business continuity and environment"

From the viewpoint of structural fire design, the stability or load bearing resistance (or structural performance) must be maintained for a specified period (i.e. 30, 60, 90 and 120 minutes under standard fire conditions) to ensure occupants can safely evacuate and fire services can obtain access in the event of a fire. Other aspects of fire safety, including limiting the spread of fire and smoke, are addressed through active (e.g. sprinklers) and passive (e.g. intumescent coating) fire protection and are not the focus of this research.

There are two main approaches to structural fire design: prescriptive rules or performance-based design. Prescriptive design involves protecting all exposed steelwork using fire protection material, such as intumescent coatings, to limit the maximum temperature to 550°C for steel

columns and 620°C for steel beam supporting a concrete slab (Bailey, 2006). In this temperature range, it is assumed that a heavily loaded steel element with a uniform temperature distribution will lose its design safety margin (ASFP, 2014). It is a straightforward method that focuses on isolated members and ensures that each structural element meets its required fire resistance period. However, the prescriptive approach gives no indication on how a structure may perform in a fire scenario, particularly after the fire resistance period when the fire protection may no longer be adequate. This is unsurprising, since standard fire tests were originally developed as comparative tests for insurance companies to rank different types of construction elements and not to predict the structural performance (Lamont, 2001; Bukowski, 2003). Assuming the fire protection is not damaged, if the fire is still ongoing once the fire resistance period is over, the structural elements can fail, which could be detrimental.

The prescriptive design approach relies on tabulated data and simple calculations based upon results obtained from standard fire tests. Such tests, have adopted the standard temperature-time curve specified in ISO 834-1 (1999). This is based on a typical furnace heating cycle and not representative of real fire behaviour observed in structures as factors including the cooling phase, fuel load and ventilation are not considered as shown in Figure 2-8. Nevertheless, standard temperature-time curve is the most widely used method in estimating the steel temperature exposed to fire and is used in performance based design (Wang et al., 2012). Other nominal or design fires, include parametric fire curve and hydrocarbon fire which demonstrate that higher temperatures could be reached, which could be damaging to the structural behaviour if such temperatures are not considered in the design process.

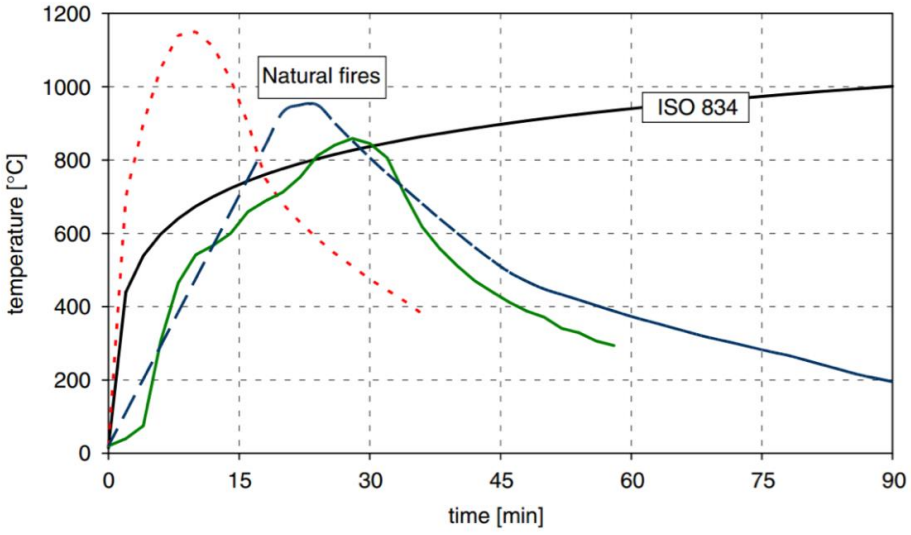

Figure 2-8 Comparison of temperature–time curves in natural fires with ISO 834 standard fire (Zehfuss and Hosser, 2007)

As a result of its simple design effort, which is understood by designers and inspection authorities, the prescriptive approach is the most common method in structural fire design (Bailey, 2006). To date, prescriptive design has generally resulted in achieving an adequate level of fire safety because it can be overly conservative and is the recommended choice when specifying fire safety strategy (Wang et al., 2012).

It is also recognised that the steel element may behave differently when part of structural system and so the safety margins may be lower than anticipated (Bailey, 2006). For this reason, the anticipated failure temperatures could be higher than the 550/620°C prescribed, suggesting that fire protection does not have to be applied to every structural element, reducing construction costs. Full scale fire tests conducted on steel-framed construction at the Building Research Establishment (BRE) facilities at Cardington, Bedfordshire revealed that the steelwork suffered damage including local buckling and distorted beams and columns as the steel was subjected to temperatures as high as 1000°C (SteelConstruction.info, 2017b). However, the structure remained structurally intact because the steelwork was able to redistribute loads from the damaged members to other parts of the structure; this is not considered in a prescriptive approach (Wang et al., 2012). Furthermore, by considering the performance of the complete structural frame rather than elements in isolation, limitations and deficiencies can be identified and improved upon resulting in a safer structure (Kirby, 1997). This is where a performance based approach is advantageous as the optimum design can be determined considering life safety, financial impact and environmental issues (Bailey, 2006).

Performance based design considers how a structure will perform in a fire scenario, taking into account the fire severity and behaviour, the thermal response where the temperature distribution through the structure is considered and the resulting structural response (Bailey, 2006). It is a complex, multidisciplinary tool that allows designers to assess the building's robustness under different fire scenarios (including the 'credible' worst case scenario). There are vast amounts of variables and uncertainty associated with fire safety engineering, and so a performance based approach is occasionally used in conjunction with a probabilistic risk approach, where the likelihood of various fire scenarios and the associated consequence is considered (Hopkin et al., 2017).

Eurocode 3 Part 1-12 (2007) gives design guidelines, which may be implemented in a prescriptive or performance based design. As mentioned earlier, the prescriptive approach is limited to member behaviour analysis, where each structural element is assessed in isolation under nominal

fire conditions (Vassart et al., 2014). In such case failure, can be defined when a critical temperature is reached. To consider part or an entire structure under fire conditions, the interaction effects between different parts of the structure and the role of compartmentation in limiting the fire spread must be considered in order to assess global stability. Advanced calculation models including finite element analysis can be used to assess the global or local structural stability. The results of the model are generally presented in terms of deformation during the whole fire duration. This could be used to assess performance in terms of the structure adhering to a specified deformation limit (Bailey, 2006; Vassart et al., 2014). Whilst the deformation limit is straightforward to define, localised behaviour such as local buckling can be more difficult to quantify as they do not necessarily result in failure (Bailey, 2006).

Figure 2-9 shows the various options available to calculate the severity of the fire, the thermal and structural response in performance based design. Relating to the fire behaviour, thermal and structural response requires knowledge on the thermal and mechanical properties at temperatures that the steel is likely to be exposed to. In the context of heat transfer, thermal properties including the specific heat and thermal conductivity determine the temperature distribution of steel elements exposed to a fire and the resulting thermal expansion. Whilst, the mechanical properties at elevated temperature, including the strength and stiffness, govern the stability of the steel elements in a fire scenario. The majority of material properties are temperature dependent, whilst few are stress and/or time-dependent (Lie, 1972). Time-dependent properties tend to only be explicitly considered for long fire durations (e.g. more than 2 hours). It should be noted that for the material properties of mild strength steel at elevated temperature, there is a comprehensive body of knowledge that exists which has been incorporated into the Eurocodes. In addition, Kodur et al. (2010) and Baconvic et al. (2005) have reviewed the thermal properties of mild strength steel in literature and compared it with the Eurocodes and American standards. With this in mind, the following sections will summarise the physical properties of HSS that are important for structural fire design purposes and assess the applicability of the material properties provided in the Eurocodes for HSS through a survey of available literature.

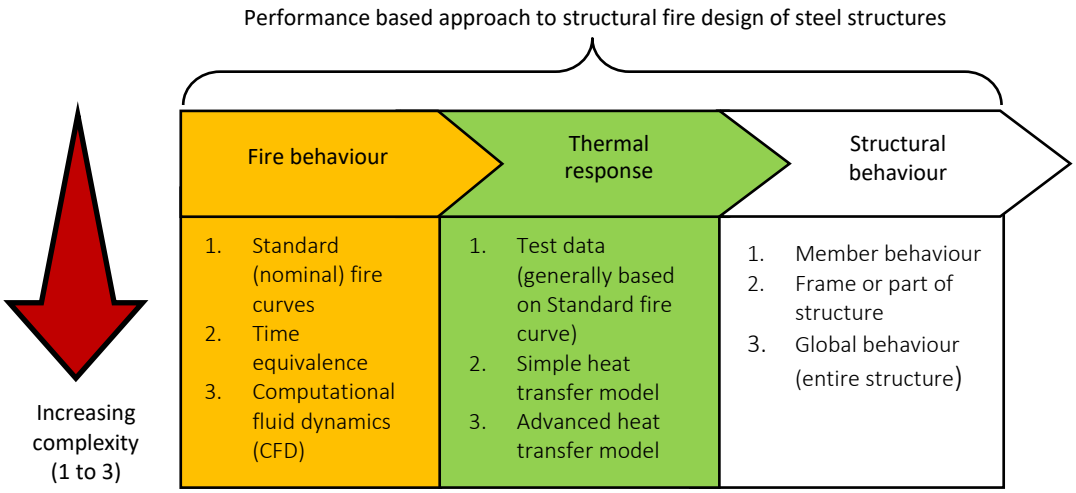

Figure 2-9 Performance based design approach to structural fire engineering adopted from Bailey (2006)

2.4.2 Thermal properties

2.4.2.1 Thermal expansion

Dependent on the changes in temperature, steel can expand or contract, which can result in large internal forces being developed in restrained structural elements or thermal bowing due to temperature gradient (Buchanan and Abu, 2017). The most common definition of thermal expansion is the linear coefficient of thermal expansion α_M, which is defined as the expansion of a unit length of a material when it is raised by 1°C (Lie, 1972) as shown in Equation (2.2).

$$\alpha_M = \frac{\varepsilon_{th}}{\Delta\theta} \tag{2.2}$$

where, ε_{th} is the thermal strain (i.e. the change of length ΔL normalised by the original length L) and $\Delta\theta$ is the change in temperature. For design purposes, Eurocode 3 Part 1-2 (2005) provides a mathematical relationship for the relative thermal elongation for conventional steel grades, illustrated in Figure 2-10 along with data in the literature for high strength steel (Choi et al., 2014; Xiong and Liew, 2016; Li and Young, 2017). Generally, it is observed that the data from the literature follows a similar trend up to about 750°C, where the steel begins to contract slightly. This is due to a phase transformation from ferrite to austenite, whereby energy is absorbed (endothermic process) and the steel adopts a denser structure (Lawson and Newman, 1996). As mentioned in Section 2.3.1, the temperature at which this phase transformation occurs is dependent on chemical composition, particularly carbon. Similarly, the degree of contraction is dependent on the heating rate, where more contraction is observed with a slower heating rate

(Cooke, 1988). Hence the Eurocode may not consider the slight contraction for design convenience.

Since there is little variation in the thermal elongations between steel grades presented in Figure 2-10, it could be concluded that the variation of the relative thermal expansion between different steel grades (i.e., yield strength, production route, alloying element) is minor. Similar remarks have been made by Lie (1972) and Anderberg (1988) based on data on mild steels.

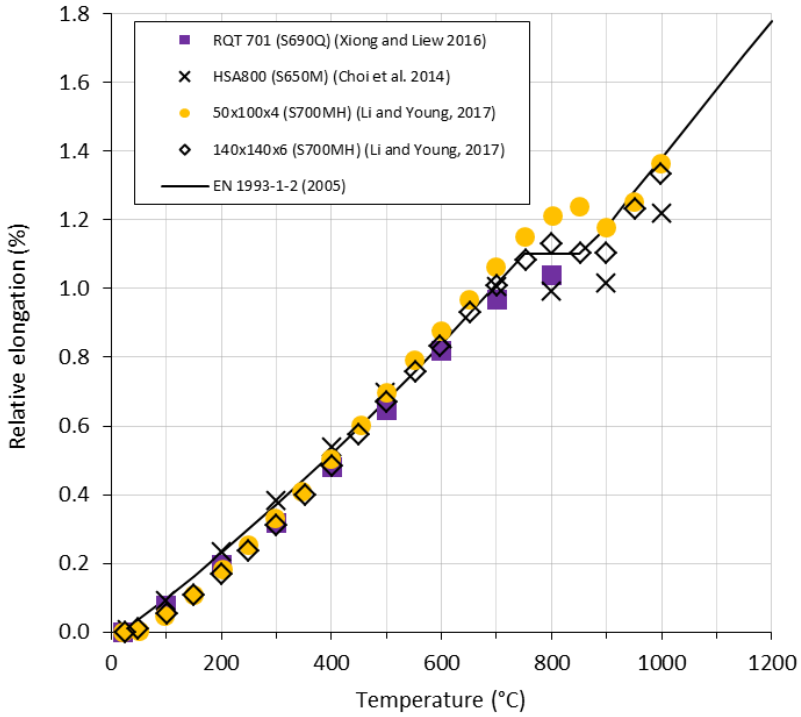

Figure 2-10 The relative thermal elongation for EN 1993-1-2 (2005) and various HSS

The linear coefficient of thermal expansion is an approximation over a temperature range, where room temperature (i.e. 20°C) is typically used as the reference temperature. This may be appropriate as structures are at similar temperatures prior to fire commencing. An alternative definition is the "true" or instantaneous thermal expansion (Bhattacher, 1997; James et al., 2001), which is the derivative of thermal strain function at the temperature of interest as described in Equation (2.3).

$$\alpha = \frac{d\varepsilon_{th}}{d\theta} = \frac{1}{L}\left(\frac{\partial L}{\partial \theta}\right) \tag{2.3}$$

For the consideration of structural behaviour under fire conditions, Banovic et al. (2005) recommended that the instantaneous coefficient should be used from room up to 700°C, prior

to the phase transformation from ferrite to austenite. However, the instantaneous coefficient of thermal expansion may be more appropriate in applications when the reference or starting temperature is much higher than room temperature, as demonstrated by Niffenger and Reichlin (2012) in nuclear applications.

2.4.2.2 Specific heat

The specific heat determines the amount of heat absorbed by a material. The relationship between specific heat and temperature as presented in the Eurocodes (EN 1993-1-2, 2005) is depicted in Figure 2-11. From Figure 2-11, the specific heat of steel gradually changes over most of the usable range. However, at the phase transformation temperature A_1 (723°C), the specific heat increases to an "infinite" value, as the energy (heat input) is no longer used to raise the temperature of the steel but rather rearrange the crystallographic structure from ferrite to austenite (Wang et al., 2012). There is limited data on the specific heat of structural steels at elevated temperature, but what is available implies that the specific heat of various steels is very close to that of iron and this property is independent of chemical composition and production route (Banovic et al., 2005; Choi et al., 2014; Kodur et al., 2010). Hence it could be concluded that the Eurocode approach depicted in Figure 2-11 is applicable for HSS.

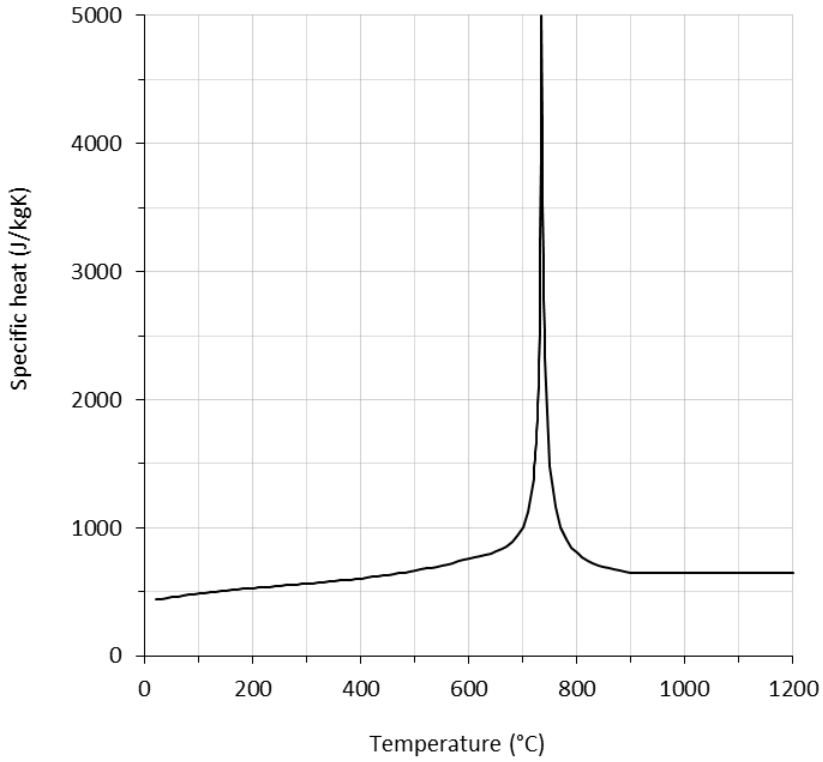

Figure 2-11 Variation of spepcific heat with temperature for mild strength steel taken from EN 1993-1-2 (2005)

2.4.2.3 Thermal conductivity

The thermal conductivity λ_c of steel is the coefficient that dictates the rate at which heat is conducted through the steel (Wang et al., 2012). Published work suggests that unlike the thermal expansion and specific heat, the chemical composition and processing route does influence the thermal conductivity and there is no generic relationship between the thermal conductivity and steel grade (Luecke et al., 2005). Between 20 and 100°C, the thermal conductivity of conventional steel grades can vary between 40 and 60 W/m°C and decreases with increasing temperature (Banovic et al., 2005; Kodur et al., 2010). There is very limited data on the thermal conductivity of HSS at elevated temperature with only data presented by Choi et al. (2014) for HSA800 alloy (S650M) available. The Eurocode approach to how the thermal conductivity varies with temperature is presented in Figure 2-12. The figure shows that the thermal conductivity of steel is 54 W/m°C and decreases with temperature until 800°C, where it remains constant at 27.3 W/m°C up to 1200°C.

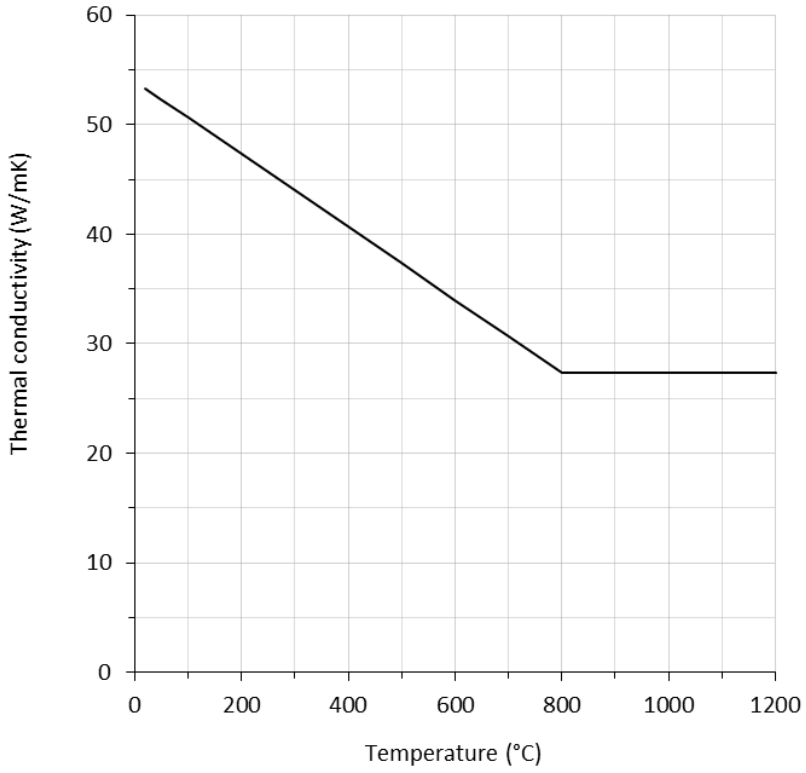

Figure 2-12 Variation of thermal conductivity with temperature for mild strength steel taken from EN 1993-1-2 (2005)

In comparison with other common building materials such as concrete and brickwork, the thermal conductivity of steel at room temperature is about 30 and 70 times higher, respectively (Wang et al., 2012). Particularly for slender members, if left unprotected, the steel temperature

can reach as high as 1100°C during a fire (Kirby, 1997) and, in this temperature range, steels regardless of the grade, the material loses more than 98% of its strength and stiffness. Hence, in many cases, steel must be insulated using fire protection methods such as intumescent coatings to limit temperature rise of steel and meet the legal/specified fire resistance time. This makes the thermal conductivity of steel less important compared to the thermal conductivity of fire protection materials, which is not readily available due to proprietary issues (Bailey, 2006). Wang et al. (2012) demonstrated the importance of using accurate temperature-dependent thermal conductivity values of fire protection materials in performance-based structural fire engineering design. A performance based approach to structural fire design may demonstrate that not all steel members need to be protected, and in such cases, accurate thermal conductivity λ_c values for various steel grades may need to be considered in the design process.

2.4.2.4 Emissivity

The Eurocode defines emissivity as the absorptivity of a surface, i.e. the ratio between the radiative heat absorbed by a given surface, and that of a black body surface (EN 1993-1-2, 2005). The emissivity of steel is only relevant if its surface is left exposed (i.e. if the steel member is non-insulated) such that the steel's surface absorbs radiated heat from a fire. Since a steel's strength is generally irrelevant to its surface finish, the Eurocode's recommended emissivity value of 0.7 could be used in heat transfer calculations for HSS (EN 1993-1-2, 2005). This value is based on the assumption of heating in a Standard fire test furnace, rather than heating conditions that are similar to an actual building fire (Wang et al., 2012). In reality, the emissivity may vary with temperature as shown by Sadiq et al. (2013). They reported an emissivity value of 0.28 at relatively low temperatures (≤320°C), which increased to 0.68 from temperatures above 520°C. The variability in emissivity is related to the surface finish, whereby a clean polished metallic surface will have a low emissivity, whereas a dull and oxidised surface will have a high emissivity (National Physical Laboratory, 2014). If the steel's surface is initially clean and polished, the surface will readily oxidise as the temperature increases. Since a high emissivity corresponds to a material heating up quickly, the Eurocode recommendation of 0.7 can be considered a conservative approach. However, it is worth noting that a very severe fire may cause the surface of the steel to heavily oxidise and reach emissivity values higher than 0.7

2.4.2.5 Density

Density is not a thermal property; however it is included in this section, as it is used in heat transfer calculations. The density of steel is 7850 kg/m^{3}and is generally independent of steel grade and temperature.

2.4.3 Mechanical properties

2.4.3.1 Material testing at elevated temperature

There are two common methods used to obtain relevant strength and stiffness properties at elevated temperatures; isothermal (steady-state) and anisothermal (transient-state) tensile tests. In an isothermal test, the temperature of the specimen is equilibrated at the target temperature before straining to failure at a controlled rate. In an anisothermal test, the specimen in held at target tensile load and then the temperature is increased at a controlled rate between 2-50°C/min until failure occurs. The total strain is recorded as a function of temperature θ and this can be converted into stress-strain curves once the effect of thermal expansion has been removed from the data using the appropriate coefficient of thermal expansion. Further details on these methods are described in Section 4.2.

2.4.3.2 Stress-strain relationship

Many advanced calculation methods such as finite element analysis require the full stress-strain response of a material to accurately depict the structural behaviour at room and elevated temperatures. Various mathematical relationships exist to capture this behaviour. Eurocode 3 Part 1-1 (2005) adopts a bilinear stress-strain response for mild steel at room temperature. In this case, the response of the steel is assumed to be linear-elastic up to the yield point (f_y) and then exhibits a yield plateau as illustrated in Figure 2-13.

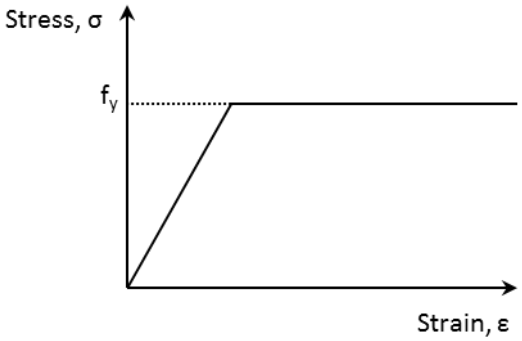

Figure 2-13 Bi-linear stress-strain relationship

At elevated temperature, it is noted that the stress-strain relationship becomes increasingly nonlinear, that is, the linear elastic region reduces and becomes difficult to distinguish from the nonlinear plastic region. Similar to the Eurocode approach for room temperature design, multi-linear functions can be used to approximate the stress-strain behaviour; these can be bilinear (Jeanes, 1985; Contro et al., 1988; Wang et al., 2013b) as presented in Figure 2-13, tri-linear (Corradi et al., 1990) or quad-linear (Ianizzi and Schleich, 1991). Although this method simplifies

the stress-strain behaviour, it is acceptable to use when deformation does not play a significant role and only the load-carrying capacity is critical for design. To get an accurate representation of the stress-strain behaviour, a large number of data lines are required (Poh, 2001).

Eurocode 3 Part 1-2 (2005) adopts Rubert and Schaumann's (1986) model derived from anisothermal tests on beams. This is a four-stage material model presented in Table 2-6 and shown in Figure 2-14. With reference to Figure 2-14, the first stage is a linear elastic region defined by a temperature dependent gradient (elastic modulus, $E_{a,\theta}$) up to the proportional limit ($f_{p,\theta}$), which is defined as the point where the curve changes from elastic to plastic. The second stage begins at the proportional limit ($f_{p,\theta}$) and is graphically represented as an elliptical curve up until the maximum strength ($f_{y,\theta}$) is achieved at a strain of $\varepsilon_{y,\theta}$ (2%). In the third stage, a constant strength is assumed between $\varepsilon_{y,\theta}$ and $\varepsilon_{t,\theta}$ (which is defined in the Eurocode as 15%) and at the fourth stage the stress drops to zero at the ultimate strain $\varepsilon_{u,\theta}$ (20% in the Eurocode).

Table 2-6 The material model for the stress-strain relationship for carbon steel at elevated temperatures taken from Eurocode 3 Part 1-2 (2005)

	Stress, σ	**Strain range, ε**
Stage 1: Elastic region (linear)	$\sigma = \varepsilon E_{a,\theta}$	for $\varepsilon \le \varepsilon_{p,\theta}$
Stage 2: Transitional region (elliptical)	$\sigma = f_{p,\theta} - c + \frac{b}{a}\left[a^2 - \left(\varepsilon_{y,\theta} - \varepsilon\right)^2\right]^{0.5}$	for $\varepsilon_{p,\theta} < \varepsilon < \varepsilon_{y,\theta}$
	with	
	$a^2 = \left(\varepsilon_{y,\theta} - \varepsilon_{p,\theta}\right)\left(\varepsilon_{y,\theta} - \varepsilon_{p,\theta} + \frac{c}{E_{a,\theta}}\right)$	
	$b^2 = c\left(\varepsilon_{u,\theta} - \varepsilon_{t,\theta}\right)E_{a,\theta} + c^2$	
	$c = \frac{\left(f_{y,\theta} - f_{p,\theta}\right)^2}{\left(\varepsilon_{y,\theta} - \varepsilon_{p,\theta}\right)E_{a,\theta} - 2\left(f_{y,\theta} - f_{p,\theta}\right)}$	
Stage 3: Plastic (constant)	$\sigma = f_{y,\theta}$	for $\varepsilon_{y,\theta} < \varepsilon < \varepsilon_{t,\theta}$
Stage 4: Ultimate failure	$\sigma = f_{p,\theta} f_{y,\theta}\left[\frac{1 - \left(\varepsilon - \varepsilon_{t,\theta}\right)}{\varepsilon_{u,\theta} - \varepsilon_{t,\theta}}\right]$	for $\varepsilon_{t,\theta} < \varepsilon < \varepsilon_{u,\theta}$
	$\sigma = 0$	for $\varepsilon = \varepsilon_{u,\theta}$
Parameters	$\varepsilon_{p,\theta} = \frac{f_{p,\theta}}{E_{a,\theta}}$ $\varepsilon_{y,\theta} = 0.02$ $\varepsilon_{t,\theta} = 0.15$ $\varepsilon_{u,\theta} = 0.20$	

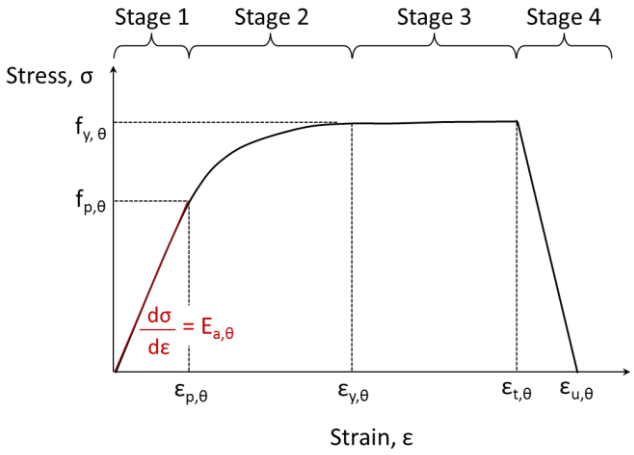

Key:

$f_{y,\theta}$	effective yield strength;
$f_{p,\theta}$	proportional limit;
$E_{a,\theta}$	slope of the linear elastic range;
$\varepsilon_{p,\theta}$	strain at the proportional limit;
$\varepsilon_{y,\theta}$	yield strain;
$\varepsilon_{t,\theta}$	limiting strain for yield strength;
$\varepsilon_{u,\theta}$	ultimate strain.

Figure 2-14 Stress-strain model for steel at elevated temperature as shown in Eurocode 3 Part 1-2 (2005)

An alternative stress-strain relationship, which incorporates strain hardening for temperatures below 400°C, is provided in Annex A of Eurocode 3 Part 1-2 (2005) and presented in Table 2-1 and shown in Figure 2-7. Provided that local or overall buckling does not lead to premature collapse, below 400°C, the stress-strain curve follows the same first two stages up to the yield strength $f_{y,\theta}$ at $\varepsilon_{y,\theta}$ (2%). Then strain hardening is assumed to be linear from the yield point ($f_{y,\theta}$) up to the tensile strength ($f_{u,\theta}$) at a strain of $\varepsilon_{s,\theta}$ (4%). Then similar to the final two stages of the previous model, the strength is assumed constant until the limiting strain $\varepsilon_{t,\theta}$ (15%), for yield strength is reached, then the stress drops to zero at the ultimate strain $\varepsilon_{u,\theta}$ (20%). In addition, the tensile strength ($f_{u,\theta}$) is assumed to be 1.25 times the yield point ($f_{y,\theta}$) below 300°C. For temperatures between 300 and 400°C the Eurocode assumes the following (Equation (2.4)):

$$f_{u,\theta} = f_{y,\theta}(2 - 0.0025\theta_a) \quad (2.4)$$

A disadvantage of the Eurocode model is that the rate of change of gradient (i.e. the curvature) from the proportional limit ($f_{p,\theta}$) and yield ($f_{y,\theta}$) points are not continuous (Wang et al., 2012). The elliptical curve used to characterise the stress-strain response at elevated temperature has been shown to overestimate the stress-strain response of some HSS including S460N, S460M (Schneider and Lange, 2009), HSA800 (S650M) (Choi et al., 2014) and RQT 701 (Xiong and Liew, 2016). It is also noted that the strain hardening response shown in Figure 2-15 is not necessarily linear and thus can result in an underestimation of the stress-strain response at elevated temperatures. Neuenschwander et al., (2017) further commented on the unsuitability of the Eurocode approach because of HSS limited strain hardening capacity, which is significantly

smaller compared with mild steel. In addition, the ultimate strain for HSS has been observed to be less than 20% at temperatures less than 500°C. Consequentially, these limiting factors may result in the overestimation of the buckling capacity of steel element in a fire scenario.

An alternative model has been proposed by Poh (2001) and is a parametric function which considers features such as the upper yield point, plastic plateau and strain hardening as shown in Figure 2-16. Deriving the parameters in this model to account for these features can be an extensive exercise; however, most of these features disappear at temperatures above 400°C.

Table 2-7 The material model for the stress-strain relationship for carbon steel including strain hardening at temperatures below 400°C taken from Eurocode 3 Part 1-2 (2005)

	Stress, σ	**Strain range, ε**
Stage 1: Elastic region (linear)	Same as Table 2-6	for $\varepsilon \leq \varepsilon_{p,\theta}$
Stage 2: Transitional region (elliptical)	Same as Table 2-6	for $\varepsilon_{p,\theta} < \varepsilon < \varepsilon_{y,\theta}$
Stage 3: Strain hardening (linear)	$\sigma_a = 50\ (f_{u,\theta} - f_{y,\theta})\varepsilon + 2f_{y,\theta} - f_{u,\theta}$	for $\varepsilon_{y,\theta} < \varepsilon < \varepsilon_{s,\theta}$
Stage 4: Ultimate load (constant)	$\sigma_a = f_{u,\theta}$	for $\varepsilon_{s,\theta} < \varepsilon < \varepsilon_{t,\theta}$
Stage 5: Ultimate failure	$\sigma_a = f_{u,\theta}[1 - 20(\varepsilon - \varepsilon_{t,\theta})]$	for $\varepsilon_{t,\theta} < \varepsilon < \varepsilon_{u,\theta}$
	$\sigma_a = 0$	for $\varepsilon \geq \varepsilon_{u,\theta}$
Parameters	$\varepsilon_{p,\theta} = \frac{f_{p,\theta}}{E_{a,\theta}}$ $\varepsilon_{y,\theta} = 0.02$ $\varepsilon_{s,\theta} = 0.04$ $\varepsilon_{t,\theta} = 0.15$ $\varepsilon_{u,\theta} = 0.20$	

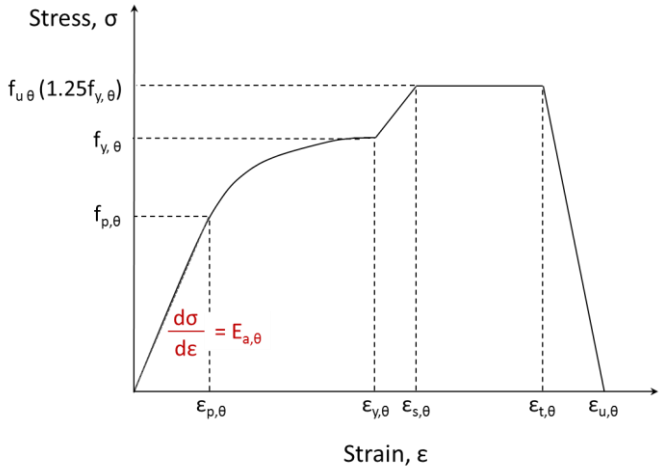

Key:

$f_{y,\theta}$	effective yield strength;
$f_{p,\theta}$	proportional limit;
$E_{a,\theta}$	slope of the linear elastic range;
$\varepsilon_{p,\theta}$	strain at the proportional limit;
$\varepsilon_{y,\theta}$	yield strain;
$\varepsilon_{s,\theta}$	strain at the tensile strength;
$\varepsilon_{t,\theta}$	limiting strain for yield strength;
$\varepsilon_{u,\theta}$	ultimate strain

Figure 2-15 Alternative stress-strain model for steel at temperatures below 400°C, allowing for strain hardening as shown in Appendix A of Eurocode 3 Part 1-2 (2005)

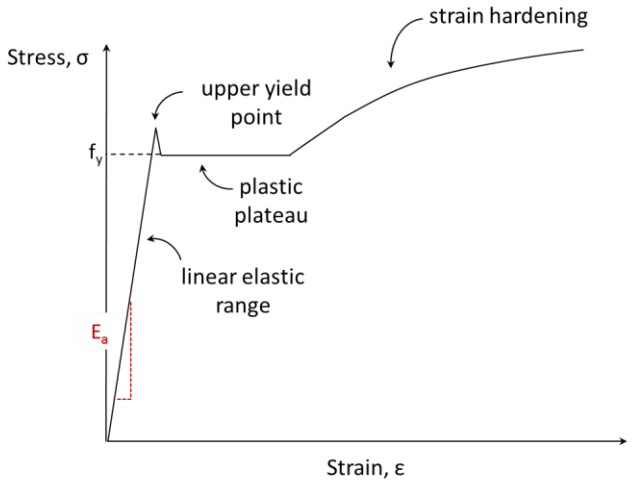

Figure 2-16 Stress-strain response for steel adopted by Poh (2001)

A popular choice amongst researchers is the modified Ramberg-Osgood model, which has been used to characterise the stress stress-strain response of conventional steel grades (Saab and Nethercot, 1991; Outinen, 1996; Knobloch et al., 2013), as well as various HSS (Chen and Young, 2008; Choi et al., 2014; Ma et al., 2015) at elevated temperatures. The original Ramberg-Osgood model was first proposed to characterise the stress-strain behaviour of materials such as aluminium, stainless steels, and certain carbon steels (e.g. chromium nickel steels) which do not follow a bilinear stress-strain response (Ramberg and Osgood, 1943). This "simple" equation presented in Equation (2.5), describes the stress-strain behaviour with 3 parameters: the elastic modulus E and two constants K and n, derived from experiments. The total strain is the summation of the elastic and plastic strains, and the curvature of the stress-strain curve is defined through the exponential n, termed the strain hardening parameter. The lower the strain hardening parameter, the more gradual the transition from elastic (linear) to the plastic (nonlinear) part of the stress-strain curve.

$$\varepsilon = \left(\frac{\sigma}{E}\right) + K\left(\frac{\sigma}{E}\right)^{n} \tag{2.5}$$

One year later, Hill (1944) modified the Ramberg-Osgood model by substituting the constant K and elastic modulus E with the plastic strain 0.002 and the 0.2% proof strength $f_{0.2p}$, respectively as shown in Equation (2.6). The strain hardening parameter n is often determined from two fixed points on the stress-strain curve. To determine the strain hardening parameter in Equation (2.6), the first point is taken close to the origin of the stress-strain curve (e.g. the 0.01% proof strength

and corresponding strain), whilst the second point is the 0.2% proof strength $f_{0.2p}$ and corresponding strain (0.002).

$$\varepsilon = \left(\frac{\sigma}{E_0}\right) + 0.002\left(\frac{\sigma}{f_{0.2p}}\right)^n \quad (2.6)$$

In comparison with measured stress-strain data for various steels at elevated temperatures the modified Ramberg-Osgood model (Equation (2.6)) showed difficulty describing the sharp curve transition from the elastic to plastic part of the stress-strain curve. As a result, the model tends to over predict the stress and cannot closely trace the stress-strain behaviour at higher strains (Wang et al., 2012; Knobloch et al., 2013; Choi et al., 2014). To address some the limitations of the modified Ramberg-Osgood further parameters may be needed.

Compound Ramberg-Osgood models have been proposed by Mirambell and Real (2000), Rasmussen (2003) and Gardner and Nethercot (2004), where different portions of the stress-strain curve are modelled using separate Ramberg-Osgood models. Both Mirambell and Real's (2000) and Rasmussen (2003) proposal was limited to tensile applications since the tensile strength at corresponding strain is used. Gardner and Nethercot's model uses the 1.0% proof strength ($f_{1.0p}$) and corresponding strain ($\varepsilon_{1.0p}$) instead of the tensile strength to make the model applicable in both tension and compression applications and achieve greater accuracy at strains of general interest in structural applications (i.e. up to 10%) (Gardner and Ashraf, 2006). In the model proposed by Gardner and Nethercot (Gardner and Nethercot, 2004), Equation (2.6) is used to characterise the stress-strain curve up to and including the 0.2% proof strength ($f_{0.2p}$). For stresses greater than 0.2% proof strength Equation (2.7) is used:

for $\sigma > f_{0.2p}$

$$\varepsilon = \left(\frac{\sigma - f_{0.2p}}{E_{0.2}}\right) + \left(\varepsilon_{p,1.0-} \varepsilon_{p,0.2} - \frac{f_{1.0p} - f_{0.2p}}{E_{0.2}}\right) \times \left(\frac{\sigma - f_{0.2p}}{f_{1.0p} - f_{0.2p}}\right)^m + \varepsilon_{p,0.2} \quad (2.7)$$

where $f_{0.2p}$ and $\varepsilon_{0.2p}$ are the 0.2% proof strength and corresponding strain, respectively, $E_{0.2}$ is the slope at 0.2% proof strength $f_{0.2p}$ and m is the strain hardening parameter determined from the points ($f_{0.2p}$, $\varepsilon_{0.2p}$) and ($f_{1.0p}$, $\varepsilon_{1.0p}$). The model proposed by Gardner and Nethercot (Gardner and Nethercot, 2004) is used in Chapter 6 to closely describe the stress-strain response of various HSS grades.

2.4.3.3 Yield strength

Since the stress-strain response becomes increasingly nonlinear as the temperature rises, it becomes difficult to distinguish the strength at which the response changes from elastic (linear) to plastic (nonlinear); this is often defined as the proportional limit. Instead, various yield strengths at elevated temperature are defined which correspond to strains at which the anticipated failure is imminent.

Prior to the Eurocode 3 Part 1-2 (2005), the British standard, BS 5950 Part 8 (2003) dealt with fire resistant design, and included strength retention factors derived from lines drawn perpendicular to the strain axis at the following strain limits: 0.5, 1.5 and 2.0%. In this case the strain limits were related to the limiting deflections observed in standard fire tests; these were in excess of 1% and 3% for columns and beams, respectively (Kirby and Preston, 1988). BS 5950 Part 8 (2003) specified that a strain limit of 0.5% should be used for columns, a strain limit of 1.5% for beams whose protection materials remain intact in a fire and a strain limit of 2.0% for composite beams.

However, since the difference between using the strength at 1% and 2% on the overall fire resistance time is marginal, the strength at 2% is specified in the analysis for all structural members including beams and columns (Twilt, 2001) .Eurocode 3 Part 1-2 (2005) adopts the term "effective" yield strength in many structural fire design calculations, and is defined as the strength at 2.0% total strain. When there is a greater chance of instability (i.e. class 4 sections), the Eurocode specifies that the 0.2% proof strength should be used.

In Eurocode 3 Part 1-2 (2005), the strength degradation of steel with rising temperature is presented as reduction factors, where the property at elevated temperature is normalised with respect to the equivalent property at room temperature. Figure 2-17 presents the reduction factors for the effective yield strength ($k_{y,\theta} = f_{y,\theta}/f_y$), 0.2% proof strength ($k_{0.2p,\theta} = f_{0.2p,\theta}/f_{0.2p}$) and proportional limit ($k_{p,\theta} = f_{p,\theta}/f_y$). The proportional limit degrades more rapidly, followed by the 0.2% proof strength and effective yield strength. It should also be recognised that the Eurocodes assume that the material properties of steel at elevated temperature can be linearly interpolated between values given every 100°C (EN 1993-1-2, 2005). The reduction factors in the Eurocodes are derived from the lower bound data obtained from anisothermal tensile tests conducted by British Steel (Kirby and Preston, 1988; Lennon et al., 2006). Extensive tests were conducted on mild steel 43A and 50B, which in accordance with BS 4360 (1979), is equivalent to S255 and S355, respectively (it is worth noting that in 1986, an updated version of BS4360 stated that 43A is S275). Currently, Eurocode 3 Part 1-12 (2007) assumes that the reduction factors for mild steel,

presented in Figure 2-17, are applicable to HSS. The next section will compare the reduction factors for the effective yield strength in the Eurocode (EN 1993-1-2, 2005) with available HSS data from the literature, to assess the suitability of the current Eurocode approach for HSS.

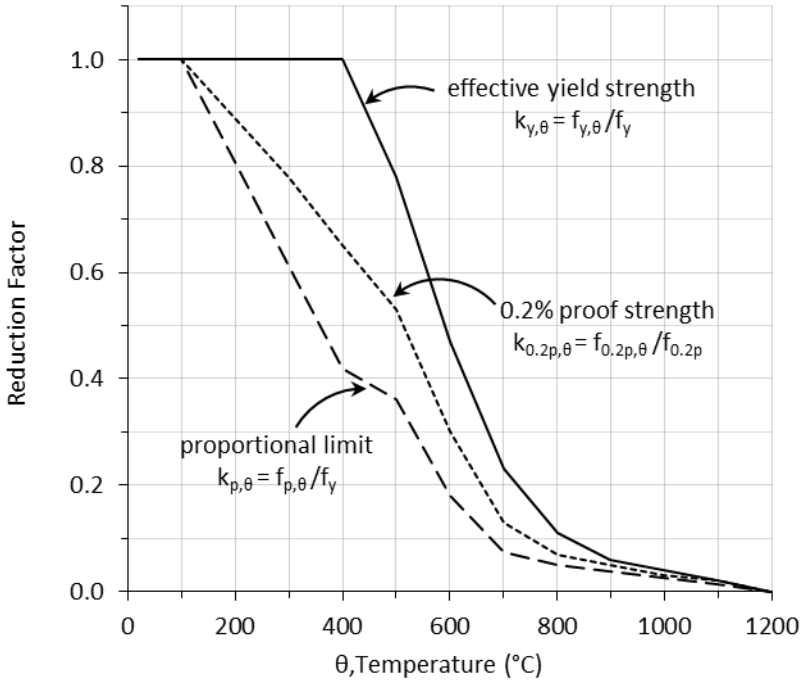

Figure 2-17 Strength reduction factors for mild strength steel at elevated temperatures θ as presented in Eurocode 3 Part 1-2 (2005)

2.4.3.4 The effective yield strength of lower HSS grades (S460)

This section is concerned with HSS grades with a nominal yield strength of 460 N/mm^2. Wohlfeil and Lange (2007) conducted anisothermal tests on hot rolled S460N and S460M plates and observed that S460M had better strength retention properties than S460N. They considered this to be due to the presence of a variety of precipitates in S460M, including niobium precipitates which helped delay recrystallisation during heating. Schneider and Lange (2009) conducted further experiments on seven commercial S460 steels (four S460M and three S460N) with different alloying compositions and heat treatments. Their results also revealed that S460M have better strength retention properties than S460N and highlights that HSS with improved high temperature performance is possible by selecting suitable alloying elements and production parameters.

Whilst Wohlfeil and Lange (2007) found the Eurocode to be conservative (i.e. safe) with respect to the reduction factors for the S460M they tested and unconservative (i.e. unsafe) for S460N

they tested, Schneider and Lange (2009) findings revealed that the Eurocode is unconservative (i.e. unsafe) for the all the S460M and S460N grades they tested. Similarly conclusions were reached by Outinen (2006), Qiang et al. (2012, 2013) and Wang et al. (2013a) who have also conducted either isothermal or anisothermal tensile tests on S460 grades or equivalent. Microstructural characterisation to deduce possible reasons for the disparity was not included in these studies.

2.4.3.5 The effective yield strength of higher HSS grades (S600-S700)

There have been several reported tests on the strength degradation of HSS with nominal yield strengths between 650 and 700 N/mm^2. A summary of the test parameters and chemical composition of these steels extracted from the published literature are presented in Table 2-8 and Table 2-9, respectively. The corresponding reduction factors are presented in Figure 2-18 which demonstrates that the reduction factors in the Eurocodes are unconservative and overestimate the strength retention properties of these HSS.

Despite this, the Rules on high strength steel (RUOSTE) report commissioned by the EU Research Fund for Coal and Steel (European Commission, 2016), concluded that the strength reduction factors in the Eurocode are adequate for the S700QL and S960QC material. This conclusion seems valid if reduction factors are derived using the nominal (design) strength. In the literature, reduction factors are typically derived by normalising the material property at elevated temperature by the average measured yield strength at room temperature, which can be 10-20% higher than the nominal strength (European Commission, 2016). Clearly, normalising the material properties by the nominal or actual yield strength will have significant discrepancies on the resulting reduction factors. However, normalising by the nominal yield strength is a "safety factor" which ensures the material meets the minimum guaranteed value specified in the Eurocodes. This is described in Equation (2.8), taken from Eurocode 3 Part 1-2 (2005):

$$X_{d,fi} = \frac{k_\theta X_k}{\gamma_{M,fi}} \tag{2.8}$$

where $X_{d,fi}$ and X_k are the design values of the mechanical properties at elevated and room temperature, respectively, k_θ is the accompanying reduction factor, and $\gamma_{M,fi}$ is the partial factor for the relevant material property for fire conditions, which takes into account variability of material strength (Lawson and Newman, 1996; Holicky et al., 2005). For fire design of steel structures the recommended partial factor is 1.0. Hence, the reduction factor k_θ, becomes the

mechanical property at elevated temperature normalised by the design strength ($X_{d,fi}$/ X_k) (Lawson and Newman, 1996). Normalising by the measured property rather than the nominal will give a better indication of how the material history (i.e. the alloying elements, production and fabrication route) will influence properties including strength at elevated temperature.

Comparisons between the reduction factors for HSS in the literature reveal that there is a considerable disparity and this includes HSS with the same steel grade (e.g. S690QL) shown in Figure 2-18. There are two plausible reasons for this. Firstly, the disparity could be due to the different testing conditions, equipment, or data collection techniques employed as shown in Table 2-8 (Lie, 1972; Loveday et al., 2004; Qiang, 2013). Secondly, the differences in the material's history will influence the microstructure and hence properties at elevated temperature as suggested by the variation in chemical composition of similar HSS grades (S650 to S700) presented in Table 2-9. The first reason highlights the challenge of obtaining "accurate" or "credible" elevated temperature properties that are representative of the anticipated fires for predicting response of HSS structures under fire conditions as mentioned by Qiang (2013). The second reason highlights that generalising the reduction factors for different HSS grades at elevated temperature may result in compromising the safety of structures under extreme loading conditions such as fire. Hence, tests on various HSS have been conducted by many researchers to contribute towards a larger pool of experimental data to be used in the performance based approach to structural fire design. Gaps still exist in the database, including the reduction factors for S700MC specified in Eurocode 3 Part 1-12 (2007), of which there is currently no data in the published literature. For this reason, an experimental investigation to obtain the reduction factors for S700MC was conducted and the work is presented in Chapter 4.

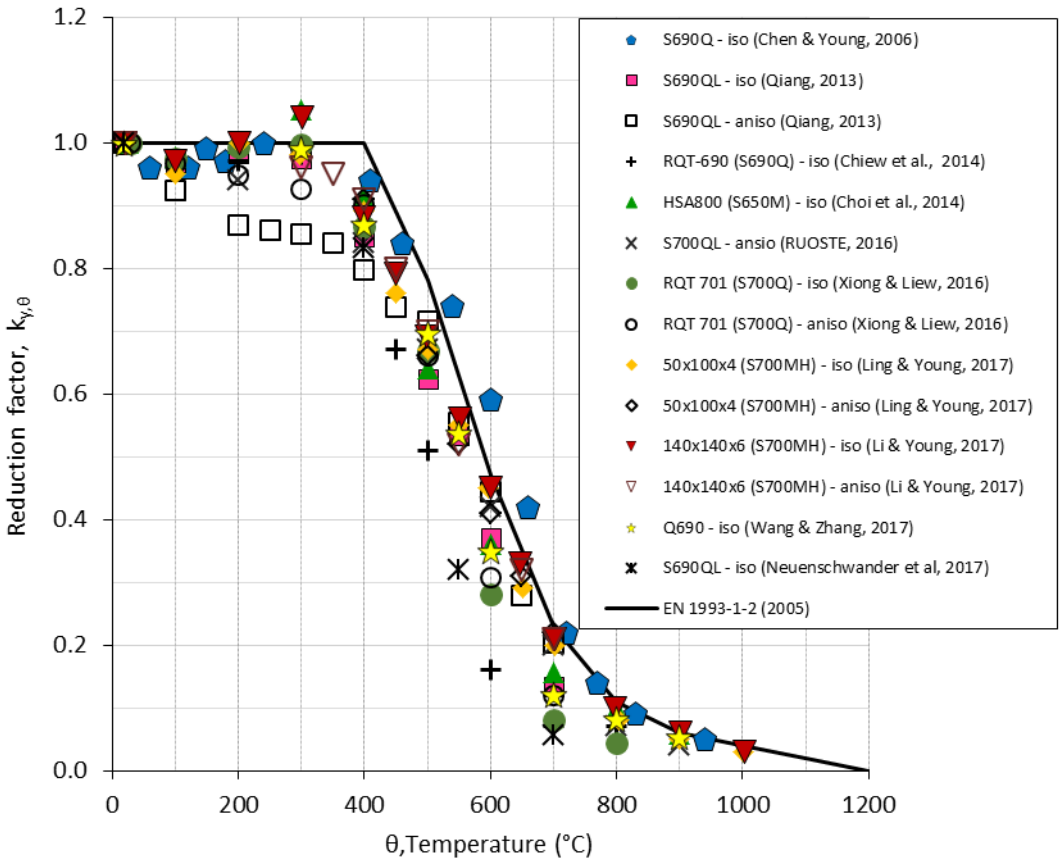

Figure 2-18 Comparrison of reduction factors for effective yield strength at 2% total strain ($k_{y,\theta} = f_{y,\theta} / f_y$) for steel grades between S650 and S700

2.4.3.6 Elastic modulus

The elastic modulus E_a is used to determine the stiffness of a structural element, which is of importance when designing with HSS as stability issues could arise. It is defined as the ratio of the stress and strain at stresses applied below the yield point which corresponds with the initial slope of the linear elastic region of the stress-strain curve.

The Eurocode (EN 1993-1-2, 2005) approach to the decline of stiffness of mild steel at elevated temperature is presented in Figure 2-19, where the reduction factors for the elastic modulus at temperature θ is normalised by the value at room temperature (i.e. $E_{a,\theta}/E_a$). Figure 2-19 shows that the elastic modulus decreases more rapidly with increasing temperature compared with the effective yield strength $f_{y,\theta}$. This suggests that the failure mode of a steel member may change at elevated temperature. For example, a steel member designed to fail under overload by reaching its strength limit at room temperature may experience buckling failure at elevated temperature. This is likely to be particularly important for HSS structures, as these members tend to be made

from more slender elements compared to members made from conventional steel grades, and so stability calculations are often critical.

As the elastic modulus of steel is essentially the same for mild strength and HSS grades at room temperature, it is rational to assume that HSS should follow a similar decline in stiffness at elevated temperature as presented in Figure 2-19. Particularly, since the decline in stiffness at elevated temperature is attributed to the predominately iron atoms moving further apart and the subsequent decline in bond strength. However, comparisons of the Eurocode approach with reduction factors for the elastic modulus of HSS in the literature, presented in Figure 2-20, reveal that the Eurocodes can be unconservative and not safely predict the decline of the elastic modulus of HSS at elevated temperatures. In Figure 2-20, the reduction factors derived from design recommendations in the American Society of Mechanical Engineers (ASME) standard B 31.1 for power piping (ASME, 2007) and a NIST report (Luecke et al., 2005) are also presented. It is worth mentioning that the Eurocode curve is considered the most appropriate for structural fire design scenarios because anisothermal conditions were used, where additional strain due to creep effects is implicitly included. It is not known how the values in ASME B31.3 (2007) were obtained, however design scenarios where the values are used reflect isothermal conditions, where creep effects are normally considered separately. Similarly, the NIST (Luecke et al., 2005) recommended curve were obtained using a dynamic mechanical analyser and also reflect isothermal conditions. Further studies on the elastic modulus at elevated temperature are presented in Chapter 4 of this thesis.

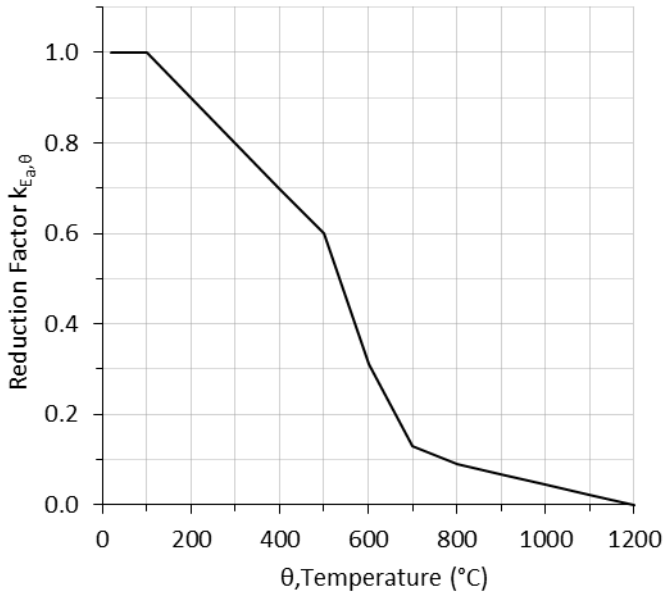

Figure 2-19 Reduction factors of the elastic modulus for mild strength steel at elevated temperatures as presented in Eurocode 3 Part 1-2 (2005)

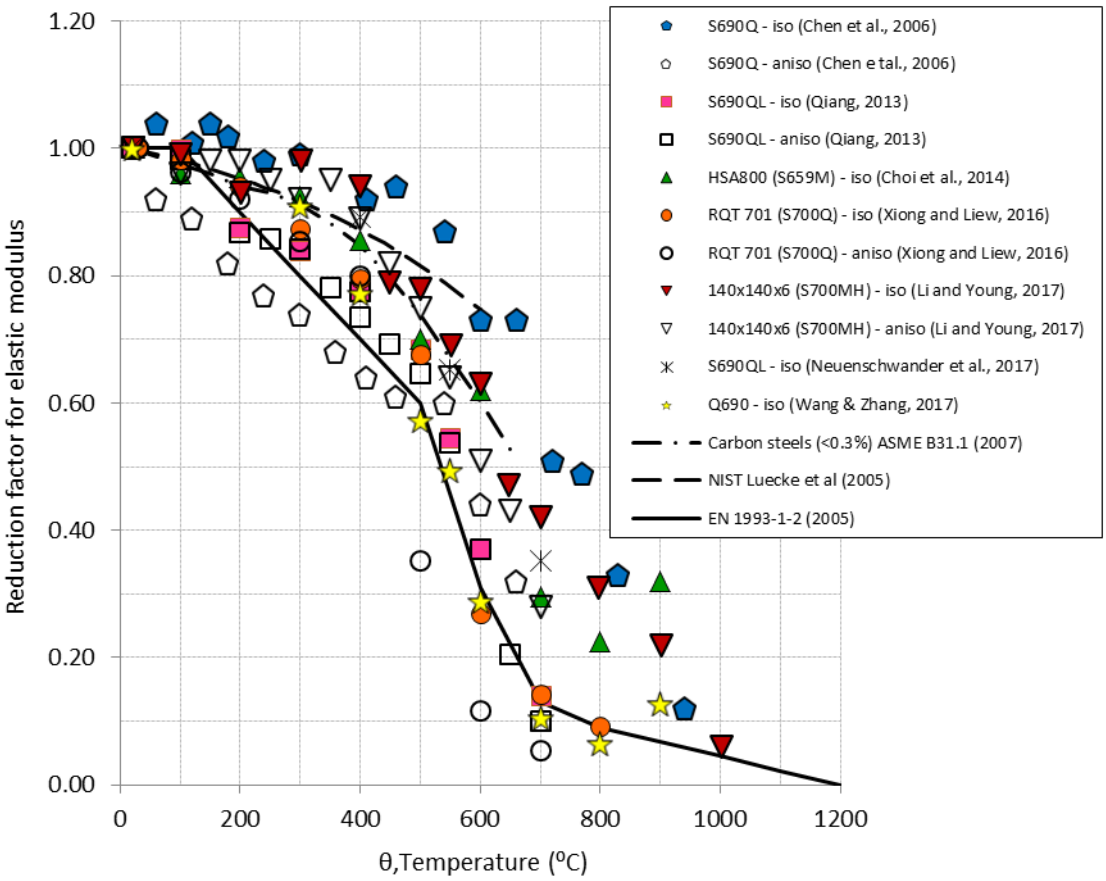

Figure 2-20 Comparrison of reduction factors for elastic modulus ($k_{y,\theta} = f_{y,\theta}/f_y$) for thermomechanical control processed (TMCP) steel grades and recommendations given in Eurocode (EN 1993-1-2, 2005), Luecke et al. (2005) and ASME B31.1 (2007)

2.4.3.7 Poisson's ratio

When a body is pulled, it becomes longer and thinner and when compressed, shorter and thicker. This phenomenon is defined as Poisson's ratio ν, which is the ratio between the lateral strain and longitudinal strain (Cooke, 1988). Eurocode 3 Part 1-1 (2005) defines this value as 0.3 at room temperature. Similar to other elastic constants including the elastic modulus, the small alloying amounts has minimal influence of the Poisson's ratio as reported by Cooke (1988) and is dependent on the crystal orientation (texture) of steel (Meyers and Chawla, 2009). The variation of Poisson's ratio of structural steels at room temperature as reported in the literature range from 0.27 to 0.3 (Cooke, 1988; Engineers Edge, n.d.). Similarly, the variation of Poisson's ratio has been shown to gradually increase in the ranges of 0.29 to 0.33 between 20 and 800°C (Cooke, 1988; Davis, 1997; Luecke et al., 2005). Hence, the value of 0.3 specific in the Eurocodes is reasonable value for design of all structural steel grades at room and elevated temperatures.

Table 2-8 Summary of test programmes on steel grades between 650-700 N/mm² in published literature

Reference	f_y (N/mm²)	Production route	Test method	Temperature range (°C)	Heating rate (°C/min)	Test parameters
Chen et al., (2006)	690	QT•	iso	22 - 940	10	Displacement: 0.2 mm/min (approximate strain: 0.006/min)
Chen et al., (2006)	690	QT•	aniso	100-1000	not specified	not specified
Qiang et al. (2013)	690	QT•	Iso	20 - 700	50	Strain: 0.005/min
Qiang et al. (2013)	690	QT•	aniso	20 - 700	10	Load: not specified
Choi et al. (2014)	650	TMCP◦	iso	25 - 900	10	Strain 1 (yield): 0.004/min Strain 2 (100-400°C): 0.015/min Strain 2 (500-900°C): 0.008/min
Chiew et al. (2014)	690	RQT˜	iso	25 - 800	20	Displacement: 0.2 mm/min (approximate strain: 0.003/min)
RUOSTE (2016)	700	QT•	aniso	20-900	20	Load: not specified
Xiong and Liew (2016)	700	QT•	iso	30-800	10	Displacement: 0.15 mm/min
Xiong and Liew (2016)	700	QT•	aniso	30-800	10	Load: 1.5kN/min
Hai-Ting and Young (2017)	700	TMCP◦ and CF*	iso	20-1000	50	Displacement: 0.3 mm/min
Hai-Ting and Young (2017)	700	TMCP◦ and CF*	aniso	20-1000	10	Load: not specified
Wang and Zhang (2017)	690	QT•	iso	20-900	20	Strain 1 (<1%): 0.003/min Strain 2 (≥1%): 0.02/min
Neuenschwander et al. (2017)	700	QT•	iso	20-900	15	Strain: 0.002/min or 0.01/min

• QT: quench and tempered
◦ TMCP: Thermo-mechanical control processed
˜ RQT: reheated, quench and tempered
*CF: cold-formed

Table 2-9 Chemical composition of various HSS grades in the published literature tested at elevated temperature

Reference	Steel grade	Chemical composition (%)															
		C	**Mn**	**Cr**	**Si**	**Ni**	**Cu**	**N**	**Mo**	**Al**	**Ti**	**Nb**	**V**	**B**	**S**	**P**	**CE_{IIW}***
Chen et al., (2006)	S690	0.16	1.1	-	0.2	-	-	-	0.2	-	-	-	-	0.001	0.003	0.01	0.38
Qiang et al. (2013)	S690QL	0.16	0.85	0.35	0.21	0.05	0.03	0.0026	0.2	0.093	0.006	0.025	-	0.0024	0.001	0.012	0.42
Chiew et al. (2014)	RQT-690	0.14	1.35	0.01	0.4	0.01	0.01	-	0.12	0.035	0.025	0.035	0.05	0.002	0.003	0.012	0.40
Choi et al. (2014)	S650M	0.2	3	0.8	0.55	2	1.5	-	0.6	-			0.12	-	0.01		0.65
Outinen (2014)/ RUOSTE (2016)	S700QL	0.169	1.01	0.59	0.316	0.19		0.0043	0.194	0.044	0.02	0.001	0.01	0.0014	0.0001	0.011	0.51
Xiong and Liew (2016)	RQT 701	0.14	1.44	0.022	0.44	0.023	0.018	0.003	0.003	0.038	0.029	0.032	0.059	0.002	0.003	0.011	0.40
Hai-Ting and Young (2017)/ Ma et al. (2015)	S700MH	0.06	1.78	0.052	0.2	0.04	0.025	0.004	0.007	0.034	0.11	0.082	0.015	0.003	0.003	0.007	0.38
Wang and Zhang (2017)	Q690	≤0.18	≤2	≤1.00	≤0.6	≤0.8	≤0.8	≤0.015	≤0.30	≥0.015	≤0.20	≤0.11	≤0.12	≤0.004	≤0.020	≤0.025	-
Neuenschwander et al. (2017)	S690QL	0.139	1.45	0.32	0.28	0.022	0.018	0.0039	0.008	0.063	0.002	0.022	0.001	0.00016	0.0011	0.01	0.45

*CE_{IIW} = C + Mn/6 + (Cr +Mo + V)/5+(Ni +Cu)/15

2.4.3.8 Creep

The properties described so far have been predominately temperature dependent. Creep is influenced by temperature, stress and time and is defined as a time dependent deformation that occurs when a material is subjected to a load, below yield (Kodur and Dwaikat, 2010). The rate of creep increases with load and temperature and the influence of creep in steels are particularly evident at temperatures above 400°C (Anderberg, 1988). As creep is time dependent, it should be noted that it is a significant concern for insulated steel members, as they are generally heated at a slower rate (e.g. 5°C/min) compared with non-insulated elements. Therefore, the member is exposed to a given temperature window for longer periods of time leading to a greater influence of creep (Kodur and Dwaikat, 2010). This effect has been observed in the literature (Rubert and Schaumann, 1986; Anderberg, 1988; Kirby and Preston, 1988), whereby heating rates below 5°C/min in anisothermal tests resulted in lower limiting temperatures at which anticipated failure is expected to occur. In practice, this failure corresponds to when the strain approaches values corresponding to the limits of deflection or instability under fire conditions (Kirby and Preston, 1988).

Explicitly including creep in numerical models can be arduous, particularly as the amount of creep is dependent on the material history, load, temperature and time. In the Eurocodes, creep is implicitly accounted for in the material properties/reduction factors derived from anisothermal tests (Kirby and Preston, 1988). Creep is not commonly considered to contribute to isothermal test results, but a slow strain rate will allow some creep to occur, and a lower effective yield strength has been reported at lower strain rate (Anderberg, 1988; Knobloch et al., 2013; Outinen, 2007). The choice of strain rate is not currently correlated to fire resistance in the European structural fire design guidelines and so researchers have tended to use the values specified in ISO 6892-2 (2011) or ASTM E21-09 (2009) when conducting tensile tests under isothermal conditions. Tests specified in these standards are often referred to as short term elevated temperature tests, where the influence of creep is considered insignificant (Davis, 1997).

For large strains (e.g. >2 %), the influence of creep on the overall fire resistance period (typically ≤1 hour) has been found to be within the reasonable error band for elevated temperature tensile testing and therefore, it has been suggested that the effect of creep can be ignored (Twilt, 1988). On the other hand, Kodur and Dwaikat (2010) found that neglecting high temperature creep in fire resistance analysis may lead to unconservative (i.e. unsafe) fire resistance predictions,

particularly for restrained elements. However, for unrestrained elements, the data obtained from isothermal testing in line with the standards is deemed to be satisfactory.

2.4.4 Behaviour of HSS compression members at elevated temperature

The previous sections have shown that the material properties of HSS can vastly differ at elevated temperatures and this in turn will influence the structural performance. Current guidelines of structural design guidelines (EN 1993-1-2, 2005) including the buckling performance of compression members at elevated temperatures are based on data structural elements made from mild steels, which is well documented in the literature (Janss and Minne, 1981; Burgess et al., 1992; Franssen et al., 1998; Pauli et al., 2012), whereas similar data for HSS is limited; only work by Chen and Young (2008), Wang et al. (2013b) and Ebel et al. (2016) are available. Chen and Young (2008) presented parametric studies investigating the buckling behaviour of box and I-sections at temperatures up to 900°C, considering geometric imperfections, the nonlinear shape of the stress-strain response and the strength and stiffness parameters of BISPLATE 80 (S690QL) from their parallel study (Chen et al., 2006). The results were compared with international standards including the Eurocode and showed the Eurocode to be conservative at predicting the buckling design strength at all temperatures up to 900°C, with the exception of the box section at 700°C. This suggests that lower buckling curves may be necessary for box sections.

In addition, Wang et al. (2013b) presented a numerical study on the behaviour of axially loaded HSS columns utilising a bilinear stress-strain response and strength and stiffness parameters of BISPLATE 80 (S690QL) from Chen et al., (2006) study. The limitations of a bilinear stress-strain response were discussed earlier (Section 2.4.3.2) and the results demonstrated that the critical temperature for S690QL column is lower than for columns made from conventional steel grade (S355). It was also found that the influence of residual stress, section shape and initial flexure have little influence on the load bearing capacity at room and elevated temperatures.

Most recently, Ebel et al. (2016) presented data on S690 beams utilising nonlinear stress-strain response and reduction factors derived from different strain rates. The results demonstrated a wide range of scatter suggesting that individual buckling curves are needed for each temperature rather than the current Eurocode approach of one buckling curve for all temperatures.

All the above studies mentioned were focused on quench and tempered steels and were conducted using finite element methods where experimental work on HSS at room temperature was used to validate the model. This is because at the time, there were no experimental studies on the behaviour of HSS members at elevated temperature mainly owing to the significant

expense associated with high temperature structural testing as well as lack of reliable material properties which are needed to develop computation design models. Experimental data on HSS at elevated temperature is currently only available for Q460 (where Q in the Chinese phonetic alphabet of the word "Qu", which stands for the steel yield strength (Wang and Lui, 2016)). Wang et al. (2014) conducted an experimental investigation into the local buckling of Q460 at 25, 450 and 650°C and demonstrated the Eurocode approach to be unconservative, predicting higher buckling loads than the experimental results (Wang et al., 2014). Although the Eurocode 3 Part 1-12 (2005) specifies the use of TMCP steels in structural design, to date, only experimental studies on the buckling behaviour of columns made from TMCP steels at room temperature is available; the influence of the material properties of TMCP on the buckling behaviour at elevated temperature is yet to be investigated.

2.5 Concluding remarks

There are many advantages to using HSS in structural applications. However, there are several challenges and knowledge gaps, including the structural performance of HSS under fire conditions, which need addressing in order to provide reliable and economical design guidance for HSS in structural applications. This section has presented an overview of previous research into the behaviour and design of HSS, including the metallurgical and structural aspects, with emphasis given to the material properties required to determine the structural response in a fire. From this literature survey the following conclusions can be drawn:

- Of the strengthening mechanisms mentioned, strain hardening and grain refinement become increasingly ineffective at contributing to strength from temperatures above 400 and 600°C, respectively. Only solid solution strengthening and secondary (precipitation) hardening can help retard the strength loss at temperatures as high as 700°C.
- There is sufficient evidence that suggests that the specific heat, thermal expansion and Poisson's ratio or steels are independent of the material history meaning that the values presented in Eurocode 3 Part 1-2 (2005) are suitable for HSS. However, the thermal conductivity is influenced by the material history and so further data for various HSS grades may be necessary.
- The current Eurocode approach to strength degradation at elevated temperatures is generally unconservative (i.e. unsafe) for various types of HSS grades at elevated temperatures.

- Vast differences in the strength degradation at elevated temperature was observed in the published literature. This is attributed to the differences in the chemical composition and production route as well as variation is testing techniques including the heating and strain rate which will influence the amount of creep present. In this thesis, consistent test parameters will be used in order to minimise the influence of using different test parameters when comparing the material properties of different types of HSS at elevated temperatures. Test parameters need to be selected to be representative of anticipated fire scenarios which will be addressed further in Chapter 4.
- In general, previous research was mainly focused on obtaining accurate material properties at elevated temperature and very limited metallurgical work was conducted, so it is not clear which HSS, if any, have better strength retention properties at elevated temperature and why (i.e. the influence of the microstructural parameters is not clear)? Hence, as well as obtaining material properties for different HSS grades at room and elevated temperatures, the metallurgical properties are also investigated; the study is presented in Chapter 5 and the links between the material properties, chemical composition and microstructure discussed in Chapter 7. This should help indicate
- There are very limited studies on the behaviour of columns made from S650 to S700 steels at elevated temperature. The behaviour of compression members in a fire scenario is dependent on the material properties and this will be studied in Chapter 6.

Chapter

3

Material properties of high strength steels at room temperature

3.1 Introduction

Before considering the influence of temperature on the properties of HSS grades for structural fire design guidelines, the properties at ambient temperature need to be obtained as a baseline for comparison. Since the material properties of HSS are great influenced by their alloying composition and production route, different types of HSS are examined in this study. Information on the material strength and stiffness are obtained from uniaxial tensile or compression tests, where a tensile or compression load is applied to a coupon to assess how the strain changes as a function of the applied load. This chapter is divided into two parts. The first part presents the steel grades examined and includes the chemical composition obtained through optical emission spectrometry (OES). In the second part of this chapter, the experimental method and results from uniaxial tensile tests are described and presented. From this the material properties are presented and compared with the recommendations given in Eurocode 3 Part 1-12 (2007) to check whether the HSS grades presented are suited for design at ambient temperature.

3.2 High strength steel examined

3.2.1 Steel grades

The designation for structural steels in accordance with EN 10027-1 (2005) were introduced in Section 2.3.4.1. A similar approach is adopted in EN 10025-3 (2004), EN 10025-6 (2004), EN 10149-2 (2013) and EN 10210-1 (2006), where by the structural steel grades are denoted by a prefix 'S' followed by the nominal yield strength at ambient temperature and then the production route/delivery condition. The steel grades that were included in the experimental investigation, covering a range of nominal yield strengths between 460 and 700 N/mm^2 at ambient temperature, are presented in Table 3-1. The suffix 'Q' in the designation S690QL refers to the quench and tempered production process, and the 'L' indicates that the material meets the minimum impact energy requirement of 30 J at −40°C (EN 10025-6, 2004). The suffixes 'M' and 'C' in S700MC indicate thermomechanical control processing (TMCP) and cold-formed materials, respectively (EN 10149-2, 2013). The suffix 'N' in the designation S460N and S460NH refers to the normalised condition and 'H' in the designation S460NH and S690QH indicates a hollow section product form. It is worth noting that currently structural hollow sections are specified up to S460, however with the growing use of HSS in structural applications it is likely that higher steel grades will be incorporated into the standards in the near future.

With reference to Table 3-1, steels A-C are commercial steels in plate form obtained from various European steel manufacturers. All the plates were hot rolled, with steels A and C (S690QL) subsequently quenched and tempered at 600°C and steel B (S700MC) thermomechanical controlled processed in line with EN 10025-6 (2004) and EN 10149-2 (2013), respectively. Steels D and E are commercial structural hollow sections used in previous beam tests at Imperial College (Wang et al., 2017). The hollow sections were hot rolled from continuously cast round ingots and then hollowed out in a piercing mill to the final section shape. Steel D (S460NH) was subsequently normalised, while steel E (S690QH) was quenched and tempered (Wang et al., 2017). The structural hollow sections are categorised as hot-finished seamless tubes and no welding process was used during their manufacture (Wang and Gardner, 2017).

Table 3-1 Grades of commercial HSS included in the programme

Steel designation	Steel Grade	Nominal yield strength (N/mm^2)	Manufacturing route	Product form	Dimension (mm)
Steel A	S690QL	690	Quenched and tempered	Plate	16 × 600 × 1000
Steel B	S700MC	700	Thermomechanical controlled processed (suitable for cold-forming)	Plate	12 × 500 × 2000
Steel C	S690QL	690	Quenched and tempered	Plate	15 × 500 × 900
Steel D	S460NH	460	Normalised	Structural hollow sections	3.6 × 90 × 90
Steel E	S690QH	690	Quenched and tempered	Structural hollow sections	5.6 × 90 × 90

3.2.2 Chemical composition

For structural steels, the standards including EN 10025-6 (2004) and EN 10149-2 (2013) give a range or set a maximum limit on the quantity of each alloying element of the steel's chemical composition. This prevents steel producers adding other elements which could compromise the required properties and ensures that the steel meets a guaranteed benchmark of adequate design properties at ambient temperature.

The chemical compositions of the steels tested in this programme were obtained by direct spark optical emission spectrometry (OES), a quantitative analysis technique in which atoms in the solid sample are excited by the absorption of energy from an electrical source. The excited atoms emit their characteristic electromagnetic radiation in the form of light, the wavelength and intensity of which is then used to determine the composition (Stevens, 1982).

Table 3-2 presents the chemical compositions for steels A-E obtained by OES and the carbon equivalent. The carbon equivalent describes the magnitude of the effect of elements which exert the greatest influence on hardenability; this was calculated following the International Institute for Welding (CE_{IIW}) formula presented in Equation (3.1). Although other elements which influence the hardenability including boron are not included in Equation (3.1), CE_{IIW} has been incorporated into many international material standards including EN 10025-1 (2004). This is possibly because it is a convenient way to evaluate the weldability from the standpoint of hydrogen cracking (Ginzburg and Ballas, 2000).

$$\%\ \mathrm{CE_{IIW}} = \mathrm{C} + \frac{\mathrm{Mn}}{6} + \frac{\mathrm{Cr} + \mathrm{Mo} + \mathrm{V}}{5} + \frac{\mathrm{Ni} + \mathrm{Cu}}{15}\ (\text{in weight \%}) \quad (3.1)$$

The full chemical composition of some of the steel B (S700MC) is not shown for confidentiality reasons. The chemical compositions of all of the steels presented comply with the following standards: EN 10025-3 (2004), EN 10025-6 (2004), EN 10149-2 (2013) and EN 10210-1 (2006). Steels A (S690QL) and C (S690QL) were both quench and tempered plates; the key difference between these steels is the chemical composition. Although both steels are alloyed with chromium, nickel, boron, and molybdenum and micro-alloyed with titanium and vanadium, steel A (S690QL) is alloyed with significantly more chromium (0.56% in steel A vs. 0.02% in steel C), molybdenum (0.21% in steel A vs. 0.002% in steel C) and boron (0.009% in steel A vs. 0.006% in steel C) which are known to have positive influence in the high temperature performance of steel as mentioned in Section 2.3.6. The lower alloying levels in steel C (S690QL) result in a lower carbon equivalent (CE_{IIW}) than steel A (S690QL) and hence better weldability properties. It is worth noting that steel C (S690QL) contains more microalloying elements than steel A (S690QL), where the total of niobium, titanium and vanadium is 0.090% in steel C (S690QL) compared with 0.006% in steel A (S690QL). These microalloying elements can contribute to the strength retention at elevated temperature. Steel E (S690QH) contains more chromium than steel A (S690QL) which contributed to the slightly higher carbon equivalent (CE_{IIW}). Steel B (S700MC) has the lowest carbon content of the steels included in this study, but the highest manganese and combined microalloying elements (niobium, titanium and vanadium) of 0.22% compared to the quenched and tempered steels (steels A, C and E). This is typical of TMCP steels, as microalloying elements play a key role in achieving strength as mentioned in Section 2.3.6.9

Table 3-2 Typical chemical composition of the HSS included in the programme

Chemical composition (weight %)	Steel designation				
	Steel A (S690QL)	Steel B (S700MC)	Steel C (S690QL)	Steel D (S460NH)	Steel E (S690QH)
Carbon (C)	0.17	<0.08	0.15	0.21	0.14
Manganese (Mn)	1.29	<2.00	1.42	1.57	1.58
Chromium (Cr)	0.56	♦	0.02	0.089	0.67
Silicon (Si)	0.29	<0.20	-	0.30	0.29
Nickel (Ni)	0.46	♦	0.16	0.045	0.11
Copper (Cu)	0.18	♦	0.01	0.036	0.042
Molybdenum (Mo)	0.21	residual	residual	0.029	0.20
Aluminium (Al)	0.037	<0.050	0.056	0.036	0.02
Titanium (Ti)	0.002	<0.15•	0.003	0.005	0.004
Niobium (Nb)	0.002	<0.090•	0.029	<0.002	0.019
Vanadium (V)	0.003	<0.20•	0.058	0.11	0.064
Boron (B)	0.003	0.0001	0.0019	0.0006	-
Sulphur (S)	<0.002	0.003	<0.002	<0.002	<0.002
Phosphorus (P)	0.009	0.015	0.006	0.017	0.011
CEIIW*	0.58	<0.50	0.41	0.52	0.61

* as calculated using Equation (3.1)
♦Cr + Ni + Cu < 0.5
•Ti + Nb +V < 0.22%

3.3 Experimental method

3.3.1 Testing device

Tensile tests were conducted on a Zwick Kappa 100 SS electromechanical testing machine with a maximum return speed of 100 mm/min. The machine consisted of a load frame with a maximum capacity of 100 kN and testXpert II V3.6 software that monitored and controlled the mechanical variables of the system through a digital closed loop control. The machine was compliant with ISO 7500-1 (2015).

To measure the strain a contact extensometer, compliant with ISO 9513 class 1 (2012), was used, where the total bias error is either 1% or ±3 μm (dependent on which value is the highest). The rods of the extensometer were made from high purity alumina ceramic and each had a knife-edge that formed a point of contact perpendicular to the gauge length of the tensile specimen. This meant that the extension of the specimen was directly measured during testing. The extensometer had a gauge length of 25 mm with the capacity to extend up to 50% and 10% in tension and compression, respectively. The extensometer was used to measure the strain up to 5% before switching to crosshead displacement to estimate the strain for the remainder of the

test, to avoid damaging the alumina ceramic rods. During initial tests, it was observed that a low contact force (<100g) resulted in the knife edges of the ceramic rods of the extensometer slipping during the test, whilst a high contact force (200g) added a bending moment from the frame where the extensometer was attached to the tensile specimen. For reliable results, the contact force on the extensometer was set to 150g. In addition, conventional strain gauges were used which are capable of measuring the strain up to 4% before debonding occurred. In each test, two linear strain gauges were attached to the midpoint at both sides of each tensile specimen to minimise the influence of bending and verify the accuracy of the readings from the extensometer; since strain gauges are known to be more accurate (Huang and Young, 2014). An example of this comparison is shown in Figure 3-1. Generally, there was good agreement between the measured elastic modulus from the strain gauge and the extensometer. The test set-up for one of the experiments is shown in Figure 3-2.

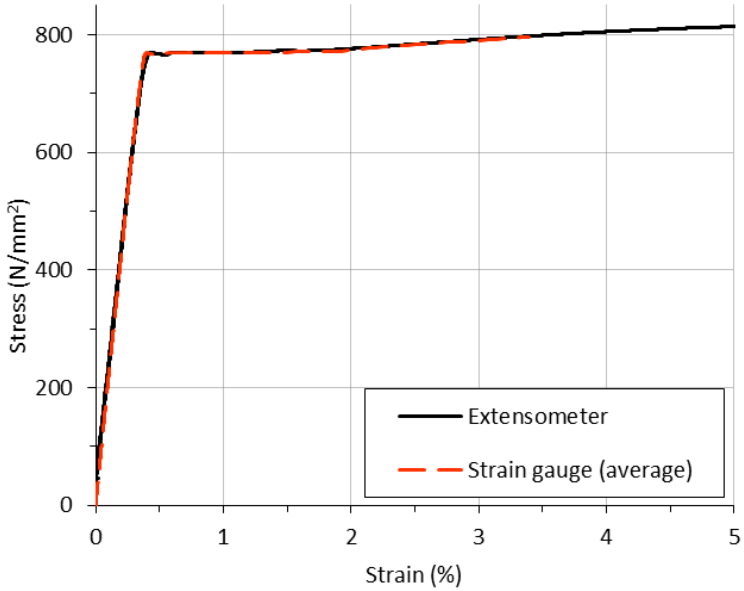

Figure 3-1 Comparison between strain measurements for steel C (S690QL) obtained from an extensometer and the average of two strain gauges

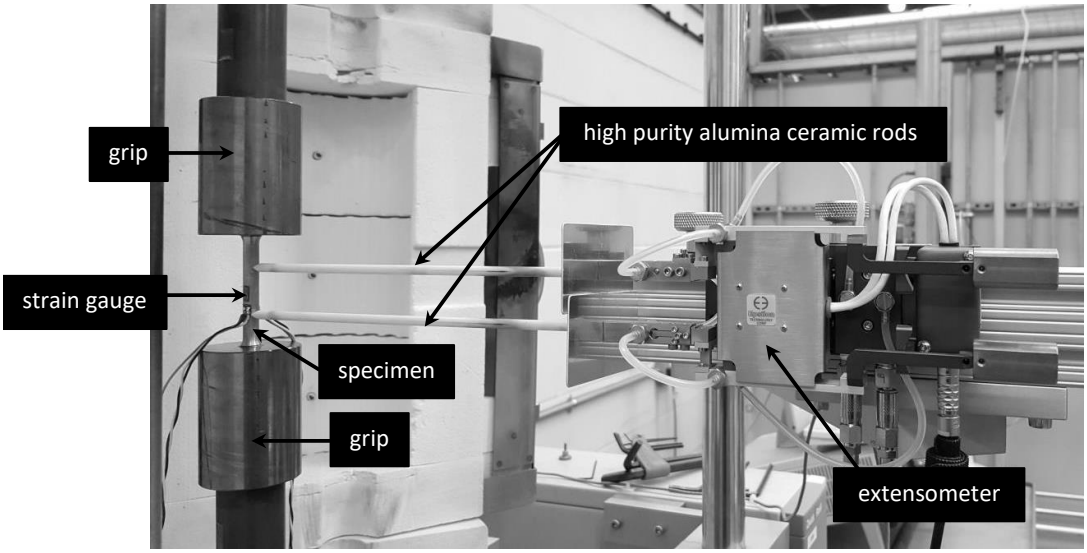

Figure 3-2 Experimental set up

3.3.2 Test specimens

The dimensions and geometry of tensile specimens was based on the recommendations provided for tensile testing at elevated temperature in ISO 6892-2 (2011) and ASTM E29-1 (2009) for consistency. ASTM E29-1 (2009) states the following:

> 'When the dimensions of the material permit, except for sheet and strip, the gauge length of the specimen should have a circular cross-section.'

Recommended dimensions for cylindrical specimens in ISO 6892-2 (2011) start at M6, which is the standard name of cylindrical specimen with a thread size of 6 mm. The thicknesses of the material in this programme varied from 3.6 to 16 mm and so for material with thicknesses less than 6 mm, flat specimens were machined. This meant that the HSS in plate form (steels A-C) were machined into cylindrical tensile specimens, whilst the HSS in structural hollow sections were machined into flat specimens. All specimens were machined parallel (or longitudinal) with respect to the rolling direction from each plate or the four flat faces of the structural hollow sections as shown in Figure 3-3. The variation in tensile properties, including the yield strength, as a result of the specimen geometry and size should be minor (Pierron et al., 2003). It is important to ensure that the specimens are proportional, where the relationship between the gauge length L_o and cross sectional area A_o, is expressed in Equation (.3.2), in order to allow comparison of the material ductility (Loveday et al., 2004).

$$L_0 = 5.65\sqrt{A_0} \tag{3.2}$$

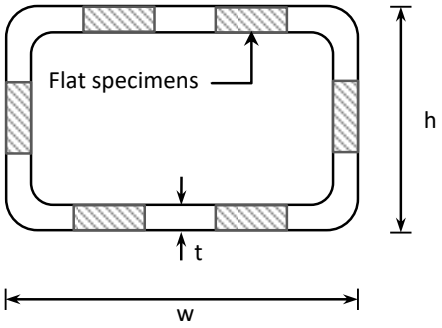

Figure 3-3 Location of the flat tensile specimens

The nominal dimensions of the tensile specimens based on the recommendations provided in ISO 6892 Part 1 (2009) and Part 2 (2011) are presented in Figure 3-4, Figure 3-5, Table 3-3 and Table 3-4. The cylindrical tensile specimens had a diameter of either 6 mm (M10) or 8 mm (M12) in the gauge length L_0. This was the maximum standard size possible from each plate.

For S460NH, the thickness t_0 of the flat tensile specimens matched the thickness of the structural hollow sections. The same was intended for S690QH however, the surface of the hollow sections was, covered in mill scale, a 'flaky' iron oxide which made the surface irregular (not flat) and could peel off when a tensile force is applied. This made the coupons unsuitable for the attachment of strain gauges which require a flat and relatively clean surface for good adherence. Furthermore the presence of mill scale could influence the strains recorded from the extensometer output if the surface is not relatively flat. Hence the mill scale was removed using a linisher.

The actual dimensions of the cylindrical and flat specimens were measured using a digitised travelling light microscope and Vernier callipers, respectively. The diameter or thickness and width of the specimens were measured three times along the gauge length and then averaged to determine the cross-sectional area A_0 for each tensile specimen. The standard gauge length was calculated using Equation (3.2) for proportional tensile specimens. L_0 was rounded to the nearest multiple of 5 mm, as recommended in ISO 6892-1 (2009) and ISO 6892-2 (2011). Such approximation is only valid if the difference between the calculated gauge length and approximate gauge length is less than 10%. This was the case for all tensile specimens presented in Tables 3-3 and 3-4. For cylindrical tensile specimens, $A_0 = ¼\pi d_0^2$, and so Equation (3.2) can be approximated to five times the gauge length diameter ($5d_o$).

The approximate gauge length was marked on the cylindrical specimens using Vernier callipers and a lathe, whilst for the flat specimens, Vernier callipers and a metal ruler were used. Once the tests were completed, the final gauge length after fracture, L_u, was measured by carefully fitting back together the broken specimen and using a digitised travelling light microscope. The plastic strain at failure ε_f, was then calculated using Equation (3.3).

$$\varepsilon_f\ (\%) = \frac{L_u - L_0}{L_0} \times 100 \qquad (3.3)$$

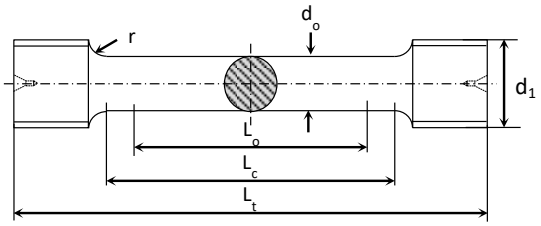

Figure 3-4 Schematic of the cylidrical tensile specimen

Table 3-3 Nominal dimensions for the cylindrical specimens from steels A-C

Nominal dimensions in mm

Steel	d_0	L_0	d_1	r min.	h min.	L_c min.	L_t min. [a]
A & C (S690QL)	8	48	M12	6	10	-	90
B (S700MC)	6	40	M10	6	8	-	80

[a] The minimum value is only sufficient when the transition radius r, the length of the gripped ends h and the parallel length L_c meet the miniumum values

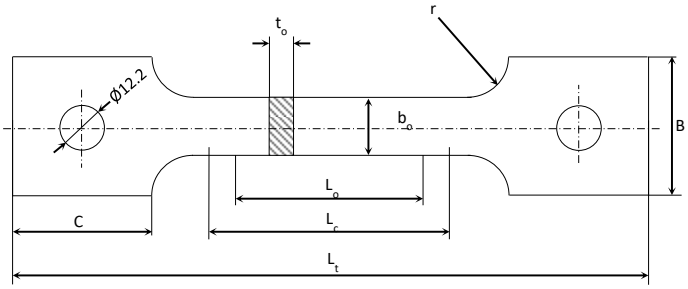

Figure 3-5 Schamitc of the flat tensile specimen geometry

Table 3-4 Nominal dimensions for flat specimens from steels D and E

Nominal dimensions in mm

Steel	a_0	b_0	L_0	r	B	C	D	E	L_c min.	L_t min.[a]
D (S460NH)	3.6	12.5	40	25	35	31	10	17	54	142
E (S690QH)	5.0	12.5	45	25	35	31	10	17	61	149

[a] The minimum value is only sufficient when the parrallel length Lc is the minimum value

3.3.3 Test procedure

The tests were conducted following the recommendations given by Huang and Young (2014), which included strain rates significantly lower than those presented in ISO 6892-1 (2009) (0.0009 vs. 0.015/min). The strain rates used in the current test programme are presented in Table 3-5. A lower strain rate (0.0009/min) was specified at strains below 0.2% in order to obtain more data points in the elastic region and hence more accurate value for the elastic modulus. From a strain of 0.2% onwards, the strain rate was increased to 0.0070/min as less data points are required. The strain rate was gradually increased around the 0.2% strain to avoid a sharp transition in the stress-strain response. The cylindrical tensile specimens were strained to failure, whilst the flat tensile specimens machined from steels D (S460NH) and E (S690QH) were strained up to 6 and 3%, respectively. This is because the flat tensile specimens were longer in length compared with the cylindrical tensile specimens; hence, for the flat specimens, the maximum displacement of the testing machine was reached before the specimen failed. Data on the full stress-strain response are available elsewhere (Wang et al., 2017) and for the purpose of obtaining values for prescriptive approach to structural fire design purposes, strains of up to 2% are of primary interest.

Table 3-5 Strain rates used in testing

Strain (%)	Strain rate (/min)
0 – 0.2	0.0009
0.2 – fracture	0.0070

3.4 Experiment results

3.4.1 Stress-strain response

Examples of the engineering stress-strain responses of steels A to E obtained from the strain gauges are presented in Figure 3-6. There is a wide variation in stress-strain responses amongst the HSS grades tested and this is related to the differences in the steels microstructure (as presented in Section 5.7.1) which is attributed to the differences in chemical compositions and production/fabrication routes. Eurocode 3 Part 1-1 (2005) adopts a bilinear stress-strain response, that is a linear-elastic response up to the distinct yield point, followed by a yield plateau, where the stress remains constant as the strain increases. Although alternative stress-strain models which consider strain hardening are presented in Eurocode 3 Part 1-5 (2006), not all HSS grades tested are represented by such models.

Amongst the quench and tempered steels, the stress-strain response for steels C (S690QL) and E (S690QH) depicted in Figure 3-6 (c) and Figure 3-6 (e) respectively, follows a bilinear response

adopted in Eurocode 3 Part 1-1 (2005), whilst steel A (S690QL) presented in Figure 3-6 (a) shows strain hardening soon after yielding. The structural hollow section that was supplied in the normalised condition, steel D (S460NH) shown in Figure 3-6 (d) has an upper and lower yield point, followed by a short yield plateau up to 0.8% total strain and then shows strain hardening. In the case of steels C (S690QL), D (S460NH) and E (S690QH), after the (lower) yield point is reached, the stress remains constant with increasing strain as different portions of the tensile specimen successively undergo yielding (Pauli, 2013). Once the entire specimen reaches yield, strain hardening usually commences where the pile up of dislocations oriented in different directions induces further strengthening through work hardening. For steel A (S690QL) and B (S700MC) (Figure 3-6 (a) and Figure 3-6 (b), respectively), strain hardening commences soon after the material yields. Although it is not fully understood why steel A (S690QL) and B (S700MC) work or strain hardens soon after yielding, the reason is related to the differences in the material microstructure and chemical compositions.

The accepted reason behind the occurrence of a distinct yield point including the upper and lower yield point, relates to the concentration of carbon and nitrogen solute atoms around dislocations, which help minimize the total strain energy associated with the distorted atomic crystal structure (Bhadeshia and Honeycombe, 2006). The segregation of carbon and nitrogen solute atoms around dislocations, known as the Cottrell atmosphere, was first shown by Cottrell and Bilby (1949). The presence of a Cottrell atmosphere means a higher stress is needed to propagate dislocation movement resulting in an upper yield point. Once yielding commences, the dislocations are freed from the solute atoms and the yield stress abruptly drops to a lower yield point. The magnitude of the upper yield point is also determined by the test parameters, particularly the speed of the test, where a high strain or displacement rate would result in a higher peak stress. It should be noted that a slow strain rate was adopted in this study hence the chances of observing an upper and lower yield point are reduced. This phenomenon was only observed in steel D (S460NH) which was alloyed with most carbon (i.e. 0.21% in steel D vs. 0.14% in steel E) compared to the rest of the HSS tested in this study. In contrast, the carbon content of steel B (S700MC) was less than half that of the other steel grades tested (i.e. 0.06% vs 0.15%), and this is likely to be linked to the nonlinear stress-strain response observed in Figure 3-6 (b). The carbon content does not necessarily indicate if a material will have a distinct yield point since the distinct yield point is attributed to the presence of carbon and nitrogen solute atoms in the iron matrix (i.e. the carbon and nitrogen that have not combined to form carbides and nitrides).

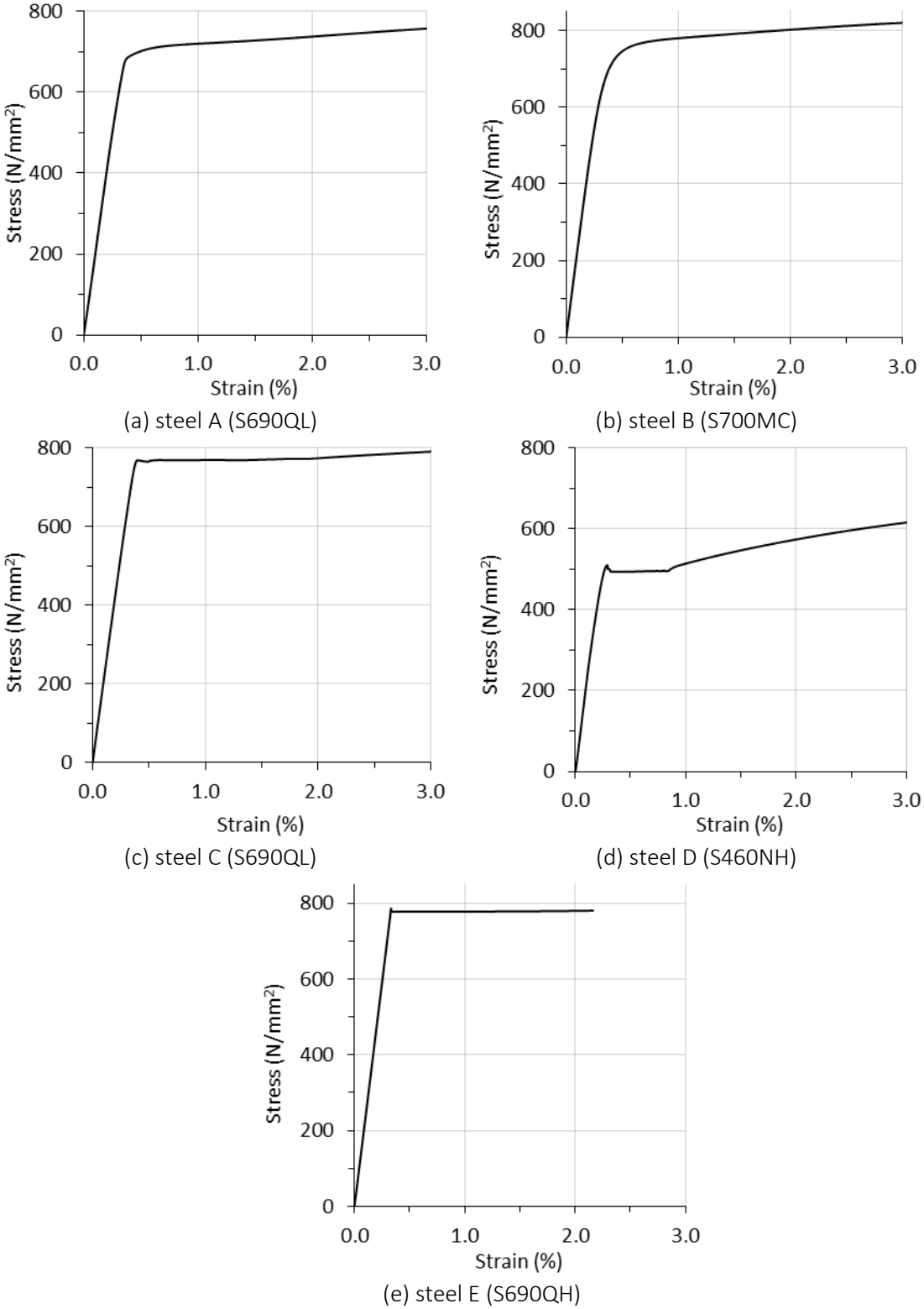

(a) steel A (S690QL)

(b) steel B (S700MC)

(c) steel C (S690QL)

(d) steel D (S460NH)

(e) steel E (S690QH)

Figure 3-6 Examples of a stress-strain response for (a) steel A (S690QL), (b) steel B (S700MC), (c) steel C (S690QL), (d) steel D (S460NH) and (e) steel E (S690QH).

3.4.2 Tensile properties

From the engineering stress-strain curves for steels A to E, the following measurements were made: (i) the proportional limit ($f_{p,20}$), defined as the point where the stress–strain response changes from being linear to nonlinear, (ii) the 0.2% proof strength ($f_{0.2p,20}$), defined as the point where the initial elastic modulus offset at 0.2% strain intersects the stress–strain curve, (iii) the effective yield strength ($f_{y,20}$), typically defined as the point where the total strain at 2% intercepts the stress–strain curve, (iv) the ultimate strength ($f_{u,20}$), defined as the maximum tensile strength measured, and (v) the elastic modulus ($E_{a,20}$). These properties are depicted in Figure 3-7. In addition, the elongation after fracture was determined using Equation (3.3).

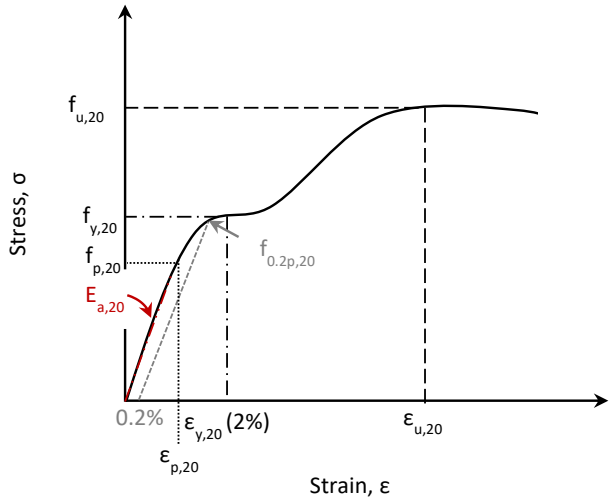

Figure 3-7 Key parameters measured from the stress-strain response at ambient temperature

Table 3-6 to Table 3-10 presents the mean data obtained from the tensile tests for each material along with the standard deviation defined in Equation (3.4) and coefficient of variation (COV), which is defined as a ratio of the standard deviation over the mean value from the tests.

$$\text{Std. Dev} = \sqrt{\frac{1}{N}\sum_{i=1}^{N}(x_i - \bar{x})^2} \tag{3.4}$$

where N is the number of specimens, x_i is the measured value and $\bar{x}$ is the mean value. In total, 3 tensile specimens for steels A-C and 2 tensile specimens for steels D and E were tested at ambient temperature. The COV values presented in Table 3-6 to Table 3-10 demonstrate good repeatability for all the tensile properties of steels A-E. These tensile properties are used later in Chapter 4 as a baseline for comparison with the elevated temperature tensile tests. All the HSS

grades tested (steels A-E) surpassed the minimum yield and tensile strengths (f_y and f_u, respectively) specified in Eurocode 3 Part 1-12 (2007).

Table 3-6 Tensile properties of steel A (S690QL) at ambient temperature

	$E_{a,20}$ (GPa)	$f_{p,20}$ (N/mm^2)	$f_{0.2p,20}$ (N/mm^2)	$f_{y,20}$ (N/mm^2)	$f_{u,20}$ (N/mm^2)
Mean	199.3	593.3	706.3	739.3	791.9
Std. Dev	2.8	9.4	0.5	2.5	6.9
CV (%)	1.4	1.6	0.1	0.3	0.9

Table 3-7 Tensile properties of steel B (S700MC) at ambient temperature

	$E_{a,20}$ (GPa)	$f_{p,20}$ (N/mm^2)	$f_{0.2p,20}$ (N/mm^2)	$f_{y,20}$ (N/mm^2)	$f_{u,20}$ (N/mm^2)
Mean	224.69	418.33	749.33	800.70	836.32
Std. Dev	0.89	8.50	11.58	11.87	1.86
CV (%)	0.4	2.0	0.3	0.1	0.2

Table 3-8 Tensile properties of steel C (S690QL) at ambient temperature

	$E_{a,20}$ (GPa)	$f_{p,20}$ (N/mm^2)	$f_{0.2p,20}$ (N/mm^2)	$f_{y,20}$ (N/mm^2)	$f_{u,20}$ (N/mm^2)
Mean	210.1	757.6	769.0	768.2	815.7
Std. Dev	1.1	7.9	5.7	5.2	3.3
CV (%)	0.5	1.0	0.7	0.7	0.4

Table 3-9 Tensile properties of steel D (S460NH) at ambient temperature

	$E_{a,20}$ (GPa)	$f_{p,20}$ (N/mm^2)	$f_{0.2p,20}$ (N/mm^2)	$f_{y,20}$ (N/mm^2)
Mean	213.4	496.5	499.0	571.2
Std. Dev	3.0	3.5	1.0	7.9
CV (%)	1.4	0.7	0.2	1.4

Table 3-10 Tensile properties of steel E (S690QH) at ambient temperature

	$E_{a,20}$ (GPa)	$f_{p,20}$ (N/mm^2)	$f_{0.2p,20}$ (N/mm^2)	$f_{y,20}$ (N/mm^2)
Mean	225.6	778.5	776.5	777.3
Std. Dev	6.4	13.5	13.5	12.4
CV (%)	2.9	1.7	1.7	1.6

3.4.3 Ductility

Ductility is of paramount importance to all steels in structural applications, as it is assumed in many design scenarios, including the design of structural connections, that the material will undergo a sufficient plastic deformation prior to failure. Higher strengths in steels are normally obtained at the expense of ductility, and this is considered in Eurocode 3 Part 1-12 (2007), where less stringent limiting values are recommended for the ultimate to yield strength ratio f_u/f_y, the elongation at failure ε_f determined based on the gauge length ($L_0 = 5.65\sqrt{A_0}$) and ultimate to yield strain ratio $\varepsilon_u/\varepsilon_y$ (where yield strain $\varepsilon_y = f_y/E_a$) for HSS, compared to Eurocode 3 Part 1-1 (2005).

The recommended f_u/f_y, ε_f and $\varepsilon_u/\varepsilon_y$ values in the Eurocode for elastic and plastic analysis, applicable to steel grades up to and including S460, as well as the ductility requirements for high strength steels up to S700 are summarised in Table 3-11.

Table 3-11 Ductility requirements presented in the Eurocodes

	f_u/f_y	ε_f (%)	$\varepsilon_u/\varepsilon_y$
Eurocode 3 Part 1-1 (2005) – elastic analysis	≥1.10	≥15	≥15
Eurocode 3 Part 1-1 (2005) – plastic analysis	≥1.15	≥15	≥20
Eurocode 3 Part 1-12 (2007)	≥1.05*	≥10	≥15

* in the UK annex the recommended value is 1.10 for highway structures such as bridges and other structures including buildings.

In accordance with Eurocode 3 Part 1-1 (2005), the lower recommended ductility requirements limit the use of HSS in plastic analysis and semi-rigid joints, however, it is worth noting that plastic resistance may still be used for Class 1 and 2 cross-sections and the structural analysis can be conducted through nonlinear finite element methods (Johansson and Collin, 2005). The assessment of these limits has been evaluated by Wang (2016), who demonstrated that HSS including steels D (S460NH) and E (S690QH) from the present study, can meet the ductility requirements for elastic analysis listed in Eurocode 3 Part 1-1 (2005). A summary of the ductility properties of steels A-E are presented in Table 3-12.

Table 3-12 Ductility properties for steels A-E

	$f_{u,20}/f_{p,20}$	$f_{u,20}/f_{0.2p,20}$	ε_f (%)	$\varepsilon_u/\varepsilon_y$
Steel A (S690QL)	1.33	1.12	20.1	19.6
Steel B (S700MC)	2.00	1.12	16.6	24.4
Steel C (S690QL)	1.10	1.06	15.7	19.5
Steel D (S460NH) (Wang, 2016)	-	1.31*	27.9	-
Steel E (S690QH) (Wang, 2016)	-	1.02*	20.1	-

*f_u/f_y where f_y is taken from the upper yield strength in accordance with Eurocode 3 Part 1-1 (2005)

It should be noted that for design at ambient temperature, the Eurocode (EN 1993-1-1, 2005) uses f_y, in calculations. Generally, for steels with a bilinear stress-strain response, where the transition from elastic (linear) to plastic (nonlinear) is straightforward, f_y can either be defined as nominal yield strength or the upper yield strength (R_{eH}) in accordance with Eurocode 3 Part 1-1 (2005) and EN 10025-1 (2004). For steels with a nonlinear stress-strain response, where no distinct yield point is present, the 0.2% proof strength is typically used in accordance with the product standard (i.e. EN 10025-1 (2004)). Since no distinct yield point was observed in the stress-strain responses in the HSS grades in this study, the ratio f_u/f_y was determined using both the proportional limit $f_{p,20}$ and 0.2% proof strength $f_{0.2p,\,20}$. Normalising the tensile strength f_u by the $f_{p,20}$ instead of $f_{0.2p,20}$, results in higher ratios, particularly for steel B (S700MC) which is linked

to the nonlinear response of the stress-strain curve. For this reason, $f_{0.2p,\ 20}$ is a more suitable parameter compared to $f_{p,20}$ and hence ε_y was determined as the corresponding strain at $f_{0.2p,20}$. From Table 3-12, it can be seen that steels A (S690QL) to C (S690QL), meet the ductility requirements for HSS as specified in Eurocode 3 Part 1-12 (2007), with steels A (S690QL) and B (S700MC) meeting the slightly more stringent requirements in the UK National Annex to Eurocode 3 Part 1-12 (2007). Although steels A-C met the elongation at failure ε_f and ultimate to yield strain ratio $\varepsilon_u/\varepsilon_y$ (if rounded to the nearest integer) requirements for plastic analysis, none of the steels met the f_u/f_y requirement of 1.15. However, it has been demonstrated experimentally that sufficient rotation capacity can still be achieved in steel girders with little strain hardening (Johansson and Collin, 2005), highlighting that f_u/f_y limit may be too stringent. There are other tools available to designers such as finite element modelling which can demonstrate the suitability of HSS in plastic analysis, however further experimental studies may be necessary in order to validate such models.

3.5 Concluding remarks

This chapter has presented the experimental method as well as the stress-strain response and tensile properties of five different HSS grades with different alloying, heat treatments and/or production route at room temperature. It was demonstrated that the shape of the stress-strain response is strongly dependent on the material history; in particular, steel B (S700MC) which exhibited a nonlinear stress-strain response was most likely related to the significantly lower carbon levels present compared to the other steel grades tested (0.06% vs 0.15%). In addition, the ductility properties of steels A (S690QL), B (S700MC) and C (S690QL) were assessed following the recommendations specified in the Eurocodes 3 Part 1-1 (2005) and 1-12 (2007). It was found that steels A-C met the requirements in Eurocode 3 Part 1-12 (2007) and steels A (S690QL) and B (S700MC) met the slightly more stringent requirements in the National Annex to Eurocode 3 Part 1-12 (2007). However, steels A (S690QL) and B (S700MC) did not meet the ultimate to yield strength ratio f_u/f_y required for plastic analysis despite meeting the strain at fracture and ultimate to yield strain ratio. This does not necessarily mean that these steels are unsuitable for plastic analysis; further work may be needed to demonstrate design scenarios where HSS are suitable. The tensile properties obtained in this section are used in Chapter 4 as a baseline for comparison with the elevated temperature tensile tests.

Chapter

4

Material properties of high strength steels at elevated temperature

4.1 Introduction

Over recent years, there has been increased effort in obtaining accurate material property data for HSS at elevated temperature, which is necessary to predict the structural response during a fire using both simple analytical methods and advanced finite element analysis. The effort has revealed discrepancies amongst HSS grades which are either due to the different experimental parameters employed or differences in the chemical composition and production/fabrication route. In this chapter, the stress-strain responses of various HSS grades at elevated temperatures were obtained through either isothermal or anisothermal tensile testing. Following a detailed explanation of the experimental study, which considers the influence of strain and heating from the available literature, the material properties of several HSS are presented as reduction factors where the property at elevated temperature is normalised by the corresponding room temperature property presented in the previous chapter. The results are compared with the literature and current Eurocode guidelines (EN 1993-1-2, 2005). It is anticipated that by being consistent with the experimental procedures, discrepancies due to experimental factors will be minimal.

4.2 Elevated temperature tensile testing

4.2.1 Summary of tensile test methods at elevated temperature

Tensile testing at elevated temperature may be conducted under isothermal (steady-state) or anisothermal (transient-state) conditions. In an isothermal test, the temperature of the specimen is equilibrated at the target temperature before straining to failure at a controlled rate. Isothermal tests can also be performed under a controlled stress rate although this method is seldom used because the softening part of the stress-strain diagram is not obtained (Dotreppe, 1997). In an anisothermal test, the specimen is held at a target tensile load and then the temperature is increased at a controlled rate until failure occurs. The total strain (which comprises of mechanical, thermal and sometimes creep strains) is recorded as a function of temperature θ and this can be converted into stress-strain curves (see Figure 4-1) once the effect of thermal expansion has been removed from the data using the appropriate coefficient of thermal expansion.

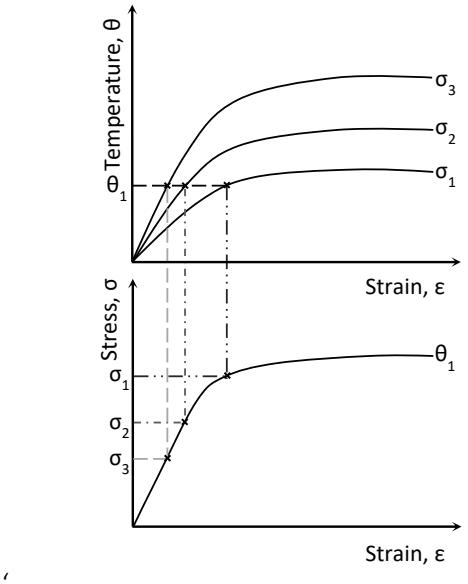

Figure 4-1 Converting temperature-strain curves from transient (anisothermal) test results into stress-strain curves once thermal strain has been removed

Isothermal tests are more commonly conducted because of experimental ease and control and the full stress-strain curves generated can be directly incorporated into complex structural fire resistance analysis (Kodur and Dwaikat, 2010). However, anisothermal tests are considered to be more representative of what steel members would experience in a fire scenario (i.e. constant mechanical loads, transient temperature) and the current European design guidelines are derived from such tests. In a real fire scenario, the behaviour of steel members is complex due to factors

such as creep, irregular rise in temperature and dynamic loads (and strains) and so in reality both test methods have their limitations. The choice of strain rate in isothermal tests or heating rate in anisothermal tests will influence the material properties at temperatures greater than 400°C due to creep effects (Anderberg, 1988). For this reason, test parameters should be chosen to be representative of the expected behaviour of steel members under fire conditions. In this investigation both test methods were used and further details on the experimental methods including equipment and test parameters are explained, hereafter.

4.2.2 Testing device

Identical to the room temperature tensile tests, a Zwick Kappa 100 SS electromechanical testing machine described in Section 3.3.1 was used. In addition, a three-zone electrical furnace, a temperature controller with a maximum temperature capability of 1200°C and the testXpert II V3.6 software which monitored and controlled the mechanical and thermal variables of the system through a digital closed loop control were used.

Three K-type thermocouples were used to monitor the top, middle and bottom temperature of each tensile specimen, which were pressed on to the surface of the specimen. In addition, three K-type thermocouples were placed in the centre of each zone of the electrical furnace. The same extensometer described previously in Section 3.3.1 was used to measure the strain up to 5% before switching to crosshead displacement to estimate the strain for the remainder of the test, to preserve the extensometer. Similar to the room temperature tests, the contact force between the high purity alumina ceramic rods of the extensometer and the tensile specimen was set to 150 g. The extensometer was calibrated up to 1000°C in accordance with ISO 9513, class 1 (ISO 9513, 2012).

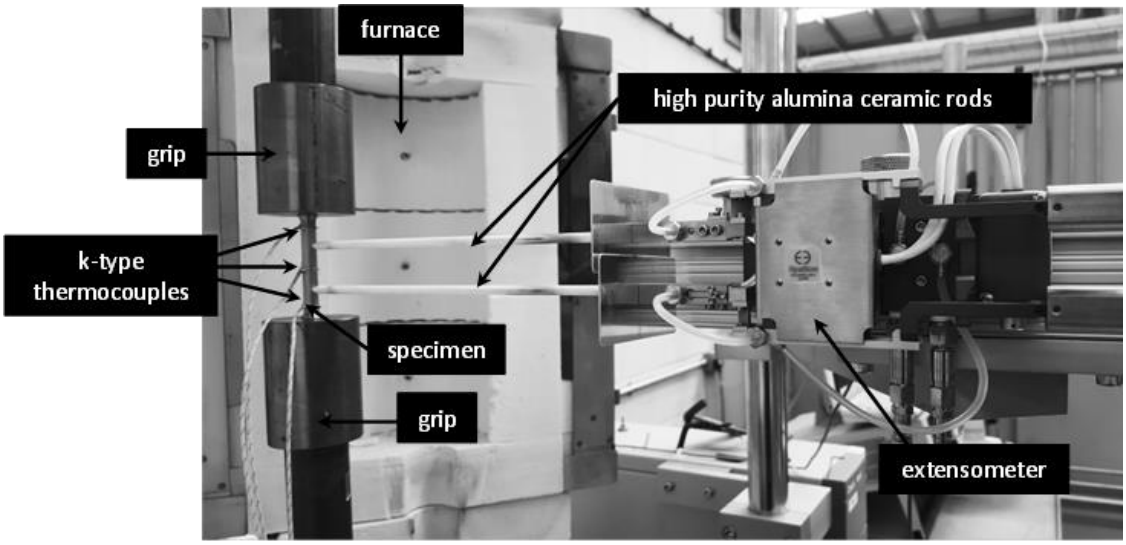

Figure 4-2 Experimental set-up (furnace open)

4.2.3 Test specimens

The same specimen dimensions described in Section 3.3.2 were used. It should be noted that at elevated temperatures, oxidation and creep occur more readily which could influence the effectiveness of the gripping system employed. This, in turn, could lead to unreliable tensile test results. ISO 6892-2 (2011) recommends that when testing above 250°C, flat tensile specimens should be gripped with a bolt or with shouldered holders (form fit) as friction gripping (e.g. wedge grips, parallel grips) may be problematic. Kelly (1998) experienced slippage when using compressive grips for tensile tests from 300°C to 750°C. To eliminate this effect in the present study pinned grips were used. For round specimens, threaded ends are typically used (ISO 6892-2, 2011). In other similar work, flat specimens were held with pinned joint and round specimens with a threaded grip (Outinen, 2007).

4.2.4 Isothermal (steady-state) testing

4.2.4.1 Standards

Isothermal tests for metallic materials are standardised in ISO 6892-2 (2011) and ASTM E21-09 (2009). Although these standards were not intended for obtaining properties specifically for structural fire design guidelines (i.e. parameters such as the strain rate may not necessarily correlate with the anticipated strain rate in a fire scenario), these standards are useful for considering how the strength and stiffness change with temperature.

4.2.4.2 Experimental method

Isothermal tests were conducted on steels A-D at selected temperatures. In the isothermal tests for steels A (S690QL) and B (S700MC), the temperature of the specimen was equilibrated at the target temperatures of 100, 200, 300, 400, 500, 600, 700 and 800°C with additional duplicate tests at 100, 400, 500 and 600°C. Similarly, for steels C (S690QL) and D (S460NH), the temperature of the specimen was equilibrated at the target temperatures of 400, 500 and 600°C. Heating rates in isothermal tests need to be controlled to ensure uniform and stable temperature distribution, in a time frame that does not allow any significant change in microstructure or properties to occur. The heating rates used in this study are shown in Table 4-1. In cases where the target temperature was greater than 400°C, a rate of 10°C/min was employed although this was reduced to 3°C/min when the temperature reached 80% of the target value in order to avoid temperature overshoot and to ensure the prescribed temperature was reached within the limits of ±3°C. This ensured that the entire parallel length of the specimen reached thermal equilibrium by the time the target temperature was achieved. Tests conducted at 100, 200, 300 and 400°C took approximately one hour to reach, and stabilise at, the target temperature. At such

temperatures, a one hour heating time has a minimal effect on the strength or stiffness, as limited microstructural effects would be expected (Smith et al., 1981). Once thermal equilibrium was reached, a pre-load of 300N was used to remove any slack introduced to the components of the testing machine due to thermal expansion during the heating process. Then the extensometer was placed in contact with the specimen through the slot of the furnace prior to straining of the specimen at a controlled rate.

Table 4-1 Heating rates used in this experimental programme

Target temperature (°C)	Heating rate (°C/min)
100	2
200	3
300	5
>400	10

4.2.4.3 Strain rate

At room temperature, moderate changes in strain rate have minor influences on the resulting tensile properties. However, at elevated temperature, moderate changes in the strain rate can have a significant influence on the resulting tensile properties because the strain-rate sensitivity increases at elevated temperatures. For this reason, ISO 6892-2 (2011), recommend using strain rate control to "minimise the variation of the test rates during the moment when strain rate sensitive parameters are determined and to minimize the measurement uncertainty of the test results" (ISO 6892-2, 2011). The effect of strain rate on the material properties of S355 at elevated temperature have been studied by Knobloch et al. (2013). In their study, three different strain rates were considered: 0.0002, 0.001 and 0.005/min. Their findings showed that the strength degradation of S355 at elevated temperatures did not correlate well with recommended reduction factors in the European design guidelines when the strain rate was 0.0002/min or 0.001/min. However, there was good agreement between the experimental data on S355 and the European design guidelines when the strain rate was 0.005/min, which is the same strain rate recommended in the standards for elevated temperature tensile testing (ISO 6892-2, 2011; ASTM, 2009). There is little evidence to suggest if this strain rate (i.e. 0.005/min) is representative of the strain rates likely to be encountered in a fire scenario. In addition, with the inherent variability of various factors mentioned earlier (i.e. creep, irregular rise in temperature and dynamic loads and strains), it is likely that the strain rate may not even be constant during a fire. Studies from standard fire resistance tests on beams (which follow the ISO 834 heating curve and not a natural fire behaviour) reported by Rubert and Schaumann (1986), showed that the strain (measured at the mid span deflection of the beam) rose steadily with increasing temperature,

and then rapidly increased near the limit of deflection. The strain rates in the steady region was approximately 0.001/min. However, choosing an appropriate strain rate to use for obtaining material properties to reflect the behaviour in a real fire scenario is not clear.

In order to be consistent with previous research (e.g. (Chen et al., 2006; Qiang, F. Bijlaard, et al., 2012)), so that the data from this study can be fairly compared with the literature, a strain rate of 0.005± 0.002/min was adopted throughout the current investigation. This strain rate is in line with ASTM E21 (2009) and is less stringent compared with ISO 689-2 (2011) recommended strain rate of 0.0042 ± 0.00084/min.

4.2.4.4 Experimental results

Examples of the tensile specimen for steels A (S690QL), B (S700MC) and C (S690QL) which were strained to failure are shown in Figure 4-3 to Figure 4-5. All specimens necked prior to fracture and steel A (S690QL) at 800°C did not fracture as the maximum extension of the testing machine was reached before fracture General observations are the noticeable discolouration on the surface of the tensile specimens which is evident at temperatures of 300°C and above due to oxidation. Further analysis of the fractured tensile specimens is presented in Section 5.3.2.

The engineering stress-strain curves obtained from isothermal tests for steels A to D are shown in Figure 4-6 to Figure 4-12. For steel D (S460NH), tests were recorded up to 6% strain because the maximum displacement of the testing machine was reached before the specimen failed as mentioned in Section 3.4.1. General observations are that as the temperature increases the strength decreases and it becomes harder to distinguish between the linear and nonlinear portions of the stress-strain response as the linear elastic part of the stress-strain curve also decreases. This is particularly evident for steel C (S690QL) and D (S460NH), where at room temperature (20°C) the stress-strain curve is bilinear.

It is noteworthy that the ductility (represented by final strain) presented in Figure 4-6, Figure 4-8 and Figure 4-10 is based on the gauge length of the extensometer. Typically, the gauge length L_0 (where $L_0=5.65\sqrt{A_0}$) would be marked on the specimen surface to measure the ductility in accordance with Eurocode 3 Part 1-1 (2005), but these marks were difficult to determine on some of the specimens because the specimens oxidised when exposed to elevated temperatures. The ductility of steels A (S690QL) and B (S700MC) from 100 to 400°C is lower than that at room temperature (20°C) as shown in Figures 4-8 and 4-10 and this is attributed to the metallurgical phenomenon known as dynamic strain ageing (DSA) or “blue brittleness”. DSA occurs as a result of simultaneous influence of plastic deformation and temperature; the temperature should be

high enough for solute atoms, primarily carbon and nitrogen to diffuse ahead of dislocations post yield to further hinder dislocation movement but not so high that the solute atoms move together with the dislocations (Dolzhenkov, 1967; Kubin and Estrin, 1991). DSA is typically accompanied by "serrations" or "saw tooth shape" in the stress-strain response, however it can still occur in materials without these physical observations (Atkinson and Yu, 1997). For both steels A (S90QL) and B (S700MC), the ductility was lowest at 200°C. Reduced ductility between 100 and 400°C has also been observed in other elevated temperature tensile tests on other types of steels (Calado et al., 2008; Hu et al., 2009; Wang et al., 2013a).

Differentiating steels which suffer a reduced ductility between 100 and 400° is a challenge because of the numerous metallurgical influences linked to the differences in the chemical composition and manufacturing route of various steels. As little as 0.01% of carbon or nitrogen solute atoms in solution are required for DSA to occur (Total Materia, 2013). Whilst all steels contain carbon and/or nitrogen, both can interact with other elements such as vanadium, titanium and niobium to form carbides or nitrides, which can reduce the chances of DSA occurring due to the lack of carbon or nitrogen solute atoms. The reduced ductility of HSS in this temperature range, raises questions about the anticipated failure modes at elevated temperature, and may need to be considered in the design of HSS in scenarios such as connections where plastic analysis is important.

Figure 4-3 Steel A (S690QL) tensile specimes after isothermal tensile tests at various elevated temperatures

Figure 4-4 Steel B (S700MC) tensile specimes after isothermal tensile tests at various elevated temperatures

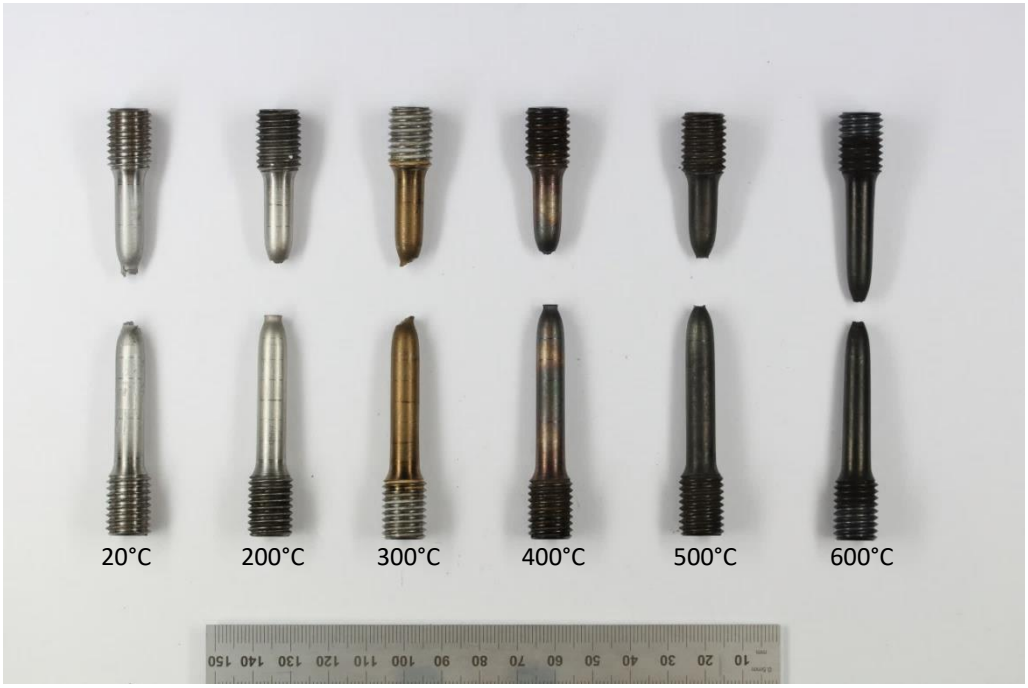

Figure 4-5 Steel C (S690QL) tensile specimes after isothermal tensile tests at various elevated temperatures

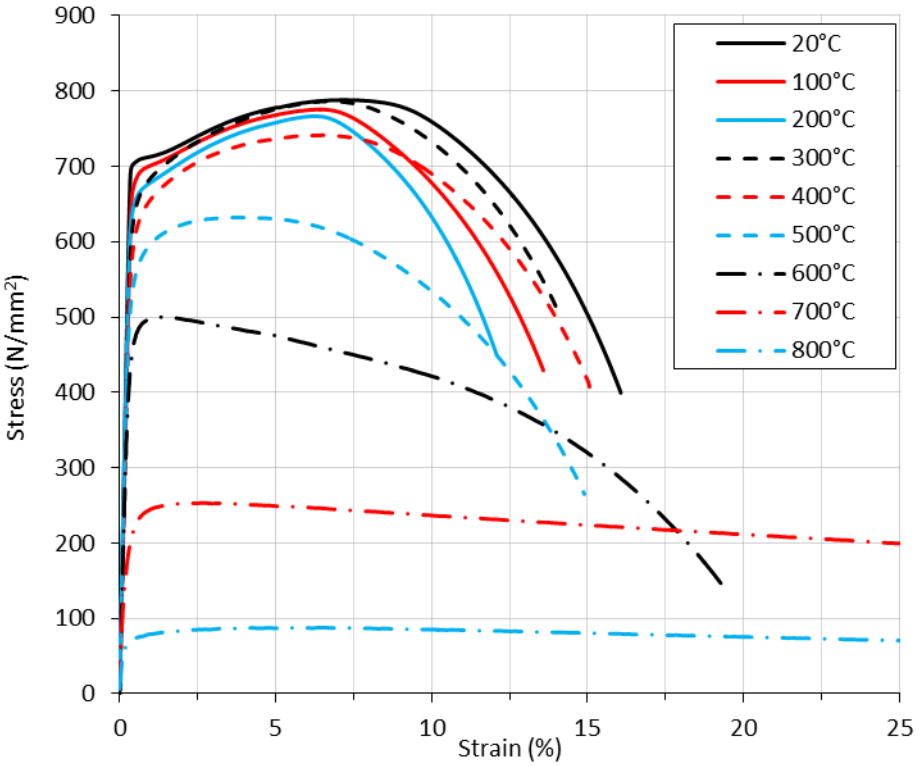

Figure 4-6 Engineering stress-strain response for steel A (S690QL) at strains up to 25%

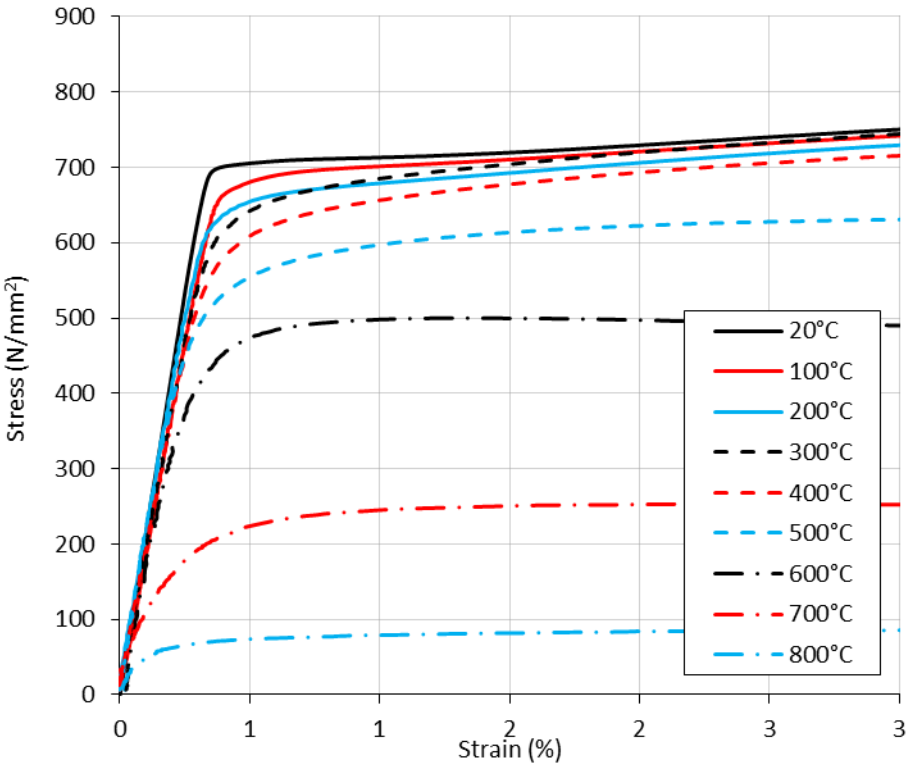

Figure 4-7 Engineering stress-strain response for steel A (S690QL) at strains up to 3%

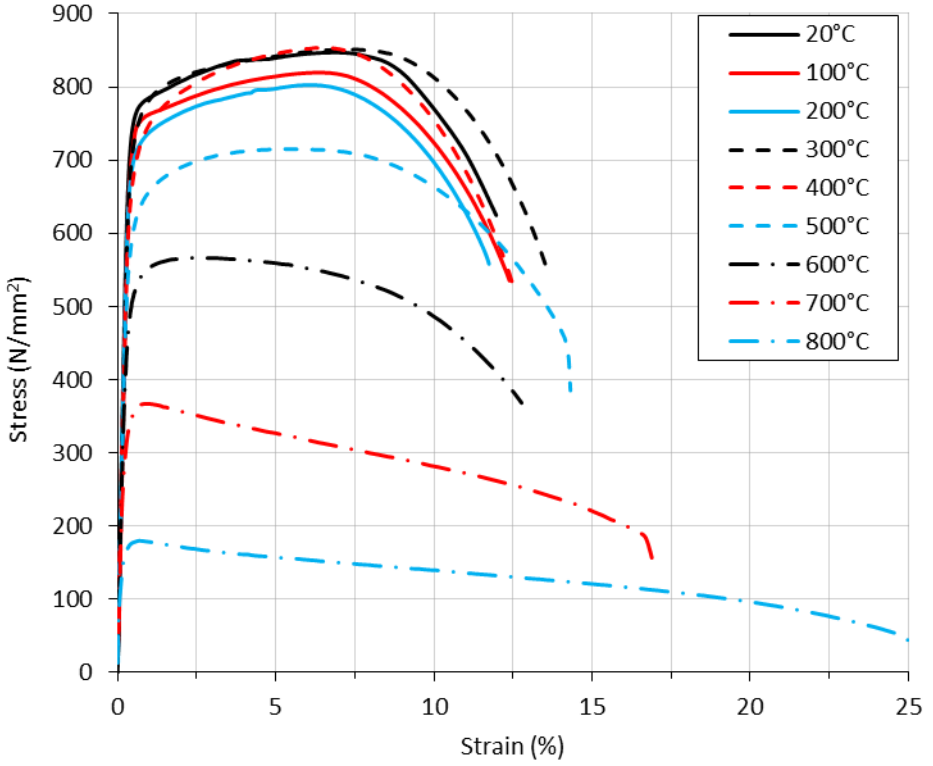

Figure 4-8 Engineering stress-strain response for steel B (S700MC) at strains up to 25%

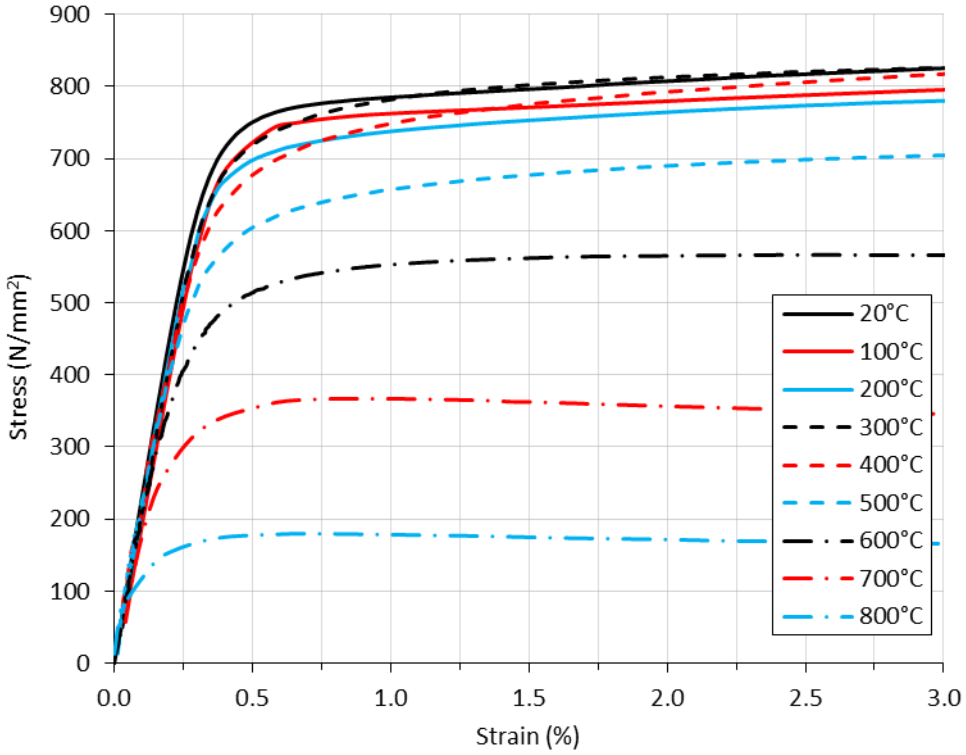

Figure 4-9 Engineering stress-strain response for steel B (S700MC) at strains up to 3%

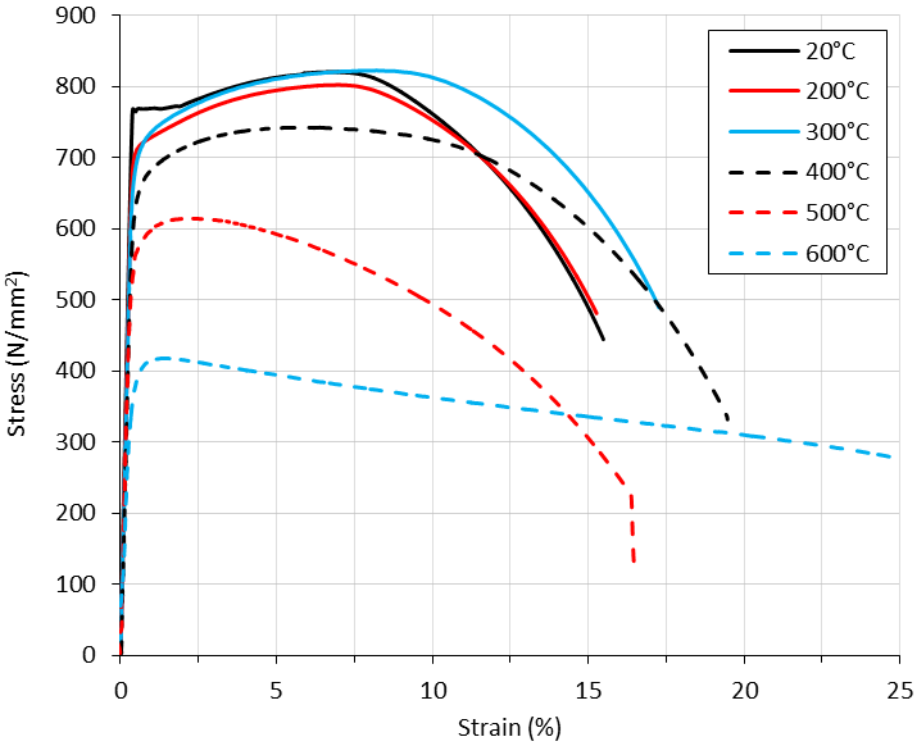

Figure 4-10 Engineering stress-strain response for steel C (S690QL) at strains up to 25%

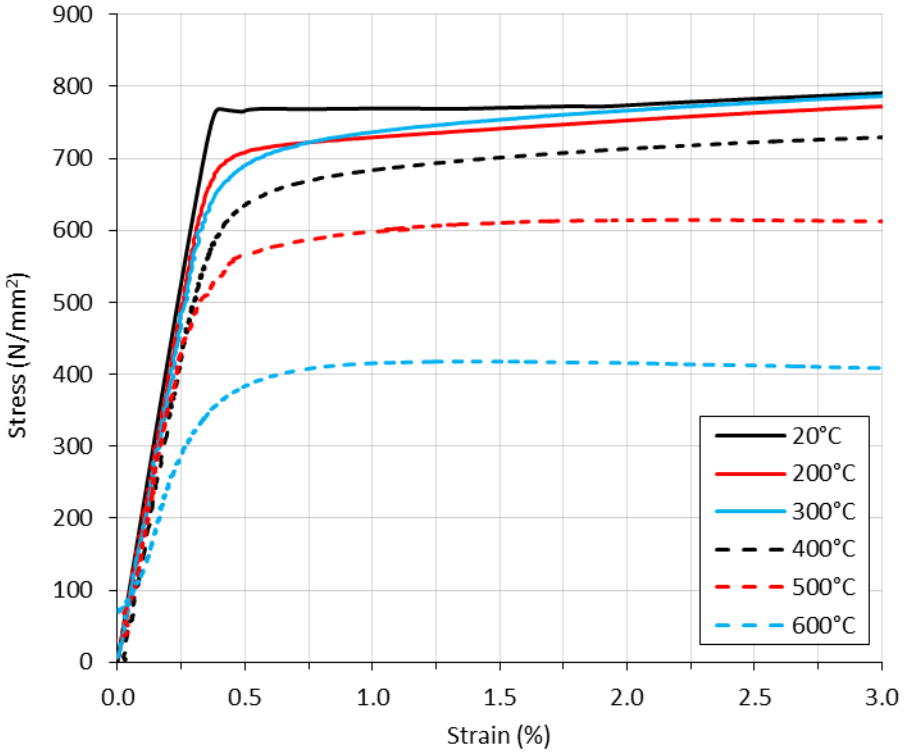

Figure 4-11 Engineering stress-strain response for steel C (S690QL)) at strains up to 3%

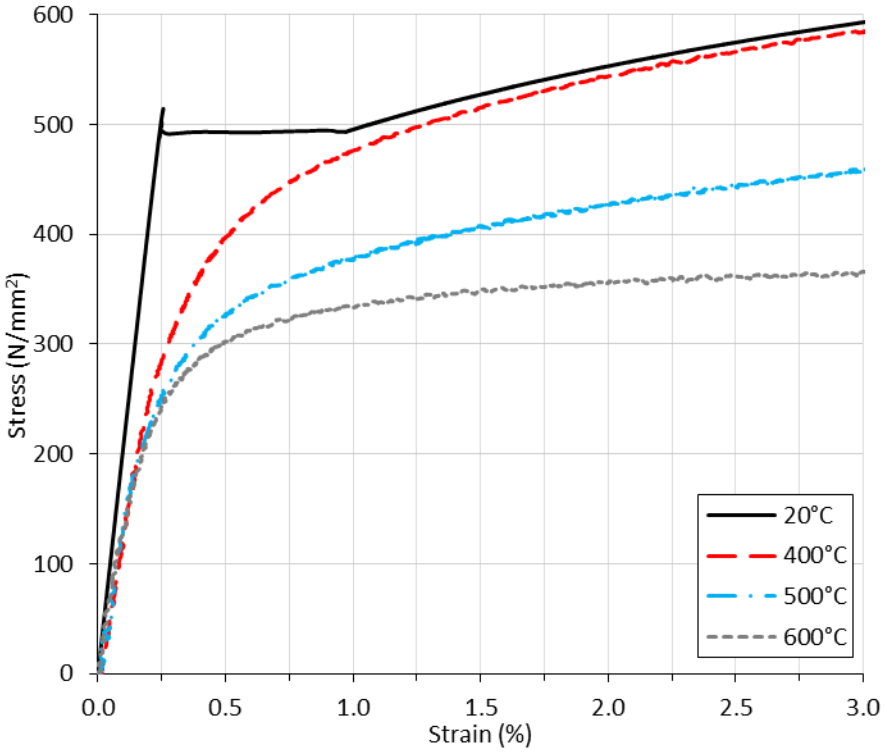

Figure 4-12 Engineering stress-strain response for steel D (S460NH) at strains up to 3%

4.2.5 Anisothermal (transient-state) testing

4.2.5.1 Standards

To date, there are no standardised procedures for anisothermal testing at elevated temperature, however as previously mentioned, the reduction factors presented in Eurocode 3 Part 1-2 (2005) are derived from such tests. This method is considered to be more representative of the conditions that a structural material may experience under real fire conditions because the influence of creep is implicitly included in the stress-strain response through the choice of mechanical load(s) and heating rate. Moreover, real fire occurs in an anisothermal manner. Generally, creep influences are more prominent at higher mechanical loads and/or slow heating rates.

4.2.5.2 Experimental method

In the anisothermal tests, the specimens were held at a target tensile load for the duration of the test whilst the temperature was increased at a controlled rate of 10°C/min until a temperature of 900°C was reached or the tensile load could no longer be maintained at the 'runaway' strain (which could be correlated to strains reached in steel beams or columns where failure is imminent (Kirby and Preston, 1988)). Owing to time and cost constraints, it was not feasible to conduct anisothermal tests on all materials considered in this study. Therefore, steels

A (S690QL) and B (S700MC) were selected for detailed transient testing because they demonstrated better strength and stiffness retention properties compared with the other steels C (S690QL) and D (S460NH) in the isothermal tests.

Nine tensile loads were chosen as multiples of 80, ranging from 80 to 720 N/mm^2 (i.e., 80, 160, 240 N/mm^2, etc.). For steel B (S700MC), additional tests were conducted at 760 and 800 N/mm^2 to obtain sufficient data to determine the effective yield strength at 2.0% total strain at temperatures between 100 and 800°C. The loads were chosen to lie within 10-90% of the measured tensile strength at room temperature and calculated based on the initial cross-section of the tensile specimen. Duplicate tests were conducted at 80, 160, 240, 320, 400 and 480 N/mm^2. Throughout the test, the total strain was recorded using the axial contact extensometer as a function of the average temperature θ taken from the top, middle and bottom thermocouples attached within the gauge length of the specimen and included the following: (i) the mechanical (elastic and plastic) strain introduced when the tensile load was applied at room temperature, (ii) the creep strain which is implicitly accounted for and (iii) the thermal strain as a result of thermal expansion (Anderberg, 1988). In order to deduct the influence of the thermal expansion from the total strain, separate tests were conducted using minimal load of 1 N/mm^2, which is similar to other researchers (Manninen and Säynäjäkangas, 2012).

The results from these tests are presented in Figure 4-13. The key observation is that the measured strains with a minimal load of 1 N/mm^2 for steel A (S690QL) and B (S700MC) are lower than the Eurocode values. The relative elongation is independent of production route and small changes in the chemical composition as mentioned in Section 2.4.2.1 and so the discrepancy is most likely related to the experimental set-up. One possible reason is the influence of the minimal load, 1 N/mm^2 on the specimen, as similar results have been observed in the work of Chen and Young (2008).

It is noted that to get a true measurement of the thermal expansion of the material would require alternative experimental set ups. The set-up used by Li and Young (2017) involved gripping only one end of the specimen and allowing the other end to freely expand. Alternatively, Xiong and Liew (2016), used much longer specimens compared to the specimens in this work (i.e. 597.5 vs 90 mm), with the gripping system outside the furnace. This meant that any possible interference between the specimen and the grips was far from the region of the specimen where strain was measured. Such experimental set-ups were not possible with the testing device used in this work. However, due to the experimental set-up used in this work, the measured strain using minimal

load of 1 N/mm^2 is considered representative of the thermal strains measured during the anisothermal tests.

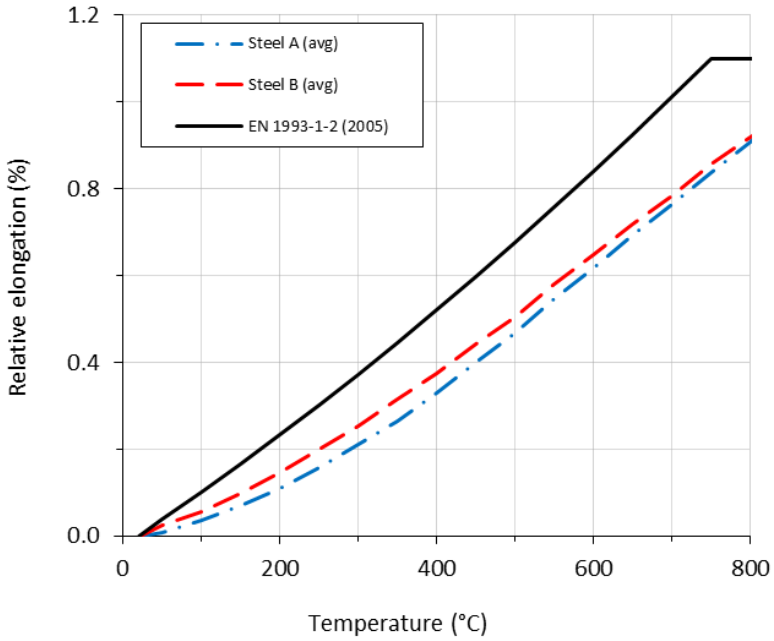

Figure 4-13 Thermal strains measured using 1 N/mm^2 load vs. Eurocode approach

4.2.5.3 Heating rate

In structural fire design, heating rates for steel should be within the range of 2 to 50°C/min as specified in Eurocode 3 Part 1-2 (EN 1993-1-2, 2005) in order to reflect real fire behaviour. Typically, a rate of 3°C/min is representative of a heavily insulated steel member in a typical building fire whilst 50°C/min is more characteristic of a non-insulated steel member (Twilt, 1988). A heating rate of 10°C/min represents a heavily loaded steel member (i.e. a load ratio of 0.6) surviving for approximately 1 hour in accordance with the ISO 834 (1999) standard fire resistance tests. For such a time frame, some creep will develop but its significance to the overall fire resistance of a steel member is dependent on factors such as boundary conditions (e.g. restrained ends). A heating rate of 10°C/min has been regularly used in literature (e.g. Kirby and Preston, 1988; Qiang et al; Choi et al., 2014) and the reduction factors in Eurocode 3 Part 1-2 (EN 1993-1-2, 2005), where derived using this heating rate (Kirby and Preston, 1988). Hence, to be able to compare the results from this programme with Eurocode 3 Part 1-2 (EN 1993-1-2, 2005) and other researchers a heating rate of 10°C/min was adopted throughout these tests.

4.2.5.4 Experimental results

The engineering stress-strain curves obtained from anisothermal tests for steels A (S690QL) and B (S700MC) are shown in Figure 4-14 and Figure 4-15, respectively. General observation is that the shape of the stress-strain responses are not as smooth as those obtained from the isothermal tests (presented in Figure 4-6 to Figure 4-9). This is because each point in the anisothermal stress-strain response was determined from one coupon test at a particular temperature. At higher temperatures (such as 700°C), there was a limited number of data points available since the failure temperature decreased as the applied tensile load increased.

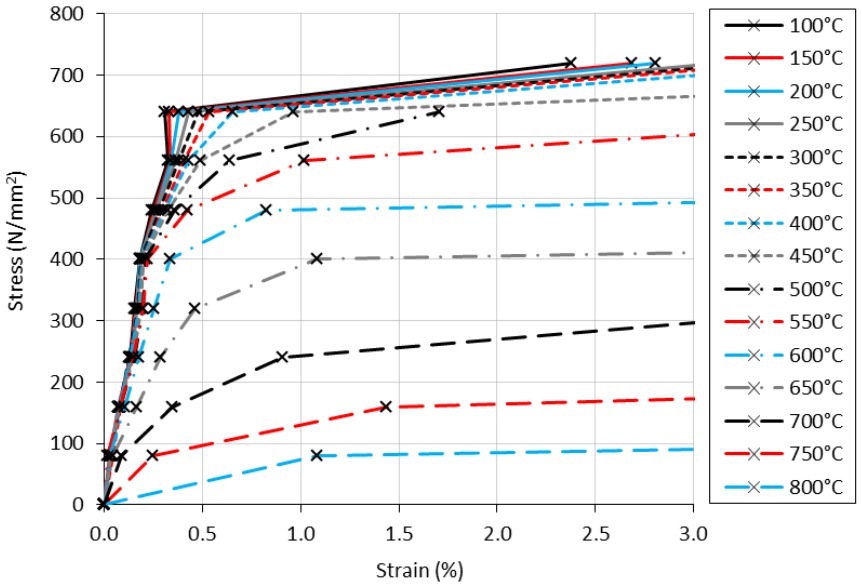

Figure 4-14 Engineering stress-strain curve of steel A (S690QL)

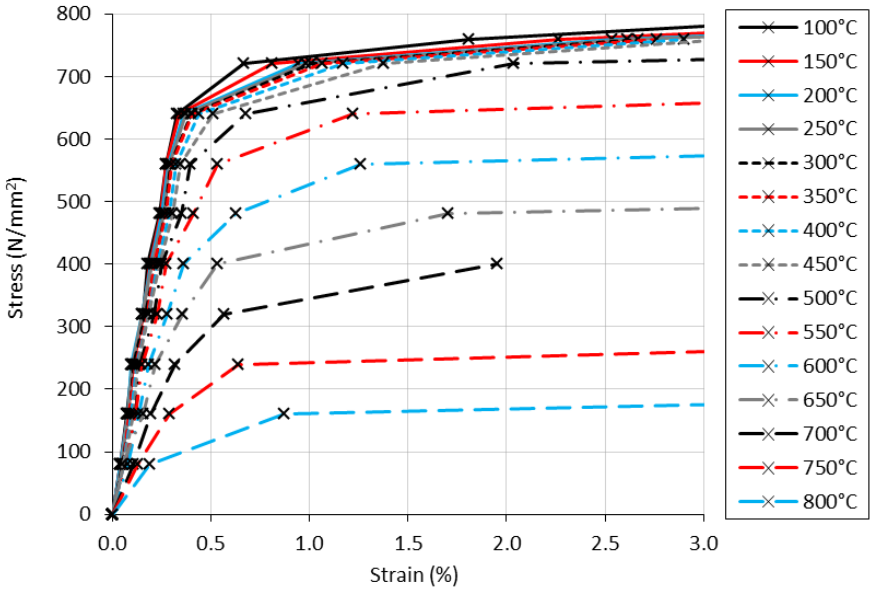

Figure 4-15 Engineering stress-strain curve of steel B (S700MC)

4.3 Reduction factors

4.3.1 Definition

Reduction factors are used in the Eurocodes (including Eurocode 3 Part 1-2 (2005)) to express how the strength and stiffness properties degrade with increasing temperature and are defined as the ratio between the mechanical property being considered at elevated temperature θ and the corresponding property at room temperature, which could be the measured or the nominal (design) property. Reduction factors are also commonly used to compare material properties derived from isothermal and anisothermal conditions.

4.3.2 Key parameters measured

At elevated temperature, the yield strength becomes increasingly difficult to quantify because of the large strains exhibited and the increasing nonlinearity of the stress-strain response. Eurocode 3 Part 1-2 (2005) idealises the stress-strain response at elevated temperature as illustrated in Figure 4-16. The response is assumed to be linear up to the proportional limit ($f_{p,\theta}$) and this is followed by an elliptical representation until the maximum stress ($f_{y,\theta}$) is achieved at a strain of $\varepsilon_{y,\theta}$, where $\varepsilon_{y,\theta}$ is commonly defined as the total strain level at 2.0% (Wang et al., 2012). Following this, a constant strength is assumed between $\varepsilon_{y,\theta}$. The 0.2% proof strength ($f_{0.2p,\theta}$) also shown Figure 4-16 is defined as the strength where the proportional line offset at 0.2% strain intersects the stress-strain curve.

The following section presents the reduction factors for the proportional limit, 0.2% proof strength, the effective yield strength (i.e. the strength at 2% total strain) and elastic modulus of steels A-D obtained under isothermal and/or anisothermal conditions. The reduction factors obtained are also compared with published data for similar steel grades where tests were similarly conducted under isothermal or anisothermal conditions (e.g. (Chen et al., 2006; Qiang, F. Bijlaard, et al., 2012; Choi et al., 2014)) and the design curves given in Eurocode 3 Part 1-2 (2005).

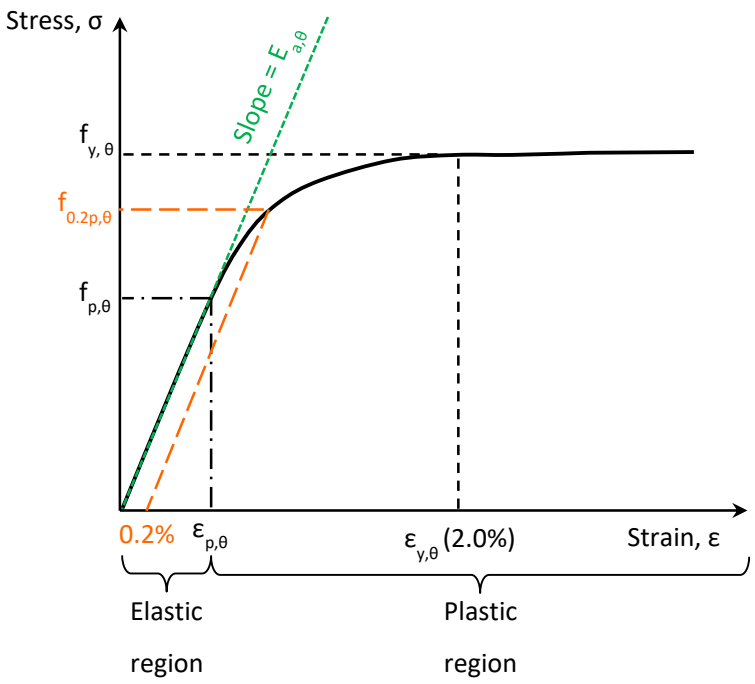

Figure 4-16 Key parameters measured from the stress-strain response at temperature θ

4.3.3 Proportional limit

As stated in the previous section, the proportional limit ($f_{p,\theta}$) is defined as the point where the stress-strain response changes from linear to nonlinear. This was determined as the point where the stress-strain curve deviates from the initial elastic modulus. The rationale for introducing the proportional limit values into the Eurocodes at elevated temperatures was to capture the viscoelastic behaviour, which is partly due to creep (Kodur et al., 2010).

The reduction factors for the proportional limit (i.e. $k_{p,\theta} = f_{p,\theta}/f_{y,20}$) of steels A-D were derived by normalising the measured yield strength at room temperature $f_{y,20}$ and the nominal (design) yield strength. $f_{y,20}$ was taken as the 0.2% proof strength for consistency as distinct yield points were not observed in the stress-strain response of the HSS grades tested. Table 4-2 shows the reduction factors obtained under isothermal conditions for steels A-D. Proportional limits for the anisothermal tests were not obtained because to determine the transition of the stress-strain response from linear to nonlinear requires conducting tests at much smaller load intervals than those used (i.e. less than 80 N/mm^2).

The reduction factors of the proportional limits for the steels A-D are presented in Figure 4-17 along with the Eurocode approach (EN 1993-1-2, 2005). Figure 4-18 also presents the reduction factors along with similar results from another test programme (i.e. (Lange and Wohlfeil, 2010;

Choi et al., 2014)) and Eurocode 3 Part 1-2 (2005). From Figure 4-17 it can be seen that the Eurocode predictions for the proportional limit are generally unconservative (i.e. not safe) at temperatures below 300°C and 200°C, when the proportional limit was normalised by the measured and nominal yield strength, respectively. Only the behaviour of steels C (S690QL) and D (S460NH) are safely or conservatively predicted by the Eurocode curve.

A similar trend is observed when examining the results from published literature, as shown in Figure 4-18. From Figure 4-18 it can be seen that at low levels of elevated temperature (i.e. from 20 up to 400°C), the reduction factors provided in the Eurocode are unconservative for the remaining steels tested in this programme and those reported by Lange and Wohlfeil (2010), Choi et al, (2014) and Xiong and Liew (2016). The standard predicts that the material will have greater strength retention than indicated by the test results because it is assumed that at 20 and 100°C the stress-strain curve is perfectly bilinear, meaning that the steel behaves in a linear-elastic manner up to the proportional limit and then exhibits a yield plateau such that $f_{p,\theta} = f_{y,\theta}$. However, for steels A (S690QL), B (S700MC) and D (S460NH), the stress-strain response is not perfectly bilinear at 20 and 100°C, especially for steel B (S700MC) where no distinctive yield point was observed as shown earlier in Figure 4-9. Above 300°C for steels A (S690QL) , HSA800 (as discussed by Choi et al. (2014)) and RQT 701 (Xiong and Liew, 2016), and 400°C for steel B (S700MC), the reduction factors provided in the Eurocode are conservative and are shown to provide a good representation of the behaviour. For S460N and S460M tested by Lange and Wohlfeil (2010), the Eurocode is unconservative and over predicts the proportional limit at 800 and 900°C.

Table 4-2 Reduction factors for the proportional limit obtained from isothermal tests

Temperature (°C)	Steel A (S690QL)	Steel B (S700MC)	Steel C (S690QL)	Steel D (S460NH)
20	0.84	0.56	0.99	0.99
100	0.76, 0.70	0.73 0.80	-	-
200	0.76	0.64	0.90	-
300	0.69	0.61	0.78	-
400	0.62 0.65	0.48, 0.50	0.65	0.50
500	0.47, 0.49	0.47, 0.46	0.59	0.38
600	0.41, 0.41	0.42, 0.43	0.34	0.42
700	0.16	0.25	-	-
800	0.06	0.15	-	-

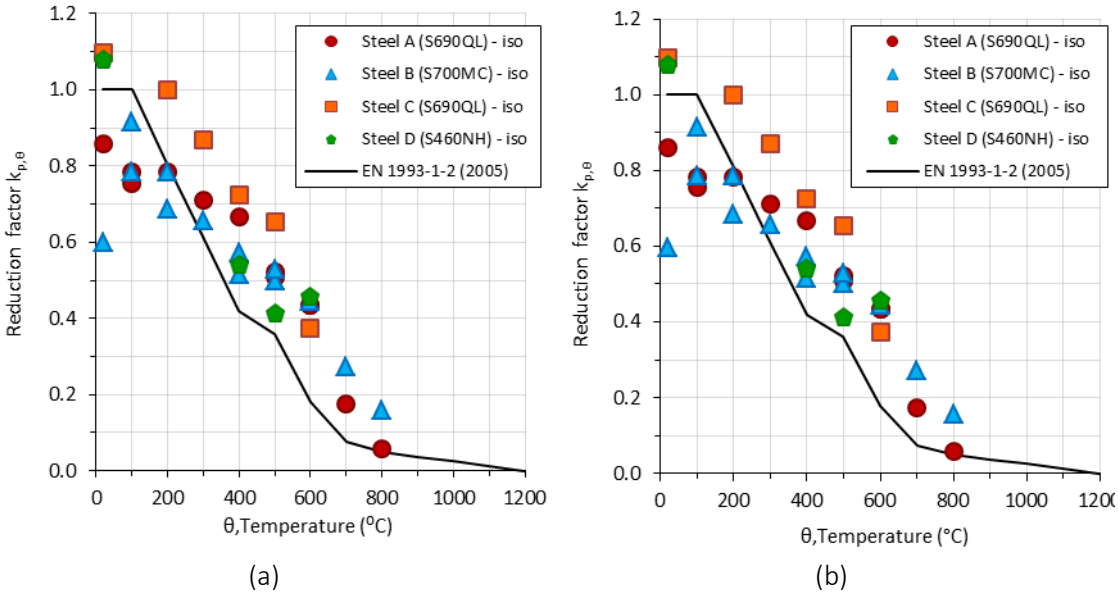

Figure 4-17 Comparison of the reduction factors for the proportional limit ($k_{p,\theta} = f_{p,\theta}/f_{y,20}$) normalised by the (a) measured 0.2% proof strength at room temperature and (b) the nominal yield strength with EN 1993-1-2 (2005)

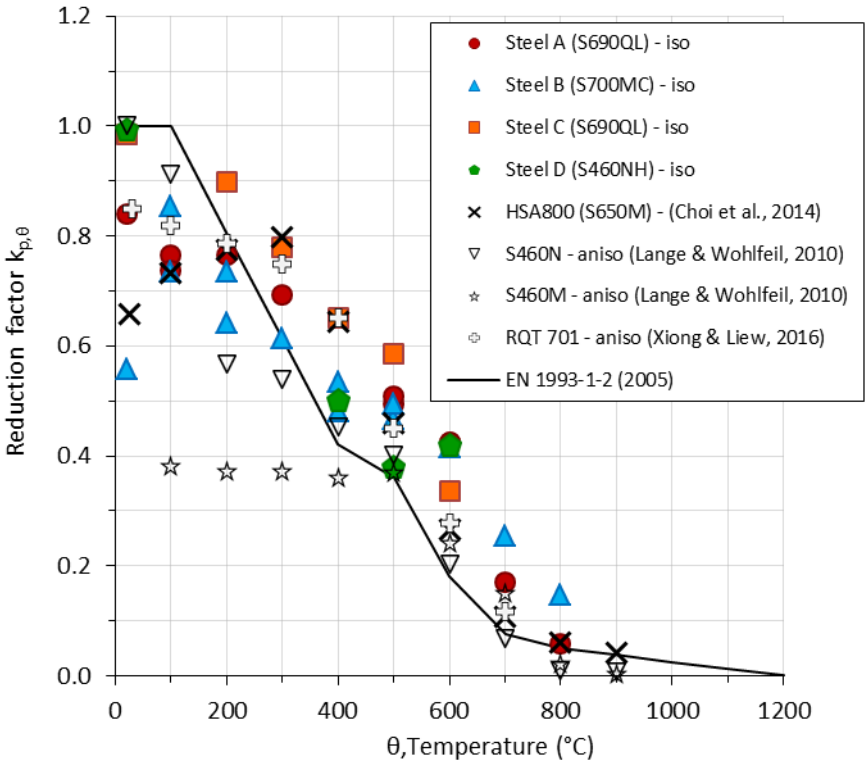

Figure 4-18 Comparison of the reduction factors for the proportional limit ($k_{p,\theta} = f_{p,\theta}/f_{y,20}$) normalised by the measured yield strength at room temperature with EN 1993-1-2 (2005) and available literature

4.3.4 0.2% proof strength

As the yield stress is difficult to identify in materials with a nonlinear stress-strain response where no distinctive yield point is observed (e.g. TMCP steel and stainless steel), the yield strength at room temperature is usually defined in terms of a proof stress at a particular offset strain, typically 0.2% strain (see Figure 4-16). The 0.2% proof stress is also used in the design of class 4 (slender) steel members in accordance with the Eurocode 3 Part 1-1 (2005), where local buckling will occur before the yield strength is reached in one or more parts of the cross-section.

The reduction factors for the 0.2% proof strength for steels A-D at elevated temperatures (i.e. $k_{0.2p,\theta} = f_{0.2p,\theta}/f_{0.2p,20}$) under isothermal and anisothermal conditions are presented in Table 4-3 and Table 4-4, respectively. Figure 4-19 depicts the reduction factors of the 0.2% proof strength at elevated temperatures (i.e. $k_{0.2p,\theta} = f_{0.2p,\theta}/f_{0.2p,20}$) for steels A-D with the Eurocode approach provided in Annex E of the Eurocode 3 Part 1-2 (2005). Similar to the previous section, the reduction factors presented in Figure 4-19 (a) and (b) are derived by normalising by the measured 0.2% proof strength and nominal yield strength, respectively. Similar data for S460 grades in the literature are limited, with only Qiang et al. (2012), presenting data on S460N under anisothermal conditions. A comparison of the reduction factors for steel D (S460NH) with S460N tested by Qiang et al. (2012) are presented in Figure 4-20. Figure 4-21 presents comparisons of the reduction factors of the 0.2% proof strength at elevated temperatures for steels A-C with similar steel grades ranging from S650-S700 from the literature.

From Figure 4-19 (a), it can be seen that generally, the reduction factors provided in the Eurocode are conservative and adequate for depicting the reduction in the 0.2% proof strength at temperatures greater than 100°C under isothermal conditions for steels A-C and 200°C under anisothermal conditions for steel A (S690QL) and B (S700MC), when normalised by the measured property. Figure 4-19 (b), demonstrated that the reduction factors provided in the Eurocode are conservative with respect to the reduction factors for steels A-D under isothermal conditions, and conservative from temperatures greater than 150°C for steels A (S690QL) and B (S700MC) under anisothermal conditions. From 700°C onwards, steel B (S700MC) retained a higher proportion of its 0.2% proof strength compared to steel A (S690QL).

From Figure 4-20, it can be seen that the reduction factors presented by Qiang et al. (2012) are unconservatively and unsafely depicted by the Eurocode approach between 100 and 300°C. However, from 300°C the Eurocode approach is conservative (i.e. safe) with respect to the reduction factors for S460N.

With reference to Figure 4-21, steels A-C follow the same trend to the steels from literature. The scatter amongst the different steel grades in the literature is very large with many of the steels including S690QL tested by Qiang (2013) at 700°C, RQT S690 tested by Chiew et al. (2014) at temperatures greater than 500°C and S690QL from Neuenschwander et al. (2017) above 550°C, unconservatively (i.e. not safely) represented by the Eurocode curve. The large discrepancy with the Eurocode is most likely related to the material history, particularly the chemical composition which was presented in Table 3-2. The influence of the material history is discussed further in Chapter 7. Only HSA800 a TMCP steel tested by Choi et al. (2014) under isothermal conditions met or exceeded the $k_{0.2p,\theta}$ reduction factors from the Eurocode at all temperatures.

Table 4-3 Reduction factors for the 0.2% proof strength obtained from isothermal tests

Temperature (°C)	Steel A (S690QL)	Steel B (S700MC)	Steel C (S690QL)	Steel D (S460NH)
20	1.00	1.00	1.00	1.00
100	0.98, 0.94	0.99, 0.99	-	
200	0.95	0.94	0.93	
300	0.92	0.98	0.92	
400	0.91, 0.85	0.92, 0.80	0.84	0.78
500	0.80, 0.72	0.81, 0.80	0.74	0.63
600	0.63, 0.67	0.68, 0.66	0.50	0.60
700	0.32	0.47	-	
800	0.10	0.23	-	

Table 4-4 Reduction factors for the 0.2% proof strength obtained from anisothermal tests

Temperature (°C)	Steel A (S690QL)	Steel B (S700MC)
20	1.00	1.00
100	0.92	0.91
150	0.91	0.89
200	0.88	0.88
250	0.88	0.89
300	0.89	0.87
350	0.88	0.87
400	0.90	0.87
450	0.86	0.86
500	0.79	0.82
550	0.71	0.76
600	0.60	0.61
650	0.46	0.54
700	0.24	0.43
650	0.14	0.30
800	0.11	0.15

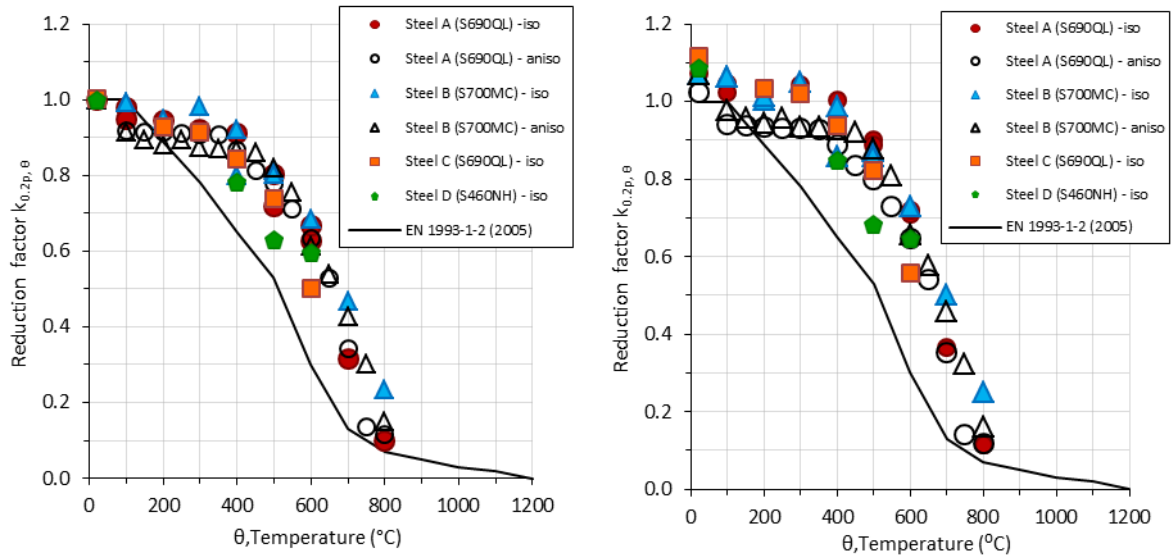

Figure 4-19 Comparison of the reduction factors of the 0.2% proof strength ($k_{0.2p,\theta} = f_{0.2p,\theta}/f_{0.2p,20}$) normalised by the (a)measured 0.2% proof strength at room temperature and (b) the nominal yield strength with EN 1993-1-2 (2005)

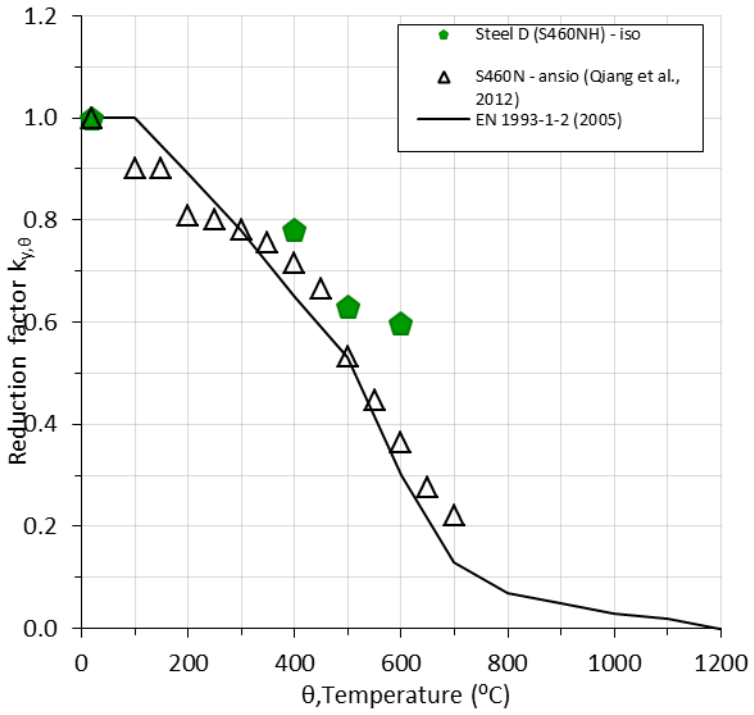

Figure 4-20 Comparison of the reduction factors of the 0.2% proof strength ($k_{0.2p,\theta} = f_{0.2p,\theta}/f_{0.2p,20}$) normalised by the measured 0.2% proof strength at room temperature with EN 1993-1-2 (2005) and Qiang et al. (2012)

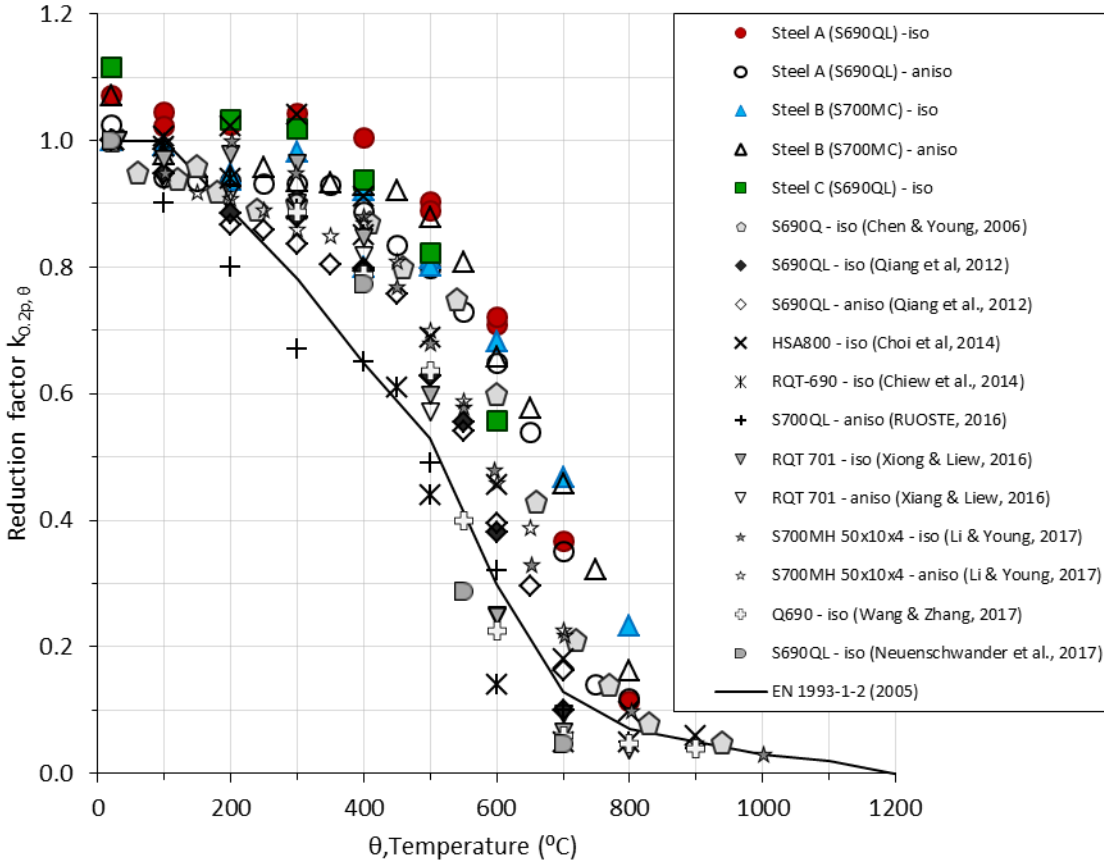

Figure 4-21 Comparison of the reduction factors of the 0.2% proof strength ($k_{0.2p,\theta} = f_{0.2p,\theta}/f_{0.2p,20}$) normalised by the measured 0.2% proof strength at room temperature with EN 1993-1-2 (2005) and available literature on S650-S700

4.3.5 Effective yield strength

As mentioned in Section 2.4.3.3, the effective yield strength is often defined as the strength at 2.0% total strain. The reduction factors for the effective yield strength (i.e. $k_{y,\theta} = f_{y,\theta}/f_{y,20}$) of steels A-D under isothermal conditions are presented in Table 4-5, whilst the reduction factors for steels A and B under anisothermal conditions are shown in Table 4-6.

Figure 4-22 (a) and (b) presents the effective yield strengths for steels A-D normalised by the measured yield strength at 2.0% total strain and the nominal yield strength at room temperature, respectively, along with the Eurocode approach. In Figure 4-23 and Figure 4-24, the reduction factors for steels A-D and the Eurocode approach are presented along with data from the literature for S460 and S650 to S700 grades, respectively, using the measured effective yield strength.

In Figure 4-22 (a), the reduction factors for steels A-D derived by the normalising by the measured yield strength at room temperature, are below the Eurocode curve at temperatures less than

400°C, meaning that the Eurocode recommendations are unconservative (i.e. not safe). However, the reduction factors for steels A-D are conservative (i.e. safe) at all temperatures when normalised by the nominal yield strength as shown in Figure 4-22 (b).

Comparisons of Figure 4-19 with Figure 4-22, shows that the reduction factors from the isothermal (coloured shapes) and anisothermal (uncoloured shapes) are closer together when based on 2% rather than 0.2% proof strength. This in agreement with other researchers (e.g. (Kirby and Preston, 1988; Gardner, Insausti, et al., 2010)) who found that the disparity between isothermal and anisothermal tests reduced at relatively high strains (e.g. ≥2%).

Figure 4-23, demonstrates that Eurocode approach is unconservative for S460 grade steels when normalised by the measured effective strengths at room temperature. The effective yield strength of Q460 tested by Wang et al. (2013a), increased to a value greater than 1 between 200 and 450°C which Wang et al. (2013a) attributed to "blue brittleness" effect discussed in Section 4.2.4.4. However, it is worth noting that there is a lot of scatter in their data, which is believed to be related to the test conditions used. Wang et al. (2013a) conducted their tests under stress-control rather than strain-control method, with the latter (strain-control) being the recommended test method in the standards (ISO 6892-2, 2011; ASTM, 2009). Hence, it is also likely that the vast differences in their reduction factors is due to fluctuations in the strain rate during each test.

The reduction factors for the steels grades between S650 and S700, normalised by the measured effective yield strength at room temperature as shown in Figure 4-24, illustrate a much larger scatter than the S460 grades in Figure 4-23. This highlights the danger of generalising reduction factors for HSS grades as discussed by Burgan (2001). The scatter is likely to be due to the increased number of variables in the composition and production route for the higher strength steels. With reference to Figure 4-24, the Eurocode is shown to provide unconservative (i.e. not safe) reduction factors for the effective yield strength for many of the S650-S700 steel grades reported in the literature, including RQT 701 tested by Xiong and Liew (2016) and S690QL tested by Neuenschwander et al. (2017).

Steel B (S700MC), a thermomechanical control processed material, showed better strength retention properties compared with all tested steel grades in the literature from temperatures greater than 400°C as depicted in Figure 4-24. This steel contained the highest amount of combined microalloying elements which suggests that this steel may contain a stable, fine dispersion of carbides/nitrides, or even form these as the temperature increases, though

Transmission Electron Microscopy (TEM) studies are necessary to verify this. Such precipitates have been reported play a crucial role in retention of steel strength at temperatures up to 650°C. The metallurgical properties of steel B (S700MC) are discussed further in Chapter 5.

Table 4-5 Reduction factors for the effective yield strength obtained from isothermal tests

Temperature (°C)	Steel A (S690QL)	Steel B (S700MC)	Steel C (S690QL)	Steel D (S460NH)
20	1.00	1.00	1.00	1.00
100	0.98, 0.95	0.97, 0.96	-	-
200	0.96	0.94,	0.98	-
300	0.97	1.02	1.00	-
400	0.94, 0.92	0.99, 0.96	0.93	0.96
500	0.84, 0.83	0.86, 0.88	0.80	0.76, 0.77
600	0.66, 0.67	0.71, 0.68	0.54	0.63
700	0.34	0.45	-	-
800	0.11	0.21	-	-

Table 4-6 Reduction factors for the effective yield strength obtained from anisothermal tests

Temperature (°C)	Steel A (S690QL)	Steel B (S700MC)
20	1.00	1.00
100	0.95	0.95
150	0.94	0.94
200	0.94	0.94
250	0.93	0.94
300	0.92	0.93
350	0.92	0.93
400	0.91	0.93
450	0.88	0.92
500	0.85	0.90
550	0.79	0.81
600	0.66	0.71
650	0.55	0.61
700	0.37	0.50
650	0.22	0.32
800	0.11	0.22

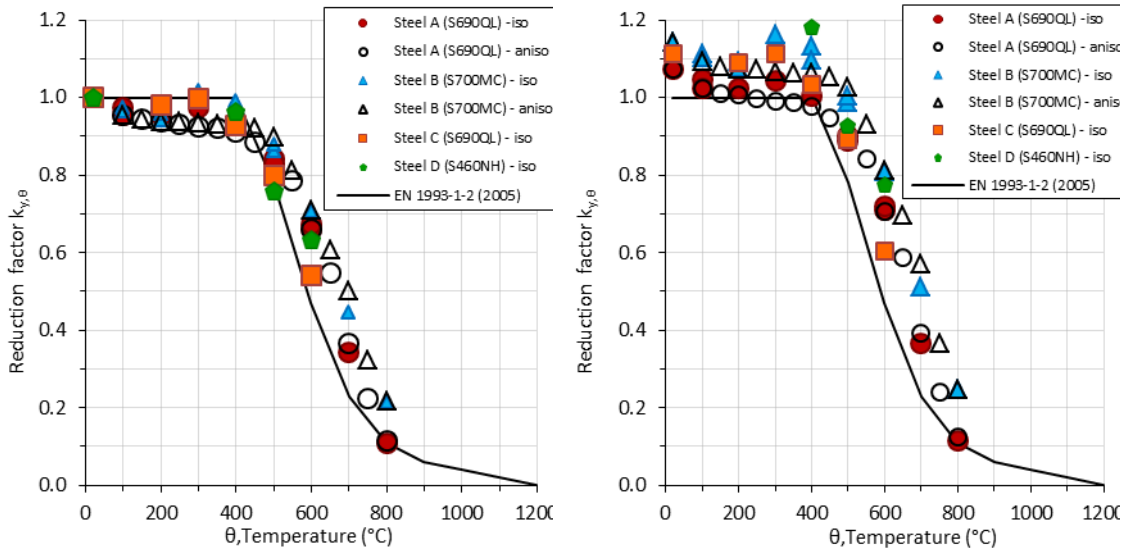

Figure 4-22 Comparison of the reduction factors of the effective yield strength ($k_{y,\theta} = f_{y,\theta}/f_{y,20}$) normalised by (a) measured yield strength at room temperature and (b) the nominal yield strength with EN 1993-1-2 (2005)

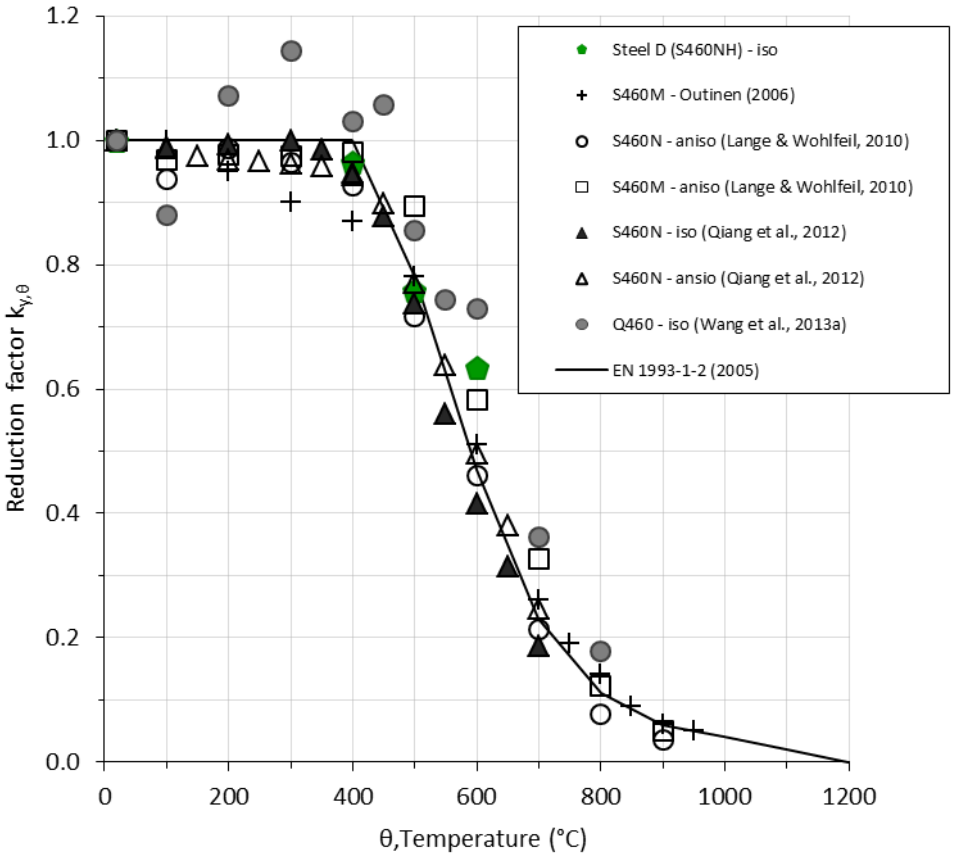

Figure 4-23 Comparison of the reduction factors of the effective yield strength ($k_{y,\theta} = f_{y,\theta}/f_{y,20}$) normalised by the measured yield strength at room temperature with EN 1993-1-2 (2005) and available literature on S460

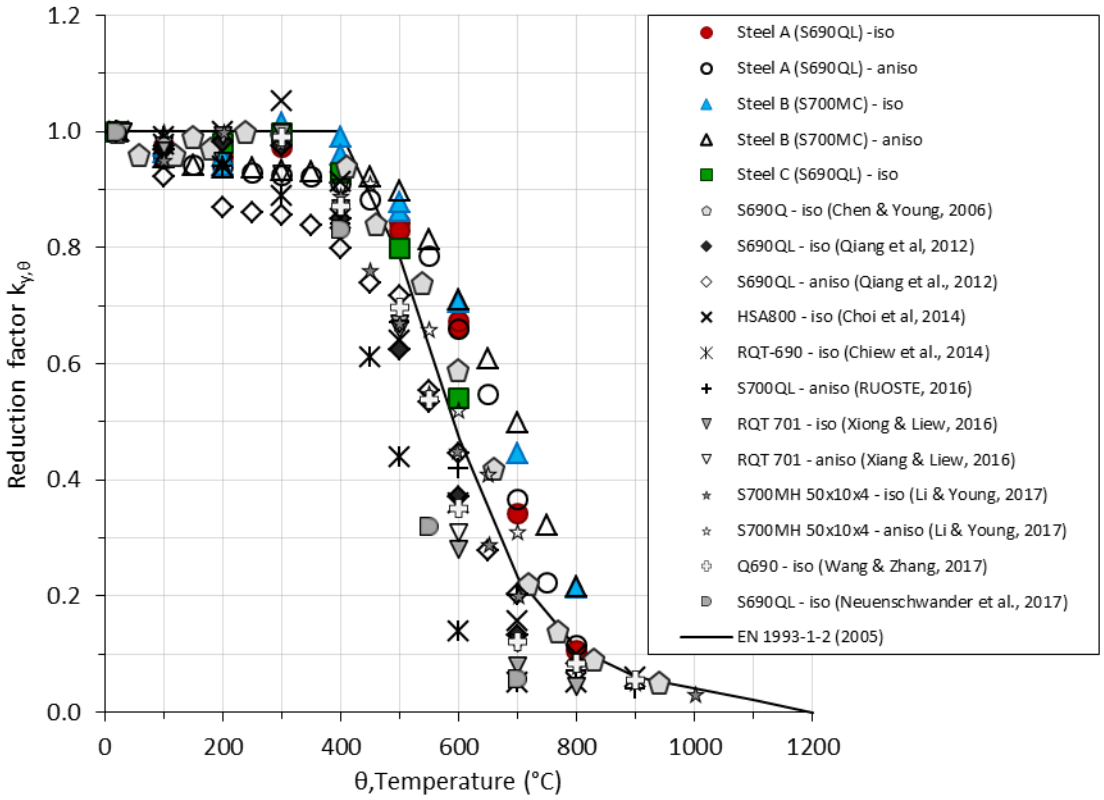

Figure 4-24 Comparison of the reduction factors of the effective yield strength ($k_{y,\theta} = f_{y,\theta}/f_{y,20}$) normalised by the measured yield strength at room temperature with EN 1993-1-2 (2005) and available literature on S650-S700

4.3.6 Elastic modulus

The elastic moduli at room and elevated temperature θ (i.e. $E_{a,20}$ and $E_{a,\theta}$, respectively) were determined from the slope of the initial linear elastic region of the stress-strain curve (see Figure 4-16). It is noteworthy that at temperatures above 700°C, the linear elastic region of the stress-strain curve was small, particularly under anisothermal conditions where there was a limited number of data points available to determine the elastic modulus at small strains (i.e. below 0.2%). The reduction factors for the elastic moduli of steels A and D under isothermal conditions are presented in Table 4-7 , whilst the reduction factors for steels A and B under anisothermal conditions are shown in Table 4-8.

Figure 4-25 (a) presents the reduction factors for the elastic modulus (i.e. $k_{E,\theta} = E_{a,\theta}/E_{a,20}$) for steels A-D derived by normalising by the measured elastic modulus at room temperature and Figure 4-25 (b) presents the reduction factors derived by normalising by the nominal elastic modulus (210 GPa). In Figure 4-26 and Figure 4-27 the reduction factors for steels A-D and the Eurocode

approach are presented along with data from the literature for S460 and S650-S700 grades, respectively, using the measured elastic modulus.

From Figure 4-25 (a), the Eurocode curve is conservative in the prediction of the reduction in the elastic modulus of steels A-D, with the exception of steel A (S690QL) and B (S700MC) at 100°C under isothermal and anisothermal conditions, steel A (S690QL) at 800°C under anisothermal conditions and steel D (S460NH) at 400°C. Comparing Figure 4-25 (a) with (b) shows that normalising by the nominal yield strength only increased the reduction factors for steel B (S700MC) under isothermal conditions because the measured elastic modulus was higher than the nominal (224.7 vs. 210 GPa). Although texture studies (i.e. the crystal orientation of the grains) was beyond the scope of this study, it is expected that the higher elastic modulus is a result of a high density of grains orientated in the direction where the elastic modulus is stronger (i.e. (111) crystallography direction).

In Figure 4-25, it can be seen that the reduction factors obtained from isothermal and anisothermal tests for steels A (S690QL) and B (S700MC) are similar up to 400°C. Above 400°C, reduction factors obtained from isothermal tests are higher than the reduction factors obtained from anisothermal tests. At temperatures greater than 400°C, creep effects are particularly evident and suggest that for a given load, the additional influence of creep deformation may possibly account for the lower elastic modulus reading. Hence, the resulting elastic modulus from anisothermal data does not represent the true elastic modulus.

The discrepancies between the test methods, is also seen in the published literature shown in Figure 4-26 and Figure 4-27. From these figures, it can be seen the reduction factors obtained from isothermal tests generally demonstrate that the Eurocode approach is overly conservative and do not allow the good stiffness retention properties to be exploited in design. This is as expected because the reduction factors in the Eurocode were derived from anisothermal test data, which Kirby and Preston (1988) believe are more appropriate for structural fire design purposes. However, the converse is true for reduction factors obtained from anisothermal tests including S460N tested by Qiang et al. (2012), S690Q tested by Chen and Young (2006) and RQT 701 tested by Xiong and Liew (2016), which showed the Eurocode approach to be unconservative (i.e. not safe), as presented in Figure 4-26 and Figure 4-27. The choice of which reduction factors to use in design is dependent on whether the influence of creep is significant. If creep is to be considered implicitly in the design process, then the reduction factors obtained from isothermal

tests are more appropriate, otherwise, it is recommended that reduction factors from anisothermal tests should be used.

Table 4-7 Reduction factors for the elastic modulus obtained from isothermal tests

Temperature (°C)	Steel A (S690QL)	Steel B (S700MC)	Steel C (S690QL)	Steel D (S460NH)
20	1.00	1.00	1.00	1.00
100	0.95, 0.97	0.91, 0.89	-	-
200	0.96	0.97	0.94	-
300	0.92	0.94	0.90	-
400	0.89, 0.89	0.91, 0.95	0.87	0.66
500	0.89, 0.9	0.85, 0.85	0.80	0.64, 0.66
600	0.75, 0.85	0.79, 0.78	0.60	0.46
700	0.38	0.63	-	-
800	0.27	0.39	-	-

Table 4-8 Reduction factors for the elastic modulus obtained from anisothermal tests

Temperature (°C)	Steel A (S690QL)	Steel B (S700MC)
20	1.00	1.00
100	0.98	0.97
150	0.95	0.95
200	0.96	0.96
250	0.95	0.97
300	0.91	0.96
350	0.90	0.92
400	0.89	0.85
450	0.86	0.79
500	0.80	0.70
550	0.75	0.65
600	0.64	0.58
650	0.46	0.46
700	0.44	0.37
650	0.16	0.27
800	0.04	0.19

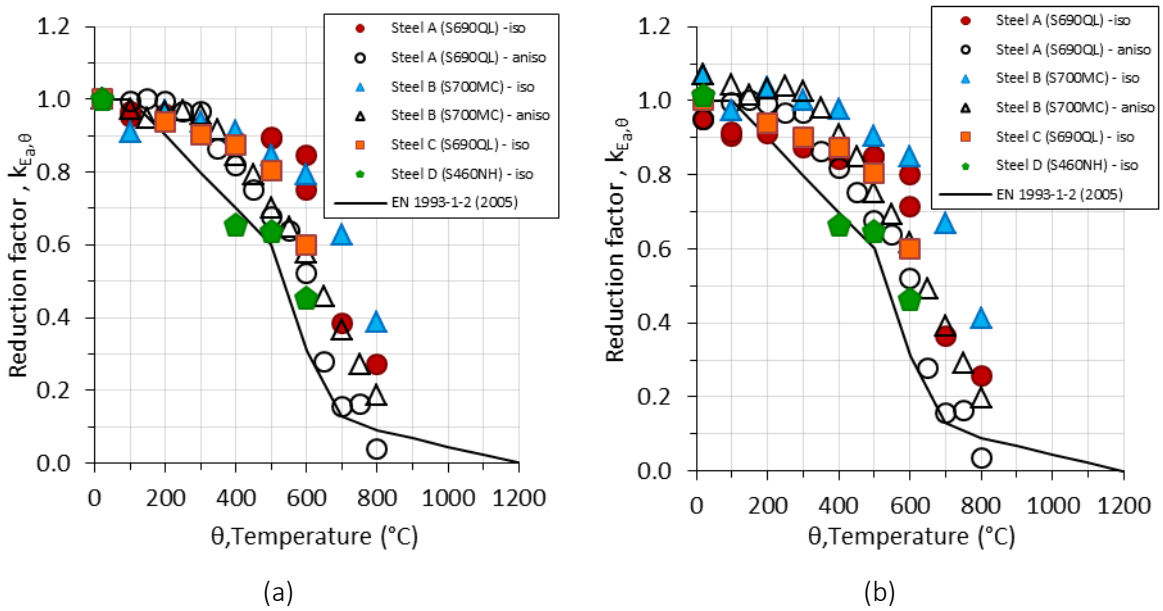

Figure 4-25 Comparison of the reduction factors of the elastic modulus ($k_{E,\theta} = E_{a,\theta}/E_{a,20}$) normalised by the (a) measured elastic modulus at room temperature and (b) the nominal elastic modulus (210 GPa) with EN 1993-1-2 (2005)

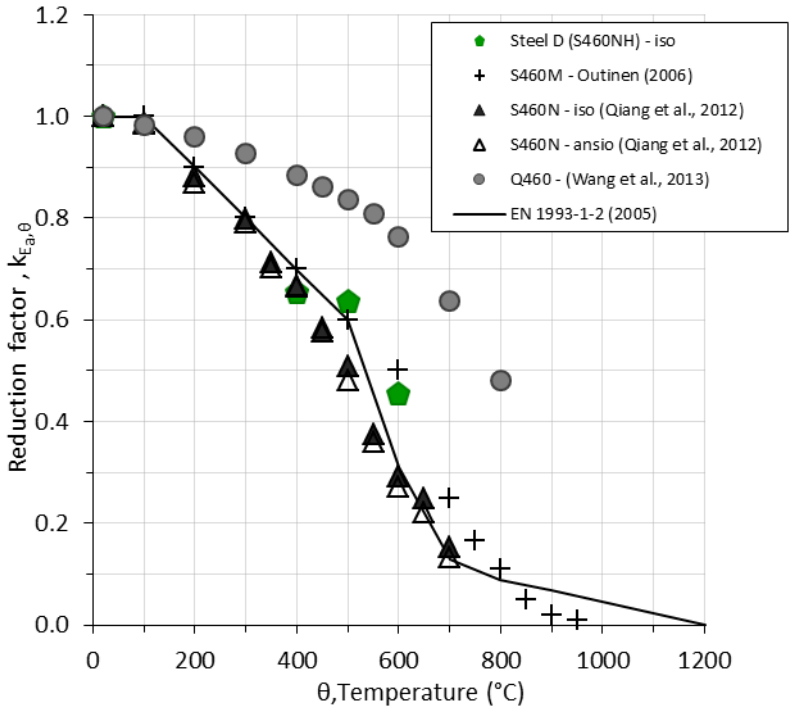

Figure 4-26 Comparison of the reduction factors of the elastic modulus ($k_{E,\theta} = E_{a,\theta}/E_{a,20}$) normalised by the measured elastic modulus at room temperature with EN 1993-1-2 (EN 1993-1-1, 2005) **and available literature on S650-S700**

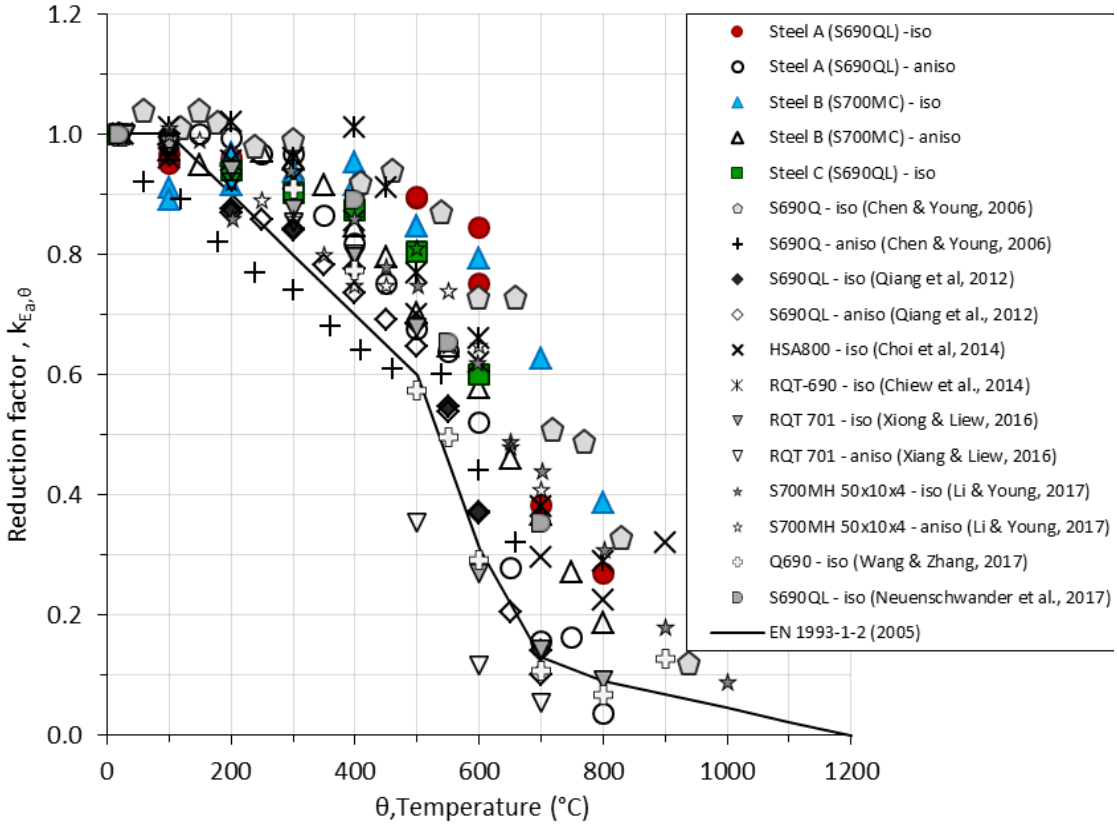

Figure 4-27 Comparison of the reduction factors of the elastic modulus ($k_{E,\theta} = E_{a,\theta}/E_{a,20}$) normalised by the measured elastic modulus at room temperature with EN 1993-1-2 (EN 1993-1-1, 2005) **and available literature on S650-S700**

4.4 Concluding remarks

This chapter has presented a detailed experimental investigation on the strength and stiffness properties of various HSS at elevated temperature, considering the influence of strain and heating rate as described in the literature. Isothermal and anisothermal tensile tests were conducted at temperature up to 800°C and the results were presented as reduction factors and compared to published data and the Eurocode 3 Part 1-2 (2005).

The reduction factors presented in the Eurocode were shown to be unconservative when compared against the reduction factors for steels A-D, derived by normalising the elevated temperature by the nominal (design) properties for the proportional limit, 0.2% proof strength, and elastic modulus given in the Eurocodes as well as the corresponding measured values from this experimental programme. However when normalising the experimental data for steel A-D by the nominal effective yield strength, the Eurocode approach was demonstrated to be conservative (i.e. safe). This was not the case for similar data in the literature, which showed the Eurocode approach for the effective yield strength to be unconservative (i.e. unsafe). These

results suggest that revised (lower) reduction factors for HSS may need to be proposed, considering the 'worse case' scenario. Furthermore, the scatter amongst the reduction factors presented further indicates that the strength and stiffness degradation at elevated temperature is strongly influenced by the material history including chemical composition and production/fabrication route and support the argument that reduction factor for HSS should not be generalised; particularly if steels with better strength retention properties at elevated temperatures can be exploited in design.

The discrepancy between isothermal and anisothermal results for steels A (S690QL) and B (S700MC) as well as the data from the literature, including RQT 701 test by Xiong and Liew (2016) and S700MH tested by Li and Young (2017), which is evident at temperatures greater than 400°C, highlights the importance of considering which data are appropriate for structural fire design purposes. For a prescriptive design approach where higher strains such as the effective yield strength at 2.0% are used in the calculations, the results produced by either test method are suitable because the difference between the two approaches is small. However, for the elastic modulus, data from isothermal tests show higher stiffness retention than data from anisothermal tests at elevated temperature and this is believed to be due to creep. Creep properties are material specific and for HSS these data are sparse, hence it is recommended that anisothermal data should be used to avoid overestimating the performance of HSS members, particularly after long fire durations where the influence of creep becomes more significant. However, if the anticipated fire duration is short enough such that creep is not a concern, then the isothermal data could be used.

Of the steel grades tested in this project and in the literature, steel B (S700MC) demonstrated the best overall strength and stiffness properties from room up to 800°C. Steel B (S700MC) contained the highest amount of combined microalloying elements (niobium, vanadium and titanium) as reported in Chapter 3 which are known to form thermally stable precipitates around 600°C (Bhadeshia and Honeycombe, 2006) as well as molybdenum which can reduce the coarsening rate of niobium carbides/nitrides above 500°C (Wan et al., 2012a, 2012b; Bhadeshia and Honeycombe, 2006). From a practical perspective, steels which retain their strength and/or stiffness for longer or to higher temperatures are clearly advantageous in prolonging the evacuation time in the event of a fire. Further studies, focused on the metallurgical influences which may be contributing to the observed strength retention at elevated temperature are presented in Chapter 5 whilst the link between the material and metallurgical properties are discussed in Chapter 7.

Chapter

5

Metallurgical properties of high strength steels

5.1 Introduction

The previous chapter confirmed that the material response at elevated temperatures differs greatly between different HSS grades. To understand these differences, it is worth examining the influence of the chemical composition and processing route on the resulting microstructure of the HSS grades. This chapter presents the microstructures of the five HSS grades (steels A-E) in the 'as-received' condition. Since steels A (S690QL) and B (S700MC) showed the best strength retention properties of the HSS grades tested in this study, these steels were examined further with the aim to characterise how their microstructures change with temperature. Selected tensile specimens from these two steels, which were influenced by the combined effect of strain and a thermal cycle, were sectioned and the microstructure assessed. Heat treatment trials have also been conducted on samples of the base steels to allow assessment of the influence of temperature only. An additional aim of the heat treatment trials was to seek evidence of secondary hardening, which could be contributing to the observed strength retention at elevated temperatures (Bhadeshia and Honeycombe, 2006). To characterise the HSS grades, the following techniques were used: light microscopy, Vickers hardness and Scanning Electron Microscopy (SEM) including Electron Backscatter Diffraction (EBSD). This chapter is mainly descriptive, summarising the experimental techniques utilised and the results; the relationship between the

microstructure, chemical composition, processing route, and the material properties are discussed later in Chapter 7.

5.2 Experimental procedures

5.2.1 Sample preparation

Samples for microstructural characterisation were cut using an abrasive wet cutting machine. Sufficient coolant was employed during the cutting process to avoid any thermal effects from the cutting operation that could alter the microstructure. Once cut, standard metallographic techniques were used to prepare the specimen surface which are summarised hereafter. Each sample was hot-mounted in conductive Bakelite, a thermosetting resin impregnated with carbon, and manually ground sequentially using 120 to 2500 grit silicon carbide papers lubricated with water. Between each grinding step, the samples were rinsed in methanol and air dried to remove grinding debris and prevent corrosion appearing on the surface of the sample. Subsequently, each sample was polished sequentially using cloths with fine diamond pastes at 3, 1 and 0.25 µm and an oil-based lubricant. Similarly, between each polishing stage, the samples were cleaned using detergent, water then methanol to remove the diamond paste and oil-based lubricant from the sample before moving to the next finer polishing step. Each sample was then examined, as polished, under the light microscope to look for any inclusions. Finally, the samples were rinsed in methanol prior to etching with 2% Nital (nitric acid and methanol) to reveal the microstructural features.

Samples for EBSD were prepared in a similar manner to that described to 0.25 µm finish; this was followed by a final polishing step with an alumina suspension (OP-AN) in water to produce a surface finish of 0.05 µm. Samples for EBSD were not etched.

5.2.2 Electron backscatter diffraction (EBSD)

To further examine the microstructure, in particular the grain morphology (size and orientation) of the as-received samples, an Oxford Instrument ‘Nordlys' EBSD detector was used. The EBSD method is an SEM technique used to obtain crystallographic information including the grain size, grain morphology, phase composition, strain and texture (i.e. the preferred orientation of each grain within the material) of a material. A schematic of a typical set up within an SEM chamber is presented in Figure 5-1. Within the SEM chamber, the sample is tilted approximately 70° from the horizontal and an electron beam targets a point on the tilted sample resulting in the formation of backscattered electrons. The backscattered electrons interact with the phosphor screen to produce a diffraction pattern often termed as Kikuchi pattern. During this interaction,

the phosphor screen converts the backscattered electrons to photons (light) and the resulting diffraction pattern is recorded using a camera located behind the phosphor screen. The diffraction pattern is then transferred to a software for analysis. In this study, the EBSD data were collected and indexed using the AZtecHKL software, whereby the resulting diffraction pattern was matched to a theoretical pattern of a grain orientation. The electron beam then moves to the next spot and the process is repeated to determine orientation of the adjacent point; the entire process is automated, resulting in a map composed of many of EBSD data points revealing the material microstructure. Further information regarding the theory and experimental set-up can be found in the following references: Engler and Randle (2010), Schwartz et al. (2000).

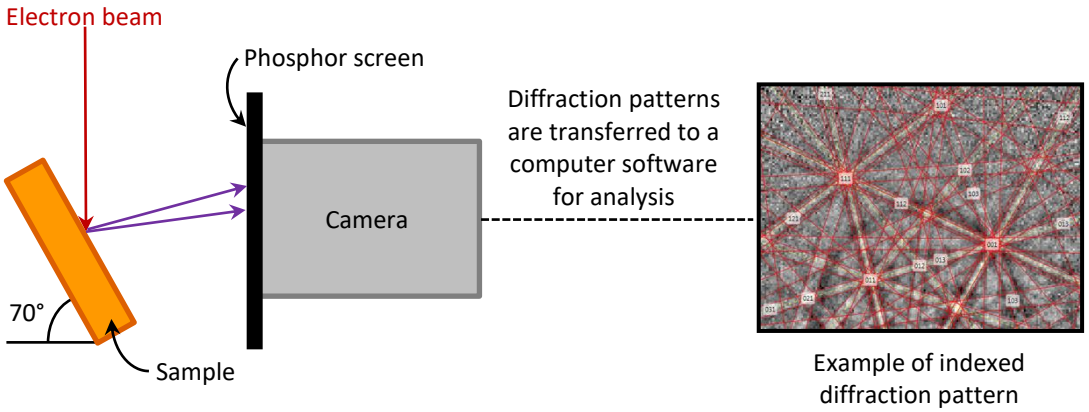

Figure 5-1 Schematic diagram of a typical EBSD set-up within the SEM

The quality of the output from EBSD analysis is highly dependent on the surface finish and the SEM settings employed. The surface preparation explained in Section 5.2.1 was employed to produce a relatively flat surface with a surface finish of 0.05 µm. The optimum SEM settings for EBSD vary depending on the specimen and machine. In this case, the working distance was set to 10 mm whilst the accelerating voltage and aperture were set to 30 kV and 120 µm, respectively. The resolution of the EBSD image is also dependent on the step size between data points and the "binning mode", which refers to the number of EBSD data points combined to create one large EBSD data point. The principle of binning is shown in Figure 5-2. The processing time is inversely proportional to the square of the binning mode. For example, a binning mode of 4x4 reduces the processing time by $1/16^{th}$, whilst an 8x8 binning mode reduces the processing time by $1/64^{th}$. Whilst a smaller step size and binning mode will increase both the quality of the EBSD data and the processing time, a larger step and binning mode can lead to some reduction in the noise level and processing time. Thus, a balance is necessary to ensure good quality EBSD data are produced

within a reasonable time frame. In this study, the step size and bin0ning mode of 0.15 µm and 4 x 4, respectively were adopted.

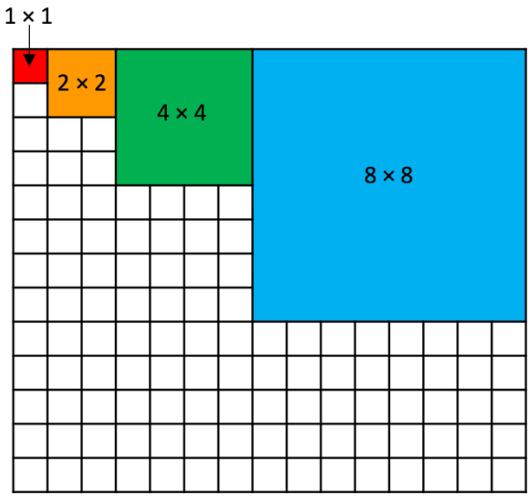

Figure 5-2 Data binning

During the indexing of the EBSD data, good agreement between the measured and theoretical data was seen, as indicated by the low average mean angular deviation (MAD) of 0.36. Following each scan, the EBSD data were processed using the HKL Channel5 software. The results are presented as pattern quality (or band contrast) and orientation maps coloured using inverse pole figure maps. Pattern quality maps are shaded (typically using a grey scale) according to the quality of the indexed pattern, where the lighter regions indicate the best pattern quality and conversely, the darker regions depict lower pattern quality. At the grain boundaries, the patterns of the two or more grains with different orientations overlap resulting in a poor pattern quality and hence grain boundaries appear as black lines (Randle, 2009).

A common method for presenting orientation maps is using the Inverse Pole Figure (IPF) colour scheme, where each grain is coloured with respect to the angle of orientation from the reference direction (e.g. the rolling direction). For cubic phases (e.g. bcc and fcc), grains that are coloured red, green, and blue represent grains orientated in the <100>, <110> and <111> directions, respectively (Maitland and Sitzman, 2007). An example of an IPF colour key maps is presented in Figure 5-3. The degree of misorientation between two grains is typically divided into two categories: high and low angle grain boundaries. In this study, the minimum misorientation angle for high angle grain boundaries was set to 10°, in accordance with conventional grain boundary theory and the misorientation of the low angle grain boundaries was set to between 2 and 10°

(Winning and Rollett, 2005). In this study, high and low angle grain boundaries are depicted in black and yellow, respectively. The resulting images were partially "cleaned" using the post-processing software to reduce the number of unindexed points (white spots), nonetheless the indexing rate (i.e. the number of successful data points indexed) for each material was ≥90%. These data are presented in the subsequent sections.

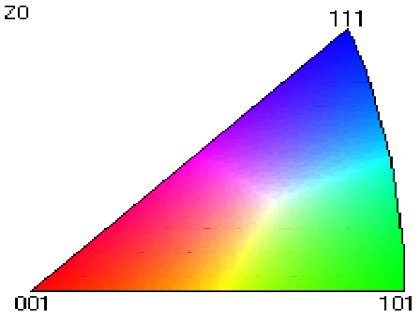

Figure 5-3 IPF colour key

5.2.3 Heat treatments

Since steels A (S690QL) and B (S700MC) showed the best strength retention properties of the HSS grades tested in this study, heat treatments were conducted on these materials in order to characterise the microstructural changes with temperature. In particular, evidence of microstructural effects including grain growth and secondary hardening were sought. The sample size for heat treatment was based on the length and thread diameter of the M12 and M10 tensile specimens, where the dimensions for steels A (S690QL) and B (S700MC) were 16 × 10 × 90 mm and 12 × 10 × 80 mm, respectively. A hole was drilled in the centre of each sample for the introduction of a k-type thermocouple to monitor the temperature of the sample. Information regarding the heating rates and maximum temperature deviation at each target temperature are summarised in Table 5-1.

Table 5-1 Temperature information from heat treatments

Target temperature (°C)	Heating rate (°C/min)	Maximum temperature deviation (±°C)
500	11.3	23
600	*	21
700	10.9	17
800	10.5	27

* the heating rate was 9.8°C/min up to 400°C and 3.1°C/min to 600°C

At each target temperature, the samples were soaked for either 5 or 60 minutes and then quenched in water to "freeze" the microstructure, in order to get an indication of the microstructure at the target temperature and prevent any further microstructural changes occurring. With reference to the Fe-C phase diagram, a section of which is presented in Figure 5-4, it is worth noting that when steels are heated between A_1 and A_3 (intercritical region) or above A_3 (supercritical region), ferrite will begin to transform to austenite. Carbon is more soluble in austenite compared with ferrite, so within the intercritical temperature regime any free carbon will diffuse to austenite. Upon quenching, any austenite present will transform to martensite or bainite. Whilst quenching steels heated above A_1 will result in a microstructure not representative of the true microstructure at elevated temperatures, the formation of martensite and bainite will give clues about any microstructural changes that would have occurred. The specific values for A_1 and A_3 for steels A (S690QL) and B (S700MC) are dependent on the heating rate and/or soaking time as well as the chemical composition.

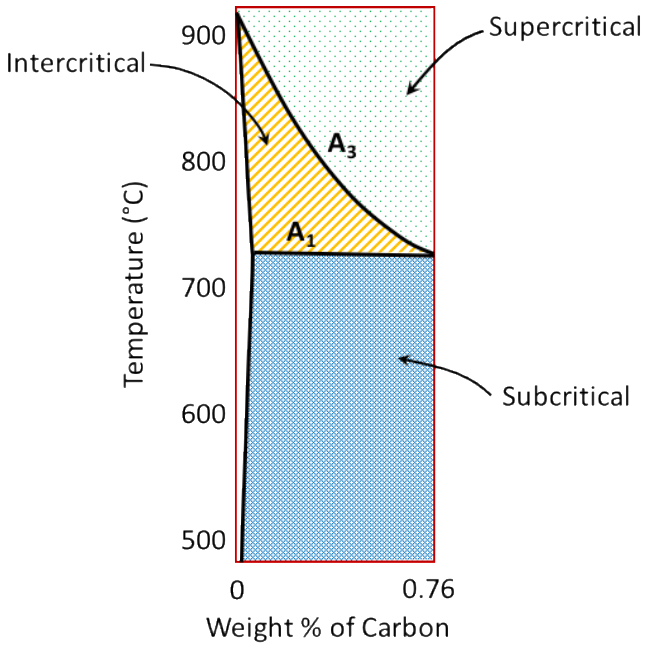

Figure 5-4 Fe-C diagram

The metallurgical processes taking place during these heat treatments are principally diffusion controlled (i.e. influenced by both time and temperature). To compare the influence of time and temperature, the Hollomon-Jaffe parameter (H-J) can be used. The H-J parameter is defined in Equation (5.1):

$$\text{H-J} = \frac{\text{T}\,(20+\log\tau)}{1000} \tag{5.1}$$

where T is the absolute temperature in Kelvin and τ is the time constant which considers the soaking time as well as the heating and cooling rate as defined in Equation (5.2).

$$\tau = \text{t} + \frac{\text{T}}{(2.3K_1(20-\log K_1))} + \frac{\text{T}}{(2.3K_2(20-\log K_2))} \tag{5.2}$$

where t is the soaking time in hours, K_1 and K_2 are the heating and cooling rate, respectively both in K/hour (Hollomon and Jaffe, 1947). In this investigation, the cooling rate was very fast and hence its contribution to H-J parameter is negligible. Thus, based on heating rates and target temperature presented in Table 5-1, and soaking times of 5 and 60 minutes, the H-J parameter values varied between 14.7 and 21.5.

5.2.4 Vickers hardness

Hardness is often defined as the capacity of a material's surface to resist plastic deformation, and is directly proportional to the yield strength, as demonstrated by Ashby and Jones (2005). In the present study, low force (1 kgf) Vickers hardness tests were conducted on as-received and heat-treated samples for the steels tested (A (S690QL) and B (S700MC)) in accordance with ISO 6507-1 (2005). The samples taken from the rolling surface (Figure 5-5) were mounted in Bakelite and polished to a 1 µm finish, using the techniques described in Section 5.2.1. Five indentations were made in each sample which was then used to determine the average hardness and standard deviation were determined for each sample.

5.3 Metallography results

5.3.1 As-received samples

Samples from the as received material for steels A-E were taken from three orthogonal directions: the rolling, transverse and normal directions, as shown in Figure 5-5. For comparison purposes, only the micrographs for steels A-E taken parallel to the rolling direction ('Rolling' surface – Figure 5-5) are presented in Figure 5-6. Similarly, the corresponding pattern quality maps from EBSD analysis for steels A-E taken from the rolling surface, are presented in Figure 5-7 to Figure 5-11. From the micrographs presented in Figure 5-6, it can be seen that the microstructure of the five HSS are very different and this is linked to the differences in the stress-strain response in Section 3.4.1.

Steels A (S690QL), C (S690QL) and E (S690QH), which were all supplied in the quenched and tempered condition, all differ slightly in microstructure which is attributed to the variation in chemical composition. The microstructures of these steels appear to be either tempered bainite or tempered martensite, which contain lath-like grains grouped together and very fine particles of cementite (iron carbide) as shown in Figure 5-6 (a), (c) and (e). The lath-like grains can be seen more clearly in the pattern quality and orientation maps shown Figure 5-7, Figure 5-9 and Figure 5-11.

The microstructure of steel B (S700MC) depicted in Figure 5-6 (b) and Figure 5-8 is ferrite and bainite as described by Gorka (2014). The grains in steel B (S700MC) are much finer compared with the other steel grades depicted, however the etchant used (2% nital) does not reveal all the grains and many of these grains are too fine to see under the light microscope. This is where EBSD becomes a useful tool. The fine grain structure of steel B (S700MC) is more evident in the pattern quality and orientation maps shown in Figure 5-8.

Orange precipitates were observed in the microstructure of steel B (S700MC) as illustrated by the arrows in Figure 5-12. These precipitates were titanium rich with niobium, nitrogen and carbon also present, as determined by energy-dispersive X-ray spectroscopy (EDX) analysis within the scanning electron microscope (SEM); the EDX results are shown in Figure 5-13. It should be noted that the EDX spectrum presented in Figure 5-13 (c) is qualitative and gives an indication only of the elements present, not the amounts of these elements. Titanium nitride is the most thermally stable precipitate out of all the carbides and nitrides precipitated from microalloying elements and can be precipitated at temperatures as high as 1500°C where the steel is liquid, depending on the amount of nitrogen and titanium present. For example, Gladman (1999) suggests that titanium nitride may precipitate in the liquid if 0.005 weight% nitrogen and 0.068 weight% titanium are present. The size of these precipitates is a further indication of when the precipitate formed, with titanium nitride precipitate sizes of up to 5 μm in the liquid state being reported. This is consistent with the size range observed in the as-received steel B (S700MC) material as shown in Figure 5-12. For comparison, Gladman (1999) has reported that the size of precipitates formed in the solid state are much finer, ranging from 10-20 nm, provided that the temperatures are not high enough for Ostwald ripening to occur. Fine precipitates (in the order of a few nm) are more effective at precipitation hardening compared with inclusions (i.e. coarse precipitates in the order a few μm), because a higher density of precipitates are present to hinder dislocation movement. To verify the presence of fine precipitates, a very high resolution microscope such as a transmission electron microscope (TEM) is required, which was beyond the scope of this study.

The microstructure of steel D (S460NH) shown in Figure 5-6 (d) is a classic ferrite-pearlite banded microstructure, where ferrite and pearlite are the light and dark-etching regions, respectively. This microstructure is characteristic of the manufacturing route and heat treatment described in Section 2.3.4.2.

Low angle grain boundaries which are also termed sub-grain boundaries are shown as yellow lines in Figure 5-7 to Figure 5-11. Sub-grain boundaries can be represented by an array of dislocations (Humphreys and Hatherly, 2004). There appears to be a greater number of sub-grains in the QT and TMCP steels compared with steel D (S460NH). The presence of sub-grains can be attributed to the deformation (hot-rolling) process, where dislocations are introduced and rearrange to form low angle boundaries through a process called polygonisation. Typically, the introduction of dislocations during hot-rolling is counteracted by recovery and recrystallisation. In the as-quenched form, martensite has a very high density of tangled dislocations. During tempering, recovery will occur, resulting in a reduction in the dislocation density and the formation of low angle grain boundaries. In the case of steel B (S700MC), a greater density of sub-grains can be seen in the larger grains. Again, this is related to the deformation process, particularly as steel B (S700MC) was hot rolled below the recrystallisation temperature ($<A_3$). As a result, the rate of recrystallisation would have been less than the rate at which dislocations were being introduced.

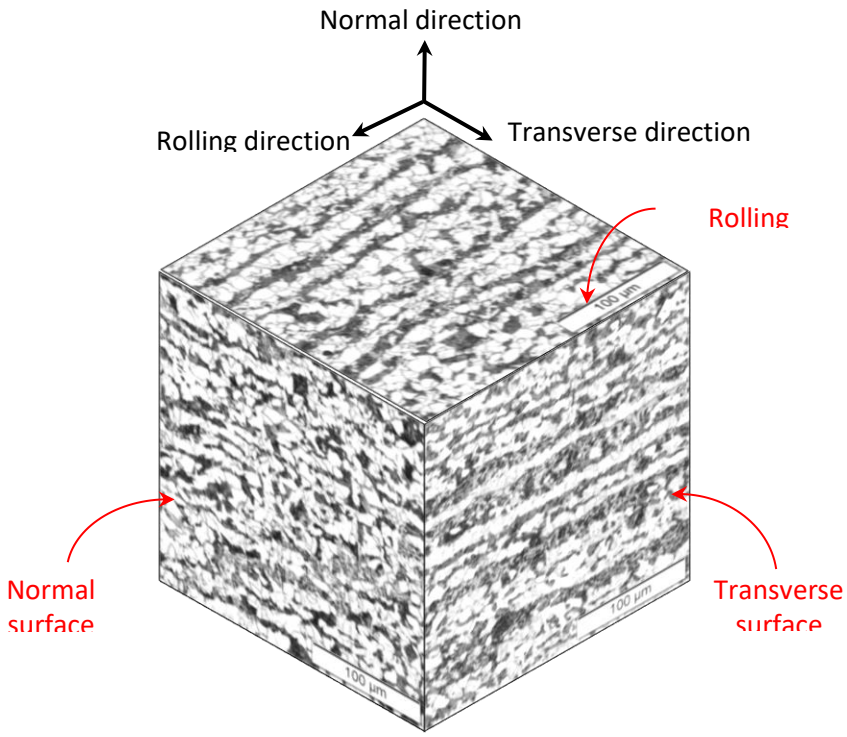

Figure 5-5 Orthogonal view of steel D (S460NH) showing the rolling, normal and transverse surface, etched with 2% nital

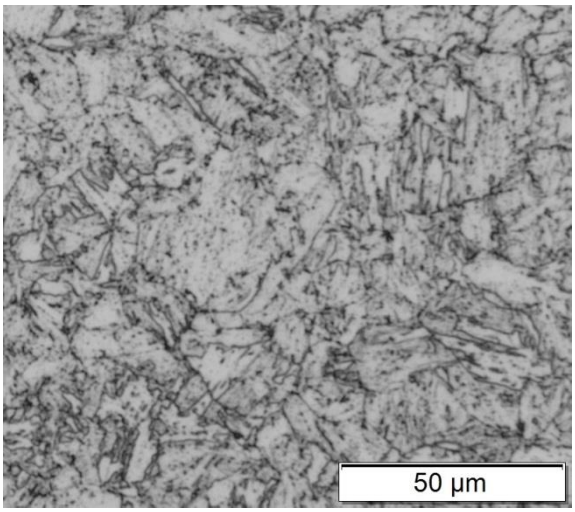

(a) Steel A (S690QL)

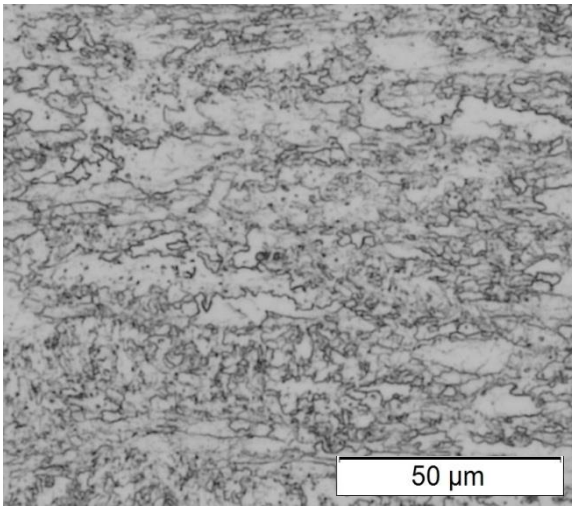

(b) Steel B (S700MC)

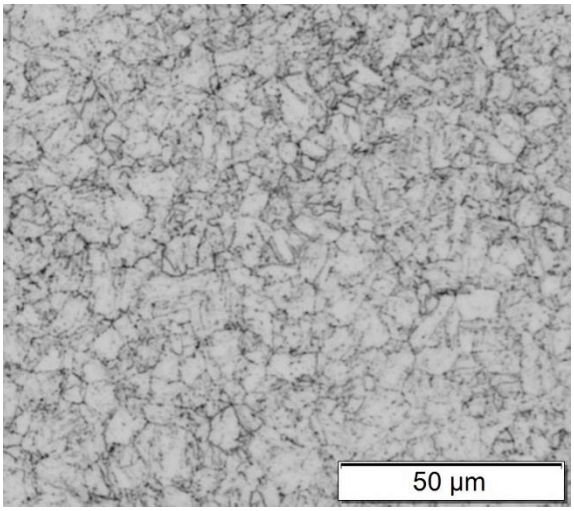

(c) Steel C (S690QL)

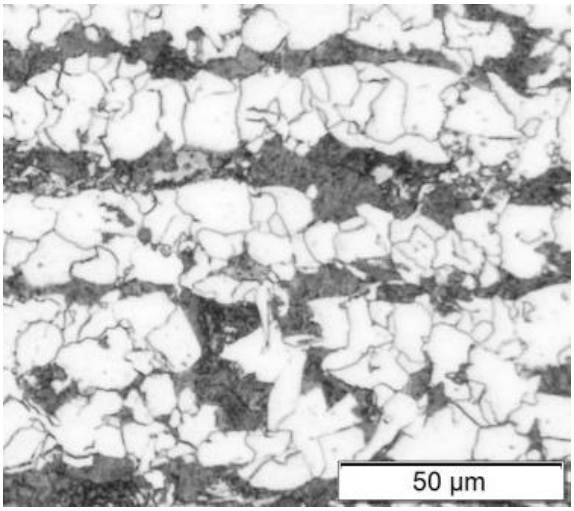

d) Steel D (S460NH)

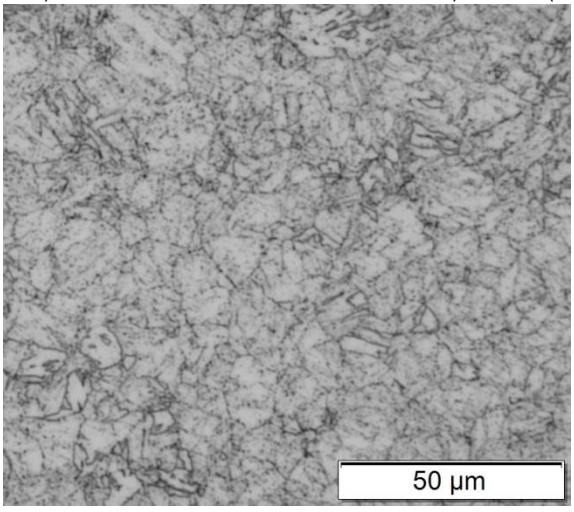

(e) Steel E (S690QH)

Figure 5-6 Light micrographs taken from the rolling surface, all etched in 2% nital

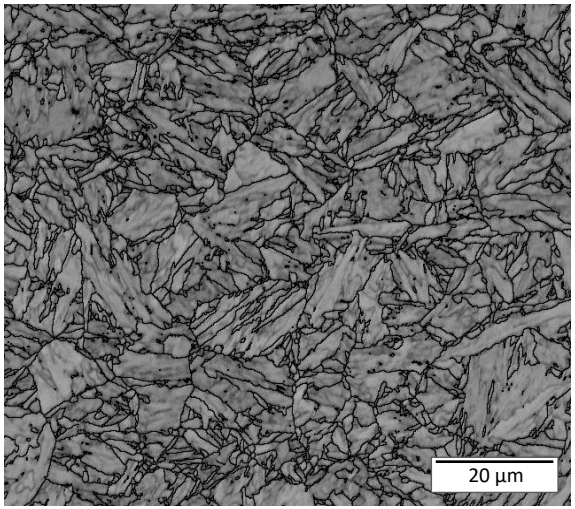

(a) Pattern quality map with high angle grain boundaries in black

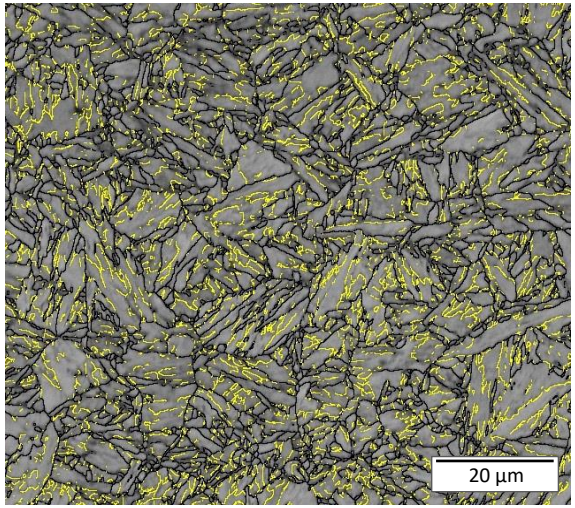

(b) Pattern quality map with high and low angle grain boundaries in black and yellow, respectively

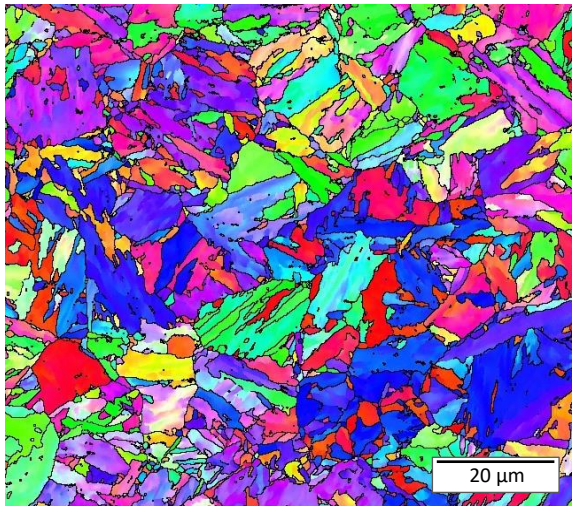

(c) Orientation map with IPF colouring (Figure 5-3)

Figure 5-7 Steel A (S690QL) taken from the rolling surface - image part cleaned from 10% to 1.6% zero solutions

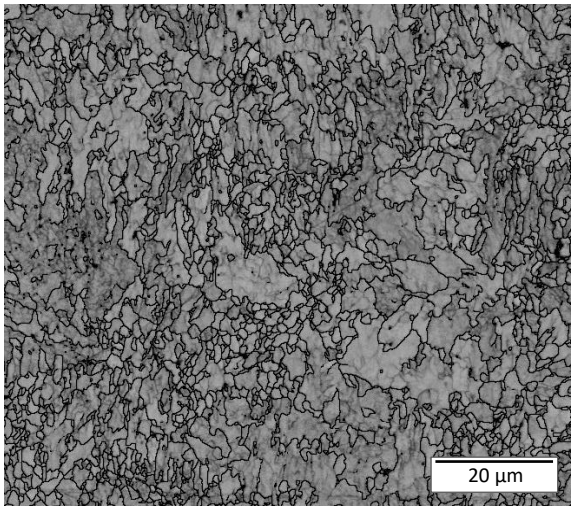

(a) Pattern quality map with high angle grain boundaries in black

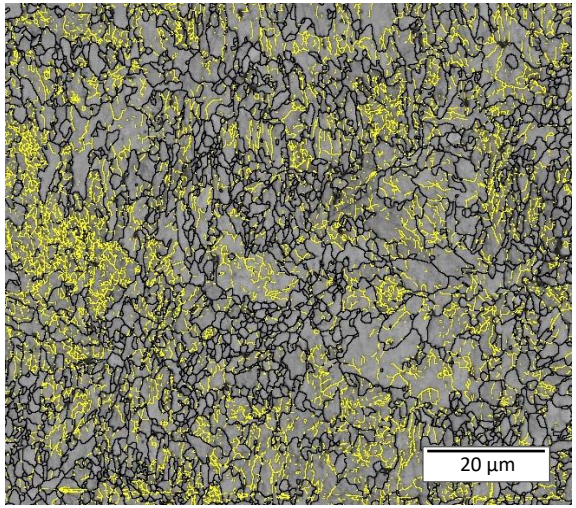

(b) Pattern quality map with high and low angle grain boundaries in black and yellow, respectively

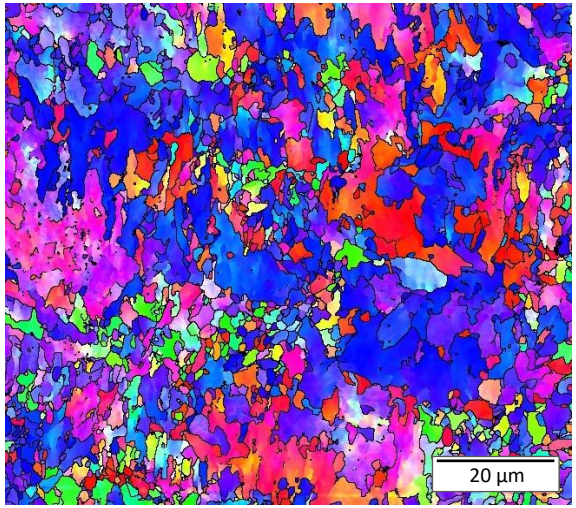

(c) Orientation map with IPF colouring (Figure 5-3)

Figure 5-8 Steel B (S700MC) taken from the rolling surface - image part cleaned from 8.3% to 1.3% zero solutions

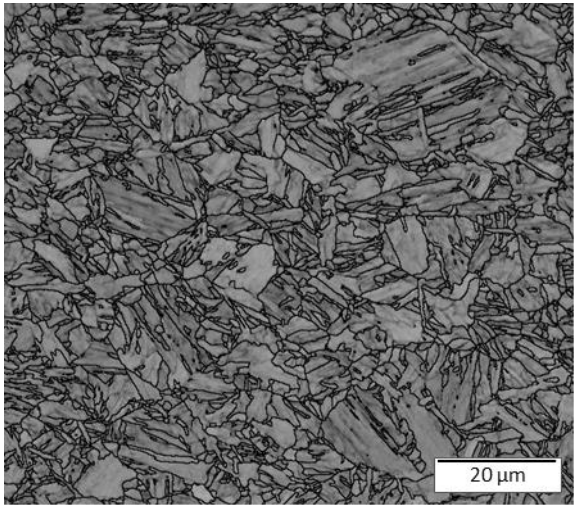

(a) Pattern quality map with high angle grain boundaries in black

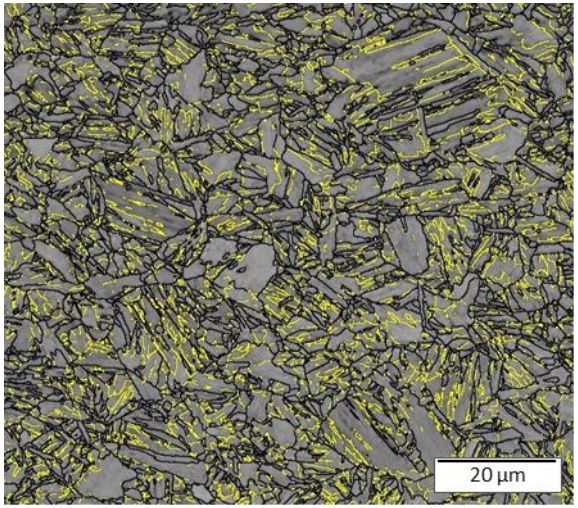

(b) Pattern quality map with high and low angle grain boundaries in black and yellow, respectively

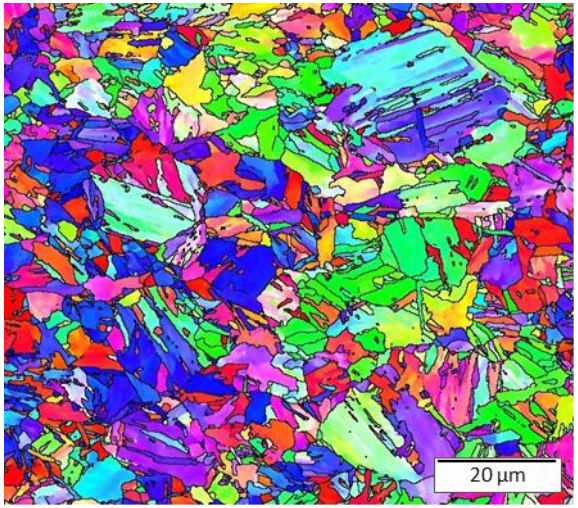

(c) Orientation map with IPF colouring (Figure 5-3)

Figure 5-9 Steel C (S690QL) taken from the rolling surface - image part cleaned from 8.5% to 1.0% zero solutions

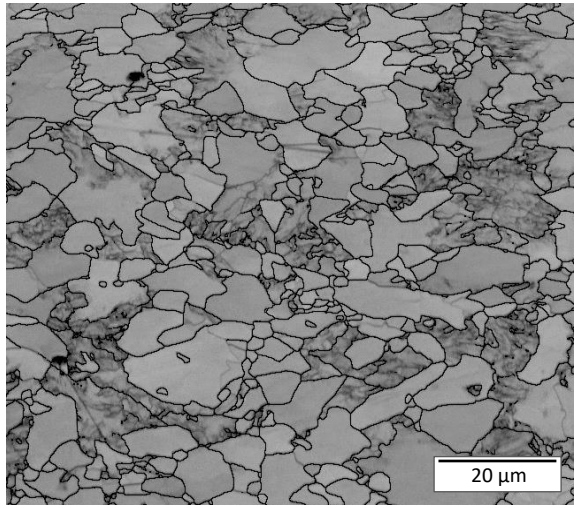

(a) Pattern quality map with high angle grain boundaries in black

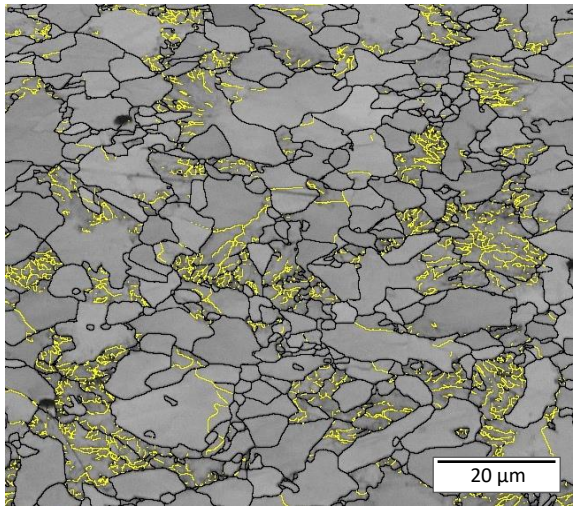

(b) Pattern quality map with high and low angle grain boundaries in black and yellow, respectively

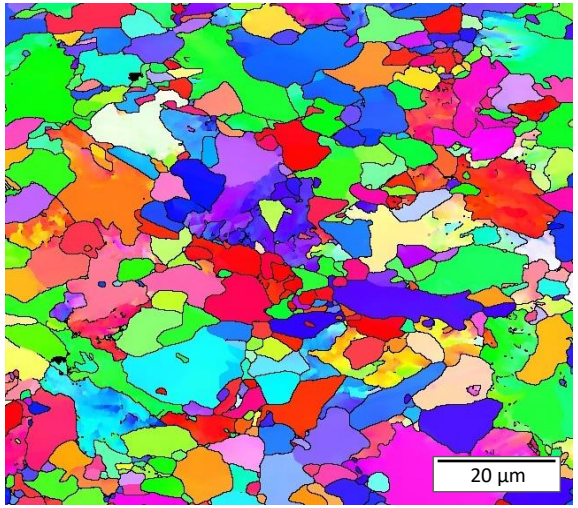

(c) Orientation map with IPF colouring (Figure 5-3)

Figure 5-10 Steel D (S460NH) taken from the rolling surface - image part cleaned from 4.6% to 1.1% zero solutions

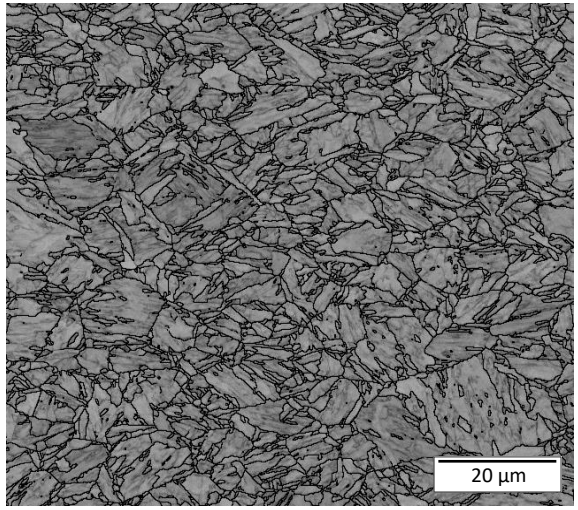

(a) Pattern quality map with high angle grain boundaries in black

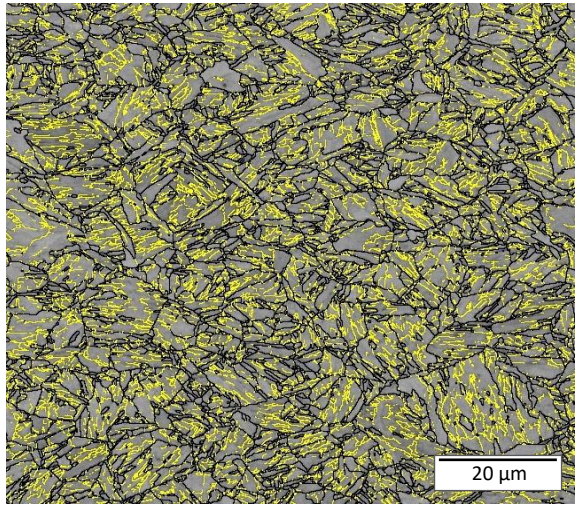

(b) Pattern quality map with high and low angle grain boundaries in black and yellow, respectively

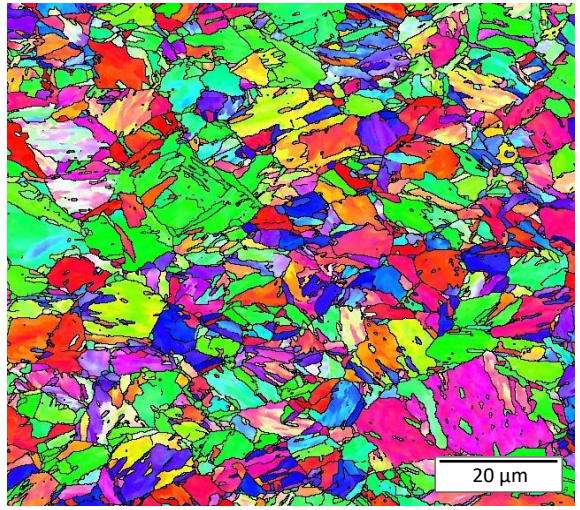

(c) Orientation map with IPF colouring (Figure 5-3)

Figure 5-11 Steel E (S690QH) taken from the rolling surface - image part cleaned from 6.9% to 0.3% zero solutions

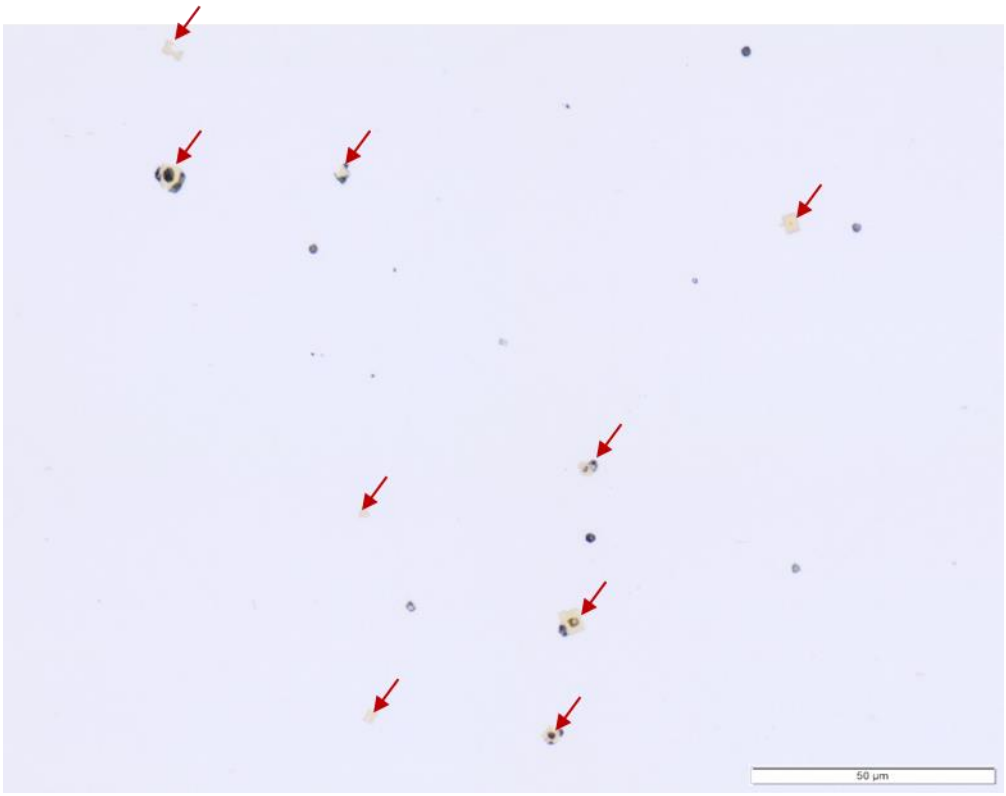

Figure 5-12 Light microscope of steel B (S700MC) - unetched

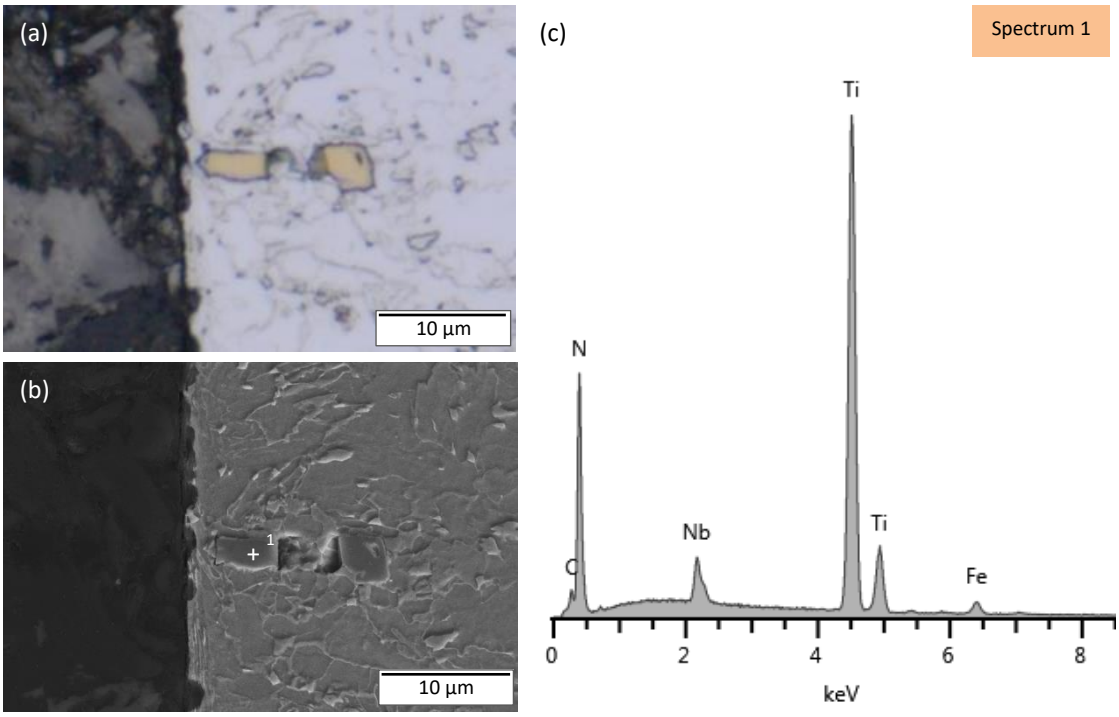

Figure 5-13 (a) light micrograph of precipitates in steel B (S700MC) – etched with 2% nital; (b) secondary electron image of a precipitate in steel B (S700MC) and (c) EDX spectrum of one of the precipitate (point 1)

5.3.2 Tensile specimens

Selected tensile specimens from steel A (S690QL) and B (S700MC) were sectioned along the rolling direction, and prepared using the techniques described in Section 6.2.1, for microstructure examination. Examples of the microstructure for the tensile specimens at 200 and 600°C are presented in Figure 5-14 to Figure 5-21. Note that following each test, the specimens were left in the furnace to cool down to room temperature (20°C). Images of the necked region of each tensile specimen presented in part (a) of Figure 5-14, Figure 5-16, Figure 5-18 and Figure 5-20, highlight that all the specimens necked prior to failure (i.e. moderate ductility).

For steel A (S690QL) at 200°C, classic 'cup and cone' failure is observed as depicted in Figure 5-14, (a) as at 600°C, with a greater reduction in the cross-sectional area at the higher temperature, as can be seen in Figure 5-16 (a). It is well known that ductile failure is initiated by the nucleation of voids under the influence of stress or strain. The presence of numerous voids is evident in the micrographs of the sectioned tensile specimens presented in Figure 5-15 and Figure 5-17. These voids generally form either by the cracking of precipitates including carbides or by decohesion between the particle and the matrix, but no evidence of these initiation mechanisms was observed.

Similarly, for steel B (S700MC) classic cup and cone failure is observed at 200°C as depicted in Figure 5-18 (a). However, in comparison with steel A (S690QL) at 600°C, the reduction in cross-sectional area of steel B (S700MC) at 600°C is less. In Figure 5-19 and Figure 5-21 many voids were observed around titanium rich precipitates. As mentioned in Section 5.3.1, these precipitates are stable up to temperatures as high as 1500°C. The bulk material around the precipitates softens at much lower temperatures (from 400°C) due to thermally activated processes including recovery. As a result, the voids around the titanium rich precipitates coalesce and grow as the material is strained at high temperatures.

Furthermore, in Figure 5-19 and Figure 5-21, there is evidence of the titanium-rich precipitates fracturing during straining. This is most likely a result of the localised interactions between concentrations of dislocations and precipitates (Gladman, 1999), although the detailed mechanism of this process is not clear from the work carried out in this study. Regardless of the mechanism, the presence of large titanium rich precipitates, is likely to have contributed to the reduced ductility observed in the stress-strain responses of steel B (S700MC) at elevated temperatures as observed in Section 4.2.4.

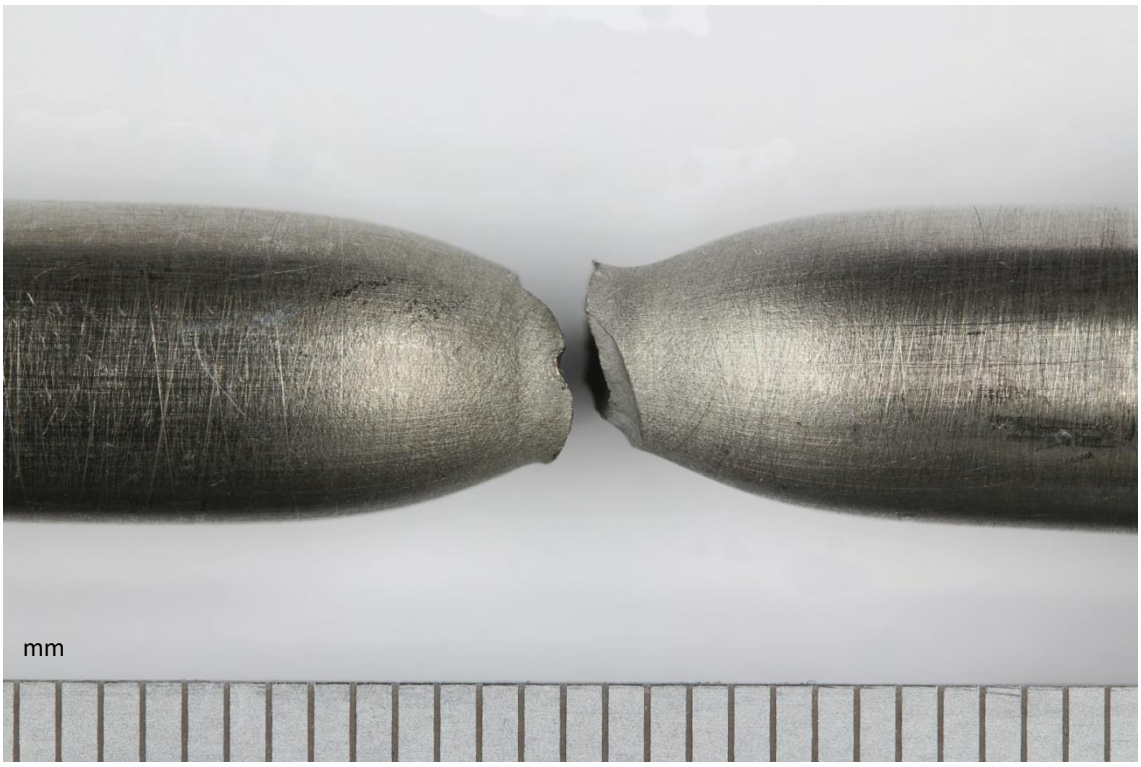

(a)

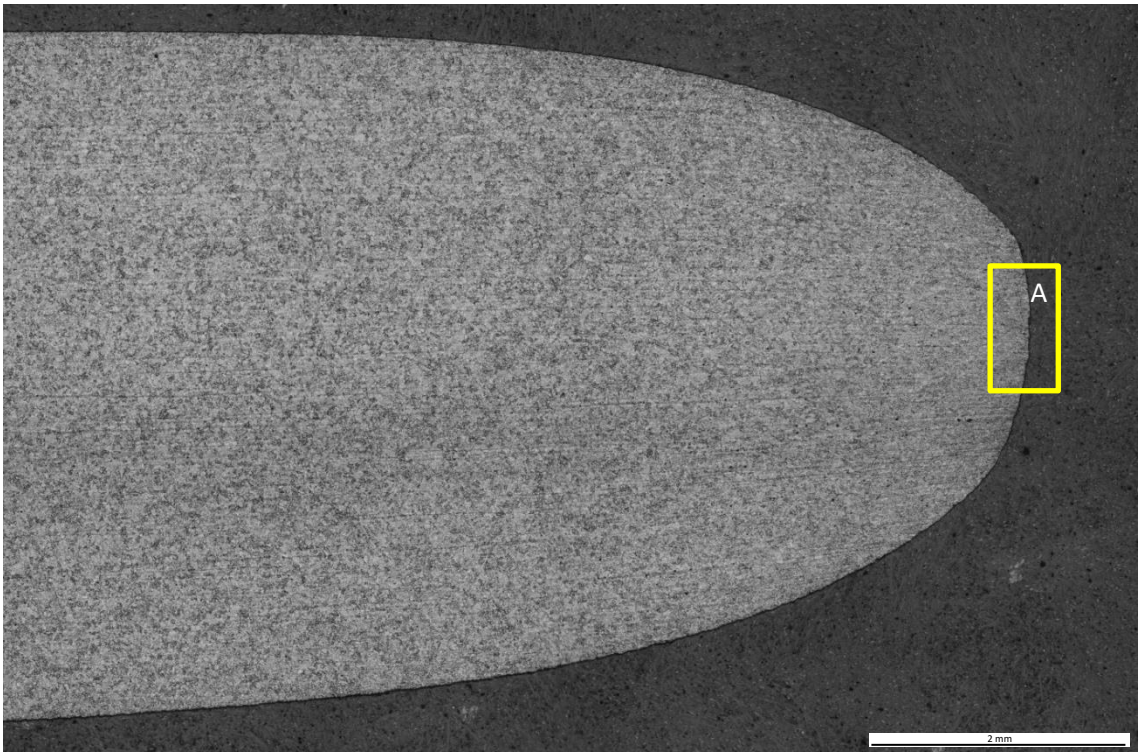

(b)

Figure 5-14 (a) focused stacked image and (b) light micrograph of cross-section of steel A (S690QL) tensile specimen tested at 200°C

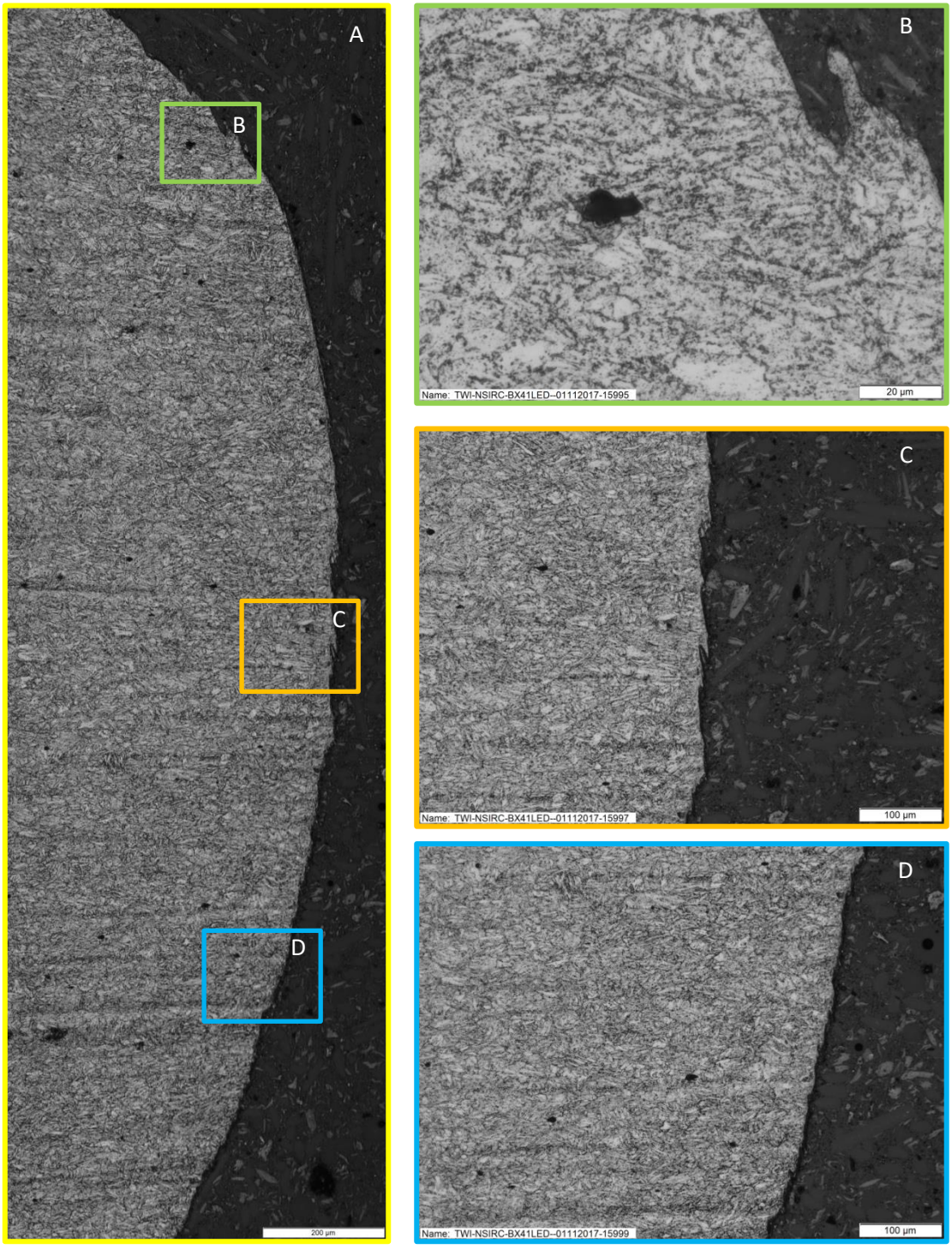

Figure 5-15 Light micrograph of cross-section of steel A (S690QL) tensile specimen tested at 200°C

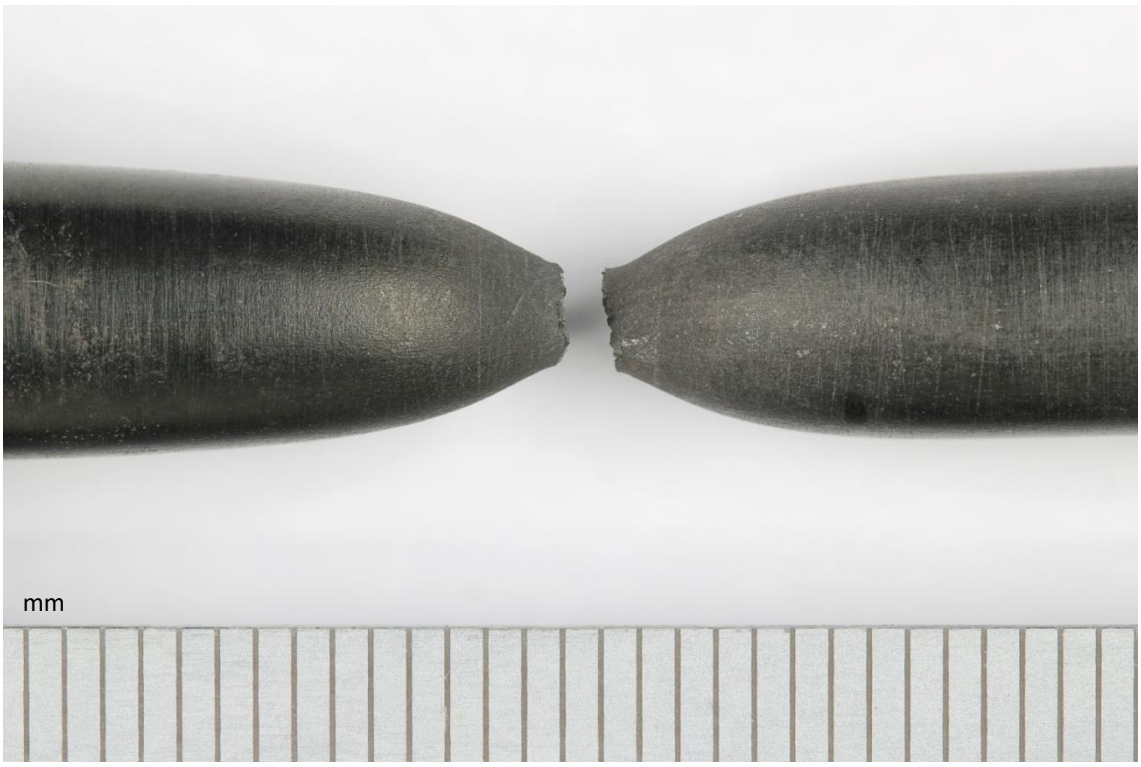

(a)

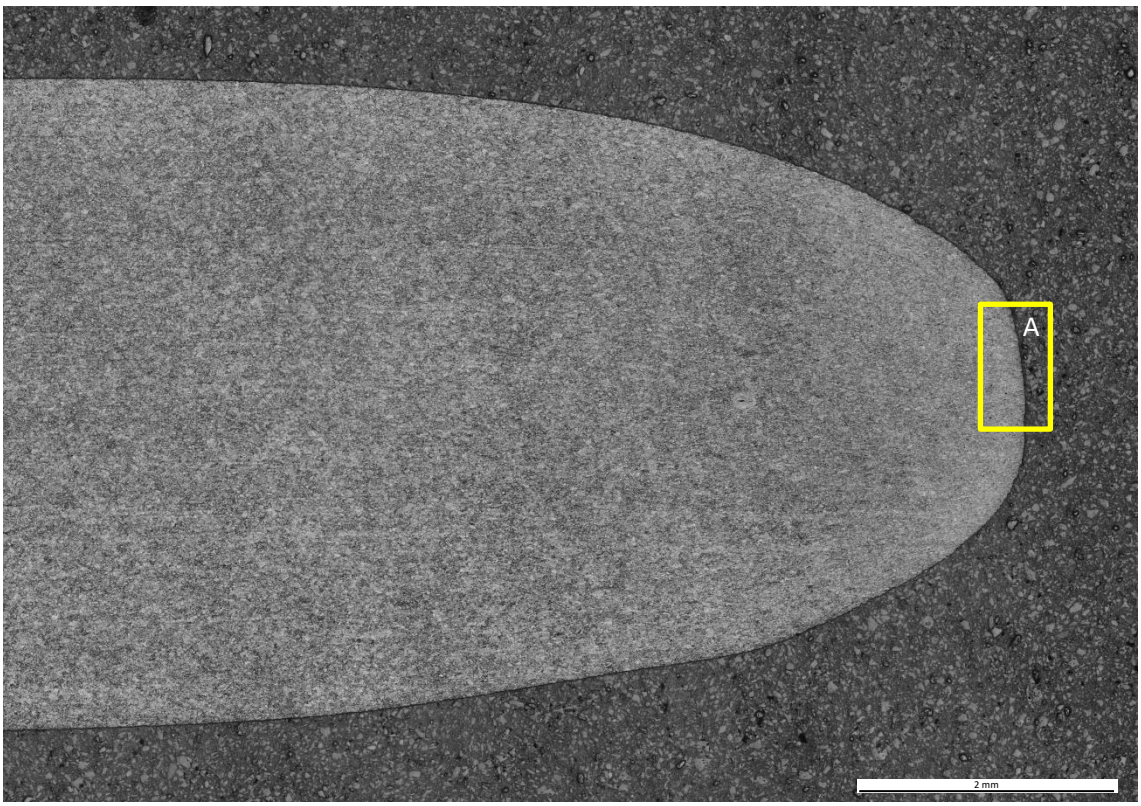

(b)

Figure 5-16 (a) focused stacked image and (b) light micrograph of cross-section of steel A (S690QL) tensile specimen tested at 600°C

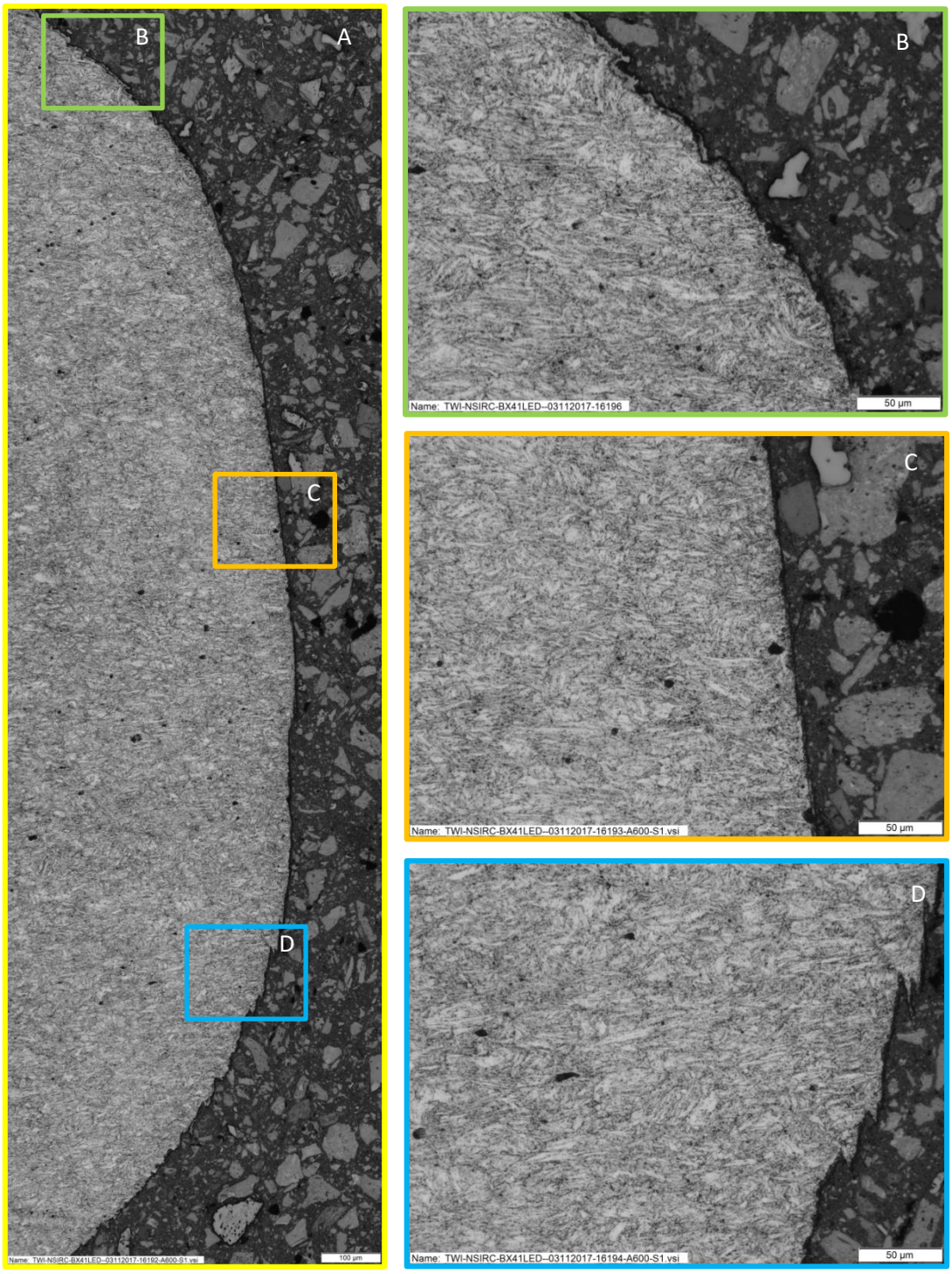

Figure 5-17 Light micrograph of cross-section of steel A (S690QL) tensile specimen tested at 600°C

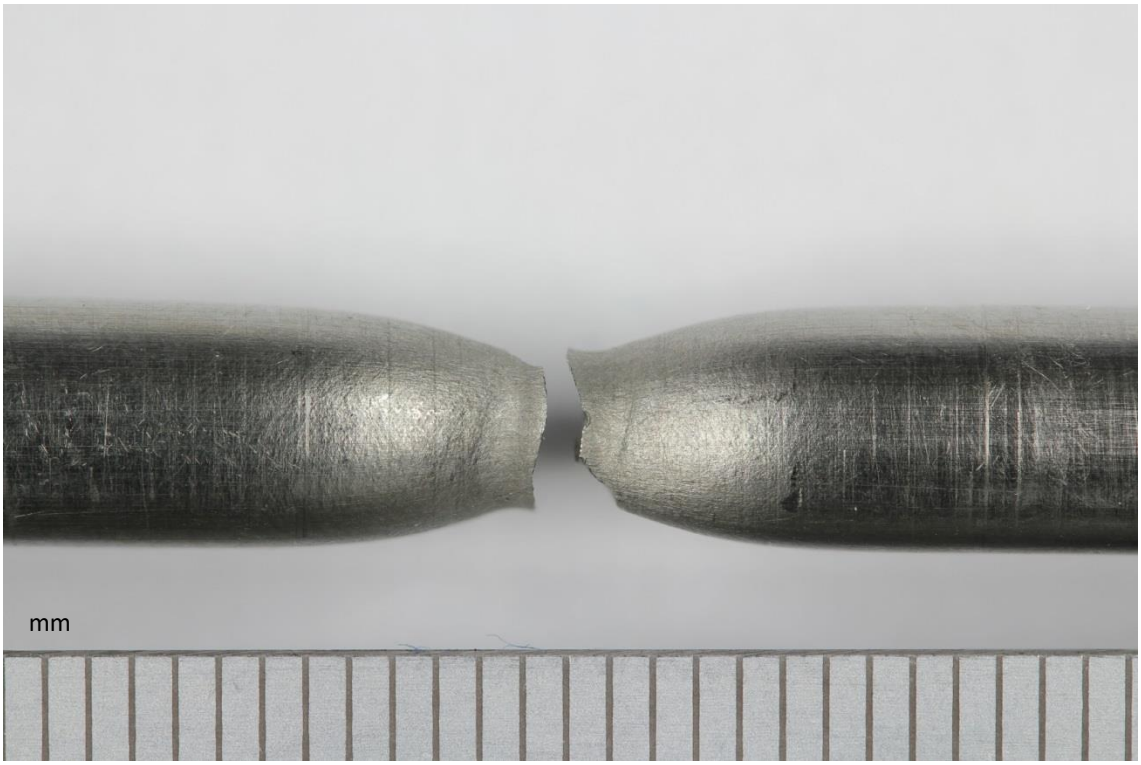

(a)

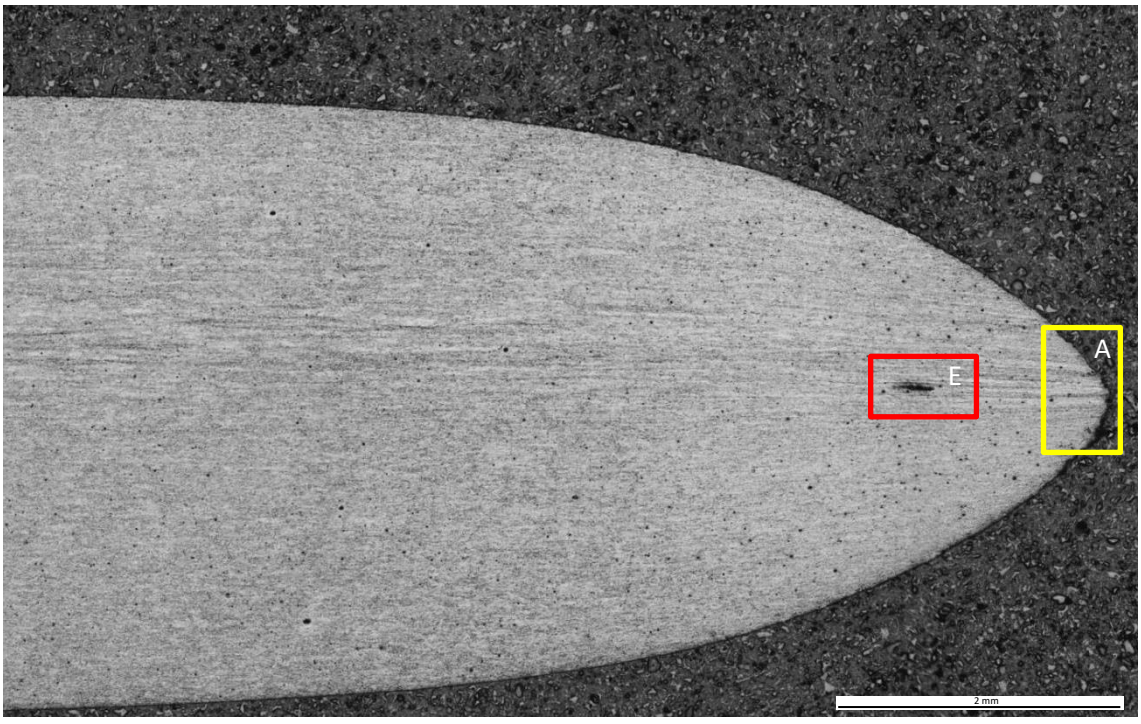

(b)

Figure 5-18 (a) focused stacked image and (b) light micrograph of cross-section of steel B (S700MC) tensile specimen tested at 200°C

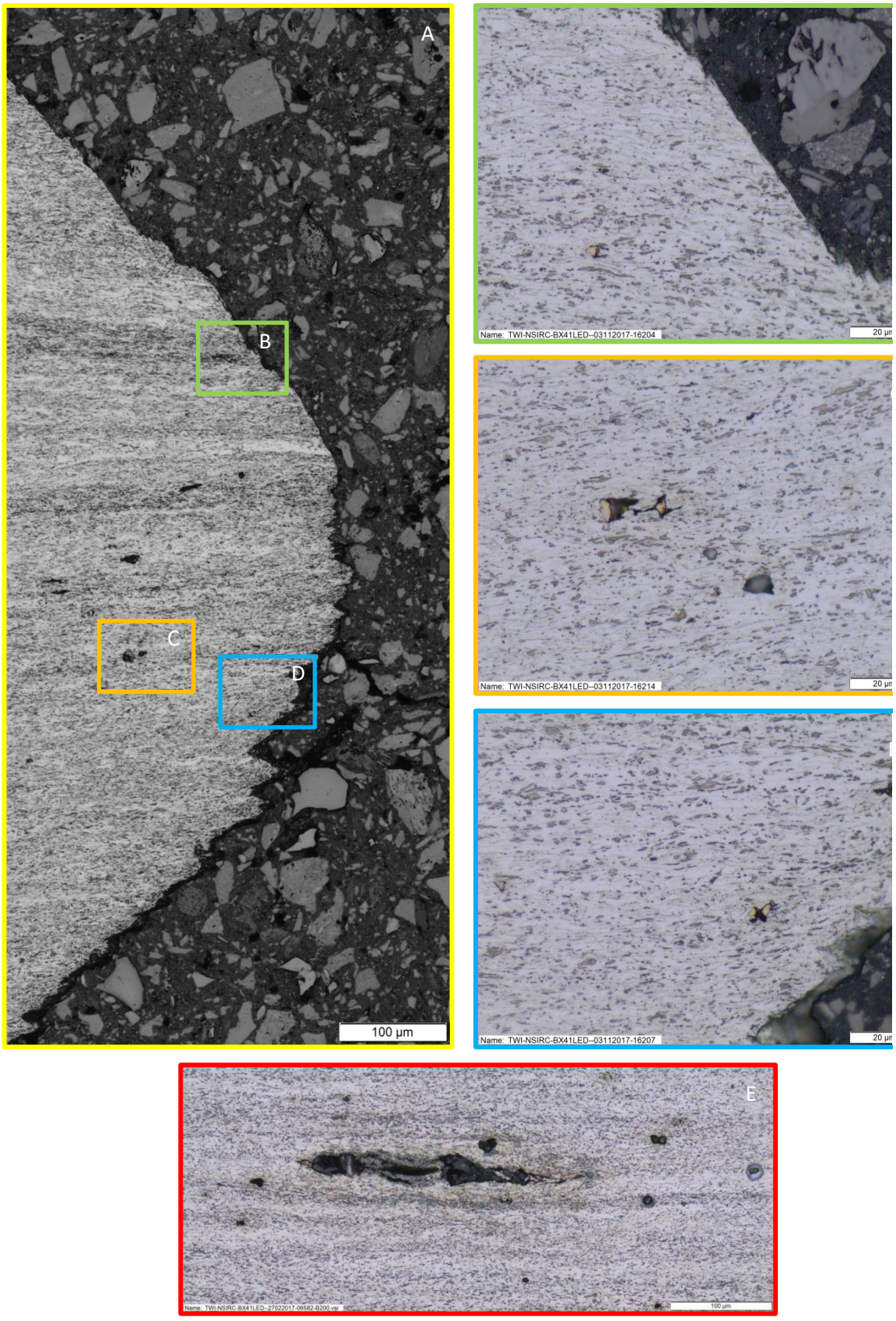

Figure 5-19 Light micrograph of cross-section of steel B (S700MC) tensile specimen tested at 200°C

(a)

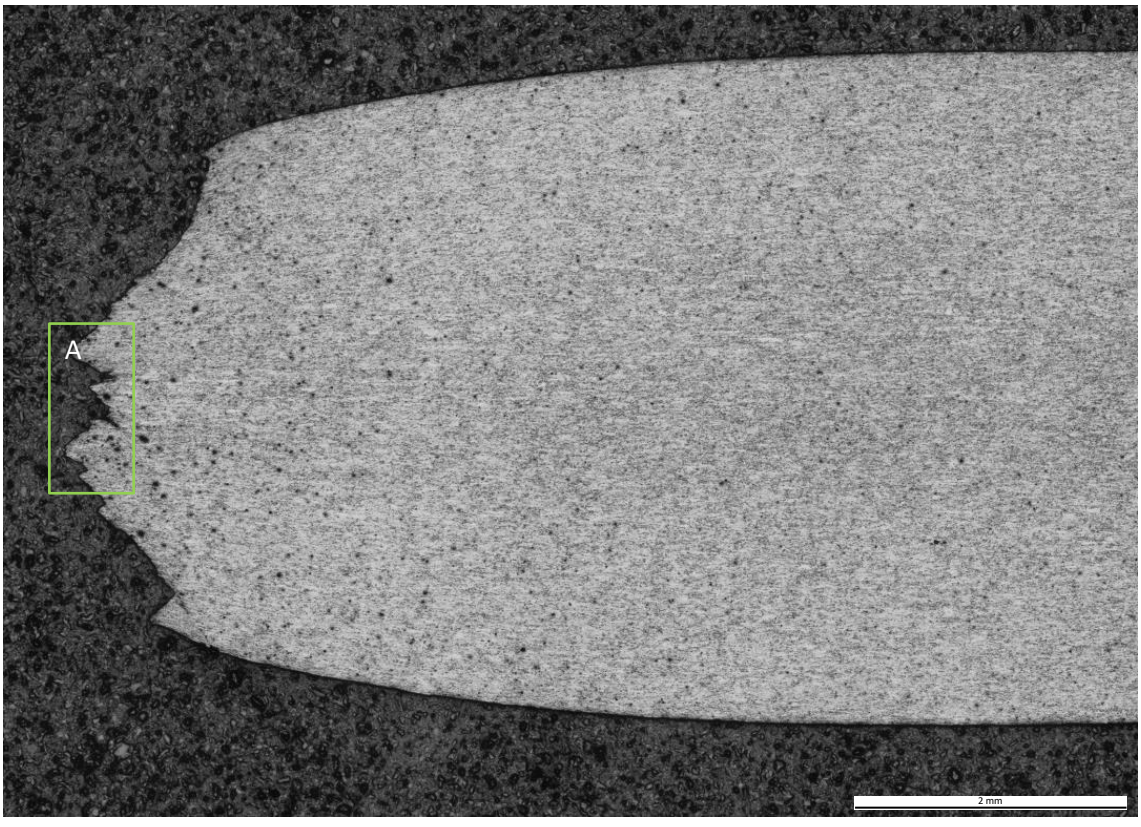

(b)

Figure 5-20 (a) focused stacked image and (b) light micrograph of cross-section of steel B (S700MC) tensile specimen tested at 600°C

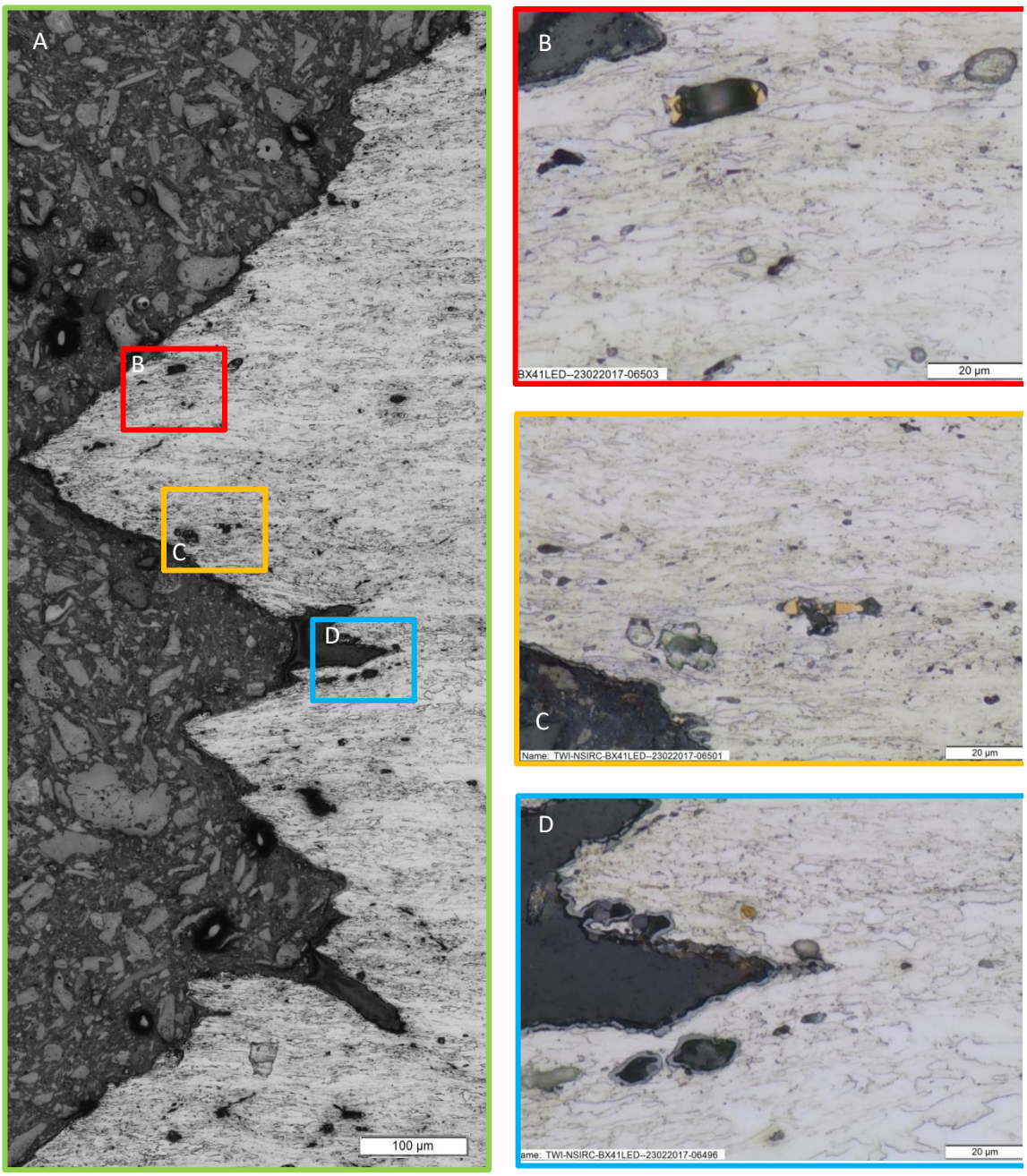

Figure 5-21 Light micrograph of cross-section of steel B (S700MC) tensile specimen tested at 600°C

5.3.3 Heat treatments

5.3.3.1 Vickers hardness

The results of the Vickers hardness tests carried out on the as-received and heat-treated specimens for steels A (S690QL) and B (S700MC) are presented graphically in Figure 5-22 and Figure 5-23, respectively. From Figure 5-22 the hardness of steel A is essentially unchanged until 600°C where the hardness drops slightly from 263 HV1 at room temperature to 251 HV1 after 5 minutes and 255 HV1 after 60 minutes. A noticeable drop in the hardness is observed at 700°C, where it decreased by 20 HV1 after 5 minute soaking time, whilst after 60 minute soaking time the hardness dropped by 45 HV1, compared with the hardness at room temperature. At 800°C, the hardness increased to 350 and 433 HV1 after a 5 minute and 60 minute soaking times, respectively, because steel A (S690L) was heated above the intercritical region (A_1) (Figure 5-4) and hence some martensite had formed upon quenching (see Figure 5-25 (h) and (i)). The standard deviations for steel A's (S690QL) hardness' are reasonably low, except for at 800°C where the values following soaking times of 5 and 60 minutes are ±31 and ±23, respectively. The high standard deviation is due to the mixed microstructure, which includes regions of hard carbon rich martensite and soft ferrite.

In the case of steel B (S700MC) shown in Figure 5-23, it can be seen that after a 5 minute soaking time, the hardness slightly dropped from 258 to 245 HV1 at 500°C, and then increased to a maximum hardness of 282 HV1 at 700°C, before decreasing to 229 HV1 at 800°C. Similarly, for 60 minute soaking time the hardness was consistent at 500°C and reached its maximum hardness of 284 HV1 at 600°C before decreasing to 225 HV1 at 800°C. Upon quenching from 800°C (intercritical region), some martensite was anticipated to have formed in steel B (S700MC), however very little evidence of martensite was seen (see Figure 5-27 (h) and (i)). It is worth mentioning that the hardness of martensite is dependent on the amount of free carbon available; generally, the hardness of martensite increases with increasing carbon content up to 0.6%. A lower carbon content of 0.06% was in steel B (S700MC) compared with 0.17% in steel A (S690QL), and the lower hardness of steel B (S700MC) following quenching at 800°C at 800°C, suggest that much less free carbon was available to form martensite compared with steel A (S690QL). The standard deviation for steel B (S700MC) was reasonable low at all soaking temperatures. Further comments on the microstructures of steels A (S690QL) and B (S700MC) are given in Section 5.3.3.2 and 5.3.3.3.

From Figure 5-22 and Figure 5-23, the influences of the time and temperature on the resulting hardness following quenching are evident. To reveal the diffusion controlled effects more clearly, the Vickers hardness was plotted against the H-J parameter defined in Equation (5.1). The use of the H-J parameter resulted in a single curve for each of steel A (S690QL) and B (S700MC), as shown

in Figure 5-24. The results following a heat treatment and quenching after 800°C are not included in this figure, as this was in the intercritical or supercritical region for these steels. From Figure 5-24, general softening in steel A (S690QL) is observed, with a slight interruption in the trend when the H-J parameter is 17.5. This increase is minor in comparison with steel B (S700MC), where a peak is observed when the H-J parameter is approximately 18. It is likely that the increase in hardness is a result of secondary hardening. Interestingly, this peak matches the H-J parameter at which Okumura et al. (1987) saw the maximum precipitation effect caused by niobium and vanadium appeared at its maximum in low alloy HSS.

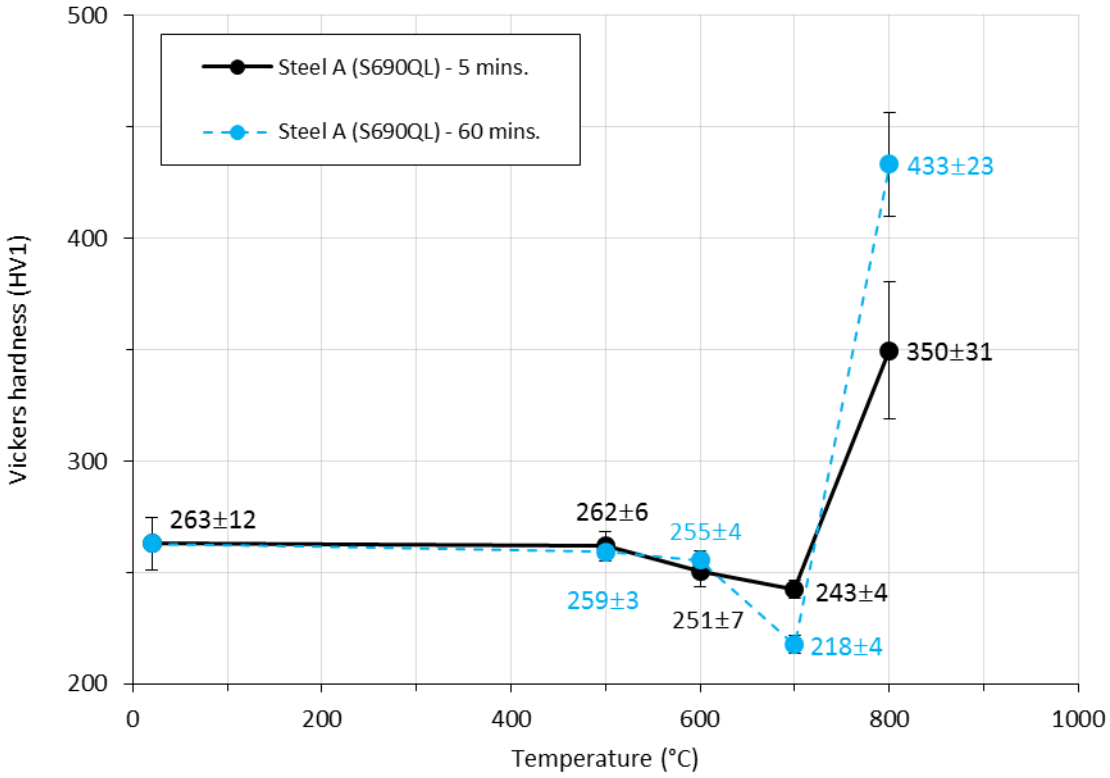

Figure 5-22 Average Vickers hardness for steel A (S690QL) in as-received condition and after heat treatment at various temperatures and quenching

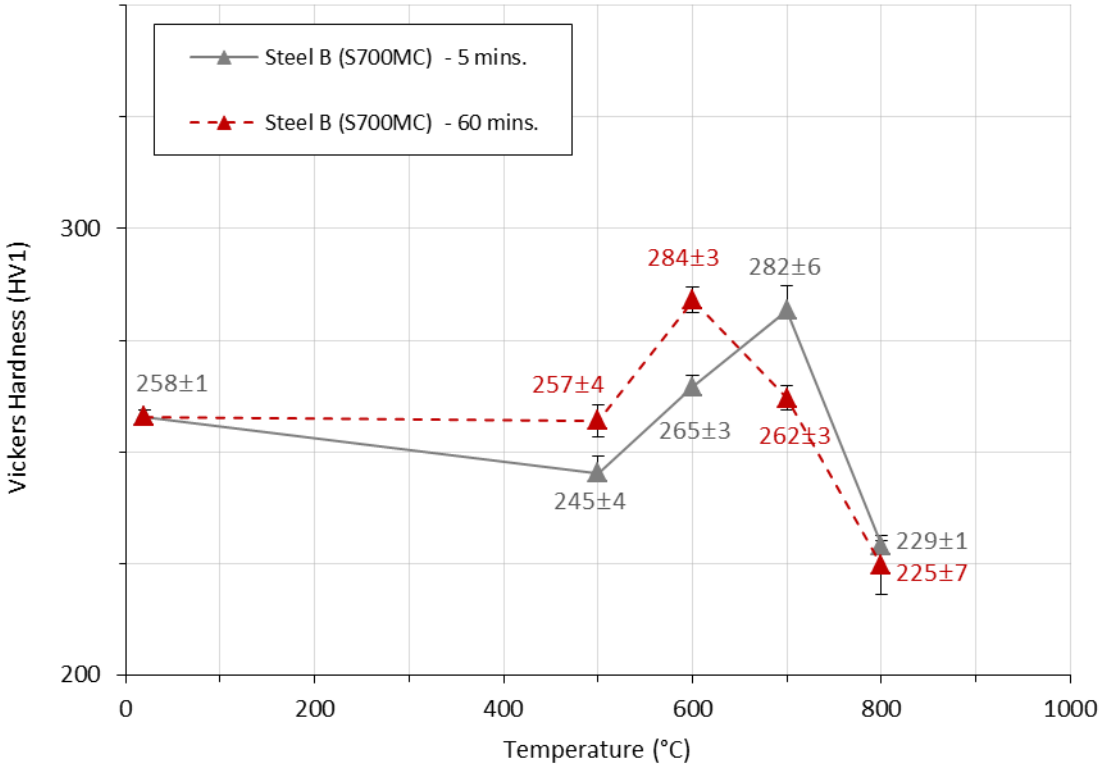

Figure 5-23 Average Vickers hardness for steel B (S700MC) in as-received condition and after heat treatment at various temperatures and quenching

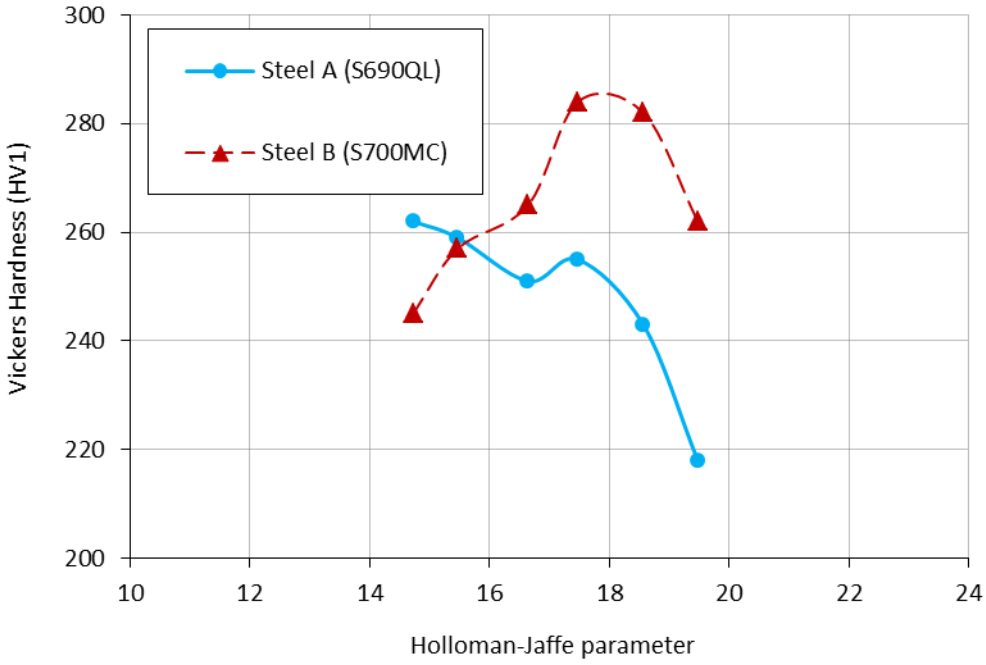

Figure 5-24 Average Vickers hardness and corresponding Hollomon-Jaffe parameters for steel A (S690QL) and B (S700MC)

5.3.3.2 Microstructural studies of steel A (S690QL)

Figure 5-25 presents the micrographs for the as-received and heat-treated and quenched steel A (S690QL) samples. In addition, images taken at a higher resolution using a Zeiss Sigma field emission gun scanning electron microscope (FEGSEM) are depicted in Figure 5-26. Compared with the as-received material, the microstructural changes are very difficult to quantify at 500°C following a 5 and 60 minute soaking time as shown in Figure 5-25 (b) and (c), respectively. Similar observations are seen after a heat treatment at 600°C for 5 minutes (Figure 5-25 (d)). However, following a soaking time of 60 minutes at 600°C (Figure 5-25 and Figure 5-26 (e)), the lath boundaries appear to gradually disappear. This is also observed after a 5 minute soaking time at 700°C (Figure 5-25 (f)). After 60 minutes soaking time at 700°C, Figure 5-25 (f), there appears to be evidence of cementite spheroidising, with much coarser precipitates observed, particularly at the grain boundaries which appear more pronounced compared with a soaking time of 5 minutes. This is likely to have contributed to the reduced hardness of 218 HV observed. The presence of larger cementite (white dots) at the grain boundaries is evident in the SEM image shown in Figure 5-26 (f).

Quenching in water after heating to 800°C has resulted in a martensitic microstructure, characterised by the collection of small plate-shaped or needle shape grains as depicted in Figure 5-25 (h) and (i). The needle shape grains can be seen more clearly in the SEM image shown in Figure 5-26 (g) and (h). The presence of martensite indicates that steel A (S690QL) was heated above A_1, in the intercritical region where austenite will begin to nucleate at the ferrite grain boundaries. Any carbon present in ferrite will diffuse into austenite, and the austenite regions richer in carbon will form martensite, with a higher associated hardness, on subsequent quenching. With a longer soaking time, more carbon will diffuse from ferrite to austenite and this explains why the corresponding mean hardness was higher following a 60 minute soaking time (433 HV1) compared with 5 minutes (350 HV1).

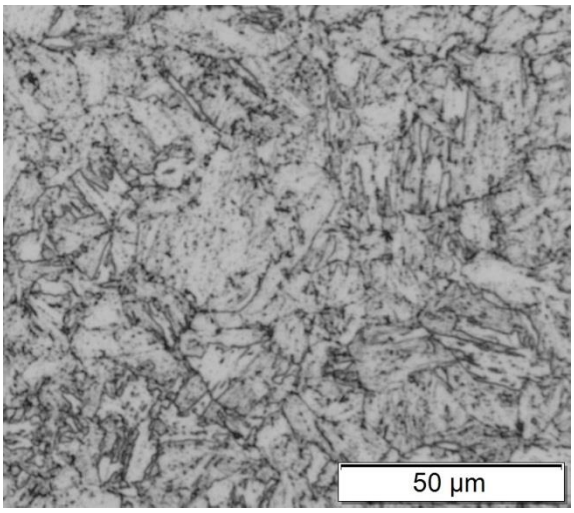

(a) As-received (263 HV1)

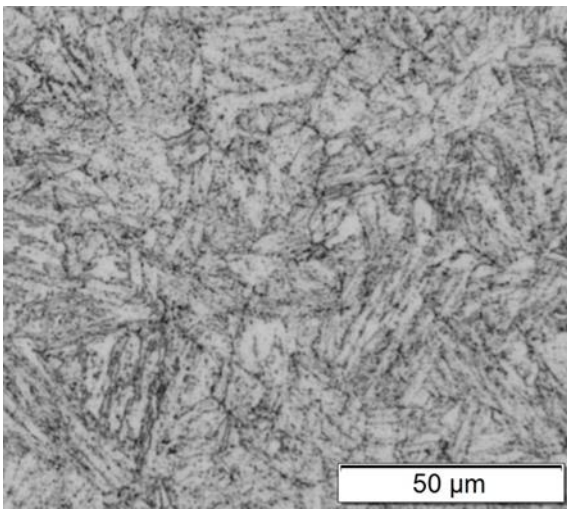

(b) 500°C + 5 minutes (262 HV1)

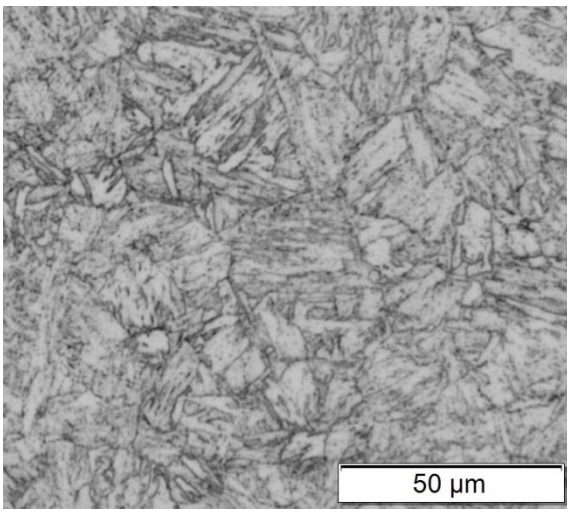

(c) 500°C + 60 minutes (259 HV1)

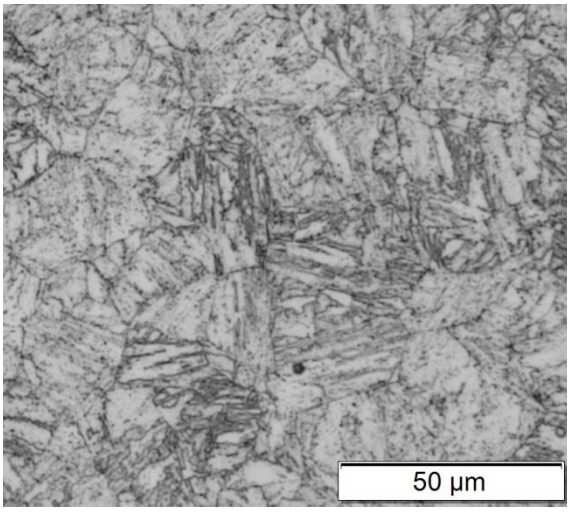

(d) 600°C + 5 minutes (251 HV1)

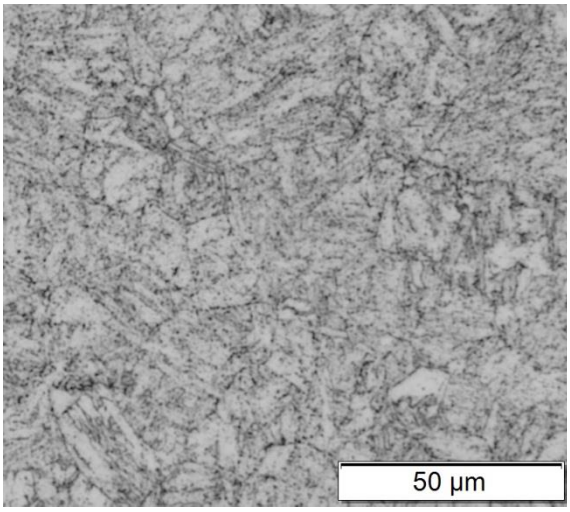

(e) 600°C + 60 minutes (255 HV1)

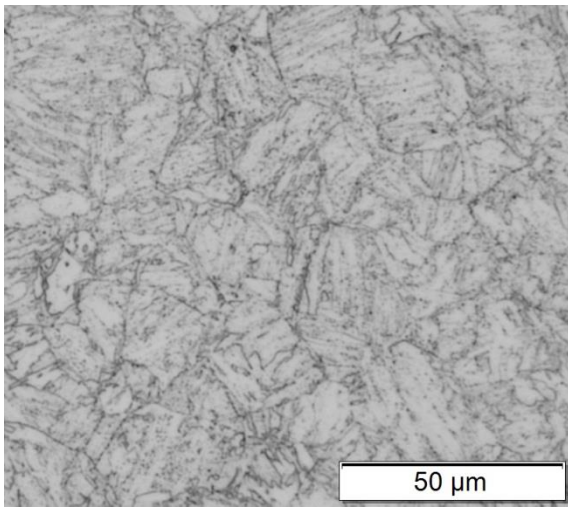

(f) 700°C + 5 minutes (243 HV1)

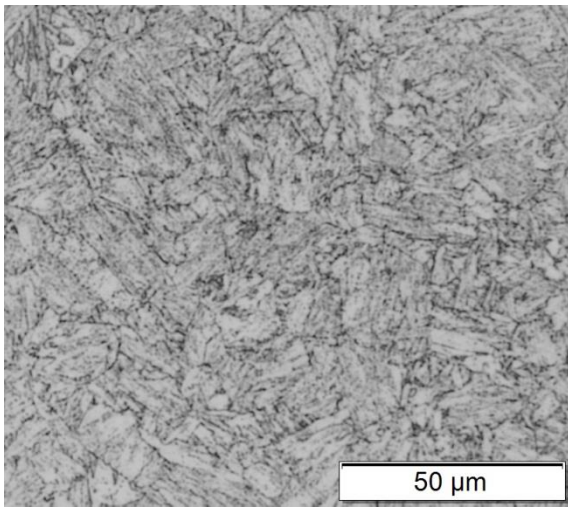

(g) 700°C + 60 minutes (218 HV1)

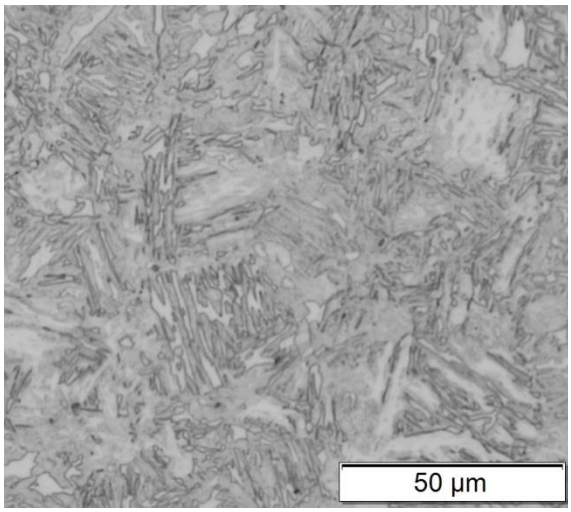

(h) 800°C + 5 minutes (350 HV1)

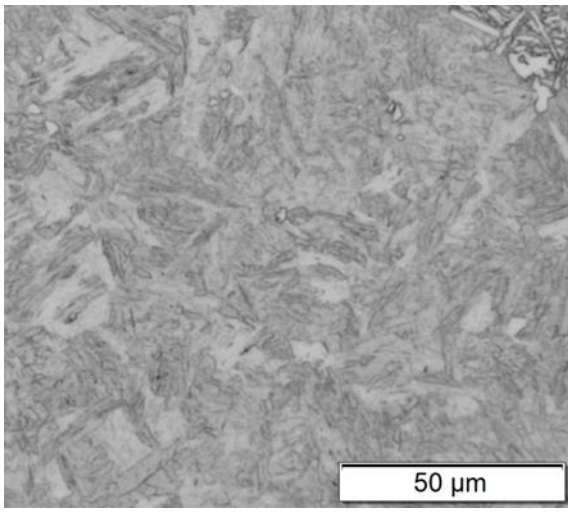

(i) 800°C + 60 minutes (433 HV1)

Figure 5-25 (a)-(i) Light micrographs of steel A (S690QL) taken from the rolling direction at various temperatures and soaking times

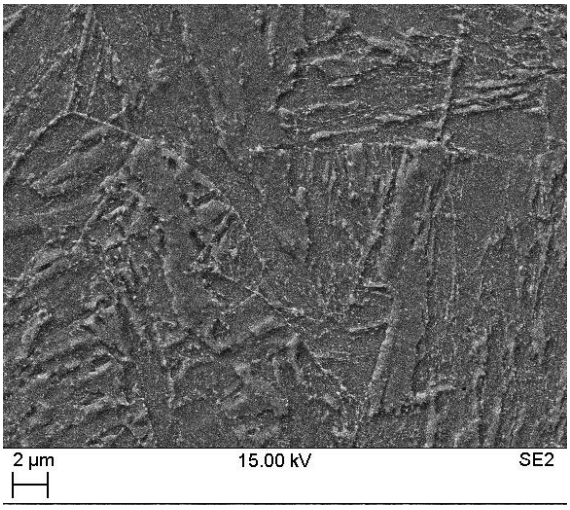

(a) 500°C + 5 minutes (262 HV1)

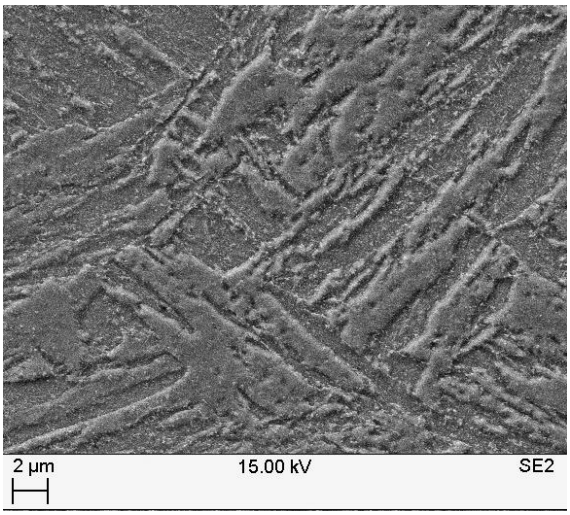

(b) 500°C + 60 minutes (259 HV1)

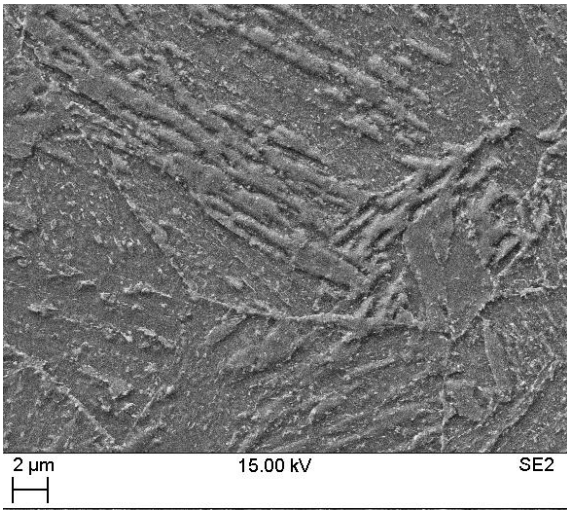

(c) 600°C + 5 minutes (251 HV1)

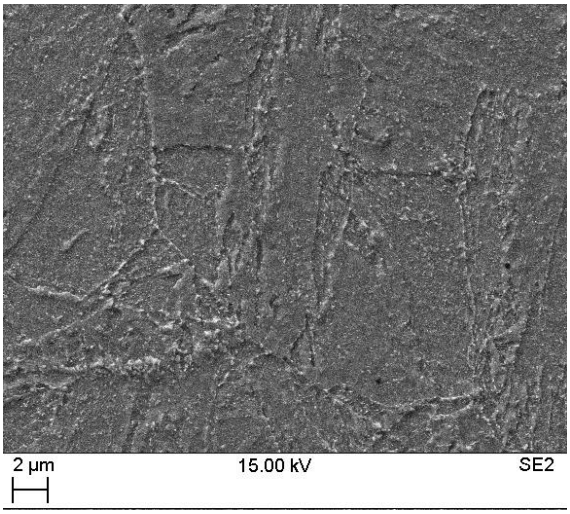

(d) 600°C + 60 minutes (255 HV1)

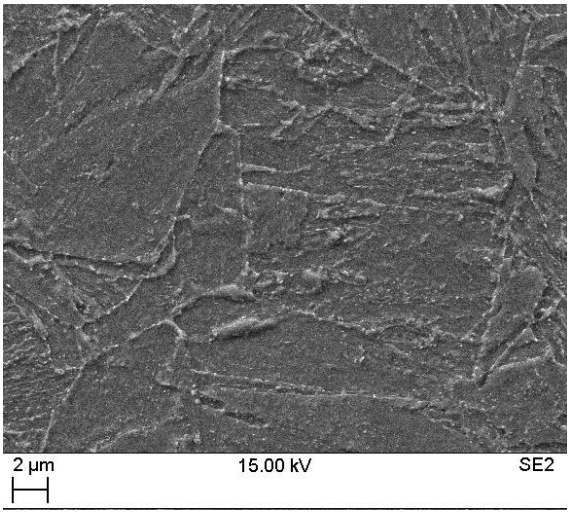

(e) 700°C + 5 minutes (243 HV1)

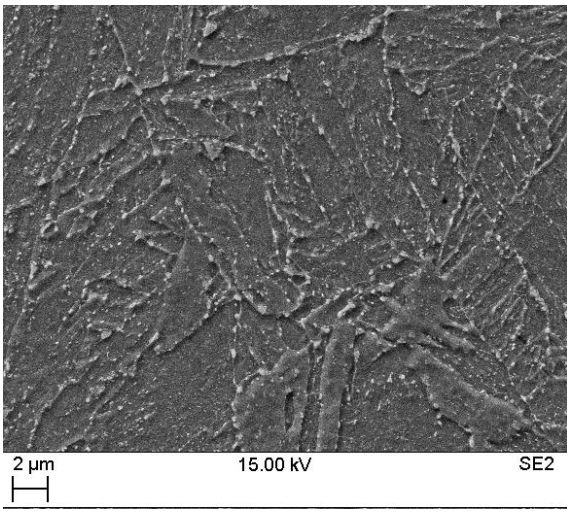

(f) 700°C + 60 minutes (218 HV1)

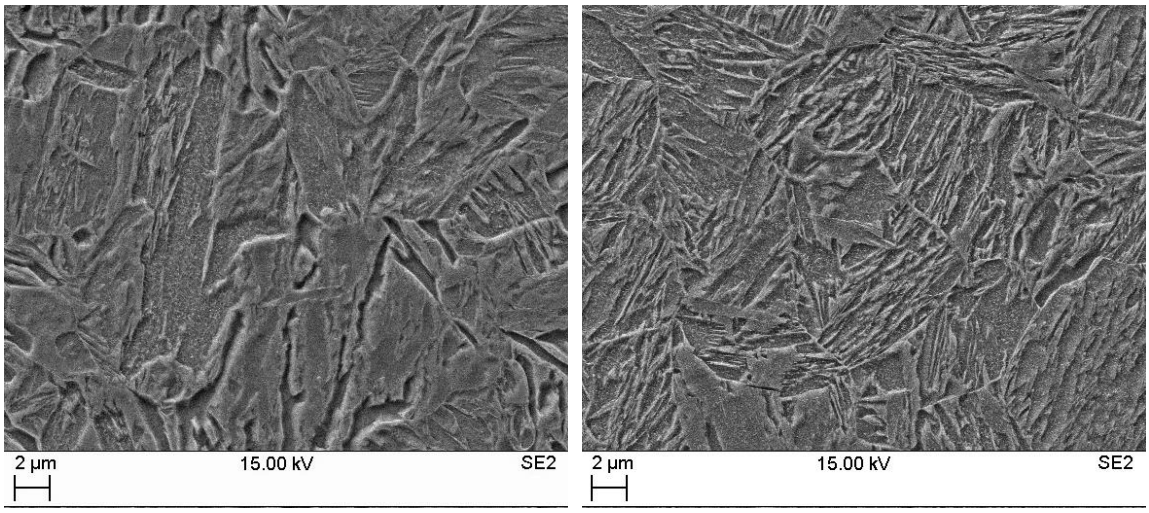

(g) 800°C + 5 minutes (350 HV1) (h) 800°C + 60 minutes (433 HV1)

Figure 5-26 (a)-(h) SEM images of steel A (S690QL) taken from the rolling direction at various temperatures and soaking times

5.3.3.3 Microstructural studies of steel B (S700MC)

The micrographs of the as-received and heat-treated and quenched steel B (S700MC) samples are presented in Figure 5-27. Compared with the microstructure of the as-received material, changes in the heat-treated samples are difficult to identify from these figures, as the etchant used (2% nital) does not reveal all the grains and many of these grains are too fine to resolve under the light microscope as mentioned in Section 5.3.1. However, compared with the microstructure of the as-received steel, presented in Figure 5-27 (a), there appears to be very little evidence of the grain morphology changing until 800°C as shown in Figure 5-27 (h) and (i). The micrographs presented in Figure 5-27 (h) and (i), suggests that steel B (S700MC) was heated just into the intercritical region, where small regions of carbon rich austenite have formed which, upon subsequent quenching, form martensite. A longer soaking time of 60 minutes, will give more time for carbon to diffuse from ferrite to austenite but no difference was seen between the hardness of these steels after 5 minutes (229 HV1) and 60 minutes (225 HV1) soaking times at 800C°C. This may be because the formation of martensite was limited due to the low carbon content in steel B (S700MC).

EBSD was conducted on the specimens exposed at 800°C for 5 and 60 minutes, to further examine the grain morphology. The resulting pattern quality maps are presented in Figure 5-28 and 5-29 and the corresponding orientation maps are presented in Figure 5-30. The grain structure following a soaking time of 60 minutes at 800°C (Figure 5-28 (c)), appears more equiaxed (i.e. same diameter in all directions) compared with the elongated 'pancake-shape' grains seen in the as-received condition shown again in Figure 5-28 (a), demonstrating that recrystallisation has occurred.

Recrystallisation typically occurs after recovery and results in the subsequent loss in material strength; hence it is thought that the number of low angle grain boundaries shown in yellow (Figure 5-29) reduced prior to recrystallisation. No evidence of grain growth was observed.

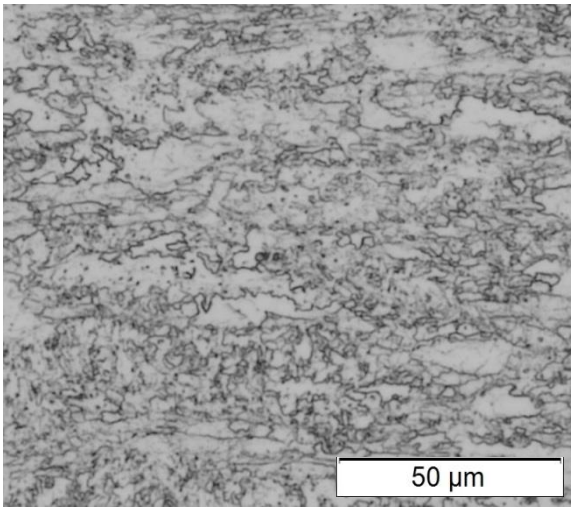

(a) As-received (258 HV1)

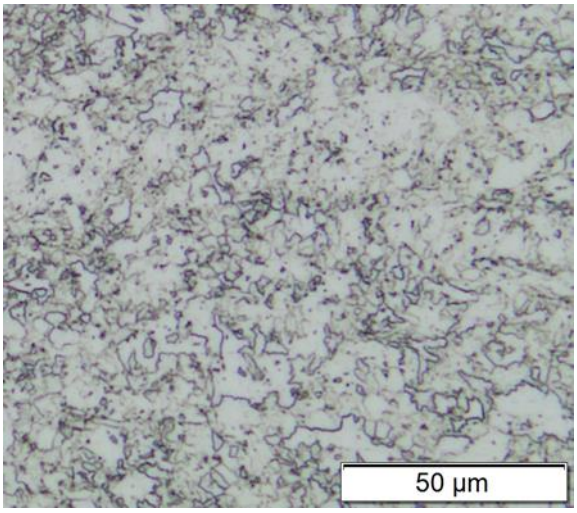

(b) 500°C + 5 minutes (245 HV1)

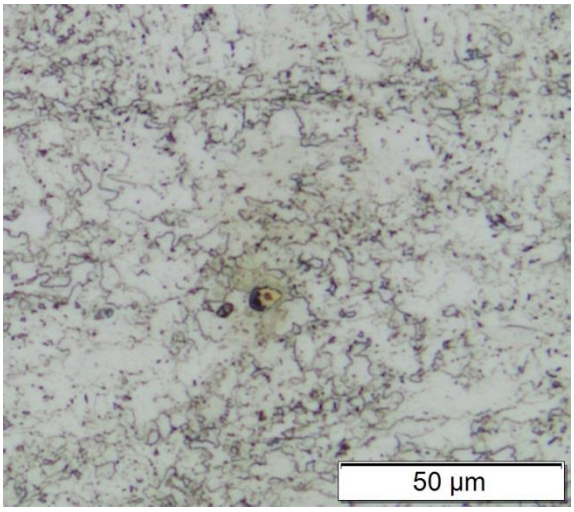

(c) 500°C + 60 minutes (257 HV1)

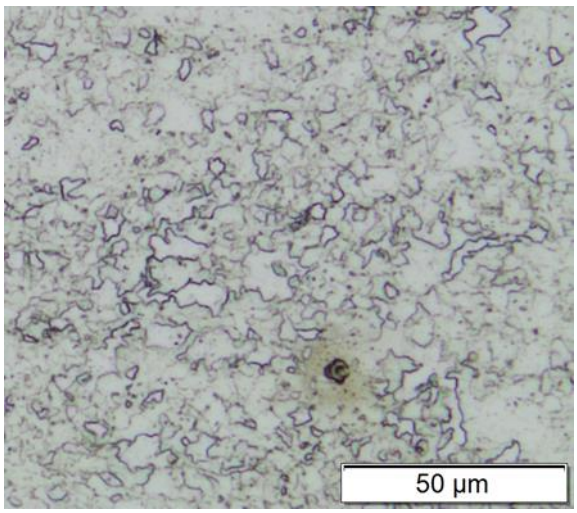

(d) 600°C + 5 minutes (265 HV1)

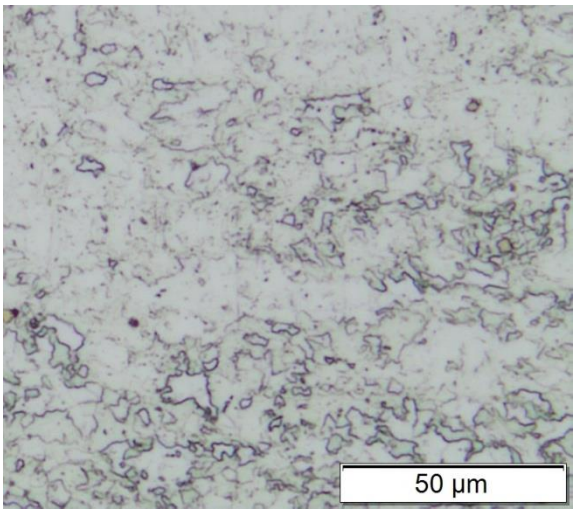

(e) 600°C + 60 minutes (284 HV1)

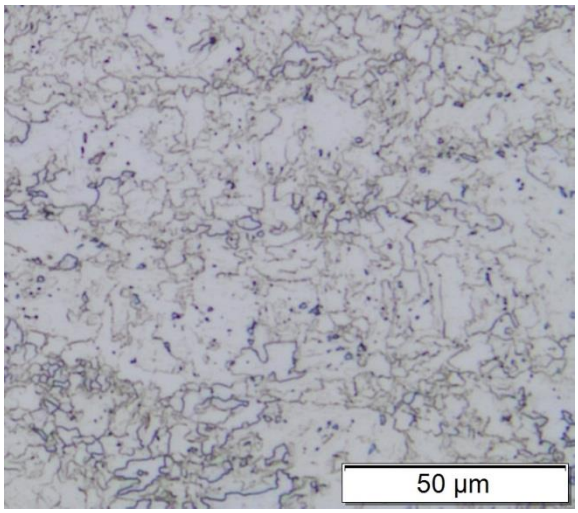

(f) 700°C + 5 minutes (282 HV1)

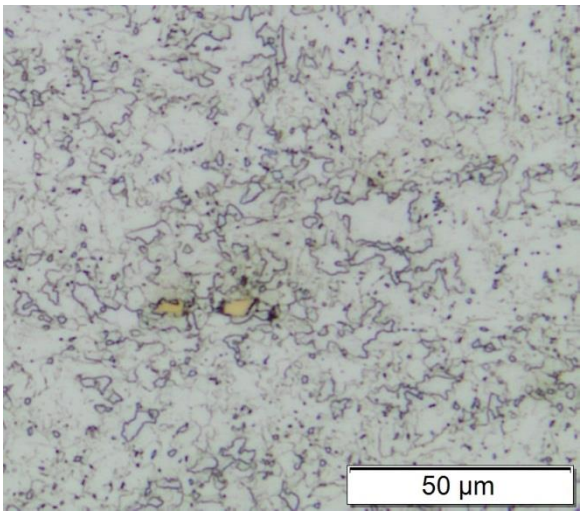

(g) 700°C + 60 minutes (262 HV1)

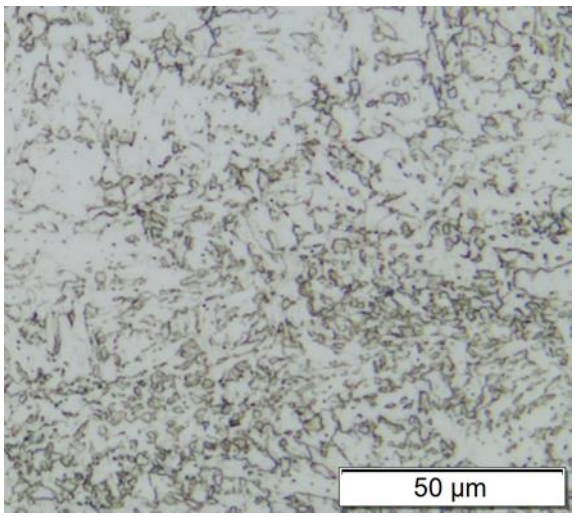

(h) 800°C + 5 minutes (229 HV1)

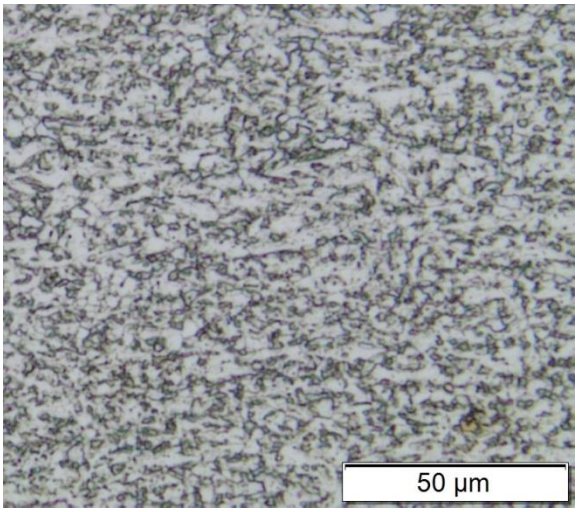

(i) 800°C + 60 minutes (225 HV1)

Figure 5-27 (a)-(i) Light micrographs of steel B (S700MC) taken from the rolling direction at various temperatures and soaking times

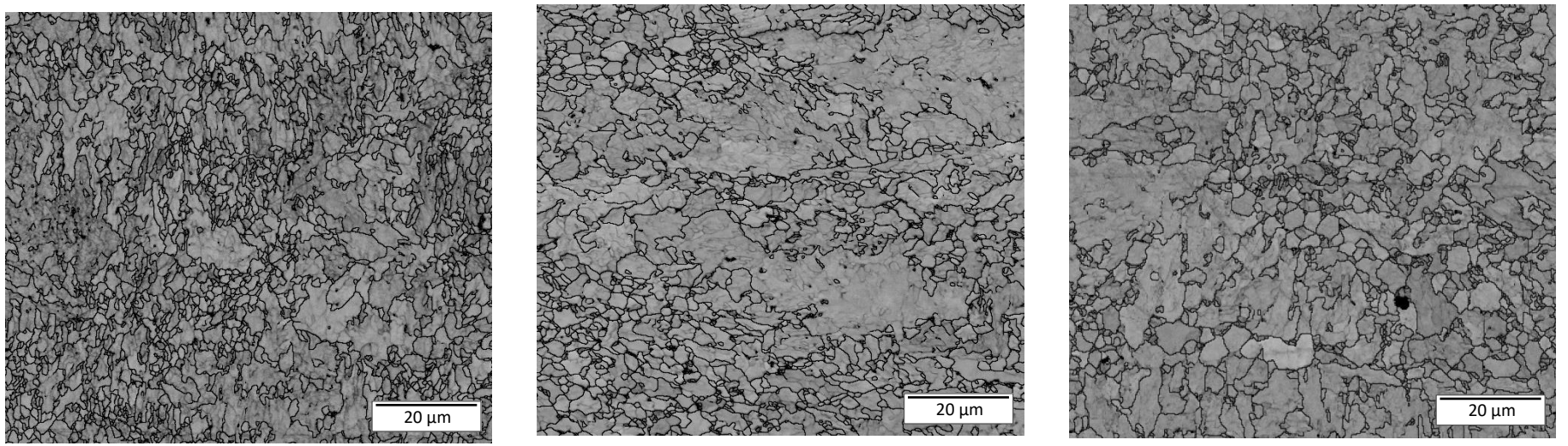

(a) As-received - image part cleaned from 8.3% to 1.3% zero solutions

(b) 800°C + 5 minutes - image part cleaned from 6.6% to 1.2% zero solutions

(c) 800°C + 60 minutes - image part cleaned from 6.8% to 0.35% zero solutions

Figure 5-28 Pattern quality maps for steel B (S700MC) taken from the rolling direction. High angle grain boundaries in black

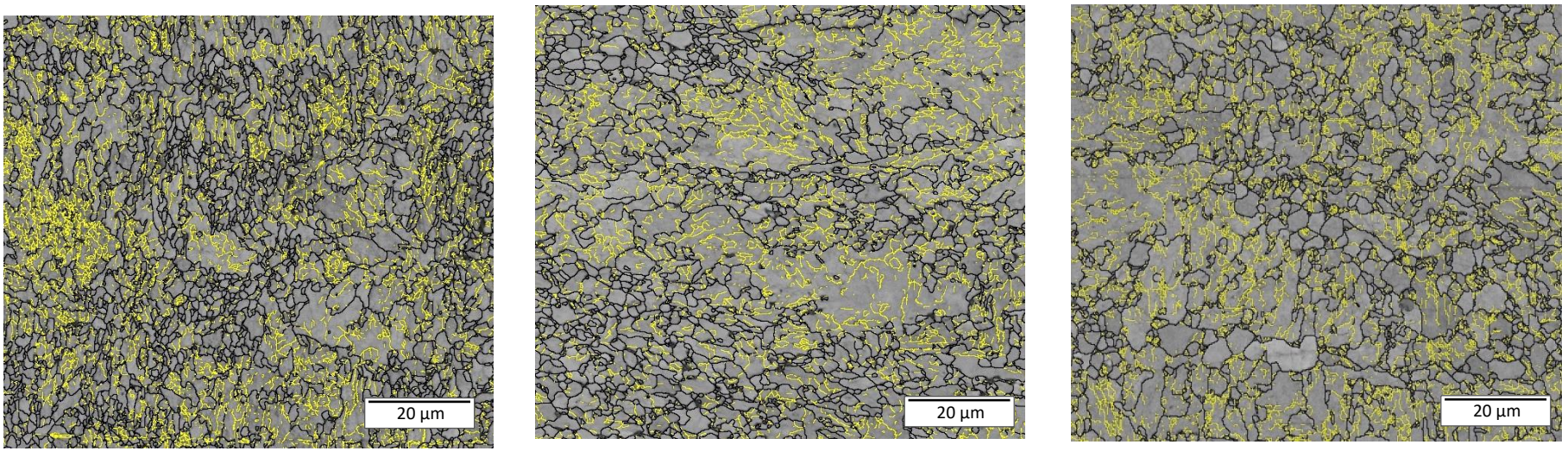

(a) As-received - image part cleaned from 8.3% to 1.3% zero solutions

(b) 800°C + 5 minutes - image part cleaned from 6.6% to 1.2% zero solutions

(c) 800°C + 60 minutes - image part cleaned from 6.8% to 0.35% zero solutions

Figure 5-29 Pattern quality map for steel B (S700MC) taken from the rolling direction. High and low angle grain boundaries in black and yellow, respectively

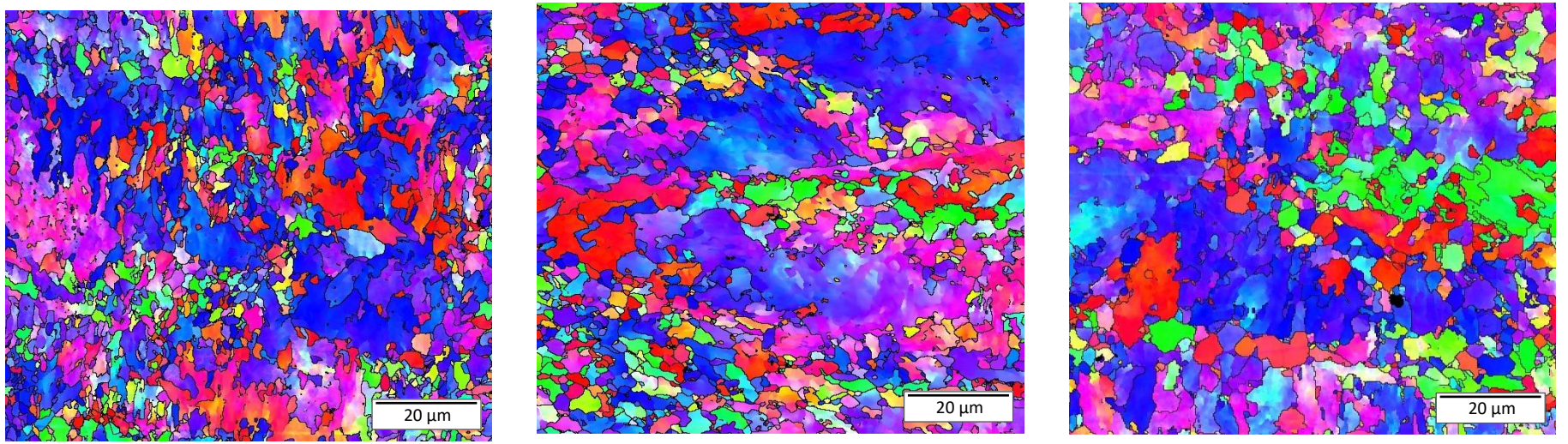

(a) As-received - image part cleaned from 8.3% to 1.3% zero solutions

(b) 800°C + 5 minutes - image part cleaned from 6.6% to 1.2% zero solutions

(c) 800°C + 60 minutes - image part cleaned from 6.8% to 0.35% zero solutions

Figure 5-30 Orientation map with IPF colouring for steel B (S700MC) taken from the rolling direction.

5.4 Summary

The microstructures of the five HSS in the 'as-received' condition have been assessed, using light microscopy, SEM and EBSD. The results revealed stark differences in the microstructures which are attributed to the differences in production route and composition and are the reason for the different stress-strain responses observed in Chapter 3.

Of the HSS grades tested, steels A (S690QL) and B (S700MC) showed the best strength retention properties at elevated temperature, hence the microstructures of these steels were studied further. Firstly the tensile specimens from isothermal tests conducted at 200 and 600°C from steel A (S690QL) and B (S700MC), were examined. Whilst all the specimens necked prior to fracture, reduced necking was seen in steel B (S700MC) at 600°C, which is likely linked to the presence of large titanium rich precipitates. Large titanium-rich precipitates are ineffective in contributing to strength (unlike a fine dispersion of precipitates) and become initiation sites for voids to form when a tensile load is applied, which can reduce the ductility of the material and hence they should be avoided by controlling the amount of titanium and nitrogen in the steel.

Secondly heat treatments were carried out on steels A (S690QL) and B (S700MC) to investigate the influence of temperature on the microstructure as well as explore possible strengthening mechanisms such as secondary hardening which may have contributed towards the observed strength retention properties presented in Chapter 4. With reference to the heat-treated and quenched samples, in steel A (S690QL), evidence of the lath grain boundaries disappear from 600°C as well as cementite spheroidisation was seen in light microscopy studies and this correlated well with decreasing hardness values in the subcritical temperature (below A_1) regime. A slight increase in hardness was observed when the H-J parameter was 17.5 and this could be due to secondary hardening which can help retard the strength loss at elevated temperatures. At 800°C, the microstructure of steel A (S690QL) was partially martensitic, indicating that the material has been partially re-austenitised prior to quenching (i.e. the material was heated into the intercritical region, i.e. between A_1 and A_3), in this region. When the steel is heated above A_1 (i.e. the transformation temperature from ferrite to austenite), many of the strengthening mechanisms including precipitation/secondary hardening may become ineffective as the precipitates including cementite dissolve into the steel matrix, this will contribute to the reduction of strength at elevated temperatures. For steel B (S700MC), the hardness increased depending on the temperature and soaking time, where the maximum hardness was observed at 600°C after 60 minute soaking time and 700°C after a 5 minute soaking time. Minimal variations in the microstructure were observed

below 800°C, after which the grain morphology changed from elongated to equiaxed and a reduction in the density of low angle grain boundaries was observed, indicating that recovery and recrystallisation had occurred. The increase in hardness observed at 600-700°C is probably due to secondary hardening, where a fine dispersion of carbides/nitrides can reduce the mobility of dislocations and retard the strength loss at elevated temperatures. The effect peaked at a H-J parameter of 18. This is in agreement with the value obtained by Okumura et al. (1987) where the maximum precipitation effect due to niobium and vanadium was observed in martensitic steels. To verify their presence would require a high-resolution microscope such as a transmission electron microscope (TEM). The links between the material and metallurgical properties are discussed in Chapter 7.

Chapter

6

The application of high strength steel material properties in structural fire design

6.1 Introduction

In the previous chapters, material properties of various HSS grades, which are essential to understanding the structural behaviour at room and elevated temperatures, have been presented. In this chapter, the stress-strain response for steels A (S690QL) and B (S700MC) are represented mathematically using the modified Ramberg-Osgood model proposed by Gardner and Nethercot (2004). Following on, the general purpose finite element software ABAQUS (version 6.14) (Dassault Systèmes, 2014) is used to develop and validate numerical models for predicting the ultimate load of columns at room and elevated temperature. Once validated, the model is then employed to conduct parametric studies incorporating the measured strengths, stiffness and stress-strain responses of steels A (S690QL) and B (S700MC). The aims of this chapter are the following:

- To understand how the material properties of different HSS grades influence the response of Class 1 and Class 3 columns at selected temperatures ranging from 20 to 800°C; and
- To assess the suitability of the current Eurocode buckling curves (EN 1993-1-2, 2005) for HSS columns in fire conditions.

6.2 Stress-strain relationship in design

6.2.1 General

Section 2.4.3.2 presented the various methods of numerically representing the stress-strain response of steel. The modified (two-stage) Ramberg-Osgood model proposed by Gardner and Nethercot (2004), shown in Equation (6.1) and (6.2), was demonstrated by Knobloch et al. (2013) to accurately trace the nonlinear stress-strain response of S355 at elevated temperatures up to strain levels of interest in structural applications (i.e. 5%). Since many materials, including HSS, exhibit a nonlinear stress-strain response at elevated temperatures, the strain hardening parameters n and m, in Equations (6.1) and (6.2), which describe the curvature of the stress-strain curve before and after the 0.2% proof strength, respectively, can be adopted accordingly for different materials (Gardner and Ashraf, 2006). Hence, the model in Equation (6.1) and (6.2) was used to trace the stress-strain response of steels A (S690QL) and B (S700MC).

For $\sigma \leq f_{0.2p}$

$$\varepsilon = \left(\frac{\sigma}{E_a}\right) + \varepsilon_{0.2}\left(\frac{\sigma}{f_{0.2p}}\right)^n \tag{6.1}$$

for $\sigma > f_{0.2p}$

$$\varepsilon = \left(\frac{\sigma - f_{0.2p}}{E_{0.2}}\right) + \left(\varepsilon_{1.0p} - \varepsilon_{0.2p} - \frac{f_{1.0p} - f_{0.2p}}{E_{0.2}}\right) \times \left(\frac{\sigma - f_{0.2p}}{f_{1.0p} - f_{0.2p}}\right)^m + \varepsilon_{0.2p} \tag{6.2}$$

where σ and ε are the engineering stress and strain respectively, E_0 is the elastic modulus, $f_{0.2p}$ and $\varepsilon_{0.2p}$ are the 0.2% proof strength and corresponding total strain, respectively, and $E_{0.2}$ is the slope at the 0.2% proof strength, $f_{0.2p}$. The strain hardening parameter n is typically determined from a point close to the origin (e.g. the 0.01% proof strength and corresponding total strain) and the 0.2% proof strength and corresponding total strain ($f_{0.2p}$, $\varepsilon_{0.2p}$), whilst the strain hardening parameter m is typically determined from the points ($f_{0.2p}$, $\varepsilon_{0.2p}$) and ($f_{1.0p}$, $\varepsilon_{1.0p}$).

6.2.2 Recommended parameters

The strain hardening parameter n and m in Equation (6.1) and (6.2) were obtained using the ordinary least square method. This is a common method used for fitting equations to a given data set, whereby the sum of the squares of the dependent variable is minimised (Afshan, 2013). The method involves a weighted total least square regression which minimises the errors on both axes

and is independent of the distribution of data points. This is represented mathematically in Equation (6.3).

$$S = \text{Min} \sum_{i=1}^{i=k} \left(W_{\varepsilon_{n,i}} r_{\varepsilon_{n,i}}^2 + W_{\sigma_{n,i}} r_{\sigma_{n,i}}^2 \right) \tag{6.3}$$

where $r_{\varepsilon_{n,i}}$ is the residual in normalised strain ε, $r_{\varepsilon_{n,i}}$ is the residual in normalised stress σ and $W_{\varepsilon_{n,i}}$ and $W_{\varepsilon_{n,i}}$ are the weighting factors for normalised ε and σ, respectively. The weighting factors consider the non-uniform distribution of data points along both axes, and are related to the interval between successive data points defined by Equation (6.4) and (6.5). A large gap corresponds to a high weighting factor (Afshan, 2013).

$$W_{\varepsilon_{n,i}} = (\varepsilon_{n,i} - \varepsilon_{n,i-1}) \tag{6.4}$$

$$W_{\sigma_{n,i}} = (\sigma_{n,i} - \sigma_{n,i-1}) \tag{6.5}$$

A summary of the parameters are presented in Table 6-1 and Table 6-2 and examples of Equations (6.1) and (6.2) fitted to experimental data for steels A (S690QL) and B (S700MC) are presented in Figure 6-1 and 6-2, respectively. Generally, the modified Ramberg-Osgood model proposed by Gardner and Nethercot (2004) closely traces the stress-strain response of steels A (S690QL) and B (S700MC) at temperatures up to 800°C. However it is noted that at room temperature (20°C), the modified Ramberg-Osgood model slightly underestimates the stress-strain response at strains greater than 2%. For greater accuracy, further Ramberg-Osgood equations and parameters can be introduced.

The transition from linear (elastic) to the nonlinear (plastic) region of the stress-strain response is more distinct for steel A (S690QL) than steel B (S700MC) at temperatures below 400°C, which is highlighted by the higher strain hardening parameter n for steel A (S690QL) (i.e. 102.0 to 32.2) compared with steel B (S700MC) (i.e. 14.8 to 13.1), as shown in Table 6-1 and 6-2. In general, the higher the strain hardening parameter value, the less "rounded" the stress-strain response of the material. The degree of "roundness" in the stress-strain response at room temperature can also be associated with the amount of free carbon and nitrogen solute atoms in the iron matrix as discussed in Section 3.4.1.

All variations of the modified Ramberg-Osgood model, including Equations (6.1) and (6.2), are only capable of tracing the stress-strain response up to the tensile or ultimate strength (i.e. maximum strength before necking occurs). The model cannot account for strain softening, which may be relevant in applications where high strains are important such as in the case of fire where anticipated strains may be greater than 2%. Nevertheless, it must be pointed out that at 600°C for steel A (S690QL) as well as 700 and 800°C for steel B (S700MC), the ultimate strength was reached at strains less than 2%.

Table 6-1 Summary of the parameters for the modified Ramberg-Osgood model proposed by Gardner and Nethercot (2004) for steel A (S690QL)

Temperature, θ (°C)	E_a (GPa)	$E_{0.2}$ (GPa)	$f_{0.2p}$ (N/mm^2)	$f_{1.0p}$ (N/mm^2)	n	m
20	199.3	3.4	706.3	717.3	102.0	1.5
100	189.7	10.0	690.0	708.0	32.5	1.5
200	191.2	9.7	667.5	688.8	32.2	1.8
300	183.4	14.9	651.0	699.6	20.1	2.4
400	176.7	16.9	643.0	673.1	16.5	2.9
500	178.0	13.6	567.0	610.2	19.0	5.2
600	149.7	15.2	442.0	499.9	14.1	3.2
700	76.3	10.0	222.5	249.2	9.7	7.6
800	53.7	4.0	70.0	80.1	8.0	3.8

Table 6-2 Summary of the parameters for the modified Ramberg-Osgood model proposed by Gardner and Nethercot (2004) for steel B (S700MC)

Temperature, θ (°C)	E_a (GPa)	$E_{0.2}$ (GPa)	$f_{0.2p}$ (N/mm^2)	$f_{1.0p}$ (N/mm^2)	n	m
20	224.7	24.5	749.3	793.3	13.8	2.4
100	204.6	24.8	744.0	769.0	13.1	2.0
200	217.6	21.4	703.0	749.2	14.8	2.8
300	210.5	26.1	735.0	798.5	12.3	4.2
400	205.6	25.9	691.0	770.1	11.5	3.4
500	190.1	19.2	610.0	672.7	14.3	4.0
600	178.3	23.8	511.5	559.7	9.3	6.9
700	140.8	14.3	350.0	367.4	11.0	3.9
800	86.7	5.5	175.0	179.8	14.9	1.7

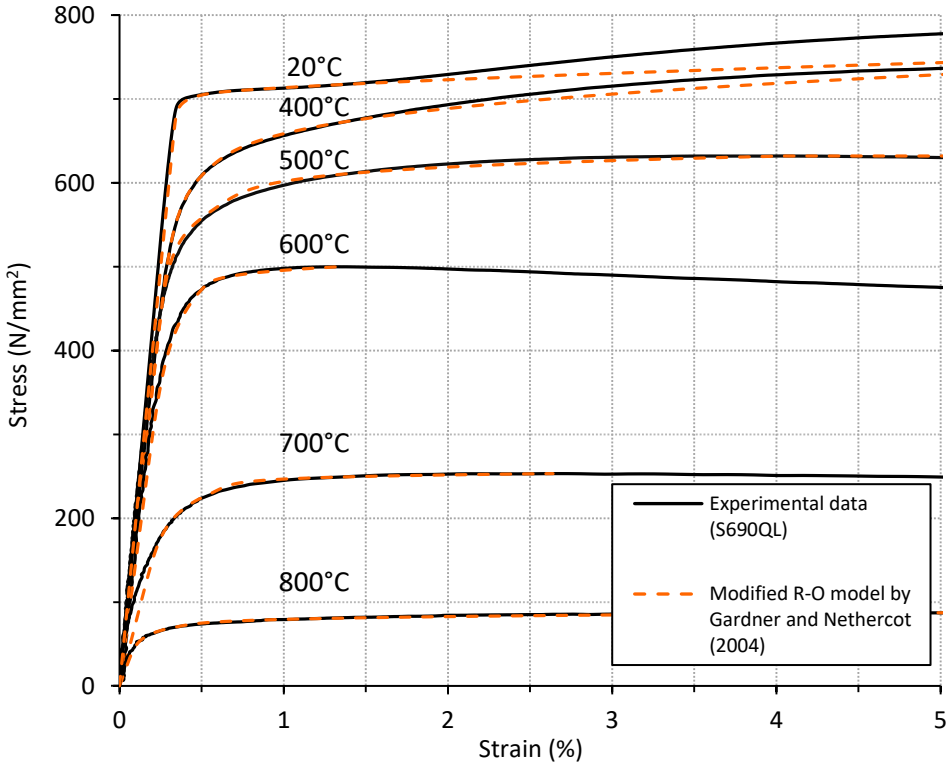

Figure 6-1 Comparisons of the stress-strain response for steel A (S690QL) with the modified Ramberg-Osgood model proposed by Gardner and Nethercot (Gardner and Nethercot, 2004)

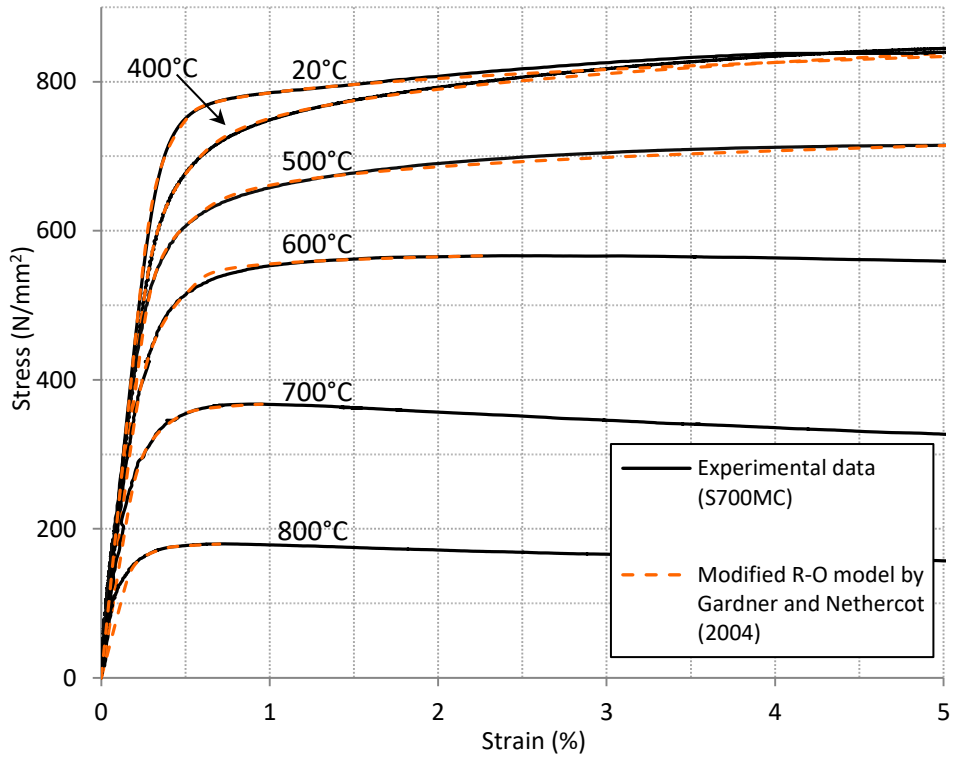

Figure 6-2 Comparisons of the stress-strain response for steel B (S700MC) with the modified Ramberg-Osgood model proposed by Gardner and Nethercot (Gardner and Nethercot, 2004)

6.3 Behaviour of high strength steel columns under fire conditions

6.3.1 Introduction

To date, there are very limited performance data and studies on the buckling behaviour of HSS columns under fire conditions, mainly owing to the significant expense associated with high temperature structural testing, as well as the lack of reliable material property data which are needed to develop computational design models. A summary of the previous studies on the behaviour of HSS compression members at elevated temperature is summarised in Section 2.4.4, where buckling performance of steel grades S690QL (Chen and Young, 2008; Wang et al., 2013b; Ebel et al., 2016) and Q460 (Wang et al., 2014) at elevated temperatures have been studied and the findings indicate the buckling parameters presented in Eurocode 3 Part 1-2 (EN 1993 1-2, 2005) to be unconservative (i.e. unsafe).

The buckling behaviour of structural members is greatly influenced by material properties including the shape of the stress-strain response of the material as reported by Knobloch (2014) and Kervalishvili and Talvik (2016). Chapters 3 and 4 have shown the broad scatter in the material responses of various HSS grades and this may lead to vast differences in the structural performances at elevated temperatures. For TMCP steels, only experimental and numerical studies on the buckling behaviour of columns at room temperature is available in the literature (Wang et al., 2017). Hence one focus of this section is to examine the buckling performance of columns made from the TMCP steel B (S700MC) at elevated temperatures. In addition, since steel B (S700MC) showed the best strength retention properties at elevated temperatures, the buckling performance will be compared with the best performing QT from Chapter 5 (steel A (S690QL)). In this section, a numerical study is carried out to investigate the influence of the material performance of steels A (S690QL) and B (S700MC) on the buckling properties of columns at elevated temperature and assess the suitability of the Eurocode fire resistant design rules for HSS columns. Details on the numerical model and Eurocode approach to steel members in buckling are described in the following sections.

6.3.2 Modelling assumptions

6.3.2.1 General

A three-dimensional finite element (FE) model has been developed using the general purpose program ABAQUS (2015) to investigate the behaviour of high strength steel columns at elevated temperature. The ABAQUS software was selected as it is commercially available and is capable of accurately depicting the material and geometric nonlinearities as well as the elevated temperature

behaviour accurately (Varol and Cashell, 2017). In the following sub-sections, the development of the model is described. This is followed by an account of the validation exercise where the model is compared with experimental results. Two types of cross-section shapes were modelled: square and rectangular hollow sections (SHS and RHS, respectively), examples of each cross-section are presented in Figure 6-3.

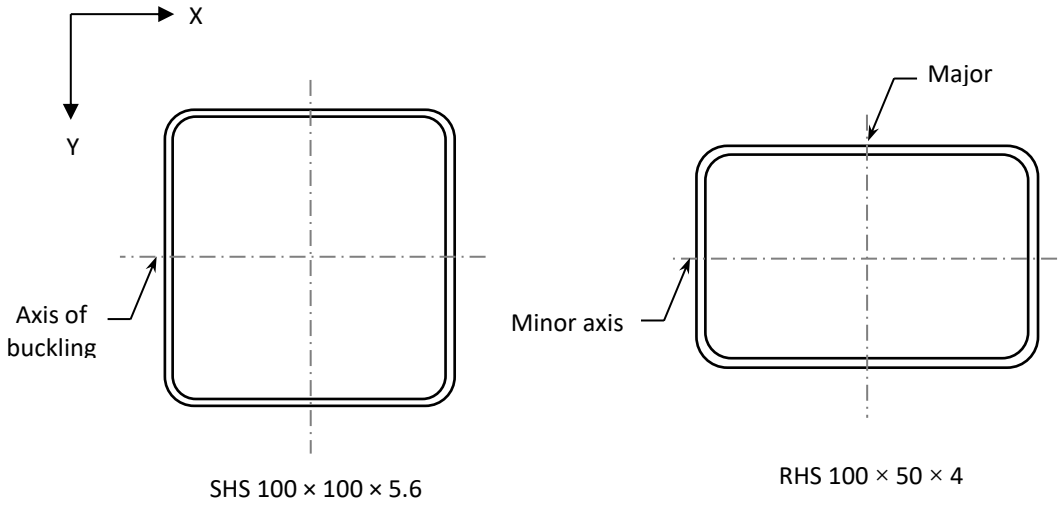

Figure 6-3 Examples of the cross-section shapes modelled

At room temperature, there are two stages to the numerical analysis, (1) a linear elastic buckling analysis using the (*BUCKLE) procedure in ABAQUS to determine the buckling mode shape, and (2) a geometrically and materially nonlinear load-displacement analysis, incorporating the buckling mode shape as an imperfection from stage (1). The stage (2) stress analysis was solved using the modified Riks method, which is a variation of the classic arc length method that enables the buckling behaviour to be examined as the structural member undergoes large deformations under an applied load. A similar two-stage modelling approach was used to determine the buckling behaviour at elevated temperatures. The columns were modelled in an isothermal manner at elevated temperatures, whereby the initial temperature was set to the target temperature using the predefined field. Although this is not necessarily representative of a real fire scenario in which the members would heat up in an anisothermal manner, numerical and experimental studies of structural members under isothermal conditions are commonly used by researchers (Davison et al., 2010; Pauli et al., 2012; Varol and Cashell, 2017). This is because testing under isothermal conditions tend to provide a reliable and controllable approach, making validation more straightforward with the result given as an ultimate load for a given temperature (Varol and Cashell, 2017). In addition, experimental studies under isothermal conditions were used to validate the

model as described later in Section 6.3.3.3. The Abaqus/Standard analysis method is used in this study.

6.3.2.2 Element type and mesh size

Shell elements were adopted to simulate HSS structural hollow section columns as have been used in similar studies on thin-walled members (e.g. Chen and Young, 2008; Wang and Gardner, 2017). The four-node shell elements with double curvature and reduced integration (S4R) were employed in all the FE models. Based on a mesh sensitivity assessment, the element size was defined as being equal to the thickness of the cross-section under consideration. This was found to provide an efficient solution without compromising the accuracy of the simulation and in line with other similar studies (e.g. Theofanous and Gardner, 2010; Wang, 2016)

6.3.2.3 Material properties

For nonlinear (plastic) analysis, ABAQUS requires the entire stress-strain response of a material in order to accurately depict the structural behaviour. The measured engineering stress-strain responses obtained from uniaxial tensile tests are unsuitable for FE analysis because the reduction of the cross-section area during deformation is not considered and so the plastic stresses reported are lower than the true values. Instead, the true stress, σ_{true}, and logarithmic plastic strain, ε_{pl}^{ln}, is used in ABAQUS and derived from the nominal engineering stress, σ_{nom}, and strain, ε_{nom}, using Equations (6.6) and (6.7), respectively:

$$\sigma_{true} = \sigma_{nom}(1 + \varepsilon_{nom}) \tag{6.6}$$

$$\varepsilon_{pl}^{ln} = \ln(1 + \varepsilon_{nom}) - \frac{\sigma_{true}}{E_a} \tag{6.7}$$

where E_a is the elastic modulus. Note that Equations (6.6) and (6.7) are only valid up to the tensile strength (i.e. onset of necking). As discussed in Section 2.4.3.7, Poisson's ratio *v* can be considered independent of temperature and steel grade (or yield strength); hence the value of 0.3 was adopted.

6.3.2.4 Geometric imperfection

All structural members contain geometric imperfections which are introduced during production, fabrication and handling. Since geometric imperfections influence the buckling response of structural members, they were considered in the present FE models. Initial geometric imperfections in the form of the lowest local and global buckling mode as shown in Figure 6-4, were

obtained from an elastic buckling analysis. This representation of geometric imperfections is commonly used by researchers (Chen and Young, 2008; Pauli, 2013; Wang et al., 2016; Gkantou et al., 2017). Local imperfections were included in the modelling of stub columns where failure will occur in the cross-section, whilst slender columns were modelled considering the global imperfections (in the form of a half-sine wave) only, because the influence of local imperfections is less significant due to the larger section geometry. The amplitude of the imperfections was set to replicate the values presented in the experimental programmes of Wag and Gardner (2017), and those of Pauli et al. (2012) used later for validation.

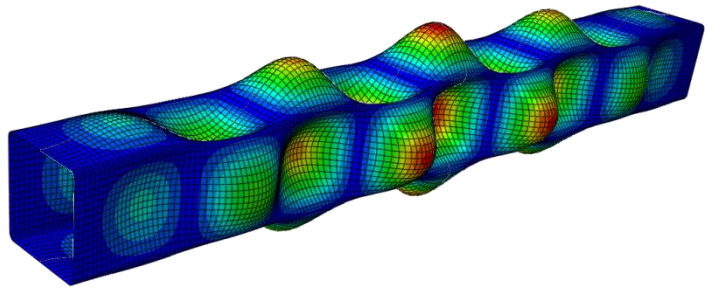

(a)

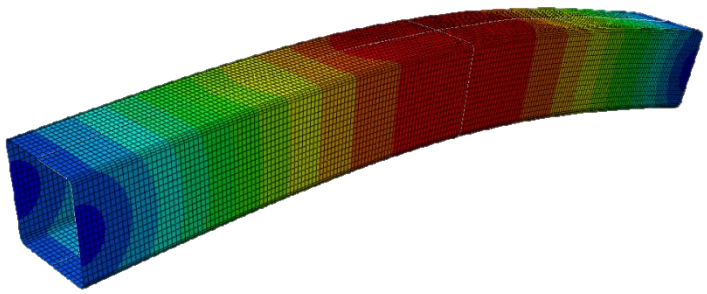

(b)

Figure 6-4 Examples of the lowest buckling mode shapes obtained from elastic analysis (a) local buckling and (b) global buckling

6.3.2.5 Residual stresses

Residual stresses are similarly introduced during the manufacturing and fabrication process including cold-forming and welding and may result in premature yielding and loss of stiffness and hence a subsequent reduction in the compressive resistance of structural members. For seamlessly hot-finished HSS structural hollow columns, Wang and Gardner (2017) demonstrated that the influence of residual stresses on the member compressive resistance is minimal due to their low

measured amount. It is noted that the influence of residual stresses can be smaller in HSS members compared with equivalent elements made from mild steel because the ratio of the residual stress over the yield strength is lower (Rasmussen and Hancock, 1995). This revelation has led to the Eurocodes (EN 1993-1-1, 2005) specifying a slightly higher buckling curve for hot finished structural hollow sections made from steel grades S460 than for conventional steel grades. However, for cold-formed structural hollow sections, regardless of the steel grade, a lower buckling curve is prescribed due to the higher influence of residual stresses.

There is a lot of uncertainty around the influence of residual stresses at elevated temperatures, with factors including geometry (e.g. width to thickness ratio), thermal gradient, strain (including thermal and creep), material and metallurgical properties, load and time influencing the distribution of residual stresses in a fire scenario (Talamona et al., 1997; Kervalishvili and Talvik, 2017). Several researchers have shown that higher buckling loads can be predicted when residual stresses are not considered in the behaviour of steel columns at elevated temperatures (Franssen, 1996; Talamona et al., 1997; Kervalishvili and Talvik, 2017). However, Yang et al. (2006) concluded that the residual stress can be ignored based on the assumption that they decrease with increasing temperature. Heating steels to temperatures below Ac_1 for specified amounts of time, is a common method employed to relive any residual stresses introduced during manufacturing; the process is termed as stress-relieving or annealing. Translating the application of stress relieving to fire scenarios suggests that residual stresses may decrease with increasing temperature, however, as mentioned earlier on in this paragraph, there are many other factors to consider and as result the behaviour of residual stresses during a fire is not understood.

With the influence of residual stresses in hot-finished structural hollow sections on the buckling response being minor and the uncertainty related to the influence at elevated temperatures, residual stresses were not explicitly incorporated into the FE models in the current chapter.

6.3.2.6 Boundary conditions and load application

In the model, the columns were assumed to be symmetric, both in terms of their geometry and the boundary conditions. Hence, only half of the cross-section and over half of the column length were included in the finite element model. Symmetry constraints about the X and Z planes (XSYMM and ZSYMM, respectively) are applied as depicted in Figure 6-5. The boundary conditions of the column were incorporated into the model based on information available on the experimental programmes (presented in Section 6.3.3) used to validate the model. Accordingly, the test boundary conditions were replicated by restraining the appropriate displacement (U_X, U_Y and U_Z) and rotation degrees

(R_X, R_Y and R_Z) of freedom at the column ends. All boundary conditions were applied through reference points in Figure 6-5, located at the centre of each column end. The reference points were linked to the nodes along the perimeter of the cross-section at the column ends through rigid body kinematic coupling. At ambient temperature, the columns were pin-ended so all degrees of freedom of the lower reference point, except rotation about buckling axis, were fixed, while the upper reference point was free to displace along the column axis and rotate about the same axis as the lower reference point (see Figure 6-5 (a)).

At elevated temperature, the stub and slender columns have fixed- and pin-ended conditions, respectively. For the fixed-ended columns, all six degrees of freedom of the lower reference point were restrained, while the upper reference point was allowed to move longitudinally along the column axis and was fixed against the other five degrees of freedom (see Figure 6-5 (b)). The elevated temperature pin-ended columns are modelled in the same way with the exception that the rotation axis is set as the minor axis in all cases. All columns at ambient and elevated temperature were concentrically loaded through their upper reference point and were free against axial thermal expansion. The modified Riks method was used to trace the load-deformation response of each of the modelled columns and to determine ultimate buckling load for each column.

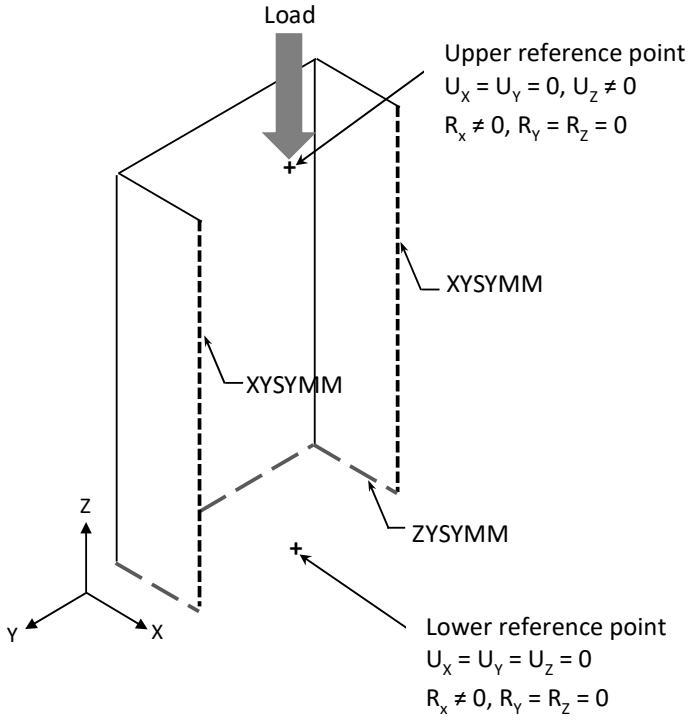

(a)

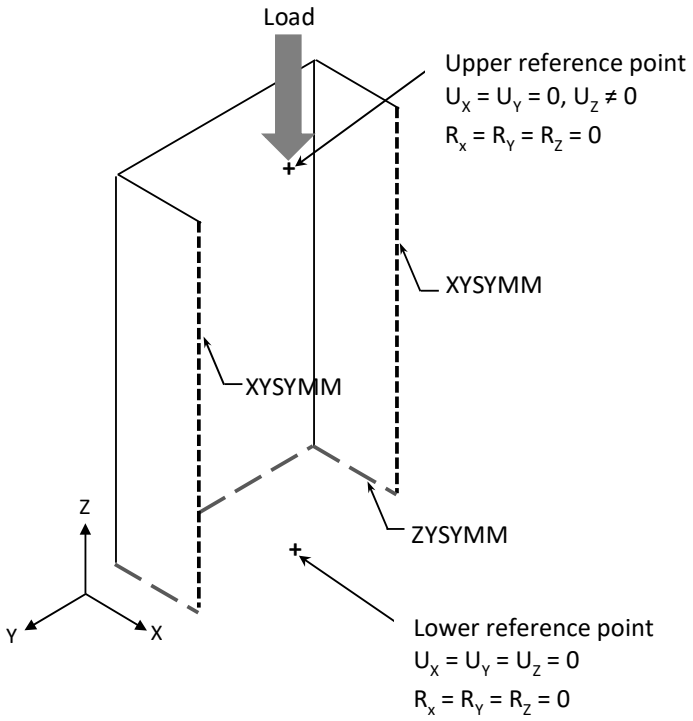

(b)

Figure 6-5 Schematic of the boundary conditions (a) pinned-end conditions (b) fixed-end conditions

6.3.3 Validation of model

6.3.3.1 General

In the absence of published elevated temperature test data on HSS columns, the finite element (FE) models are validated against (1) the room temperature experiments on high strength steel columns reported by Wang and Gardner (2017) and (2) the elevated temperature tests on columns made from mild strength steel reported by Pauli et al. (2012). Both test programmes included measurements of material properties, geometry as well as local and global geometric imperfection amplitudes of the tested columns. The same modelling procedures are employed for both the room temperature and elevated temperature tests by incorporating the material property data corresponding to the test temperature under consideration.

6.3.3.2 Column tests at room temperature (Wang and Gardner, 2017)

Wang and Gardner (2017) conducted a series of tests on S460NH and S690QH hot-finished square and rectangular hollow sections. The columns were pinned at both ends and allowed only in-plane rotation of the member about one axis. The columns were loaded under displacement control at a loading rate of $L_{cr}/2000$ per minute, where L_{cr} is the buckling length considering the member length

(L) plus 150 mm to account for the distance between the knife edge supports used to simulate the pin-ended boundary conditions.

A summary of the details from the test programme is presented in Table 6-3, which includes the failure load measured during the test ($N_{u,test}$). Tensile tests on material extracted from the flat faces of the S460NH and S690QH columns were performed to measure their basic engineering stress-strain response and these are incorporated in the FE model, once converted to true stress and strain using Equation (6.6) and (6.7).

Table 6-3 Summary of the test conditions reported by Wang and Gardner (2017) at room temperature

Specimen	Steel grade	Nominal section size (mm)	L (mm)	$N_{u,test}$ (kN)	$N_{u,FE}$ (kN)	$N_{u,test}$ / $N_{u,FE}$
C3L1	S460NH	100 × 100 × 5	708	878	888	0.99
C3L2	S460NH	100 × 100 × 5	1609	798	850	0.94
C3L3	S460NH	100 × 100 × 5	2799	557	576	0.97
C4L1	S690QH	50 × 50 × 5	276	690	705	0.98
C4L2	S690QH	50 × 50 × 5	518	637	588	1.08
C4L3	S690QH	50 × 50 × 5	756	562	520	1.08
C4L4	S690QH	50 × 50 × 5	1070	391	360	1.09
C4L5	S690QH	50 × 50 × 5	1379	248	230	1.08
C4L6	S690QH	50 × 50 × 5	1550	201	195	1.03
C4L7	S690QH	50 × 50 × 5	1710	166	165	1.01
C4L8	S690QH	50 × 50 × 5	2000	119	126	0.94
C5L1	S690QH	100 × 100 × 5.6	709	1571	1608	0.98
C5L2	S690QH	100 × 100 × 5.6	1609	1420	1376	1.03
C5L3	S690QH	100 × 100 × 5.6	2800	680	679	1.00

Examples of the load-lateral deflection curves of the C4L6 and C5L3 members derived from the numerical models compared with their respective test response are presented in Figure 6-6. Figure 6-6 demonstrates that the numerical provide an accurate depiction of the load-deformation history of the high strength steel columns. A summary of the comparisons between the ultimate test load ($N_{u,test}$) and ultimate FE load ($N_{u,FE}$) reached is provided in Table 6-3, as well as the ratio of these two figures. It is shown that the FE model gives a mean $N_{u,test}/N_{u,FE}$ value of 1.01 and a COV of 5.0%. From the results provided in Table 6-3 it is concluded that the FE model is adequate of predicting the ultimate strengths of HSS columns at room temperature.

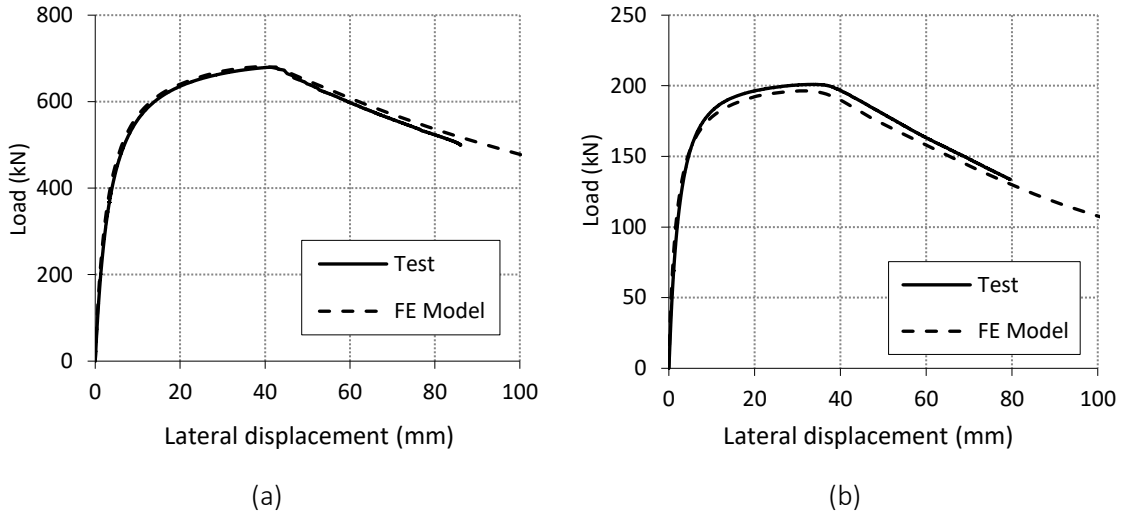

(a) (b)

Figure 6-6 Comparison of the load–lateral displacement curves for column (a) C4L6 and (b) C5L3 (Wang and Gardner, 2017)

6.3.3.3 Column tests at elevated temperature (Pauli et al., 2012)

The FE model described previously is employed to analyse the columns tested by Pauli et al. (2012). Although these experiments were conducted on columns made from conventional S355 steel, they are used in the current study for validation of the model owing to a lack of experimental results for HSS columns in fire. This test programme included tests on SHS and RHS, and included both stub (short) and slender (long) columns. All structural members were made from hot finished sheets which were formed into shape at room temperature and welded closed. The experiments were performed under isothermal loading conditions whereby the columns were first heated to a target temperature of 400, 550 and 700°C and then, once thermal equilibrium had been established at the desired temperature, a mechanical load was applied at a strain rate of 0.1 %/min, until the horizontal displacement increased rapidly and the vertical load could no longer be maintained. The stub columns were fixed against displacement and rotation at both ends, apart from axial displacement at the loaded end, while the slender columns were pinned at both ends and allowed in-plane rotation of the member about either the major or minor axis. The details of the tests are presented in Table 6-4. Similar to the room temperature validation, the elevated temperature model incorporates the material properties corresponding to the test temperature under consideration. In the test programme, tensile coupons were extracted from flat faces of the S355 columns and then tensile tests were conducted at room, 400, 550 and 700°C under isothermal conditions at a strain rate of 0.1%/min. These tests were analysed (Knobloch et al., 2013) and the proposed input parameters for the modified Ramberg-Osgood model as developed by Gardner and Nethercot (2004) and given in Equations (6.1) and (6.2), were included in the FE model.

Table 6-4 Summary of the test conditions reported by Pauli et al. (2012) at elevated temperature

Specimen	Nominal section size (mm)	L (mm)	θ (°C)	End-condition	$N_{u,test}$ (kN)	$N_{u,FE}$ (kN)	$N_{u,test}$ / $N_{u,FE}$
S3	160 × 160 x 5	480	400	Fixed	795	767	1.04
S6	160 × 160 x 5	480	550	Fixed	468	474	0.99
S5	160 × 160 x 5	480	700	Fixed	138	128	1.08
S02	60 × 120 × 3.6	360	400	Fixed	408	330	1.24
S03	60 × 120 × 3.6	360	550	Fixed	257	218	1.18
S06	60 × 120 × 3.6	360	700	Fixed	74	71	1.04
L2	160 × 160 x 5	1840	400	Pinned	760	701	1.08
L5	160 × 160 x 5	1840	550	Pinned	467	443	1.05
L6	160 × 160 x 5	1840	700	Pinned	130	119	1.10
L08	60 × 120 × 3.6	1840	400	Pinned	242	262	0.92
L10	60 × 120 × 3.6	1840	550	Pinned	186	165	1.13
L05	60 × 120 × 3.6	1840	700	Pinned	71	64	1.10

Comparisons of the load-vertical displacement response from the test and FE model are depicted in Figure 6-7, whilst the results from the validation study are presented in Table 6-4, where $N_{u,test}/N_{u,FE}$ is a measure of how accurately the FE model predicts the ultimate load. For the stub columns, the FE model gives a mean $N_{u,test}/N_{u,FE}$ value of 1.09 and a coefficient of variation of 7.9%. On the other hand, for the slender columns the FE model gives a mean $N_{u,test}/N_{u,FE}$ value of 1.04 and a coefficient of variation of 8.3%. Figure 6-7 demonstrates that the model moderately traces the load deflection response of the columns; whilst Table 6-4 shows that the model generally underestimated the ultimate load of the columns and thus provides a safe prediction for the fire resistance of steel columns. The discrepancy is relatively small and most likely attributed to various factors such as the use of nominal dimensions (including the corner radii of the cross-section) and the mean value for the global imperfection as well as idealised boundary conditions which can be difficult to replicate experimentally. In addition, the influence of residual stresses introduced during welding are not considered in the model. In summary, from the results provided in Table 6-4, it is concluded that the FE model is adequate of predicting the ultimate strengths of S355 structural hollow sections at elevated temperature.

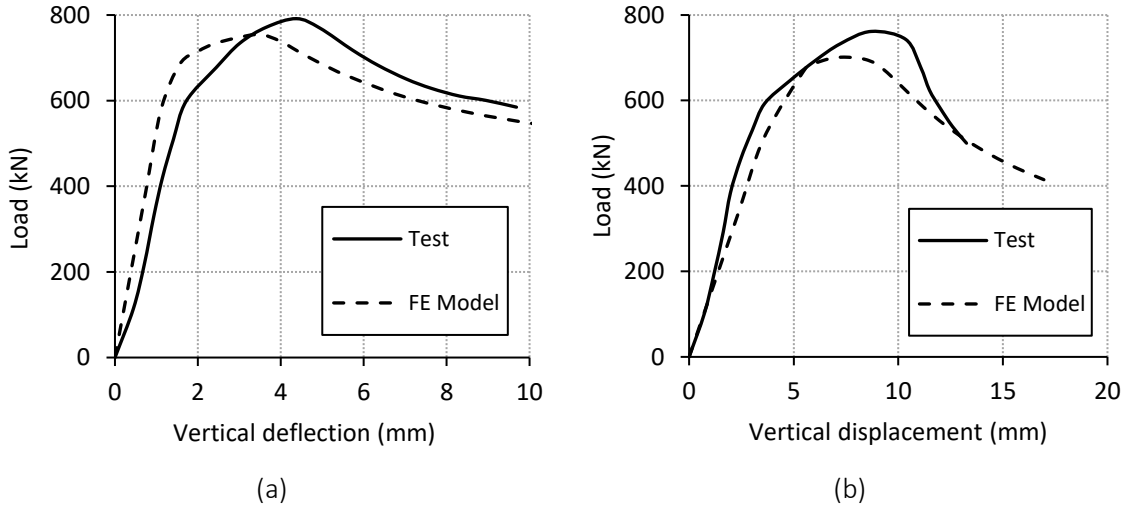

Figure 6-7 Comparison of the load–lateral displacement curves for column (a) S3 and (b) L2 (Pauli et al., 2012)

6.3.4 Parametric study

Following the validation of the FE models against experimental data, a series of parametric studies were performed in order to generate structural performance data, which are then employed to assess the suitability of the Eurocode 3 Part 1-2 (2005) buckling curves for HSS compression members in fire and propose appropriate developments. The influence of a number of salient parameters was investigated including material grade, cross-sectional geometry and member length. Two grades of HSS, namely steel A (S690QL) and B (S700MC) were included in the study as well as four cross-section geometries with varying member lengths. The same modelling procedures as explained in the previous sections were employed for the parametric study models.

The outer dimensions of the parametric study models were selected as a 100 × 100 mm square hollow section and a 100 × 50 mm rectangular hollow section, for both grades, which resulted in two different cross-section aspect ratios (i.e. h/b=1.0 and 2.0, where h is the height of the section and b is the width). The effect of cross-section slenderness was investigated by varying the cross-section thickness, while maintaining the cross-section outer dimensions. Thus, two different thicknesses were selected for each of the considered cross-sections such that one Class 1 (with a thickness of 5.6 mm) and one Class 3 (thickness of 4 mm) cross-section was modelled in each case, in accordance with the classification specifications in Eurocode 3 Part 1-1 (2005).

For the RHS models, buckling about both major and minor axes was considered to investigate if different buckling curves are required for each case. All columns were modelled as pin-ended providing a member non-dimensional slenderness range ($\bar{\lambda}$) of 0.5 to 2.5. The measured

engineering stress-strain curves for steel A (S690QL) and B (S700MC) were first modified into the true stress versus plastic strain values (Equations 6.6 and 6.7) and then incorporated into the models.

The global imperfection amplitude was taken as L/1000, where L is the column length, in accordance with the recommendations in Eurocode 3 Part 1-2 (2005). The local imperfection amplitude (ω_0) was determined using the Dawson and Walker model (Dawson and Walker, 1972), adopted by Gardner et al. (2010) and has also been used for a similar study on HSS members (Wang et al., 2016), and is given as:

$$\omega_0 = 0.028t\,(f_y/f_{cr})^{0.5} \tag{6.8}$$

where t is the thickness, f_y is material yield strength (in this case was taken as the 0.2% proof strength) and f_{cr} is the elastic critical buckling stress of the most slender constituent plate element in the section. Owing to the symmetry in the geometry and the boundary conditions of the models, only half of the section, and over half of the member length, is included in the model. The results from the parametric study are presented and analysed in the following section and used to assess the design recommendations in the Eurocodes.

6.3.5 Results and analysis

6.3.5.1 General

In this section, the design rules given in the Eurocodes are briefly described and then compared with the results from the parametric study. The design rules in Eurocode 3 Part 1-2 (2005) are mainly based on the work by Talamona et al. (1997) and Franssen et al. (1998) on H and I-section columns made from conventional steel grades. These design rules were extended to steels with yield strengths up to 700 N/mm^2 as specified in Eurocode 3 Part 1-12 (2007). However, there was very limited data available when Eurocode 3 Part 1-12 (2007) was published, hence further data is necessary to assess the applicability of the design guidelines to ensure that the standards are reliable for structures made from HSS. The design guidelines relevant for compression members are summarised, hereafter.

6.3.5.2 Cross-section classification

In classifying cross-sections at room temperature in accordance with Eurocode 3, the material factor (ε) given in Equation (6.9) for carbon steel is used to allow for variation in material yield strength $f_{y,20}$ and Young's modulus E:

$$\varepsilon = \sqrt{\frac{235}{f_{y,20}}} \tag{6.9}$$

At elevated temperature, a reduction factor of 0.85 is applied to ε, as shown in Equation (6.10), to account for the decline in strength ($k_{y,\theta}$) and stiffness ($k_{Ea,\theta}$) in a fire situation:

$$\varepsilon = \sqrt{\frac{k_{E,\theta}}{k_{y,\theta}}}\sqrt{\frac{235}{f_{y,20}}} \cong 0.85\sqrt{\frac{235}{f_{y,20}}} \tag{6.10}$$

The variation in $(k_{E,\theta}/k_{y,\theta})^{0.5}$ as a function of temperature for steels A (S690QL) and B (S700MC) derived from the reduction factors presented earlier in Chapter 4, are depicted in Figure 6-8. The corresponding Eurocode values (EN 1993-1-2, 2005), determined from the recommended reduction factors are also presented. From Figure 6-8, it can be seen that 0.85 is generally conservative for these HSS grades and can be considered as an additional safety factor. For steels A (S690QL) and B (S700MC) the variation of $(k_{E,\theta}/k_{y,\theta})^{0.5}$ is close to unity until around 450-500°C. At temperatures greater than 500°C, $(k_{E,\theta}/k_{y,\theta})^{0.5}$ is greater than unity and thus the cross-section classification may not change but will improve. This highlights the fact that 0.85 may be too conservative for members made from HSS and could result in underestimating the overall buckling resistance. Based on the reduction factors for steels A (S690QL) and B (S700MC), an appropriate value for cross-section classification of HSS columns would be 0.95. However, due to the inherent variability in material properties resulting from the differences in chemical composition and production route, a reliability analysis considering a large pool of data should be conducted before proposing an appropriate reduction parameter for HSS. In the meantime, it may be more appropriate to directly incorporate the material strength and stiffness reduction factors (i.e. $(k_{E,\theta}/k_{y,\theta})^{0.5}$) rather than use a reduction factor of 0.85 derived from conventional steel grades.

Following the Eurocode approach, the cross-section classification of a square hollow section with dimensions 100 × 100 × 4 made from steels A (S690QL) and B (S700MC), at elevated temperature, changes from Class 3 to Class 4, owing to the reduction factor of 0.85 as presented in Equation (6.10). Similarly, a 100 × 50 × 4 rectangular hollow section also changes from Class 3 to Class 4. On the other hand, the Class 1 sections assessed in the parametric study (i.e. 100 × 100 × 5.6 SHS and 100 × 5.0 × 5.6 RHS) retain their Class 1 classification.

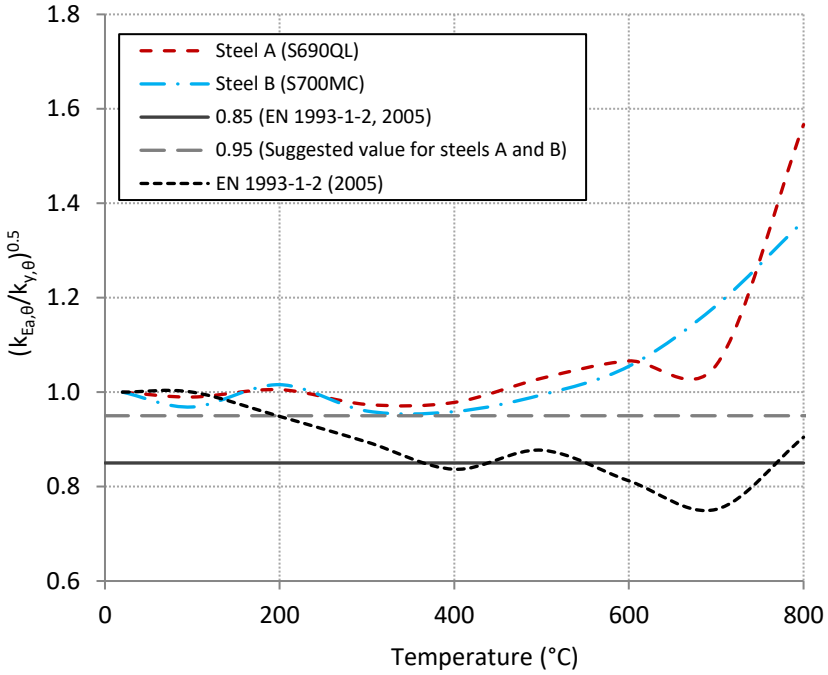

Figure 6-8 Variation of $(k_{E,\theta}/k_{y,\theta})^{0.5}$ reduction factors with temperature

6.3.5.3 Stability of compression members

In accordance with Eurocode 3 Part 1-2 (2005), the design buckling resistance ($N_{b,fi,t,Rd}$) of a compression member with Class 1, 2 or 3 cross-section with uniform temperature θ is determined as:

$$N_{b,fi,t,Rd} = \frac{\chi_{fi} A k_{y,\theta} f_{y,20}}{\gamma_{M,fi}} \quad (6.11)$$

where A is the gross cross-sectional area of the structural member, $k_{y,\theta}$ is the reduction factor for the effective yield strength (presented in Chapter 4), $f_{y,20}$ is the yield strength at room temperature (presented in Chapter 3), $\gamma_{M,fi}$ is the partial factor for fire situation which is taken as 1.0, in accordance with the recommendations in Eurocode 3 Part 1-2 (2005), and χ_{fi} is the reduction factor for flexural buckling in the fire design situation given by Equation (6.12):

$$\chi_{fi} = \frac{1}{\varphi_\theta + \sqrt{\varphi_\theta^2 - \bar{\lambda}_\theta^2}} \quad (6.12)$$

In this expression, φ_θ is determined from Equation (6.13)

$$\varphi_\theta = \frac{1}{2}\left[1 + \alpha\bar{\lambda}_\theta + \bar{\lambda}_\theta^2\right] \tag{6.13}$$

and the imperfection factor α is found from Equation (6.14)

$$\alpha = 0.65\sqrt{\frac{235}{f_{y,20}}} \tag{6.14}$$

In these equations, $\bar{\lambda}_\theta$ is the non-dimensional slenderness at temperature θ as defined by Equation (6.15), $\bar{\lambda}$ is the non-dimensional slenderness at room temperature and $k_{Ea,\theta}$ is the reduction factor for the elastic modulus at temperature θ.

$$\bar{\lambda}_\theta = \bar{\lambda}\sqrt{\frac{k_{y,\theta}}{k_{E_a,\theta}}} \tag{6.15}$$

For Class 4 sections, where local buckling instabilities must be considered, a similar approach to room temperature design can be used. The cross-sectional area A and reduction factor $k_{y,\theta}$ in Equations (6.11) and (6.15) are replaced by the reduced effective area A_{eff} and the reduction factor for the 0.2% proof stress $k_{0.2p,\theta}$ presented in Equation (6.16), as specified in Appendix E of Eurocode 3 Part 1-2 (2005). However, the Eurocode has limited the critical temperature of Class 4 sections to 350°C which is considered overly conservative and could be improved (Lawson and Newman, 1996).

$$\bar{\lambda}_\theta = \bar{\lambda}\sqrt{\frac{k_{0.2p,\theta}}{k_{E_a,\theta}}} \tag{6.16}$$

The aforementioned Equations (6.12) to (6.15) are used to produce buckling curves for fire scenarios for Class 1-3 cross-sections, which are presented in Figure 6-9. It should be noted that the buckling curves at elevated temperature differ from those presented in Eurocode 3 Part 1-1 (2005), for the design of steel structures at room temperature, which is presented in Figure 6-10 for reference. Firstly, at elevated temperature, there is no plateau in the buckling curve (i.e. at low values of $\bar{\lambda}_\theta$). In addition, at room temperature, five different buckling curves (a_0, a, b, c and d) are provided where the choice of appropriate buckling curve is dependent on the yield strength, geometry of the cross-section, manufacturing process (e.g. hot finished or cold formed) and the

buckling axis. On the other hand, the elevated temperature buckling curves shown in Figure 6-9 are dependent on the yield strength $f_{y,20}$ at room temperature. In Figure 6-9, the buckling curves for S275 and S460 were derived using the reduction factors in Eurocode 3 Part 1-2 (2005) whilst steel A (S690QL) and B (S700MC) utilised the reduction factors presented in Chapter 4. It can be seen that the buckling coefficient increases with (nominal) yield strength as mentioned by Talamona et al. (1997) and Franssen et al. (1998). It should also be noted that the use of $\bar{\lambda}_\theta$ defined in Equation (6.15) allows for all buckling curves at temperature θ to be represented by a single curve for a given yield strength.

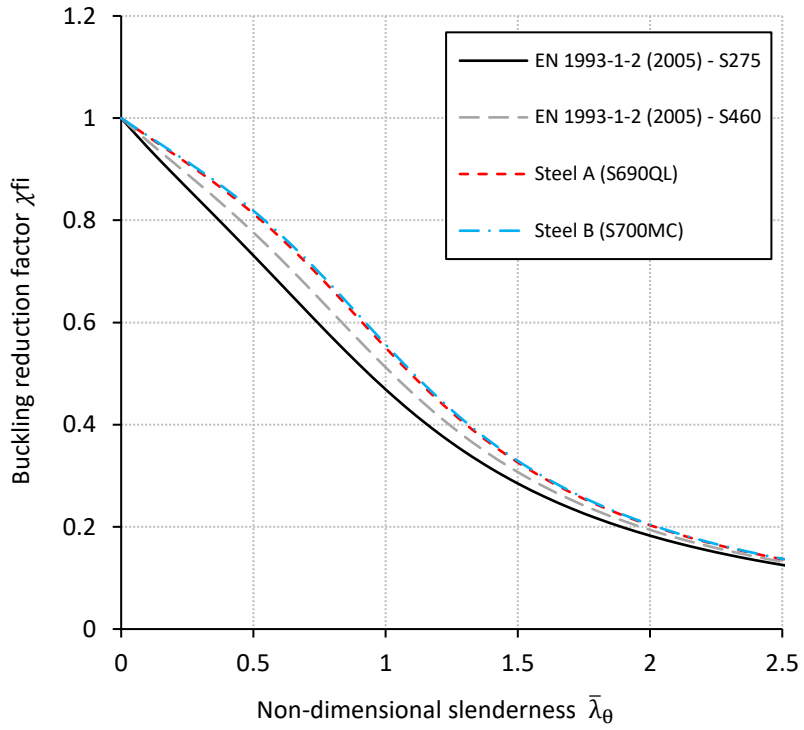

Figure 6-9 Buckling curves for various steel grades at elevated temperatures in accordance with EN 1993-1-2 (2005)

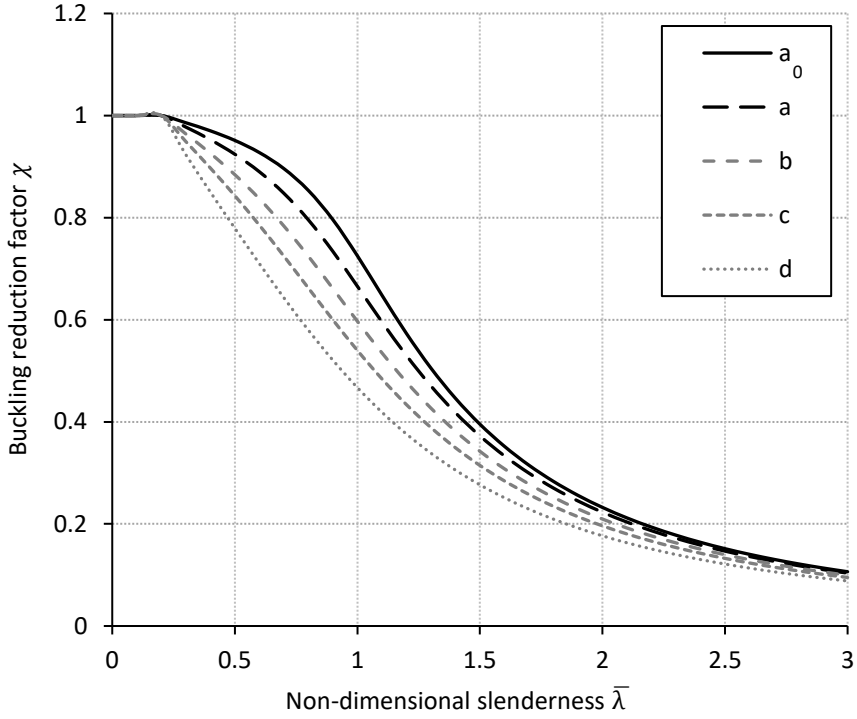

Figure 6-10 Buckling curves at room temperature in accordance with EN 1993-1-1 (2005)

6.3.5.4 Results from the parametric studies

This section presents a comparison of the results from the parametric studies with the recommendations in Eurocode 3 Part 1-2 (2005) outlined previously. For Class 1 SHS and RHS columns, the ultimate buckling load obtained from the FE models is normalised by $Af_{y,\theta}k_{y,\theta}$ and the non-dimensional slenderness $\bar{\lambda}_{\theta}$ is calculated using Equation (6.15). Since the Class 3 classification changes to Class 4 when taking into account the reduced value ε mentioned in Equation (6.10), the ultimate buckling load is normalised by $A_{eff}f_{0.2p,\theta}k_{0.2p,\theta}$ and the non-dimensional slenderness $\bar{\lambda}_{\theta}$ is calculated using Equation (6.16). The reduction factors ($k_{y,\theta}$ and $k_{0.2p,\theta}$) presented in Chapter 4 were used in the calculations.

The buckling curves and FE results for Class 1 and Class 3 SHS and RHS members, respectively made from steel A (S690QL) and B (S700MC) are presented in Figure 6-11 and 6-12. The buckling coefficients at 100, 200 and 300°C are not presented here, however it is rational to assume that the buckling coefficients will be between 20 and 400°C. With reference to Figure 6-11 (a), the Eurocode buckling curve is generally conservative with respect to the buckling coefficients for steel A (S690QL), with the exception of 800°C at non-dimensional slenderness $\bar{\lambda}_{\theta}$ values below unity.

Similarly, in Figure 6-11 (b) the Eurocode buckling curve is conservative and adequately predicts the ultimate buckling load for steel B (S700MC) at all temperatures which is related to the better strength and stiffness properties of this material. In

Figure 6-12 (a), it can be seen that generally, the Eurocode curve is conservative with respect to the buckling coefficients and safely predicts the buckling behaviour of Class 3 sections which change to Class 4 sections at temperatures up to 800°C, even though the Eurocode limit the application of the buckling curves for Class 4 sections to temperatures up to 350°C only. There is little disparity between the major and minor buckling axes for RHS sections.

At non-dimensional slenderness $\bar{\lambda}_{\theta}$ values below 1.0, steel A (S690QL) has higher buckling coefficients and more scatter between the buckling coefficients compared to steel B (S700MC). This is related to the shape of stress-strain curve of the two materials, which strongly influences the stability behaviour of the steel members at low non-dimensional slenderness values ($\bar{\lambda}_{\theta}$<1.0). For steel B (S700MC), the shape of the stress-strain curve shown in Figure 6-2 is nonlinear at all temperatures and quite consistent in shape. This is further demonstrated by the strain hardening parameter, n in Table 6-2, which are relatively similar at all temperatures varying between 9.3 and 14.9. However, for steel A (S690QL), the stress-strain response at room temperature (20°C) displays an almost bi-linear elastic-plastic response up to the 2% total strain, and shows more nonlinear behaviour at higher temperatures as shown in Figure 6-1. This is demonstrated by the great disparity between the strain hardening parameters, n in Table 6-1, which varies between 8.0 and 102.0. The varying degree of nonlinearity of the steel A (S690QL) with temperature leads to different buckling responses and hence results in the increased scatter in the obtained results. Members with a non-dimensional slenderness greater than 1.5 buckle elastically, where the average stress falls in the elastic part of the stress-strain curve, and as expected there is little difference in the elevated temperature buckling strength of columns of steel A (S690QL) and B (S700MC).

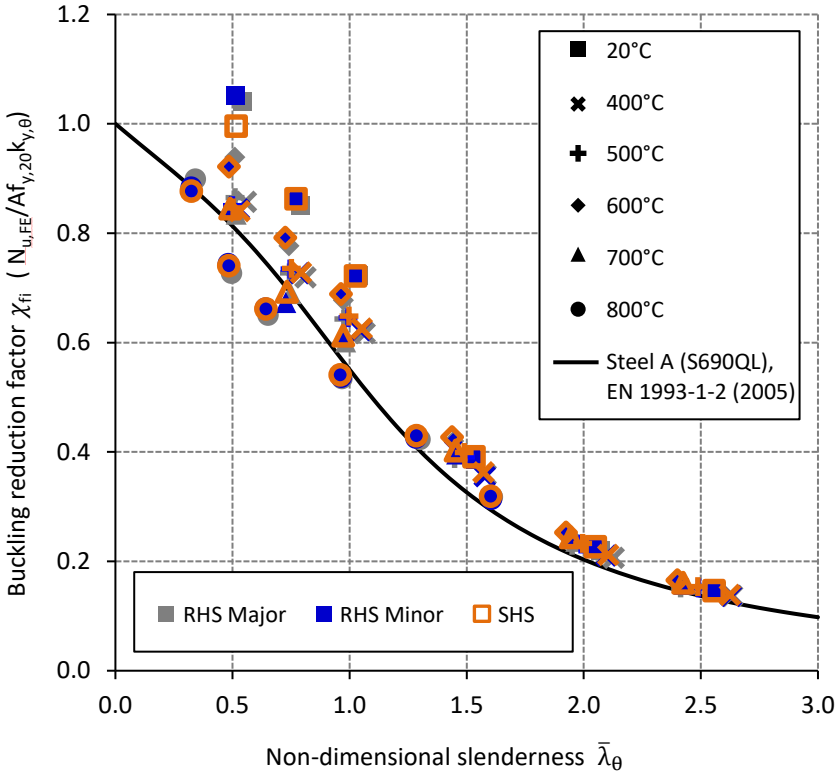

(a)

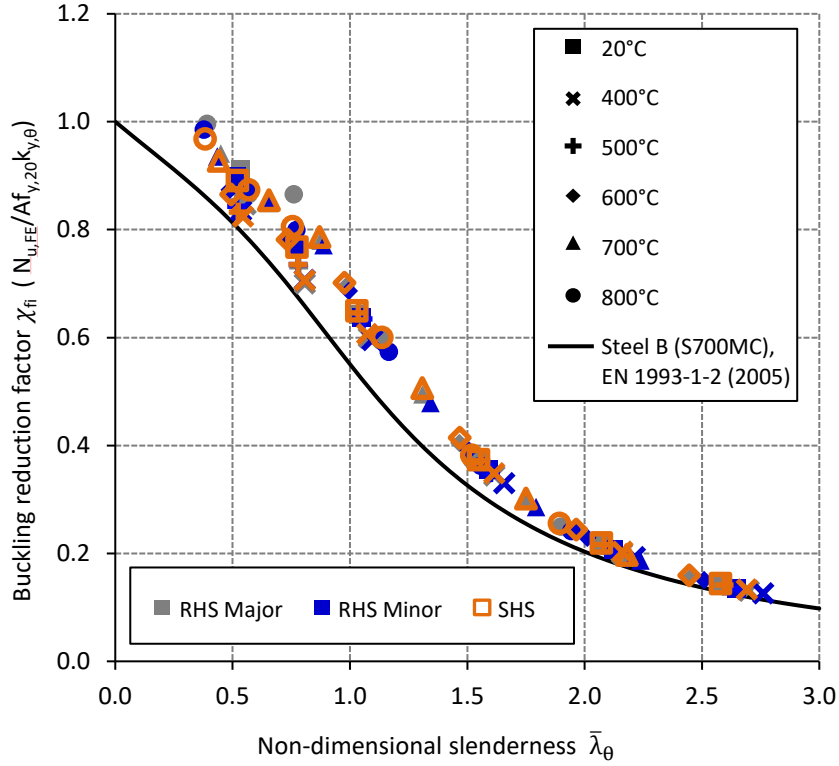

(b)

Figure 6-11 Comparison of EN 1993-1-2 (2005) buckling curve and FE results for Class 1 SHS and RHS (a) A (S690QL) and (b) steel B (S700MC)

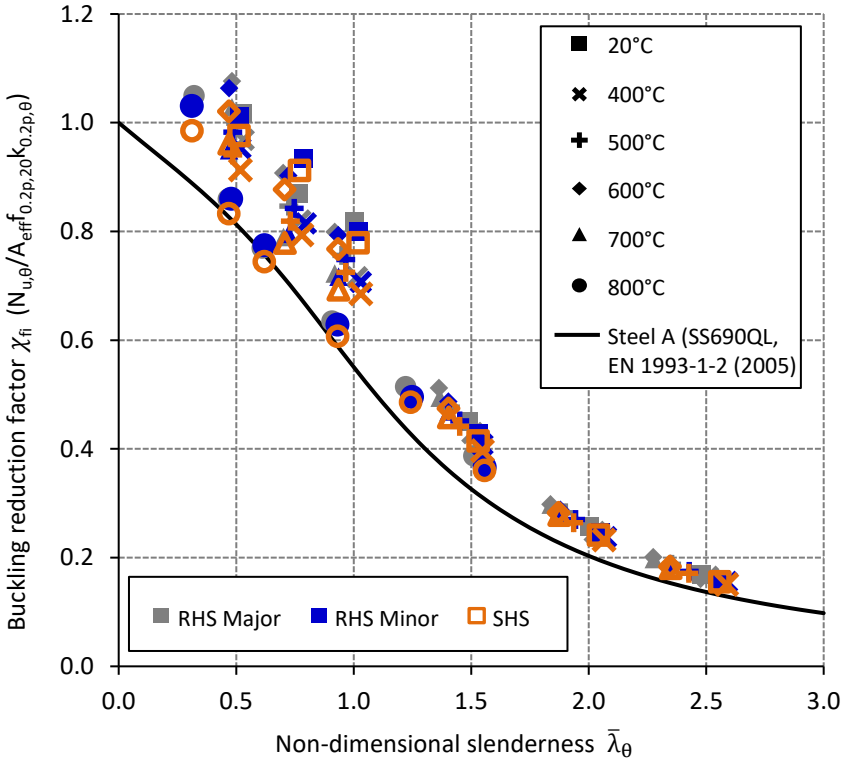

(a)

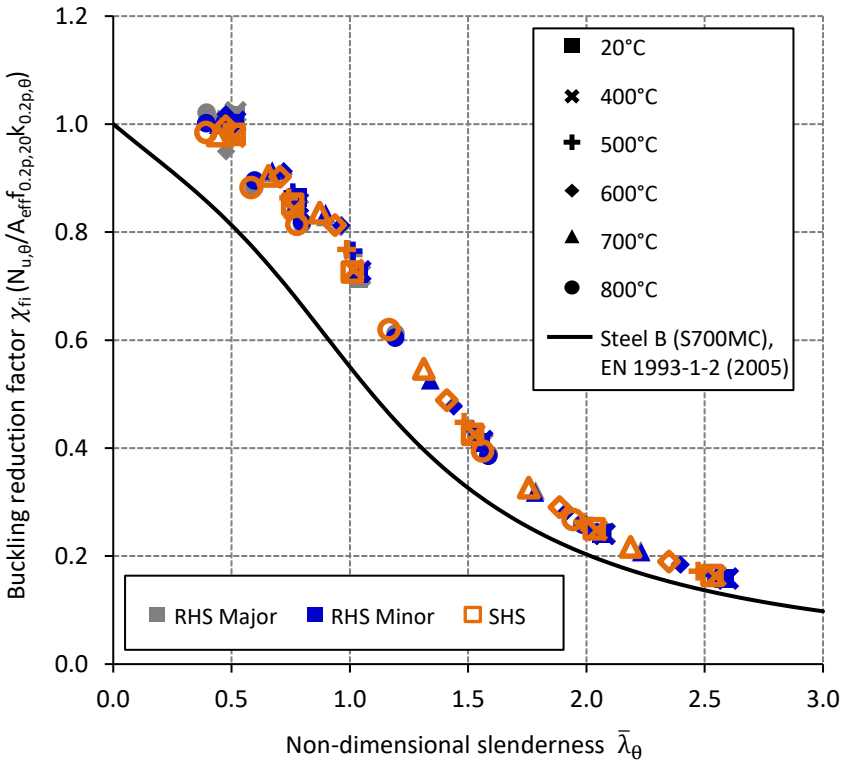

(b)

Figure 6-12 Comparison of EN 1993-1-2 (2005) buckling curve and FE results for Class 3 SHS and RHS (a) steel A (S690QL) and (b) steel B (S700MC)

The strain hardening parameter further explains why steel A (S690QL) has a high buckling coefficient than steel B (S700MC) at 20°C for non-dimensionless slenderness values less than 1. For comparison, the buckling coefficient at 20°C derived from normalisation with the yield strength taken at 0.2% proof strength are presented in Figure 6-13 along with the five design buckling curves (a_0, a, b, c, and d) presented in Eurocode 3 Part 1-1 (2005). In the case of steel A (S690QL), the buckling coefficient at 20°C is greater than 1 at a non-dimensionless slenderness of 0.5 due to the material strain hardening after yield (0.2% proof strength). In contrast, the buckling coefficient of steel B (S700MC) at 20°C is below 1, owing to the nonlinearity of the stress-strain response where the stiffness reduces prior to reaching the 0.2% proof strength. The results from the parametric study demonstrate that for design at room temperature, 'curve a_0' is suitable for steel A (S690QL) which is in line with the current recommendations in Eurocode 3 Part 1-1 (2005). However, 'curve a' is appropriate for steel B (S700MC), highlighting the importance of considering the stress-strain response. At higher temperatures, the stress-strain response becomes increasingly nonlinear, and the advantage of steel B's (S700MC) superior strength and stiffness retention properties, results in better buckling coefficients compared to steel A (S690QL). This is evident from non-dimensionless slenderness values less than 1.5 as shown in Figure 6-11 and Figure 6-12, particularly at 700 and 800°C.

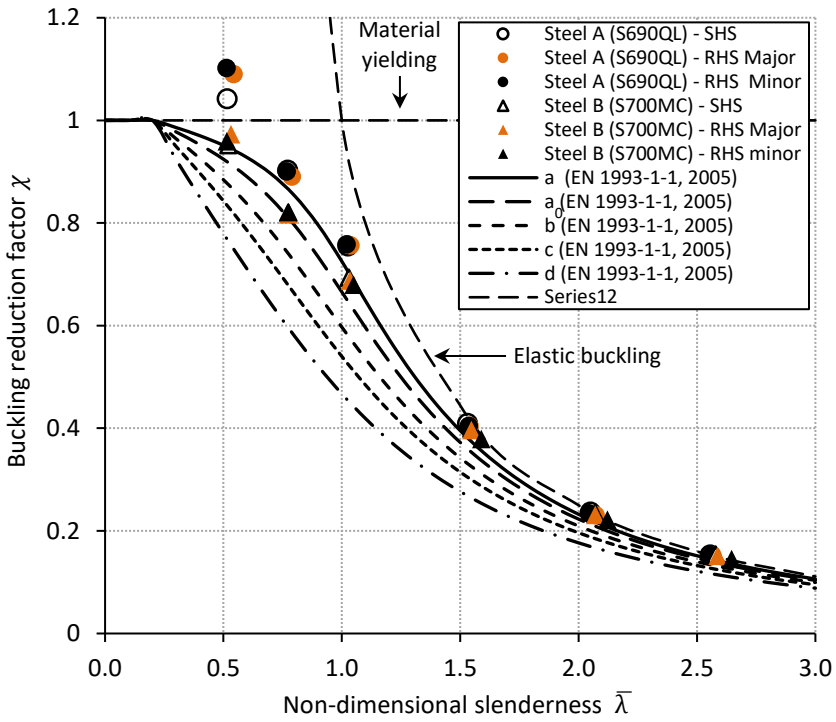

Figure 6-13 Comparison of EN 1993-1-1 (2005) buckling curves and FE results for Class 1 SHS and RHS made from steel A (S690QL) and steel B (S700MC)

6.4 Summary

In this chapter, the stress-strain response of steels A (S690QL) and B (S700MC) obtained from tensile tests at room and elevated temperatures (presented earlier in Chapters 3 and 4), were described using the modified Ramberg-Osgood model proposed by Gardner and Nethercot (2004). Following on, a numerical study investigating the flexural behaviour of HSS columns, including a detailed description of the FE model and validation results in ABAQUS, was presented, considering the material properties and geometric imperfections. Once validated, the model was used to perform parametric studies on the behaviour of columns made from steel A (S690QL) and B (S700MC) at room and elevated temperature, incorporating the measured stress-strain response. The results from the parametric studies were analysed and it was shown that the Eurocode generally provides conservative results with respect to the buckling coefficients and safely predicts the buckling resistance of steel B (S700MC) columns, while a lower buckling curve may be needed for steel A (S690QL) columns. Minimal difference was observed between buckling about the major and minor axis, which was similarly reported by Franssen et al. (1998). It was also shown that the shape of the stress-strain response, in particular the curvature of the stress-strain response before reaching the 0.2% proof strength, as described by the strain hardening parameter n, strongly influences the stability behaviour of the steel members at low non-dimensional slenderness values ($\bar{\lambda}_{\theta}$<1.0). In such scenarios, a higher strain hardening parameter results in better buckling coefficient because the reduction of stiffness occurs at much higher strength. At room temperature, the strain hardening parameter for steels A (S690QL) and B (S700MC) was 102.0 and 13.8, respectively. As a result, the Eurocode 'curve a_0' is suitable for steel A (S690QL), whilst 'curve a' is more appropriate for steel B (S700MC).

Chapter

7

Discussion

7.1 Introduction

At the outset, it is suspected that the variety of production routes and chemical compositions used to produce a HSS compliant with the standards at room temperature, could lead to a wide variation in the material response in fire. This raised questions about the suitability of the current elevated temperature material performance data presented in the Eurocodes for HSS, since the Eurocode approach is derived from mild steel grades. To support the safe design of HSS structures under fire conditions, there has been increased effort in obtaining material property data for HSS at elevated temperature. The data has been compared with the Eurocode guidelines (EN 1993-1-2, 2005) and show that the reduction factors presented in the Eurocode are unconservative (i.e. unsafe) for majority of HSS grades (Chen et al., 2006; Schneider and Lange, 2009; Qiang, 2013; Choi et al., 2014; Chiew et al., 2014; Xiong and Liew, 2016 and Neuenschwander et al., 2017). However, the Eurocode was conservative (i.e. safe) for a few HSS with differing chemical composition and/or heat treatment (Chen and Young, 2006 and the (RUOSTE) report commissioned by the EU Research Fund for Coal and Steel (European Commission, 2016)). From these studies, it is not clear why certain HSS grades have better reduction factors properties than others. The focus of this study is to document the changes in strength and stiffness of different HSS at elevated temperatures and compare the findings with the current Eurocode approach. In addition, there is an interest to explore whether any benefits could be derived (when compared to lower strength alternatives) from metallurgical effects including grain size and secondary hardening gained from the microalloying additions, which might improve the strength retention at elevated temperatures.

Hence, microstructural characterisation was conducted on selected HSS grades. It is noteworthy that the microstructural study was limited to explore possible reasons for the strength retention of the two best performing steels (steels A (S690QL) and B (700MC)) at elevated temperatures; the stiffness retention was beyond the scope of this thesis. This chapter discusses the links between the material history and changes in the microstructure at elevated temperatures, and relates these to the material and buckling performance at elevated temperature.

7.2 Strength

7.2.1 General

Strength is one of the key properties required to determine a structures load bearing capacity. With increasing temperature, strength loss becomes inevitable and this can lead to the total or partial collapse of a structure under fire conditions. Hence, it is important to ensure that the material properties of HSS used in design are reflective of the material under fire conditions and it is worth exploring whether the strength loss can be delayed at elevated temperature.

At room temperature, the difference between the nominal (design) and measured yield strengths for the HSS grades tested in this study (Chapter 3) was up to 14%. This is within the 10-20% range specified in the European commissioned study (European Commission, 2016). With increasing temperature, it was found that the high temperature performance of HSS varied significantly more than mild strength steels. In the literature, the Eurocode approach was shown to be unconservative (i.e. unsafe) for many HSS grades. However, in this study, the Eurocode approach was at times overly conservative (i.e. safe) with respect to all the HSS grades tested. This is particularly true when the reduction factors are derived by normalising the effective yield strength at elevated temperature by the nominal yield strength at room temperature.

In Chapter 4, the reduction factors of various HSS grades at elevated temperature were presented. Following the Eurocode approach, in which the reduction factors were derived from the lower bound results from anisothermal tests on mild steels, a lower reduction curve should be specified for HSS, considering the 'worse case' scenario. However, lower reduction factors for HSS will penalise the steels that demonstrate better strength retention properties and have cost implications as more fire protection will be required in order to meet the legal fire resistance period in accordance with the standards. Separate reduction curves for different HSS based on the production route or chemical composition could be specified, and this will require obtaining the elevated temperature material properties of various types of HSS; this is an onerous task.

Alternatively, a clause could be introduced to the Eurocodes, which allows for HSS grades which demonstrate better strength retention properties to be utilised in design.

The reduction factors for steel D (S460NH) support the applicability of the current Eurocode approach for S460NH. Compared with the mild steel grades used for the derivation of the reduction factors in the Eurocode (i.e. S235 and S355), the higher strength of S460N type steel is typically a result of a higher carbon content as indicated by the European material standards (EN 10025-3, 2004). This could be a reason why S460NH behaved in a similar matter to the mild steel grades. To produce HSS with higher yield strengths up to 700 N/mm^2, QT and TMCP processes are used. Both processes resulted in different material behaviour at elevated temperatures, and this is discussed further in Section 7.2.3.

7.2.2 Experimental influences

Before evaluating the metallurgical influences, which could account for the variation in the differences in strength at elevated temperatures, it is worth considering the possibility of scatter due to experimental approach used. The inconsistencies in the experimental approach employed amongst researchers including different strain rates and soaking times at elevated temperatures, will influence the strength. It is well established that a high strain rate will result in a higher effective yield strength with increasing temperature (as discussed in Section 4.2.4.3). However, the influence of soaking times at elevated temperatures, which may influence the microstructure and hence material properties, is often not considered. As part of the metallurgical study presented in Chapter 5, heat treatments were conducted on steels A (S690QL) and B (S700MC) at various target temperatures ranging from 500 to 800°C and two soaking times: 5 and 60 minutes. After each heat treatment, the steels were quenched in water to get an indication of the microstructure and Vickers hardness studies were carried out on the heat-treated material. The Vickers hardness results for steel A (S690QL), demonstrated a considerable drop in hardness at 700°C, following a soaking time of 60 minutes compared with 5 minutes, because of rapid coarsening of cementite occurring by diffusion. Alloying elements including chromium, molybdenum, niobium and vanadium can reduce the rate of cementite coarsening. In the absence of these elements, coarsening may occur at temperatures as low as 400°C, resulting in subsequent decreases in hardness (Bhadeshia and Honeycombe, 2006). Since hardness is proportional to strength, long soaking times may result in material softening and subsequent reduction in strength. Hence it is relevant to consider the soaking time when presenting and analysing reduction factors.

Specifying an appropriate soaking time is challenging because, on the one hand, it is important to ensure that the entire specimen is equilibrated to the target temperature prior to testing whilst, on the other hand, long soaking times can result in rapid strength degradation from temperatures of 400°C and above (depending on the production route and alloying elements). This is where considering the volume of the tensile specimen and appropriate heat transfer calculations can be beneficial to ensure that an appropriate soaking time is used. The variability of elevated temperature strengths due to differences in experimental techniques within the literature, which included the strain and heating rates as well as soaking times, highlight the need for a consistent experimental approach. As of date, there is not standardised method for obtaining elevated temperature material properties for structural fire design purposes.

Whilst it is evident that the experimental technique can affect the strength, genuine material effects will also influence the material properties including strength and this is discussed further in the following sections.

7.2.3 Metallurgical influences

7.2.3.1 Quench and tempered (Q or QT) steel

In Chapter 4, a noticeable difference in the strength reduction factors of steel A (S690QL) and C (S690QL) was seen at temperatures greater than 500°C. For example, at 600°C, the reduction factors for the effective yield strength of steel A (S690QL) and C (S690QL) were 0.67 and 0.54, respectively. Comparisons of the reduction factors with other QT steels in the literature revealed an even greater discrepancy. Again, taking the example of the reduction factors for the effective yield strength at 600°C, the highest and lowest reduction factors were 0.67 and 0.14, respectively, representing a difference greater than 50%.

The standards concerning many steel grades, including QT steels (EN 10025-6, 2004) are optimised to ensure adequate properties are achieved at room temperature. Compositional limits are specified in EN 10025-6 (2004) leading to an almost-infinite number of possible chemical compositions. This is in addition to differences in the manufacturing route, including difference in thickness, quenching rate, heating rate, tempering temperature, and holding times. The differences in chemical compositions and production routes do not lead to significant differences in the properties at room temperature as the materials are designed to meet the minimum property requirements at room temperature. However, at elevated temperatures, there is no requirement for steels to follow any reduction curve, and different effects are seen for different production and alloying routes. The large discrepancy in the reduction factors found in this work and reported in

the literature, supports the remarks by Burgan (2001) and highlights the danger in attempting to generalise the behaviour of QT (and indeed other) steels without considering the material history.

The QT steels investigated in this study, all differed slightly in microstructure (as presented in Section 5.3.1) which is attributed to the variation in chemical composition. Significantly lower amounts of microalloying elements (titanium, niobium and vanadium) were present in Steel A (S690QL) compared with steel C (S690QL) and E (S690QH), as discussed in Section 3.2.2. These microalloying elements typically form fine precipitates which pin the grain boundaries and help reduce grain growth during hot rolling process. Upon tempering the presence of the fine precipitates can reduce the coarsening rate of cementite and further hinder strength loss at elevated temperature upon reheating.

Nevertheless, steel A (S690QL) had better strength retention properties than steel C (S690QL) at elevated temperature, which highlights that the presence of microalloying elements in QT steels does not necessarily guarantee better strength retention properties under these conditions. The strengthening potential of microalloying elements at elevated temperature is dependent on the quantity as well as the presence of other elements including molybdenum which can help reduce the coarsening rate of the precipitates. As shown in Section 3.2.2, steel A (S690QL) was alloyed with more chromium and molybdenum than steel C (S690QL). Molybdenum can enhance the tensile strength of carbon steels, prior to the prevalence of creep effects. Chromium may also have a positive influence on the strength retention properties when alloyed with molybdenum. Corresponding hardness results following heat treatments on steel A (S690QL), presented in terms of Hollomon-Jaffe (H-J) parameter (Section 5.3.3.1), revealed a slight delay in softening when the H-J parameter was 17.5. This is believed to be due to the precipitation of complex chromium carbides, known as secondary hardening. Complex chromium carbides tend to form around 500-600°C when sufficient amounts of molybdenum are present but upon forming these carbides will rapidly coarsen as the temperature increases (Bhadeshia and Honeycombe, 2006). Thus, it is believed that the superior strength of steel A (S690QL) compared with steel C (S690QL) at elevated temperatures is most likely due to the higher amount of chromium and molybdenum present. In steel A (S690QL), the decomposition of the lath boundaries occurred at temperatures above 600°C and this may have contributed to this steels strength loss; further changes in the grain size were not observed until the material was in the intercritical region at 800°C.

Steel E (S690QH) which was alloyed with chromium, molybdenum and microalloying elements could not be tested at elevated temperatures because the dimensions of the flat specimens

machined, following the recommendations in ISO 6892-2 (2011), were not compatible with the test machine used in this study. The results from this study suggest that steel E (S690QH) may have better strength retention properties than the Eurocode because of the similarity in chemical composition and production route to those of steel A (S690QL). However, the microstructures of steels A (S690QL) and E (S690QH) (presented in Section 5.3.1), which is influenced by the chemical composition and production route are different. It is worth nothing that both steels have different product forms which may influence the elevated temperature performance, steel A (S690QL) is a plate and steel E (S690QH) is a structural hollow section.

7.2.3.2 Thermomechanically controlled processed (TMCP or M) steel

Of the steel grades tested at elevated temperature in Chapter 4, steel B (S700MC) had the best strength retention properties. The microstructure at room temperature (as presented in Section 5.3.1) was very fine and this is attributed to the addition of microalloying elements (e.g. vanadium, niobium and titanium) in combination with the controlled rolling regime to temperatures much lower than the temperatures used to produce QT and N steels. Although precipitates formed from microalloying additions slow down grain growth during production, these precipitates also further hinder dislocation movement at room and elevated temperatures.

The precipitates can be a useful strengthening mechanism at elevated temperature, however, their effectiveness at contributing to strength, generally decreases with increasing particle size and hence the formation of large precipitates (i.e. several microns as opposed to several nanometres in size) should be avoided. Large titanium rich precipitates (or inclusions) were present in steel B (S700MC), which are ineffective at contributing to strength enhancement through precipitation hardening. Instead, the large precipitates became initiation points for voids and cracks to form during straining of the tensile specimens (as presented in Section 5.3.2) and seem the most likely reason for the reduced ductility of steel B (S700MC) compared with the steels A (S690QL) and C (S690QL) at elevated temperature.

On the contrary, the high thermal stability of titanium nitride compared with niobium and vanadium nitrides, makes titanium nitride an attractive precipitate that can contribute to strength through grain refinement during hot rolling. The use of accelerated cooling can supress the formation of further precipitates (in particular for carbides which form at lower temperatures compared with their respective nitrides). In Section 5.3.3.1, evidence of reserved microalloying elements in solid solution was observed in steel B (S700MC), which upon reheating, contributed towards retarding the strength loss at elevated temperatures through secondary hardening. To

further investigate and characterise the fine precipitates produced during secondary hardening will require a high-resolution microscope such as a transmission electron microscope (TEM), and this was beyond the scope of this project. In addition, EBSD studies on heat-treated steel B (S700MC) material presented in Section 5.3.3.3, revealed no changes in grain morphology until 800°C which correlated with the rapid strength loss observed in Section 4.3.

7.3 Stiffness

7.3.1 General

Stability calculations are often critical for HSS members as they tend to be more slender than lower steel grade equivalents. Different stiffness retention properties were observed amongst the HSS grades tested in this study (Section 4.3.6). The findings highlight that the stiffness retention properties are dependent on the chosen test method (i.e. isothermal or anisothermal conditions) and the accuracy of the extensometer. These factors can limit the interpretation of the results, if such factors are not considered and so the experimental influences and the differences in the stiffness retention properties observed in this study are discussed in the following sections.

7.3.2 Experimental influences

A concern which arose during the experimental programme was the reliability of the elastic modulus measurements stemming from the challenges related to elevated temperature tensile testing. The elastic modulus is derived from the early (linear) part of the stress-strain curve which gets smaller as the temperature increases. As a result, obtaining a reliable and accurate elastic modulus at elevated temperature can be a challenge for several reasons including a reduction in the strain data available from which to derive the elastic modulus, the influence of thermal and creep strains (e.g. when the influence of thermal restraint is not considered when subtracting thermal expansion effects from data obtained from anisothermal tests), and experimental errors such as misalignment of the tensile specimen and the classification (hence accuracy) of the extensometer.

In this work, a class 1 extensometer with a 25mm gauge length and total bias error of 1% or ±3 µm (dependent on which value is the highest) was used, in accordance with ISO 9513 (2012). The uncertainties related to class 1 extensometers were described by Lord and Morrell (2010) as the following:

> "Because of the 1% or 3 µm lower limit, the absolute error in strain measurement increases as the strains become smaller. This means that for a 25mm gauge length and 0.1% strain, the absolute error in modulus can be as high as ±12%, and these are the typical

uncertainties that can be attributed to the measurement of strain for a class 1 extensometer."

Hence, with increasing temperature the uncertainty of the elastic modulus is aggravated as its value is derived from strain values less than 0.1%. The classifications of the extensometers used in published literature are seldom reported and hence their reliability is unknown. Ideally, a high-resolution extensometer such as class 0.2, where the total bias error is either 0.2% or ±0.6 μm (again, dependent on which value is the highest) in accordance with ISO 9513 (2012) should be used to measure the strain during tensile tests. However, class 0.2 extensometers calibrated for use from room to elevated temperatures are not widely available (Lord and Morrell, 2010; Motra et al., 2014)

As a result of the aforementioned challenges related to obtaining elastic moduli at elevated temperatures, while tensile tests can be considered a good starting point to get an indication of the corresponding elastic modulus at elevated temperatures, for more accurate and reliable elastic moduli data, alternative methods should be considered (Münstermann et al., 2014). Examples include 3 point-bend tests or dynamic methods such as flexural resonance methods, the impact excitation technique (IET), and various ultrasonic, resonance or acoustic wave propagation methods (Lord and Morrell, 2014).

7.3.3 Metallurgical influences

Despite the uncertainties related to inherent experimental errors related to elevated temperature tensile testing, significant differences in the behaviour of the elastic modulus at elevated temperature were observed and majority of the steels were safely and conservatively depicted by the Eurocode. Steels A (S690QL) and B (S700MC) showed better stiffness retention properties than steels C (S690QL) and D (S460NH). Although the metallurgical influences accounting for the differences in the elastic modulus for the HSS grades in this study were not explored, it is noted that the difference is unlikely to be related to the variations in chemical composition and heat treatments. The texture (i.e. a preferred crystal orientation) introduced during the rolling process may result in a higher density of grains oriented in a direction where the elastic modulus is stronger or weaker (as discussed in Section 2.3.3) and this may be a possible reason for the differences in the stiffness retention properties at elevated temperatures. Hence, to understand how the metallurgical properties influences the elastic modulus of different types of HSS at elevated temperatures, will require examining the texture of these materials at various temperatures.

7.4 Buckling response

7.4.1 General

Since the material response of various types of HSS differ at both room and elevated temperature, it is anticipated that the structural response will also differ. In Chapter 6, FE studies were conducted to investigate the implication of the buckling behaviour of columns made from steels A (S690QL) and B (S700MC) at elevated temperatures. The results showed that the Eurocode generally provides conservative (i.e. safe) results for steel B (S700MC) columns with respect to the buckling coefficients and safely predicts the buckling resistance, but a lower buckling curve may be needed for steel A (S690QL) columns. The influence of the steel grade on the buckling response is explained further in the following section.

7.4.2 Influence of the steel grade on the buckling response

It is clear that the material properties (including the strength, stiffness and the shape of the stress-strain response) strongly influence the buckling performance of HSS columns at elevated temperature; this is particularly true for columns with a non-dimensional slenderness from 0.5 to 1.0. For slender elements (i.e. columns with a non-dimensional slenderness value greater than and including 1.5), buckling is mainly governed by stiffness which was similar for both steels A (S690QL) and B (S700MC) at room and elevated temperature. Hence, with increasing temperature, there was no difference in the buckling response of these two HSS, as buckling occurred elastically before the material reached yield.

Although steel B (S700MC) had a higher stiffness and yield strengths (i.e. 0.2% proof strength and effective yield strength) than steel A (S690QL) at room temperature (Section 3.4.2), the columns made from steel A (S690QL), had a higher buckling coefficient compared with the columns made from steel B (S700MC). The reason for this was attributed to the shape of the stress-strain response, which was described using the strain hardening parameter in Section 6.2.2. It was found that higher strain hardening parameters translated to higher buckling responses because the corresponding strength, where the stiffness subsequently reduces, would occur at a higher temperature. At room temperature, the strain hardening parameter for steel A (S690QL) was significantly higher than steel B (S700MC) (102.0 for steel A vs 13.8 for steel B) and this resulted in the Eurocode 'curve a_0' being suitable for steel A (S690QL), whilst 'curve a' was suitable for steel B (S700MC). The differences of the stress-strain responses amongst different HSS grades is currently not considered in the Eurocode, and as a result the Eurocode specifies the 'curve a_0' for all HSS grades. Since TMCP steels tend to have a more curvilinear stress-strain response compared with most QT steels at room temperature, it is recommended that 'curve a' is specified for TMCP steels.

The results suggest that at room temperature, steel A (S690QL) is perhaps more favourable to use than steel B (S700MC) for structural elements including SHS and RHS columns with a non-dimensional slenderness between 0.5 and up to and including 1.0. However, in a fire scenario, the high buckling coefficients of steel A (S690QL), reduced to similar levels as steel B (S700MC). When the temperature reached 800°C, steel B (S700MC) had significantly higher buckling coefficients than steel A (S690QL). Whilst the Eurocode approach was conservative (i.e. safe) with respect to buckling coefficients for steel B (S700MC) at all temperatures, the Eurocode approach was unconservative (i.e. unsafe) with respect to buckling coefficients for steel A (S690QL) at 800°C. It is likely that steel A's (S690QL) lower buckling response at 800°C is linked to the low strain hardening parameter for steel A (S690QL) compared with steel B (S700MC) at this temperature and highlights that the strain hardening parameter is a useful indicator for determining the buckling response of stub columns at room and elevated temperatures.

The benefits of steel B's (S700MC) better strength retention properties compared with steel A (S690QL) on the buckling coefficients were not observed until 800°C. Following a prescriptive approach to design, at 800°C, it is not anticipated that a column will survive when loaded to 60% of its nominal strength. In reality, if one of the structural elements (e.g. column) can no longer maintain its load bearing capacity, total collapse may not occur because the load will redistribute to other (cooler) parts of the structure. Therefore, to gain a holistic understanding on the use of different types of QT and TMCP steels in a fire scenario will require investigating the behaviour of these materials in structural systems rather than singular structural elements.

7.5 Structural fire design considerations of HSS

The vast differences in the strength reduction factors of different types of HSS grades at elevated temperature, as presented in Section 4.3.5, raises the question about what should designers look out for to ensure the HSS grade they select has adequate strength retention properties in line with the Eurocodes. The answer is not straight forward as there is no requirement in the standards for HSS to meet a specified strength at elevated temperature or follow any reduction curve. The findings from this study show that HSS such as QT steels with high molybdenum (e.g. ≥0.2%) and chromium content (e.g. ≥0.5%) can have better strength retention properties; hence the mill certificate can be a first indication of the elevated temperature performance. However, for confirmation, it would be worth conducting materiel tests following a relevant standard. If driven by consumers and standards organisation bodies, steel manufacturers could demonstrate that their steel adheres to a minimum strength at elevated temperature.

A performance based approach to design, will utilise the stress-strain response in order to predict post buckling performance. Hence, it is worth considering the differences in the shapes of the stress-strain responses at both room and elevated temperatures. Steels A (S690QL) and B (S700MC) which demonstrated the best strength retention properties amongst the HSS grades tested, do not have the typical bilinear stress-strain response specified in Eurocode 3 Part 1-1 (2005). Not considering the shape of the stress-strain response could lead to underestimating the buckling performance at both room and elevated temperatures as discussed in the previous section (7.4). The strain hardening parameter from the modified Ramberg-Osgood model presented in Section 6.2 is a useful indicator of differentiating steels with a nonlinear stress-strain response from steels with a typical bilinear stress-strain response. The strain hardening parameter of steels with a bilinear stress-strain response approach infinity (for more practical approach the values can be considered ≥100), whilst for materials with a more non-linear stress-strain response, the values will be smaller (i.e. ≤20).

In addition, the stress-strain relationship at elevated temperature specified in the Eurocode (EN 1993-1-2, 2005) is specified for strains up to 20%. However, at elevated temperature, it is noted that the same strengthening mechanisms employed to retard strength loss such as secondary hardening can have detrimental effects on the ductility. In Chapter 4, the ductility of steels A (S690QL) and B (S700MC) from 100 to 400°C is lower than that at room temperature and this was attributed to a metallurgical phenomenon called dynamic strain ageing (DSA). The reduction of the ductility at elevated temperature may need to be considered in performance based approach where plastic analysis is important since the reduced ductility (ε_f) will influence the post buckling behaviour.

7.6 Concluding remarks

There is enough evidence to believe that HSS (including those of the same grade, e.g. S690QL) can have significantly different responses at elevated temperatures. These differences stem from the wide variety in the chemical composition, heat treatment and production route used to produce the HSS. The literature shows that the HSS grades are generally unconservatively represented in the Eurocodes, however the HSS grades tested in this study demonstrate that some HSS grades are overly conservatively represented in the Eurocodes. HSS with better strength retention properties could be exploited in design if the material properties were obtained following a consistent standardised method. Although a standardised approach for obtaining the properties of different materials for structural fire design purposes currently does not exist, following a consistent standardised approach will reduce the error due to experimental influences and allow the influence

of the chemical composition and production route to be much clearer. The option to utilise the material properties of HSS with enhanced strength retention properties can offer wider potential applications for HSS in structural applications.

This research has also shown that microalloying elements can be an effective strengthening mechanism for retarding the strength loss of TMCP steels at elevated temperature, through secondary hardening. In QT steels, the presence of microalloying elements does not necessarily guarantee better strength retention properties at elevated temperature. This is because the precipitates formed from the microalloying elements in the QT steels will rapidly coarsen with increasing temperature, resulting in a reduction in strength. Instead other elements including chromium and molybdenum were seen to have a positive influence on the strength retention properties at elevated temperature, as these elements can help reduce the coarsening rate of the precipitates.

The significance of utilising HSS with better strength retention properties showed that Eurocode approach to buckling response at elevated temperature to be conservative for steel B (S700MC) but unconservative for steel A (S690QL). The unconservative result at 800°C is due to a combination of the strength and stiffness properties at this temperature, as well as the 'roundness 'of the stress-strain response, described using the strain hardening parameter. Generally, the higher strain hardening parameter, the higher the buckling response, and this factor is currently not considered in the Eurocode. The key conclusions and design recommendations drawn from this discussion are summarised in Chapter 8.

Chapter

8

Conclusions and future work

8.1 Introduction

This research has explored how the material history including chemical composition and production route of different types of HSS, influences the material properties and hence structural response in a fire scenario. In this chapter, the key findings and conclusions from this thesis, as well as recommendations for further research following on from this work are presented.

8.2 Conclusions

From the experimental work carried out in this programme, the following conclusions can be drawn:

- This research has shown that, dependent on the appropriate combination of chemical composition and processing route, some commercial HSS grades, with yield strengths between 650 and 700 N/mm^2, can have better strength retention properties then the indicated from reduction factors presented in the Eurocodes. Therefore, it is recommended that a clause should be introduced in the Eurocodes, which allows for HSS that demonstrate better strength retention properties, following a standard experimental procedure, to be used in the design of structures under fire conditions.

- Based on the HSS grades tested in this study, the reduction factors for the effective yield strength, 0.2% proof strength (from temperatures above 250°C onwards) and elastic modulus, derived by normalising by the nominal (design) property, were shown to be

conservative (i.e. safe) with respect to Eurocode 3 Part 1-2 (2005). However, similar reduction factors for the effective yield strength of various HSS grades in the literature demonstrated that the Eurocode is unconservative and that revised (lower) reduction factors for HSS should be proposed, considering the 'worse case' scenario.

- The vast difference in the material properties of HSS at elevated temperature is related to differences in the chemical composition, processing route as well testing techniques including soaking time and strain rate. This highlights the need for a consistent experimental approach, which will help give a better indication of the influence of the material history.

- Amongst the steel grades tested, the TMCP steel, steel B (S700MC) alloyed with chromium and combined niobium, vanadium and titanium additions, demonstrated the best strength retention properties at temperatures up to 800°C. Results from the metallurgical study showed evidence of secondary hardening, which would have contributed to the strength loss retardation of steel B (S700MC) at elevated temperatures.

- On the other hand, the reduction factors for the QT steels A (S690QL) and C (S690QL) showed that the presence of microalloying elements, niobium, vanadium and titanium does not necessarily guarantee better strength retention properties at elevated temperatures. Amongst the QT steels tested, steel A (S690QL), which was alloyed with more chromium and molybdenum than steel C (S690QL) showed the best strength retention properties. In steel A (S690QL), a slight delay in softening was observed and this is believed to be due to secondary hardening of complex chromium carbides, which tend to form around 500-600°C when sufficient amounts of molybdenum are present.

- As well as the strength and stiffness, the shape of the stress-strain response also influences the structural response. The curvature (or roundness) of the stress-strain response, described numerically using the strain hardening parameter n, was found to influence the buckling behaviour of HSS members with slenderness value less than and including 1. In general, the higher the strain hardening parameter, the higher the buckling response because the corresponding strength, where the stiffness subsequently reduces, would occur at a higher strength.

- At room temperature, the strain hardening parameter for steel A (S690QL) and B (S700MC) was 102.0 and 13.8, respectively. As a result, the 'curve a_0' from the Eurocode is suitable for steel A (S690QL), whilst 'curve a' is more appropriate for steel B (S700MC).

- Comparisons of the results with the buckling curves at elevated temperature, derived following recommendations in Eurocode 3 Part 1-2 (2005) revealed that the Eurocode generally provides conservative (i.e. safe) results and safely predicts the buckling resistance of steel B (S700MC) columns but a lower (i.e. safer) buckling curve is recommended for columns made from steel A (S690QL). However, it is noted that the reduction factors for other types of HSS will differ, and this will influence the buckling response. Hence, it is recommended that the reduction factors for the HSS of interest should first be obtained experimentally before commencing with any structural design.

8.3 Recommendations for future research

Previous work on HSS grades implied that the current Eurocode approach to strength loss at elevated temperature is unconservative. Although this may be true for some of the HSS grades commercially available, it was observed that researchers have used varying testing conditions that will influence the resulting material properties. In particular, the material response is influenced by the increased sensitivity to strain and temperature, as well as metallurgical effects such as spheroidising at elevated temperature which is enhanced by prolonged soaking times. The addition of the microalloying elements niobium, vanadium and titanium can delay the rate of cementite spheroidising (Bhadeshia and Honeycombe, 2006; Vander Voort et al., 2004). It is therefore important to select an appropriate soaking time to ensure that the entire specimen reaches thermal equilibrium whilst also considering the metallurgical influences that will occur. Considering the challenges of obtaining suitable reduction factors that are representative of anticipated fire durations, it is proposed that a "standard" test procedure for obtaining material properties for structural fire design purposes, is developed in order to minimise the discrepancy of results due to variations in the testing parameters employed and make comparisons of different HSS grades easier. Current testing standards used to obtain elevated temperature strength and stiffness properties are limited to isothermal test conditions. Although the current reduction factors in the Eurocodes were derived from anisothermal tests, such tests are currently not standardised.

This work has highlighted that HSS can have better strength retention properties if sufficient amounts of chromium, molybdenum, vanadium, niobium, titanium and boron are present in the composition. These elements appear to have contributed to the strength of the material by

secondary hardening. Extensive studies, with a high-resolution microscope such as a transmission electron microscope (TEM), will allow for further characterisation as well as enhance the understanding of such precipitates in retarding strength loss at elevated temperatures.

Due to the large differences in the reduction factors for HSS grades S650-S700, it is not appropriate to specify a single reduction factor because this means that better strength retention factors for certain HSS cannot be exploited in design. Consideration of the steel's chemistry and processing should be explored further to distinguish steels with better strength retention properties which can be incorporated into designs of structures. This will require a more comprehensive study on a larger range of steels with varying chemical composition in conjunction with different production routes and parameters. Such an extensive task would demand a lot of resources, but the outcome could lead to a compositional parameter to classify steels with better strength retention properties.

Only the influence of temperature on the metallurgical properties of steel A (S690QL) and B (S700MC) has been studied. Strain will also influence the microstructure and hence resulting material properties at elevated temperature (parameters such as yield strength are strain sensitive at all temperatures, especially elevated temperatures). Understanding the metallurgical influences of both strain and temperature is complex. However, there have been great advancements in the field of advance microscopy techniques including in-situ tests in the SEM, which allow for the influence of strain and/or temperature on the microstructure to be observed in real time (Torres and Ramírez, 2011). Such techniques could be very useful in understanding the grain morphology and precipitation behaviour, as well as giving further insight in to the reduced ductility observed in some steels at elevated temperatures.

The Eurocode approach to stiffness from temperatures greater than 400°C was shown in this research to be conservative, owing to the influence of creep. Considering the challenges of obtaining a reliable elastic modulus at elevated temperatures (as discussed in Section 7.3.2), it appears that the reduction factors obtained for HSS grades between S690 and S700 support the notion for revised reduction factors which allow for the better strength retention properties to be utilised in design. However, further tensile tests using a high-resolution extensometer such as class 0.2 compliant with ISO 9513 (2012), or 3-point bend test may give more consistent (i.e. less scatter) results at elevated temperature. Alternatively, dynamic testing techniques such as a dynamic mechanical analyser, which does not consider creep effects, could also be used to obtain the elastic modulus at elevated temperatures. Such tests should provide further evidence to support the notion to revise the reduction factors for HSS. Additionally, the metallurgical understanding behind

higher steel grades demonstrating better stiffness retention properties at elevated temperatures is unclear and should be explored. For example, the texture or orientation of the grain structure of steels can influence the maximum attainable elastic modulus at room temperature, but it is not clear whether the texture changes with increasing temperature. Hence, to understand how the metallurgical properties influences the elastic modulus of different types of HSS at elevated temperatures, it is recommended to study the texture of these materials at various temperatures.

There could be significant cost implications associated with using HSS grades with better strength retention properties at elevated temperature, arising from the high costs of increased alloying with molybdenum, chromium, niobium vanadium and titanium. However, HSS with better strength retention properties at elevated temperature may lead to reduced costs in terms of fire protection. In order to have a holistic understanding of the economic, environmental and social impact of utilising different types of HSS, a life cycle assessment should be considered. This will provide a wider perspective on the use of HSS in more structural applications.

This research has focused on grades with yield strengths between 460-700 N/mm^2. However, there is the likelihood of the Eurocodes being expanded to accommodate steels with strengths up to 960 N/mm^2 (Baddoo and Brown, 2015). QT is the only production route that can be used to achieve strengths greater than 700 N/mm^2 and the metallurgical influences should be considered when specifying appropriate reduction factors for structural fire design.

Equally important to the understanding and safe design of structures under fire conditions, is the material performance of structural connections including welded joints at elevated temperatures. Welding is a common fabrication process used in steel structures and typically involves joining steel parts (or the parent material) together with localised heat and a filler material to create one continuous piece. The process involves a careful selection in welding parameters to avoid adverse effects such as hydrogen cracking. The material properties of welded HSS joints at elevated temperatures are scarce and hence characterisation studies on the performance of welded joints at elevated temperatures is an area requiring further exploration.

The material response is fundamental to understanding the behaviour of HSS at elevated temperature, and this was demonstrated through parametric studies on HSS columns utilising the measured stress-strain response at elevated temperatures. The studies were limited to hot finished class 1 SHS and RHS columns and thus further structural shapes should be investigated to ensure the current Eurocode approach is applicable to HSS. At room temperature, the stress-strain response of S700MC, led to the lower buckling curve “curve a” being appropriate rather than “curve

a_0", which is currently specified for all HSS grades. A comprehensive data set which includes numerical and experimental studies for other structural forms (e.g. I-beams) are necessary to validate this finding.

Residual stresses were not considered in this study due to the low amount in hot-formed structural hollow sections as measured by Wang and Gardner (2017) at room temperature. However, it is noted that in other structural members such as cold-formed or welded members, the level of residual stresses could be more significant to the cross-section capacity. Residual stresses are the internal stresses present in a material, after the material has been processed (typical examples of processes include welding, non-uniform cooling, cold-forming, and shot peening). These internal stresses are often described as "self-balanced stresses caused by incompatible internal strains" (TWI, 2017). In the case of fire, the influence of thermal and creep strain, as well as recovery, may cause the distribution of stresses in a structural member to change at elevated temperature. There is a lot of uncertainty concerning how the distribution of internal stresses changes with increasing temperature and it is noted that this is a perplexing subject.

Numerical representation of the stress-strain response was simulated using the modified Ramberg-Osgood model proposed by Gardner and Nethercot (2004). This model can only trace the stress-strain response up to the ultimate strength, which may be a problem for numerical models at certain temperatures. Nonetheless, the model, together with the reduction factors, can be utilised to assess the structural performance of other structural forms (e.g. beams), part of a composite structural system or as part of a global frame in a performance-based approach to structural fire design. Such an approach will further enhance the understanding of HSS members under fire conditions which may, in turn lead to a more economic and safe design.

References

Afshan, S. (2013) Structural Behaviour of Cold-Formed Stainless Steel Tubular Members. (October).

Anderberg, Y. (1988) Modelling Steel Behaviour. Fire Safety Journal, 13 17–26.

ArcelorMittal USA (2015) Guidelines for fabricating and processing plate steel. 1–96.

Archer, R.S., Briggs, J.Z., Loeb Jr, C.M. and Loeb, C.M. (1948) Molybdenum: steels, irons, alloys. Climax Molybdenum Co. (ed.). New York: Climax Molybdenum Co.

ASFP (2014) Fire protection for structural steel in buildings 5th Edition (Volume 1 of 2). (Yellow book). Association for Speciacilist Fire Protection, 1.

Ashby, M.F. and Jones, D.R.H. (2005) Engineering materials 1: an introduction to properties, application, and design. Elsevier Butterworth-Heinemann, Amsterdam, Boston,.

ASME (2007) B31. 1-Power Piping. The American Society of Mechanical Engineers.

Assefpour-Dezfuly, M., Hugaas, B.A. and Brownrigg, A. (1990) Fire resistant high strength low alloy steels. 6(December) 1210–1214.

ASTM (2009) ASTM E21 - 09 Standard Test Methods for Elevated Temperature Tension Tests of Metallic Materials. In: West Conshohocken, PA: ,.

Atkinson, J.D. and Yu, J. (1997) the Role of Dynamic Strain-Ageing in the Environment Assisted Cracking Observed in Pressure Vessel Steels. Fatigue & Fracture of Engineering Materials & Structures, 20(1) 1–12.

Baddoo, N. (2015) SCI Webinar: Design with High Strength Steels.

Baddoo, N. and Brown, D. (2015) High Strength Steel Available from http://www.newsteelconstruction.com/wp/high-strength-steel/ [accessed 17 March 2017].

Bailey, C.G. (2006) Advances in fire engineering design of steel structures. Proceedings of the ICE - Structures and Buildings, 159(1) 21–35.

Banovic, S.W., McCowan, C.N. and Luecke, W.E. (2005) Physical Properties of Structural Steels.

Bhadeshia, H. and Honeycombe, R. (2006) Steels: microstructure and properties: microstructure and properties. 3rd edition. Butterworth-Heinemann.

Bhadeshia, H.K.D.H. (2010) Interpretation of the Microstructure of Steels Available from https://www.phase-trans.msm.cam.ac.uk/2008/Steel_Microstructure/SM.html [accessed 7 October 2017].

Bhattacher, V.S. (1997) Instantaneous coefficient of linear thermal expansion—a new definition.

Journal of testing and evaluation, 25(5) 479–484.

Billingham, J., Sharp, J. V, Spurrier, J. and Kilgallon, P.J. (2003) Review of the performance of high strength steels used offshore.

Boehler, J.P. (1987) Applications of tensor functions in solid mechanics (Vol. 292). New York: Springer.

Bolton, W. (2013) Engineering materials technology. Elsevier.

Bolton, W. and Higgins, R.A. (2014) Materials for Engineers and Technicians. Routledge.

BS 4360 (1979) Specification for Weldable structural steels. BSI.

BS 5950-8 (2003) Structural use of steelwork in building - Part 8: Code of practice for fire resistant design. BSI.

Bukowski, R.W. (2003) Prediction of the Structural Fire Performance of Buildings. In: 8th Fire and Materials Conference. 2003.

Burgan, B. (2001) Elevated tempreature and high strain rate properties of offshore steels.

Burgan, B.A. and Sansom, M.R. (2006) Sustainable steel construction. Journal of Constructional Steel Research, 62(11) 1178–1183.

Burgess, I.W., Olawale, A.O. and Plank, R.J. (1992) Failure of steel columns in fire. Fire Safety Journal, 18(2) 183–201.

Calado, W.R., dos Santos, O.J., Castro, C.S.B., Barbosa, R.N. and Gonzalez, B.M. (2008) Effect of finishing rolling temperature on fire resistance and dynamic strain aging behavior of a structural steel. Journal of Materials Science, 43 6005–6011.

Chadwick, G.A. (1972) Metallography of phase transformations. London: Butterworths.

Chen, J. and Young, B. (2008) Design of high strength steel columns at elevated temperatures. Journal of Constructional Steel Research, 64(6) 689–703.

Chen, J., Young, B. and Uy, B. (2006) Behavior of high strength structural steel at elevated temperatures Behavior of High Strength Structural Steel. 132(12) 1948–1954.

Chiew, S.P., Zhao, M.S. and Lee, C.K. (2014) Mechanical properties of heat-treatedhigh strength steel under fire/post-fire conditions. Journal of Constructional Steel Research, 98 12–19.

Chijiwa, R., Yoshida, Y., Uemori, R., Tamehiro, H., Funato, K. and Horii, Y. (1993) Development and Practical Application of Fire - Resistant Steel for Buildings.

Choi, I.-R., Chung, K.-S. and Kim, D.-H. (2014) Thermal and mechanical properties of high-strength structural steel HSA800 at elevated temperatures. Materials & Design, 63 544–551.

Cleaves, H.. and Hiegal, J.M. (1942) Properties of high-purity iron. Journal of Research of the National Bureau of Standards, 28 643–667.

Collin, P. and Johansson, B. (2005) Design of Welds in High Strength Steel. In: 4th European Conference on Steel and Composite Structures. 2005 Maastricht, The Netherlands,: ,.

Contro, R., Poggi, C. and Cazzani, A. (1988) Numerical analysis of fire effects on beam structures.

Engineering Computations, 5(1).

Cooke, G.M.E. (1988) An introduction to the mechanical properties of structural steel at elevated temperatures. Fire Safety Journal, 13(1) 45–54.

Corradi, L., Poggi, C. and Setti, P. (1990) Interaction domains for steel beam-columns in fire conditions. Journal of Constructional Steel Research, 17(3) 217–235.

Cottrell, A.H. and Bilby, B.A. (1949) Dislocation Theory of Yielding and Strain Ageing of Iron. Proceedings of the Physical Society. Section A, 62(1) 49.

Dassault Systèmes (2014) Abaqus 6.14 Online Documentation.

Date, E.H.. and Andrews, K.W. (1969) Anisotropic and composition effects in the elastic properties of polycrystalline metals. Journal of Physics D: Applied Physics, 2 1373–1381.

Davis, C.L., Mukhopadhyay, P., Strangwood, M., Potter, M.D.G., Dixon, S. and Morris, P.F. (2008) Comparison between elastic modulus and ultrasonic velocity anisotropy with respect to rolling direction in steels. 35(5) 359–366.

Davis, J.R. ed (1997) ASM specialty handbook: heat-resistant materials. R Davis, J (ed.). ASM International.

Davison, J.B., Burgess, I.W., Plank, R.J., Yu, H. and Hu, Y. (2010) Ductility of simple steel connections in fire. Proceedings of SDSS' Rio 2010: International Colloquium Stability and Ductility of Steel Structures, 1(June 2016).

Dawson, R.G. and Walker, A.C. (1972) Post-buckling of geometrically imperfect plates. Journal of the Structural Division. Journal of the Structural Division, 98(1) 75–94.

Dolzhenkov, I.E. (1967) Influence of deformation rate on the blue brittleness temperature and dislocation density of carbon steel. Metal Science and Heat Treatment, 9(6) 423–426.

Dotreppe, J.C. (1997) Mechanical properties of quenched and self-tempered reinforcing steel at elevated temperatures compared with recommendations of Eurocode 2-Part 1–2. Materials and Structures, 30(7) 430–438.

Du, Y., Liew, J.Y.R. and Xiong, M. (2017) Effects of heat-treatment methods on mechanical performance of high-tensile strength steel subject to elevated temperatures. In: EUROSTEEL 2017. 2017.

Dunne, D. (2016) Boron As An Alloying Element In Steels & Its Weld Metals. Australian Welding (Q3) p.37–43.

Ebel, R., Scandella, C., Fontana, M. and Knobloch, M. (2016) Member buckling of high strength steel in fire. In: Proceedings of the International Colloquium on Stability and Ductility of Steel Structures. 2016 Timisoara, Romania: Weinheim, 485–492.

EN 10025-1 (2004) Hot rolled products of structural steels - Part 1: General technical delivery conditions.

EN 10025-3 (2004) Hot rolled products of structural steels - Part 3: Technical delivery conditions for normalized/normalized rolled weldable fine grain structural steels.

EN 10025-4 (2004) Hot rolled products of structural steels – Part 4: Technical delivery conditions

for thermomechanical rolled weldable fine grain structural steels.

EN 10025-6 (2004) Hot rolled products of structural steels - Part 6: Technical delivery conditions for flat products of high yield strength structural steels in the quenched and tempered condition. 3.

EN 10027-1 (2005) Designation systems for steels - Part 1: Steel names.

EN 10147 (1992) Continuously hot-dip coated strip and sheet of structural steels — Technical delivery conditions.

EN 10149-2 (2013) Hot rolled flat products made of high yield strength steels for cold forming - Part 2 : Technical delivery conditions for thermomechanically rolled steels.

EN 10210-1 (2006) Hot finished structural hollow sections of non-alloy and fine grain steels Part 2: Tolerances, dimension and sectional properties.

EN 1993-1-1 (2005) Eurocode 3. Design of steel structures – Part 1–1: General rules and rules for buildings.

EN 1993-1-12 (2007) Eurocode 3. Design of steel structures – Part 1–12 :Additional rules for the extension of EN 1993 up to steel grades S 700.

EN 1993-1-2 (2005) Eurocode 3. Design of steel structures – Part 1–2: General rules – Structural fire design.

EN 1993-1-5 (2006) Eurocode 3: Design of steel structures – Part 1-5: Plated structural elements.

Engineers Edge (n.d.) Poissons' ratio metals material chart Available from http://www.engineersedge.com/materials/poissons_ratio_metals_materials_chart_13160.htm [accessed 3 October 2017].

Engler, O. and Randle, V. (2010) Introduction to texture analysis: macrotexture, microtexture, and orientation mapping. Second. Boca Raton: CRC press.

European Commission (2017) High strength long span structures (HILONG) Final Report. Brussels, Belgium: .

European Commission (2016) Rules on high strength steel (RUOSTE) Final Report. Brussels, Belgium: .

Franssen, J.-M. (1996) Residual stresses in steel profiles submitted to the fire: an analogy. In Proc. 3rd CIB/W14 FSF workshop on modelling (pp. 103-112). TNO Building and construction researc.

Franssen, J.-M., Talamona, D., Kruppa, J. and Cajot, L.G. (1998) Stability of Steel Columns in Case of Fire: Experimental Evaluation. Journal of Structural Engineering, 124(2) 158–163.

Garcia, H., Biezma, M. V, Cuadrado, J. and Orbe, A. (2013) Study of historical developments in the use of fire resistant steels. Materials at High Temperature, 30(4) 313–320.

Gardner, L. and Ashraf, M. (2006) Structural design for nonlinear metallic materials. Engineering Structures, 28(6) 926–934.

Gardner, L., Insausti, a., Ng, K.T. and Ashraf, M. (2010) Elevated temperature material properties

of stainless steel alloys. Journal of Constructional Steel Research, 66(5) 634–647.

Gardner, L. and Nethercot, D. (2004) Experiments on stainless steel hollow sections-Part 1: Material and cross-sectional behaviour. Journal of Constructional Steel Research, 60(9) 1291–1318.

Gardner, L., Saari, N. and Wang, F. (2010) Comparative experimental study of hot-rolled and cold-formed rectangular hollow sections. Thin-Walled Structures, 48(7) 495–507.

Ginzburg, V.B. and Ballas, R. (2000) Flat Rolling Fundamentals. CRC Press.

Gkantou, M., Theofanous, M., Antoniou, N. and Baniotopoulos, C. (2017) Compressive behaviour of high-strength steel cross-sections. Proceedings of the Institution of Civil Engineers - Structures and Buildings, (August) 1–12.

Gladman, T. (1999) The physical metallurgy of microalloyed steels. London: The institute of materials.

Global Metals (2017) Section 4 : Effects of alloying elements Available from http://www.globalmetals.com.au/_pdf/Metallurgical_Overview/section_4.pdf [accessed 20 August 2017].

Gorka, J. (2014) Changes in the structure and properties of steel S700MC by heat treatment. Advanced Material Research, (1033–1036) 111–116.

Gresnigt, A.M. and Steenhuis, C.M. (1997) High strength steels. Progress in Structural Engineering and Materials, 1(1) 31–41.

Gyasi, E.A. and Kah, P. (2016) Structural Integrity Analysis of the Usability of High Strength Steels (HSS). Reviews on Advanced Materials Science, 46.

Hechler, O. (2015) The right choice of steel–according to the Eurocode. Economical Bridge Solutions Based on Innovative Composite Dowels and Integrated Abutments: Ecobridge, 1–179.

Hill, H.N. (1944) Determination of Stress–Strain Relations from the Offset Yield Strength Values. Washington: .

Holicky, M., Materna, A., Sedlacek, G., Arteaga, A., Sanpaolesi, L. and Vrouwenvelder, T. (2005) Development of Skills Facilitating Implementation of Eurocodes, Handbook 2: Reliability Backgrounds. Prague, Czech Republic: .

Hollomon, J.H. and Jaffe, L.D. (1947) Ferrous metallurgical design: design principles for fully hardened steel. Wiley.

Hopkin, D., Van Coile, R. and Lange, D. (2017) Certain uncertainty - demonstrating safety in fire engineering design and the need fo safety targets Available from http://www.sfpe.org/page/Issue7Feature2/Certain-Uncertainty---Demonstrating-Safety-in-Fire-Engineering-Design-.htm [accessed 16 October 2017].

Hu, G., Morovat, M.A., Lee, J., Schell, E. and Engelhardt, M. (2009) Elevated Temperature Properties of ASTM A992 Steel. Structures Congress 2009, 1–10.

Huang, Y. and Young, B. (2014) The art of coupon tests. Journal of Constructional Steel Research, 96 159–175.

Humphreys, F.J. and Hatherly, M. (2004) The structure and energy of grain boundaries. In:

Recrystallization and Related Annealing Phenomena. 91–119.

Ianizzi, R. and Schleich, J.B. (1991) Mechanical properties of structural steel at elevated temperatures—comparisons by numerical simulations.

ISO 6892-1 (2009) Metallic materials. Tensile Testing Part 1: Method of test at ambient temperature.

ISO 6892-2 (2011) Metallic materials. Tensile testing. Part 2: Method of test at elevated temperature. BSI.

ISO 7500-1 (2015) Metallic Materials - Verification of Static Uniaxial Testing Machines - Part 1: Tension/Compression Testing Machines - Verification and Calibration of the Force-Measuring System. BSI.

ISO 834-1 (1999) Fire-resistance tests. Elements of building construction. Part 1: General requirements.

ISO 9513 (2012) Metallic materials - Calibration of extensometer systems used in uniaxial testing. BSI.

Jacques, H. and Boris, D. (2004) Tmcp Applications in Sections , Bars and Rails. 1–8.

James, J.D., Spittle, J.A., Brown, S.G.R. and Evans, R.W. (2001) A review of measurement techniques for the thermal expansion coefficient of metals and alloys at elevated temperatures. Measurement Science and Technology, 12(3) R1–R15.

Janss, J. and Minne, R. (1981) Buckling of steel columns in fire conditions. Fire Safety Journal, 4(4) 227–235.

Jeanes, D.C. (1985) Application of the computer in modeling fire endurance of structural steel floor systems. Fire Safety Journal, 9(1) 119–135.

Johansson, B. and Collin, P. (2005) Eurocode for high strength steel and applications in construction. Super-High Strength Steels,.

Kelly, F.S. (1998) Characterisation and design of fire-resistant steels for construction. Queen's University of Belfast.

Kervalishvili, A. and Talvik, I. (2017) Influence of residual stress on the stability of steel columns at elevated temperatures. Journal of Civil Engineering and Management, 23(2) 292–299.

Kervalishvili, A. and Talvik, I. (2016) Modified procedure for buckling of steel columns at elevated temperatures. Journal of Constructional Steel Research, 127 108–119.

Kirby, B. (1997) Large Scale Fire Tests: The British Steel European Collaborative Research Programme On The Bre 8-storey Frame. Fire Safety Science, 5 1129–1140.

Kirby, B.R. and Preston, R.R. (1988) High Temperature Properties of Hot-rolled , Structural Steels for Use in Fire Engineering Design Studies. Fire Safety Journal, 13 27–37.

Kizu, T., Okuda, K., Nagataki, Y., Urabe, T. and Seto, K. (2015) Influence of Tensile Strain on Young's Modulus in High-strength Cold-rolled Steel Sheets. ISIJ International, 55(7) 1502–1511.

Knobloch, M. (2014) Stability of steel structures in fire. Stahlbau, 83(4) 257–264.

Knobloch, M., Pauli, J. and Fontana, M. (2013) Influence of the strain-rate on the mechanical properties of mild carbon steel at elevated temperatures. Materials and Design, 49 553–565.

Kodur, V., Dwaikat, M. and Fike, R. (2010) High temperature properties of steel for fire resistance modeling of structures. Journal of Materials in Civil Engineering, 22(5) 423–434.

Kodur, V.K.R. and Dwaikat, M.M.S. (2010) Effect of high temperature creep on the fire response of restrained steel beams. Materials and Structures, 43(10) 1327–1341.

Kubin, L.P. and Estrin, Y. (1991) Dynamic strain ageing and the mechanical response of alloys. Journal de Physique III, 1(6) 929–943.

Kutz, M.E. (2002) Handbook of materials selection. John Wiley & Sons.

Lamont, S. (2001) The Behaviour of Multi-Storey Composite Steel Framed Buildings in Response to Compartment Fires. University of Edinburgh.

Lange, J. and Wohlfeil, N. (2010) Examination of the Mechanical Properties of Steel S460 for Fire. Journal of Structural Fire Engineering, 1(3) 189–204.

Lange, J. and Wohlfeil, N. (2007) Untersuchungen zum Werkstoffverhalten des Feinkornbaustahls S 460 unter erhöhten. 84 711–720.

Laogan, B.T. and Elnashai, A.S. (1999) Structural performance and economics of tall high strength RC buildings in seismic regions. Structural Design of Tall Buildings, 8(November 1998) 171–204.

Lawson, R.M. and Newman, G.M. (1996) Structural Fire Design to EC3 & EC4, and comparison with BS 5950.

Lennon, T., Moore, D.B., Wang, Y.C. and Bailey, C.G. (2006) Designers' guide to EN1991-1-2, EN1992-1-2, EN1993-1-2 and EN1994-1-2.

Li, H.-T. and Young, B. (2017) Material properties of cold-formed high strength steel at elevated temperatures. Thin-Walled Structures, 115(February) 289–299.

Lie, T. (1972) Fire and buildings. Applied Science Publishers Ltd.

Lord, J.D. and Morrell, R.M. (2014) Comparison of static and dynamic methods for measuring stiffness of high modulus steels and metal composites. Canadian Metallurgical Quarterly, 53(3) 292–299.

Lord, J.D. and Morrell, R.M. (2010) Elastic modulus measurement - obtaining reliable data from the tensile test. Metrologia, 47(2) S41.

Loveday, M.S., Gray, T. and Aegerter, J. (2004) Tensile Testing of Metallic Materials : A Review Tensile Testing of Metallic Materials : A Review.

Luecke, W.E., McColskey, J.D., McCowan, C.N., Banovic, S.W., Fields, R.J., Foecke, T., Siewert, T. a and Gayle, F.W. (2005) Mechanical properties of structural steels, Federal building and fire safety investigation of the World Trade Center disaster.

Ma, J.L., Chan, T.M. and Young, B. (2015) Material properties and residual stresses of cold-formed high strength steel hollow sections. Journal of Constructional Steel Research, 109 152–165.

Mahendran, M. (1996) The modulus of elasticity of steel - is it 200 GPa? Thirteenth International Specialty Conference on Cold-Formed Steel Structures St. Louis, Missouri U.S.A., 641–648.

Maitland, T. and Sitzman, S. (2007) EBSD technique and materials characterization examples. In: Scanning Microscopy for Nanotechnology. Berlin: Springer, 41–75.

Manninen, T. and Säynäjäkangas, J. (2012) Mechanical Properties of Ferritic Stainless Steels at Elevated Temperature. Proceedings of the Fourth International Experts Seminar on Stainless Steel in Structures, 4th 1–15.

Maślak, M. and Skiba, R. (2015) ScienceDirect Fire resistance increase of structural steel through the modification of its chemical composition. Procedia Engineering, 108 277–284.

Meester, B. De (1997) The Weldability of Modern Structural TMCP Steels. ISIJ International, 37(1 997) 537–551.

Meyers, M.A. and Chawla, K.K. (2009) Mechanical Behavior of Materials. Second. Cambridge University Press.

Mirambell, E. and Real, E. (2000) On the calculation of deflections in structural stainless steel beams: an experimental and numerical investigation. Journal of Constructional Steel Research, 54(1) 109–133.

Mizutani, Y., Yoshii, K., Chijiwa, R., Ishibashi, K., Wattanabe, Y. and Yoshida, Y. (2004) 590MPa Class Fire-Resistant Steel for Building Structural Use. (90) 45–52.

Morozov, Y.D., Chevskaya, O.N., Filippov, G. a. and Muratov, a. N. (2007) Fire-resistant structural steels. Metallurgist, 51(7) 356–366.

Motra, H.B., Hildebrand, J. and Dimmig-Osburg, A. (2014) Assessment of strain measurement techniques to characterise mechanical properties of structural steel. Engineering Science and Technology, an International Journal, 17(4) 260–269.

Münstermann, S., Feng, Y. and Bleck, W. (2014) Influencing parameters on elastic modulus of steels. Canadian Metallurgical Quarterly, 53(3) 264–273.

Muratov, a. N., Morozov, Y.D., Chevskaya, O.N. and Filippov, G. a. (2007) Technology for the commercial production of fire-resistant steel for building structures. Metallurgist, 51(8) 446–453.

National Physical Laboratory (2014) What is emissivity and why is it important? (FAQ - Thermal) Available from http://www.npl.co.uk/reference/faqs/what-is-emissivity-and-why-is-it-important-(faq-thermal) [accessed 11 February 2018].

Neuenschwander, M., Knobloch, M. and Fontana, M. (2017) Elevated temperature mechanical properties of solid section structural steel. Construction and Building Materials, 149 186–201.

Neuenschwander, M., Scandella, C., Knobloch, M. and Fontana, M. (2017) Modeling elevated-temperature mechanical behavior of high and ultra-high strength steels in structural fire design. Materials & Design, 136(September) 81–102.

Niffenegger, M. and Reichlin, K. (2012) The proper use of thermal expansion coefficients in finite element calculations. Nuclear Engineering and Design, 243 356–359.

Nishioka, K. and Ichikawa, K. (2012) Progress in thermomechanical control of steel plates and their

commercialization. Science and Technology of Advanced Materials, 13 39501.

Okumura, M., Yurioka, N., Kasuya, T. and Cotton, H.J. (1987) Prediction of HAZ Hardness after PWHT. In: Stress relieving heat treatments of welded steel constructions. 1987 Sofia, Bulgaria: Pergamon Press, 61–68.

Outinen, J. (1996) Behaviour of High-strength Structural Steel S420M at Elevated Temperatures. Rakenteiden Mekaniikka, 29(3–4) 103–114.

Outinen, J. (2006) Mechanical properties of structural steels at elevated temperatures and after cooling down. In: Fire and Materials Conference. 2006 San Francisco: Interscience Coomunications Limited, UK,.

Outinen, J. (2007) Mechanical properties of structural steels at high temperatures and after cooling down. Helsinki University of Technology Laboratory.

Outinen, J., Tojakander, P., Lu, W. and Puttonen, J. (2014) Material properties of high strength steel in fire. In: EUROSTEEL. 2014.

Pauli, J. (2013) The Behaviour of Steel Columns in Fire.

Pauli, J., Somaini, D., Knobloch, M. and Fontana, M. (2012) Experiments on steel columns under fire conditions.

Pierron, O.N., Koss, D. a. and Motta, a. T. (2003) Tensile specimen geometry and the constitutive behavior of Zircaloy-4. Journal of Nuclear Materials, 312(2–3) 257–261.

Poh, K.W. (2001) Stress-strain temperature relationship for structural steel. (October) 371–379.

Porter, D.A. (2015) Weldable High-Strength Steels : Challenges and Engineering Applications. IIW International Conference High-Strength Materials - Challenges and Applications, (Portevin session).

Prabhudev, K.H. (1988) Handbook of heat treatment of steels. Tata McGraw-Hill Education.

Qiang, X. (2013) Behaviour of High Strength Steel Endplate Connections in Fire and after Fire. Delft University.

Qiang, X., Bijlaard, F. and Kolstein, H. (2012) Dependence of mechanical properties of high strength steel S690 on elevated temperatures. Construction and Building Materials, 30 73–79.

Qiang, X., Bijlaard, F.S.K. and Kolstein, H. (2012) Deterioration of mechanical properties of high strength structural steel S460N under steady state fire condition. Materials & Design, 40 521–527.

Qiang, X., Bijlaard, F.S.K. and Kolstein, H. (2013) Elevated-temperature mechanical properties of high strength structural steel S460N: Experimental study and recommendations for fire-resistance design. Fire Safety Journal, 55 15–21.

Rakshe, B. and Patel, J. (2010) Modern high strength Nb-bearing structural steels. MILLENNIUM STEEL INDIA, 69–72.

Ramberg, W. and Osgood, W. (1943) Description of Stress-Strain Curves By Thee Parameters. NACA Technical Note. No. 902.

Randle, V. (2009) Electron backscatter diffraction: Strategies for reliable data acquisition and processing. Materials Characterization, 60(9) 913–922.

Rasmussen, K.J.R. (2003) Full-range stress–strain curves for stainless steel alloys. 59(2003) 47–61.

Rasmussen, K.J.R. and Hancock, G.J. (1995) Tests of High Strength Steel Columns. Journal of Constructional Steel Research, 34(1) 27–52.

Rhodan, M. (2013) UN: Number of city-dwellers to double by 2050 Available from http://world.time.com/2013/12/09/un-number-city-double/ [accessed 3 July 2017].

Rubert, A. and Schaumann, P. (1986) Structural steel and plane frame assemblies under fire action. Fire Safety Journal, 10(3) 173–184.

Ruukki (2013) High-strength special steels create new architecture Available from http://www.ruukki.com/News-and-events/News-archive/2013/High-strength-special-steels-create-new-architecture [accessed 27 April 2015].

Saab, H.A. and Nethercot, D.A. (1991) Modelling steel frame behaviour under fire conditions. Engineering Structures, 13(4) 371–382.

Sadiq, H., Wong, M.B., Tashan, J., Al-Mahaidi, R. and Zhao, X.L. (2013) Determination of steel emissivity for the temperature prediction of structural steel members in fire. Journal of Materials in Civil Engineering, 25(2) 167–173.

Sakumoto, Y. (n.d.) Fire-Resistant Steel for Building Structures.

Samuels, L.. (1999) Light microscopy of carbon steels. ASM International.

Schneider, R. and Lange, J. (2009) Constitutive equations of structural steel S460 at high temperatures. In: Nordic Steel ’09 Construction Conference. 2009 204–211.

Schröter, F. (2006) Trends of using high-strength steel for heavy steel structures. Progress in Steel, Composite and Aluminium Structures S p.292–293.

Schwartz, A.J., Kumar, M. and Adams, B.L. (2000) Electron backscatter diffraction in materials science. New York: Kluwer Academic/Plenum Publshers.

Sedlacek, G. and Müller, C. (2001) High strength steels in steel construction. Niobium: Science & Technology, TMS: The Minerals, Metals & Materials Society, Orlando, Florida,.

Sha, W., Kelly, F.S., Browne, P., Blackmore, S.P.O. and Long, a. E. (2002) Development of structural steels with fire resistant microstructures. Materials Science and Technology, 18(3) 319–325.

Sha, W., Kelly, F.S. and Guo, Z. (1999) Microstructure and Properties of Nippon Fire-Resistant Steels. 8(October) 606–612.

Sha, W., Kirby, B.R. and Kelly, F.S. (2001) The Behaviour of Structural Steels at Elevated Temperatures and the Design of Fire Resistant Steels. Materials Transactions 42 (9) p.1913–1927.

Smith, C.I., Kirby, B.R., Lapwood, D.G., Cole, K.J., Cunningham, A.P. and Preston, R.R. (1981) The reinstatement of fire damaged steel framed structures. Fire Safety Journal, 4(1) 21–62.

SteelConstruction.info (2017a) Steel material properties Available from

http://www.steelconstruction.info/Steel_material_properties [accessed 12 June 2017].

SteelConstruction.info (2017b) Structural fire engineering Available from https://www.steelconstruction.info/Structural_fire_engineering [accessed 19 June 2017].

Steiner, R. (1990) ASM Handbook, Volume 1: Properties and Selection: Irons, Steels, and High-Performance Alloys Volume 1 of ASM Handbooks Series. 10th edition. ASM International.

Stevens, S.M. (1982) Calibration of a driect reading optical emission spectrograph. The Welding Insititute Research Bulletin p.190–193.

Stroetmann, R. (2011) High strength steel for improvement of sustainability. Eurosteel. Budapest, Hungary, 2–7.

Talamona, D., Franssen, J.M., Schleich, J.B. and Kruppa, J. (1997) Stability of steel columns in case of fire: Numerical Modeling. Journal of Structural Engineering, 123(6) 713–720.

Theofanous, M. and Gardner, L. (2010) Experimental and numerical studies of lean duplex stainless steel beams. Journal of Constructional Steel Research, 66(6) 816–825.

Torres, E.A. and Ramírez, A.J. (2011) In situ scanning electron microscopy. Science and Technology of Welding and Joining, 16(1) 68–78.

Total Materia (2009) Advanced Structural Steels Part Two: Thermomechanically Control Processed Steels Available from http://www.totalmateria.com/page.aspx?ID=CheckArticle&site=kts&NM=256 [accessed 11 May 2015].

Total Materia (2013) Strain Ageing of Steel: Part One Available from https://www.totalmateria.com/page.aspx?ID=CheckArticle&site=kts&NM=392 [accessed 10 July 2018].

Türköz, E. (2016) Material Science Available from https://www.princeton.edu/~eturkoz/materials.html [accessed 7 January 2018].

TWI (2017) Residual Stresses Available from http://www.twi-global.com/capabilities/integrity-management/engineering-critical-assessment/residual-stresses/ [accessed 10 December 2017].

Twilt, L. (1988) Strength and Deformation Properties of Steel at Elevated Temperatures : Some Practical Implications. Fire Safety Journal, 13 9–15.

Twilt, L. (2001) The new eurocode on fire design of steel structures. Seminar,.

Uemori, R., Tamehiro, H. and Chijiwa, R. (1996) AP-FIM Analsysi of Ultrafine Carbonnitrides in Fire-Resistant Steel for Building Construction.

Varol, H. and Cashell, K.A. (2017) Numerical modelling of high strength steel beams at elevated temperature. Fire Safety Journal, 89(February) 41–50.

Vassart, O., Zhao, B., Cajot, L.., Robert, F., Meyer, U. and Frangi, A. (2014) Eurocodes : Background & Applications Structural Fire Design.

Vander Voort, G.F., Lampman, S.R., Sanders, B.R., Anton, Gayle, J., Polakowski, C., Kinson, J., Kathryn, M., Henry, S.D. and Scott Jr, W.W. (2004) ASM handbook. Metallography and

microstructures. Volume 9. ASM International.

Wan, R., Sun, F., Zhang, L. and Shan, A. (2012a) Development and study of high-strength low-Mo fire-resistant steel. Materials and Design, 36 227–232.

Wan, R., Sun, F., Zhang, L. and Shan, A. (2012b) Effects of Mo on high-temperature strength of fire-resistant steel. Materials and Design, 35 335–341.

Wang, F. and Lui, E.M. (2016) Behavior of High Strength Steels under and After High Temperature Exposure: A Review. Journal of Steel Structures & Construction, 2(2).

Wang, J. (2016) Behaviour and design of high strength steel structures. Imperial College London.

Wang, J., Afshan, S., Gkantou, M., Theofanous, M., Baniotopoulos, C. and Gardner, L. (2016) Flexural behaviour of hot-finished high strength steel square and rectangular hollow sections. Journal of Constructional Steel Research, 121 97–109.

Wang, J., Afshan, S., Schillo, N., Theofanous, M., Feldmann, M. and Gardner, L. (2017) Material properties and compressive local buckling response of high strength steel square and rectangular hollow sections. Engineering Structures, 130 297–315.

Wang, J. and Gardner, L. (2017) Flexural Buckling of Hot-Finished High-Strength Steel SHS and RHS Columns. Journal of Structural Engineering, ASCE, 143(6) 1–12.

Wang, W., Kodur, V., Yang, X. and Li, G. (2014) Experimental study on local buckling of axially compressed steel stub columns at elevated temperatures. Thin-Walled Structures, 82 33–45.

Wang, W., Liu, B. and Kodur, V. (2013a) Effect of Temperature on Strength and Elastic Modulus of High-Strength Steel. (February) 174–182.

Wang, W., Ohmiya, Y. and Ma, G. (2013b) Fire Resistance Study of Axially Loaded High Strength Steel Columns. Procedia Engineering, 62 690–701.

Wang, W. and Zhang, L. (2017) Mechanical properties of high strength Q690 steel at elevated temperatures. In: EUROSTEEL 2017. 2017 Copenhagen: ,.

Wang, Y., Burgess, I., Wald, F. and Gillie, M. (2012) Performance-based fire engineering of structures. CRC Press.

Winning, M. and Rollett, A.D. (2005) Transition between low and high angle grain boundaries. Acta Materialia, 53(10) 2901–2907.

World Steel Association (2017a) Steel – the permanent material in the circular economy Available from http://circulareconomy-worldsteel.org/ [accessed 12 June 2017].

World Steel Association (2017b) World steel in figures 2016 Available from https://www.worldsteel.org/en/dam/jcr:1568363d-f735-4c2c-a1da-e5172d8341dd/World+Steel+in+Figures+2016.pdf [accessed 12 June 2017].

Wyatt, O.H. and Dew-Hughes, D. (1974) Metals, cermaics and polymers. Cambridge University Press.

Xiong, M.X. and Liew, J.Y.R. (2016) Mechanical properties of heat-treatedhigh tensile structural steel at elevated temperatures. Thin-Walled Structures, 98 169–176.

Yang, K.C., Lee, H.H. and Chan, O. (2006) Experimental study of fire-resistant steel H-columns at elevated temperature. Journal of Constructional Steel Research, 62(6) 544–553.

Zehfuss, J. and Hosser, D. (2007) A parametric natural fire model for the structural fire design of multi-storey buildings. Fire Safety Journal, 42(2) 115–126.